NATIONAL CENTER FOR EARTHQUAKE
ENGINEERING RESEARCH
State University of New York at Buffalo

TEFLON BEARINGS IN ASEISMIC BASE ISOLATION: EXPERIMENTAL STUDIES AND MATHEMATICAL MODELING

by

A. Mokha, M.C. Constantinou and A.M. Reinhorn
Department of Civil Engineering
State University of New York at Buffalo
Buffalo, New York 14260

Technical Report NCEER-88-0038

December 5, 1988

This research was conducted at the State University of New York at Buffalo and was partially supported by the National Science Foundation under Grant No. ECE 86-07591.

NOTICE

This report was prepared by the State University of New York at Buffalo as a result of research sponsored by the National Center for Earthquake Engineering Research (NCEER). Neither NCEER, associates of NCEER, its sponsors, the State University of New York at Buffalo, nor any person acting on their behalf:

a. makes any warranty, express or implied, with respect to the use of any information, apparatus, method, or process disclosed in this report or that such use may not infringe upon privately owned rights; or

b. assumes any liabilities of whatsoever kind with respect to the use of, or the damage resulting from the use of, any information, apparatus, method or process disclosed in this report.

TEFLON BEARINGS IN ASEISMIC BASE ISOLATION: EXPERIMENTAL STUDIES AND MATHEMATICAL MODELING

by

A. Mokha[1], M.C. Constantinou[2] and A.M. Reinhorn[3]

December 5, 1988

Technical Report NCEER-88-0038

NCEER Contract Number 87-2002

NSF Master Contract Number ECE 86-07591

1 Graduate Student, Dept. of Civil Engineering, State University of New York at Buffalo
2 Assistant Professor, Dept. of Civil Engineering, State University of New York at Buffalo
3 Associate Professor, Dept. of Civil Engineering, State University of New York at Buffalo

NATIONAL CENTER FOR EARTHQUAKE ENGINEERING RESEARCH
State University of New York at Buffalo
Red Jacket Quadrangle, Buffalo, NY 14261

PREFACE

The National Center for Earthquake Engineering Research (NCEER) is devoted to the expansion and dissemination of knowledge about earthquakes, the improvement of earthquake-resistant design, and the implementation of seismic hazard mitigation procedures to minimize loss of lives and property. The emphasis is on structures and lifelines that are found in zones of moderate to high seismicity throughout the United States.

NCEER's research is being carried out in an integrated and coordinated manner following a structured program. The current research program comprises four main areas:

- Existing and New Structures
- Secondary and Protective Systems
- Lifeline Systems
- Disaster Research and Planning

This technical report pertains to Program 2, Secondary and Protective Systems, and more specifically, to protective systems. Protective Systems are devices or systems which, when incorporated into a structure, help to improve the structure's ability to withstand seismic or other environmental loads. These systems can be passive, such as base isolators or viscoelastic dampers; or active, such as active tendons or active mass dampers; or combined passive-active systems.

Passive protective systems constitute one of the important areas of research. Current research activities, as shown schematically in the figure below, include the following:

1. Compilation and evaluation of available data.
2. Development of comprehensive analytical models.
3. Development of performance criteria and standardized testing procedures.
4. Development of simplified, code-type methods for analysis and design.

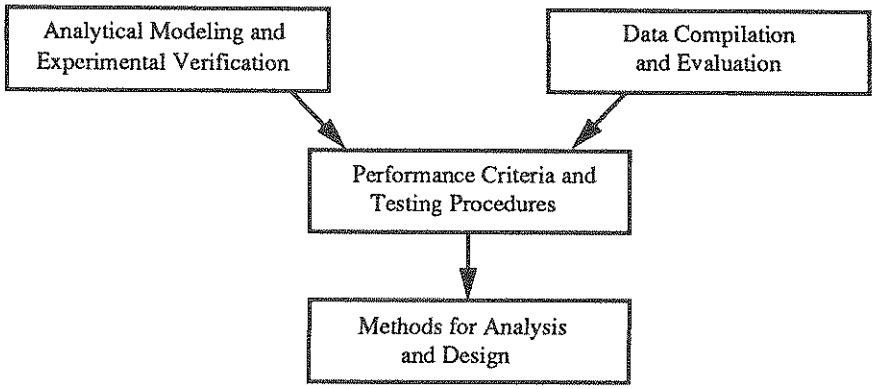

The focus of this study was on teflon sliding bearings for base-isolated buildings and bridges. The experimental program described in this report was designed to provide as much information as necessary to develop mathematical models for teflon-steel interfaces. A total of 164 tests were conducted and the effects on friction of pressure, velocity, acceleration, type and condition of the interface, and type of test were investigated. The obtained results have been used in the development of a mathematical model of uni-directional friction.

ABSTRACT

This report describes the frictional properties of Teflon-steel interfaces in relation to their application in sliding bearings for base isolated building and bridge structures. A number of laboratory tests have been conducted to determine the effect of sliding velocity, sliding acceleration, bearing pressure, type of Teflon and surface finish on the frictional characteristics of sliding bearings. Aspects of mathematical modeling and application of results in the analysis of sliding isolation systems are considered.

ACKNOWLEDGEMENTS

This work was supported by the National Center for Earthquake Engineering Research and by Watson Bowman Acme Corporation. Watson Bowman's contribution consisted of a monetary contribution, materials and the engineering services of Mr. Liberato Pietrantoni, who provided valuable assistance throughout the course of the project.

TABLE OF CONTENTS

TABLE OF CONTENTS (Cont'd)

LIST OF FIGURES

LIST OF FIGURES (Cont'd)

LIST OF TABLES

SECTION 1
INTRODUCTION

Teflon sliding bearings have been used for the past several years to accommodate the slow motions that arise in bridges due to temperature changes, creep and shrinkage of concrete. For such slow motions, the coefficient of friction of Teflon sliding on polished stainless steel is very low. AASHTO Specifications [1] recommend a coefficient of friction for design between 0.04 and 0.06 for Teflon mating with stainless steel of a surface roughness of less than 20μin RMS (0.50μm). In practice, however, the coefficient of friction may be much higher. This led California to require a surface finish of less than 3μin RMS (0.076μm) and the use of lubrication [2]. Under these conditions, the coefficient of friction for slow speeds may be as low as 0.01 [2, 3].

If such low coefficients of friction are maintained over long periods of time, Teflon sliding bearings may be particularly useful in base isolation systems for structures. In fact, five different isolation systems that incorporate Teflon-steel interfaces have been proposed, of which one has reached the stage of implementation. All these systems, which are reviewed in section 2 of this report, utilize Teflon-steel interfaces to support the weight of the structure and a separate mechanism to provide centering force capability and additional energy absorption capacity. A simple version of this mechanism may be in the form of cylindrical rubber springs that are bolted or otherwise attached to the basemat and foundation slab of the structure and carry no vertical load. The centering force in these systems need not be strong as sliding bearings may be designed to accommodate the resulting large displacements. Suggested values for the rigid body mode period of sliding isolation systems are 4 to 5 seconds.

There are two important advantages in sliding isolation systems with restoring force. First, the functions of carrying the vertical load and of providing horizontal stiffness are effectively separated. This results in a more stable system that eliminates the need of a fail-safe mechanism. Second, sliding isolation systems with a weak restoring force are less sensitive to variations in the frequency content of ground excitation and tend to limit the intensity of the force imparted to the superstructure. This insensitivity to the frequency content of the excitation is of particular importance as it distinguishes sliding from elastomeric isolation systems.

The acceptance of sliding isolation systems by the engineering profession depends largely on the experimental verification of the concept, on the establishment of design procedures and on the assessment of the characteristics of sliding bearings under conditions of interest in base isolation. The most important characteristic of sliding bearings is the coefficient of friction at the Teflon-steel interface. It is known that this coefficient depends on the sliding velocity, bearing pressure, surface condition of stainless steel, and type of Teflon. Other factors may have important effects, the extent of which is unknown.

A considerable amount of data on friction of Teflon is included in several duPont publications [4-6]. It has been common to refer to this data as representative of what might be the behavior of Teflon-steel interfaces under conditions encountered in base isolation applications. To assess the usefulness of this data in the application of interest, namely base isolation, it is necessary to review the original publications on which the duPont data is based.

A variety of testing arrangements have been used. One apparatus has been described by Flom and Porile [7] and reviewed in Reference 8. The apparatus used to obtain some of the most commonly referred data (those of high compressive loads) has been described by Thompson et al [9]. The Teflon specimen is in the form of a ring 0.25 inches wide and two inches outside diameter. It is in contact with a polished stainless steel plate that is compressed by a press. Sliding is imposed by rotation of the steel plate. The coefficient of friction is obtained from the vertical force and the torque needed to maintain motion. In deriving a relation between the frictional force and torque, it was assumed that friction is independent of velocity. The device was used to obtain values of the sliding coefficient of friction (value needed to maintain motion) at speeds of about 0.1 in/sec.

Thompson et. al. [9] have reported the sliding coefficient of friction of unfilled Teflon in contact with stainless steel of surface roughness of about 2μin RMS (0.05μm). Most of the other data on friction in duPont publications is of Teflon sliding against Teflon and at light loads. This data is useful in the design of mechanical bearings. In these applications of repetitive sliding, Teflon is transferred to the metal surfaces which are quickly coated with Teflon. Thus, the condition in actual practice is that of Teflon sliding against itself.

A significant amount of data on friction of Teflon-steel interfaces under conditions of interest in bridge applications has been generated in more recent years. Taylor [10] has conducted a comprehensive series of tests on unfilled and filled (glass, graphite, carbon and molybdenum disulphide) Teflon sliding against stainless steel. Bearing pressure was between 1,000 and 5,800 psi (7 to 40 N/mm^2) and maximum speed was less than 3 in/hr. Coefficients of friction were determined after running-in the interfaces as maximum load. This has an effect of reducing the coefficient of friction. There are practical difficulties in running-in quantities of bearings for this purpose.

Other test programs have been conducted in the U.S., England, Germany and South Africa and have been reviewed in Reference 11. The maximum speed used in these laboratory tests is 0.1 in/sec [11,12]. This speed is well below the speeds expected to occur during earthquakes.

Tyler in New Zealand [13] was the first to conduct tests on unfilled Teflon-steel interfaces under pressure of 1,100 to 4,300 psi (7.6 to 30 N/mm^2) and peak velocity (sinusoidal motion) of 2.5 to almost 15 in/sec. At each pressure level, only two or three tests were conducted at different

velocities. The stainless steel surface was polished to a finish of 2 to 6μin CLA (0.05 to 0.15μm).

Constantinou et. al. [8] have obtained indirect measurements of the sliding coefficient of friction (value needed to maintain motion) of unfilled Teflon-steel interfaces during shake table testing of a model. The studies of Tyler and Constantinou, while useful in understanding the behavior of these interfaces under earthquake conditions, have been limited to a small number of tests that precluded the development of mathematical models that could describe the behavior of Teflon-steel interfaces.

The experimental program described in this report has been designed to provide as much information as necessary to develop mathematical models of the behavior of Teflon-steel interfaces. The objective, of course, is the application of these results in the analysis and design of sliding isolation systems in building and bridge structures. The concentration has been on the frictional characteristics. The effects of bearing pressure, sliding velocity, type of Teflon and surface finish of stainless steel have been studied. Furthermore, in a limited number of tests, the effects of type of test, acceleration at sliding interface and size of specimen have been studied.

More than 160 tests have been conducted at bearing pressure of 1,000, 2,000, 3,000, and 6,500 psi (6.9, 13.8, 20.7 and 45 N/mm^2) and sliding velocity of 0.1 to about 20 in/sec. Unfilled and glass filled Teflon (at 15% and 25% composition by weight) were tested against stainless steel polished to mirror finish. The tests were conducted with the direction of sliding either parallel or perpendicular to the surface lay (direction of predominant surface pattern) that resulted in two effective degrees of surface finish. The obtained results have been utilized in the development of a mathematical model of uni-directional friction.

The tests have been conducted with a specially designed test arrangement that is capable of developing up to 250 kips of compressive force over prolonged intervals of time. The arrangement may be used to study the effect of adhesion that may develop over prolonged compression of Teflon-steel interfaces.

SECTION 2
BASE ISOLATION SYSTEMS

The concept of aseismic base isolation is one in which a building is uncoupled from the damaging horizontal components of ground motion by a mechanism that provides flexibility and energy absorption capacity.

The idea of supporting the building and letting the ground move underneath is so appealing that many inventors proposed devices to achieve this result as early as the beginning of this century. Almost all of these inventions remained unimplemented until the 1950's, when multilayer elastomeric bearings were developed. A system with no horizontal restraint such as the one described above has, in practice, to accommodate frequently occurring service loads such as minor earthquakes, wind and braking forces in bridge applications. A practical system usually consists of the following elements [14, 15]:

1. A horizontally flexible mount which lowers the fundamental frequency of the system below the predominant ground motion frequencies,

2. Additional damping to keep displacements within acceptable limits,

3. A mechanism to provide rigidity under frequent service loads, and

4. A fail-safe system that is activated in extreme situations when the flexible mount is about to fail (a second line of defense). Some isolation systems combine the first three of these elements in a single device.

Design codes require that earthquake forces be absorbed by the structural system through inelastic action which lengthens the period of the system and increases its energy dissipation capacity. This inelastic action is concentrated at beam-column connections and relies heavily on connection details or confinement and reinforcement details in concrete structures. This action involves damage, both to the structural system and nonstructural components. The paradox with this approach is that safety is ensured by allowing damage. It is acceptable because of its economic benefits in reducing construction costs. However, earthquakes have other cost impacts such as repair and disruption costs after an earthquake, earthquake insurance premiums and potential liability for losses and injuries.

The base isolation alternative reduces the forces transmitted to the structure and limits any inelastic action in a specially designed replaceable system that is placed between the building and its foundation. It provides a level of performance well beyond the normal code requirements with potential for substantial life-cycle cost reduction.

Isolation systems that either found application in modern structures or are at a stage of development that promises application in the future are described in the paragraphs below. They are classified as elastomeric bearing systems, sliding systems, sliding systems with restoring force, and other systems.

2.1 Elastomeric Bearing Systems

Elastomeric bearings provide the simplest method of isolation. Like elastomeric bridge bearings, they are made by bonding sheets of rubber to thin steel plates. The steel reinforcement increases the compressive stiffness of the unit while maintaining the desired low horizontal stiffness. Thirty years of experience with bridge rubber bearings has provided confidence in their longevity and reliability [16].

Damping that is inherent in usual rubber compounds as well as neoprene is rather low for use in aseismic isolation. Research in New Zealand resulted in the development of several energy dissipators that could enhance damping in elastomeric bearing systems [14]. Of these, the lead-rubber bearing is one of the most highly developed systems. This system is used in a 4-story building in New Zealand and about 40 bridges in New Zealand, Italy and the United States. Four more buildings have been constructed or are under construction in Japan [17] and one more has been recently rehabilitated by lead-rubber bearings in the U.S. (Salt Lake City Hall).

A considerable amount of theoretical and experimental research has been carried out on the lead-rubber bearing. Concentrating only on the experimental work, the authors refer to shake table testing of large scale models of building structures and bridges carried out at U.C. Berkeley [18, 19] and a comprehensive series of tests on such bearings in New Zealand [20]. The last series of tests revealed a problem of substantial reduction in energy dissipation with reductions in the load carried by the bearing. The tests also showed a deterioration of damping properties with the number of cycles caused by fracture of the lead plug. Mitigation of these problems was achieved by confining the lead plug by coils or steel washers [21] and by reducing the thickness of individual rubber layers [22].

The rubber used in the bearings of the Foothill Communities Law and Justice Center in California, the first major base-isolated structure in the U.S. [23], has a high degree of inherent damping, making it ideal for aseismic isolation. The shear modulus of this natural rubber compound decreases from a large value at zero strain to about 130 psi at 50% strain. At this strain, the effective damping is about 10% of critical [24]. The high initial stiffness is invoked only in wind load design. At 50% strain, the shear modulus is about the same as that of the usual natural rubber hardness 50 but with twice as much damping. Natural rubber of hardness 50 is used in lead-rubber bearings. Furthermore, the acceptance of this system by officials in California was primarily due to the substantial experimental evidence of good behavior of elastomeric bearing

systems. Almost all of this experimental work has been carried out by Professor Kelly at U.C. Berkeley. This work, in addition to providing unambiguous evidence of the validity of the concept, resulted in the development of a fail-safe system and a method of controlling uplift [25].

Despite the rather low degree of damping that is inherent in usual rubber compounds, conventional reinforced rubber bearings have been used in the earthquake protection of a school building and a three-story radioactive waste storage building in France [26,27]. This system carries the trade name GAPEC, and has been more recently applied to several houses in France. However, mild steel rods have been added for additional damping [28].

Considerable interest in aseismic base isolation by elastomeric bearing systems has developed in Japan [17]. Twenty-three structures have been constructed or are under construction on isolation systems. All but one of these single to ten-story buildings use elastomeric bearings and some additional energy dissipators in the form of steel bars or lead-rubber bearings. One structure is on a sliding isolation system.

The type of unreinforced rubber bearing used in the construction of a school building in Yugoslavia in 1969 has reappeared under the code name SEISMAFLOAT [29]. Tests were performed with a large-scale model structure at Berkeley under simultaneous vertical and horizontal table motion. Some degree of isolation in the vertical direction was evident in these tests. However, the model structure was not excited in the rocking mode and no observations were made as to its performance under these conditions. Analytical studies on the behavior of isolated structures that exhibit vertical and horizontal flexibility showed an increase both in the force imparted to the proper structure and in the displacement when R-wave type of excitation was used (as compared to vertical incidence) [30]. This subject warrants further investigation.

Recently, there has been a substantial amount of research into understanding the behavior of elastomeric bearings. Of particular interest are studies on the effect of reinforcement flexibility on the buckling load [31] and studies on overturning displacements of dowelled bearings [32]. Furthermore, many analytical studies have been performed on the response of systems with torsional and vertical-rocking coupling [33, 34] and on soil-structure interaction of structures on elastomeric bearings [35-38]. Comparison studies of the behavior of isolation systems have also been performed [39].

2.2 Sliding Systems

Spie-Batignolles (SBTP) and Electricite de France (EDF) developed a sliding-elastomeric isolation system for nuclear power plants [40]. This system has been developed to provide protection, regardless of the area seismicity, to standardized power plants designed for a seismic input of 0.2g peak acceleration. The system uses laminated neoprene bridge bearings with lead bronze-stainless steel sliding plates on top of each bearing. In principle, it is identical to the

TFE-elastomeric expansion bearing [41] except for the frictional interface. This interface provides a friction coefficient of 0.2 that is consistent with the 0.2g design of the power plant. A nuclear power plant in South Africa has been built on this system. Another nuclear power plant in Iran was scheduled to be built on the EDF system when construction was halted due to the revolution and the Iran-Iraq war. Two more plants were constructed in France but without the sliding plates. Isolation was provided only by the elastomeric bearing part of the system.

The EDF system is a highly developed and very expensive system. This cost, however, is justified in that it allows a standardized plant to be constructed at any site regardless of its seismicity. It is unlikely that this system will find application in other types of structures.

Theoretical studies on the behavior of purely sliding isolation systems have been numerous [39, 42-45].

2.3 Sliding Systems with Restoring Force

Elastomeric bearing systems provide isolation by the use of steel-rubber units that also support the weight of the structure. Prime consideration in the design of these units is stability under extreme lateral displacement. The properties of elastomeric bearings, stiffness and damping capacity, are affected by variations in the load they carry. Furthermore, these systems are sensitive to the frequency content of the ground excitation.

Isolation systems have been proposed that decouple the functions of carrying the vertical load and of providing the necessary horizontal stiffness. Five such systems have been described, all utilizing Teflon-steel interfaces for carrying the vertical load. These systems are the Earthquake Barrier System [46], Alexisismon [47], TASS [48], R-FBI [49] and Wabo-Fyfe Earthquake Protection System [50].

The Earthquake Barrier System uses woven Teflon-steel interfaces under very high pressure (about 8,000 psi) in an attempt to reduce friction to very low levels. Restoring force and energy absorption capacity are provided by a combination of high friction interfaces and steel beams designed to yield in bending. The Alexisismon uses pot bearings and cylindrical neoprene springs for centering force capability. These springs are allowed to slide at one end in a sleeve while the other end is fixed. The TASS system uses TFE - elastomeric bearings and cylindrical neoprene springs with both ends fixed to metal plates. The R-FBI system utilizes a stack of Teflon coated steel plates with a central core of rubber. The rubber core carries no vertical load and provides the needed horizontal stiffness. A steel rod is embedded in the rubber core for uniform distribution of displacement along the height of the bearing. The Wabo-Fyfe system uses Teflon-disc bearings [51] and a specially designed displacement control device for providing centering force and energy dissipation capability at an adjustable level. The system has been proposed for the protection of bridges.

Theoretical evaluations of sliding systems with restoring force have been too numerous to be referenced. All of these theoretical evaluations have been based on Coulomb's law of friction despite experimental evidence that Teflon-steel interfaces do not obey this law [5, 8, 13].

An implementation of the TASS system has been reported in Reference 17. Information on this structure is provided in Section 3 of this report.

2.4 Other Systems

One system that does not fall in the previous categories uses helical steel springs and viscous dampers and carries the code name GERB [52]. Flexibility and energy absorption capacity may be provided in all directions. The properties claimed for this system are identical to those of the SEISMAFLOAT system. Shake table testing of the GERB system has been conducted in Yugoslavia and there is one known implementation at a diesel power station in Taiwan [52]. Both GERB and SEISMAFLOAT systems appear to be appealing to the nuclear industry [17, 53].

SECTION 3
REVIEW OF DOMESTIC AND FOREIGN PRACTICE ON TEFLON BEARINGS

The design of sliding isolation systems that utilize Teflon-steel interfaces depends largely on our knowledge of the frictional properties of these interfaces. This knowledge is reflected, usually with some delay, in applicable codes and specifications.

New Zealand is the only country which has included a clause in its standards that allows the use of aseismic base isolation (eg. reference 54). Seismic isolation design requirements are under preparation in the U.S. [55] and Japan [17]. The use of sliding isolation systems is specifically allowed in Reference 55. This document provides general design requirements that are applicable to many isolation systems. A formula is presented that attempts to provide an estimate of the lateral displacement at the isolation interface. In this formula, the displacement is related to the damping coefficient in the isolation system. There is particular difficulty in obtaining an equivalent damping coefficient for sliding systems. In such cases, the document recommends the use of time history analyses for determining the design forces and displacements. Time history analyses require the availability of sufficient test data, otherwise major design alterations may be necessary at the completion of tests prior to construction. Of course, base isolation is in its infancy and as experimental data and experience accumulate, standardized design procedures will be developed.

The authors anticipate that design specifications for Teflon bearings in base isolation applications will be largely based on existing specifications on the design of Teflon bearings in bridge applications. Three types of bearings that utilize Teflon and which are commonly used in bridge applications are shown in Figure 3-1. They are the pot, disc and TFE-elastomeric bearings. It should be noted that all three types are utilized in the sliding isolation systems described in Section 2. Of interest in base isolation are those versions of these bearings that allow rotation, longitudinal and transverse motion in the bearing plane.

Pot bearings allow rotation by the elastomeric rotational part that is confined and sealed by a steel piston and a steel base pot. The rotational capability in the disc bearing is provided by a disc of high strength synthetic rubber (adiprene). Motion of the disc is restricted by a shear restriction mechanism. In the TFE-elastomeric bearing, the rotational capability is provided by the supporting plain or steel reinforced elastomeric bearing. This element provides limited lateral flexibility even when the Teflon-steel interface does not slide. The rotational capability is needed in preventing excessive local stresses on the Teflon sliding surface. In all three types of bearings the longitudinal and transverse motion capability is provided by a Teflon-stainless steel interface. The condition of this interface is important as it dictates the transmission of force to the superstructure. Various specifications and codes in the United States and abroad provide guidelines for the selection of materials for this interface and the conditions under which it should operate.

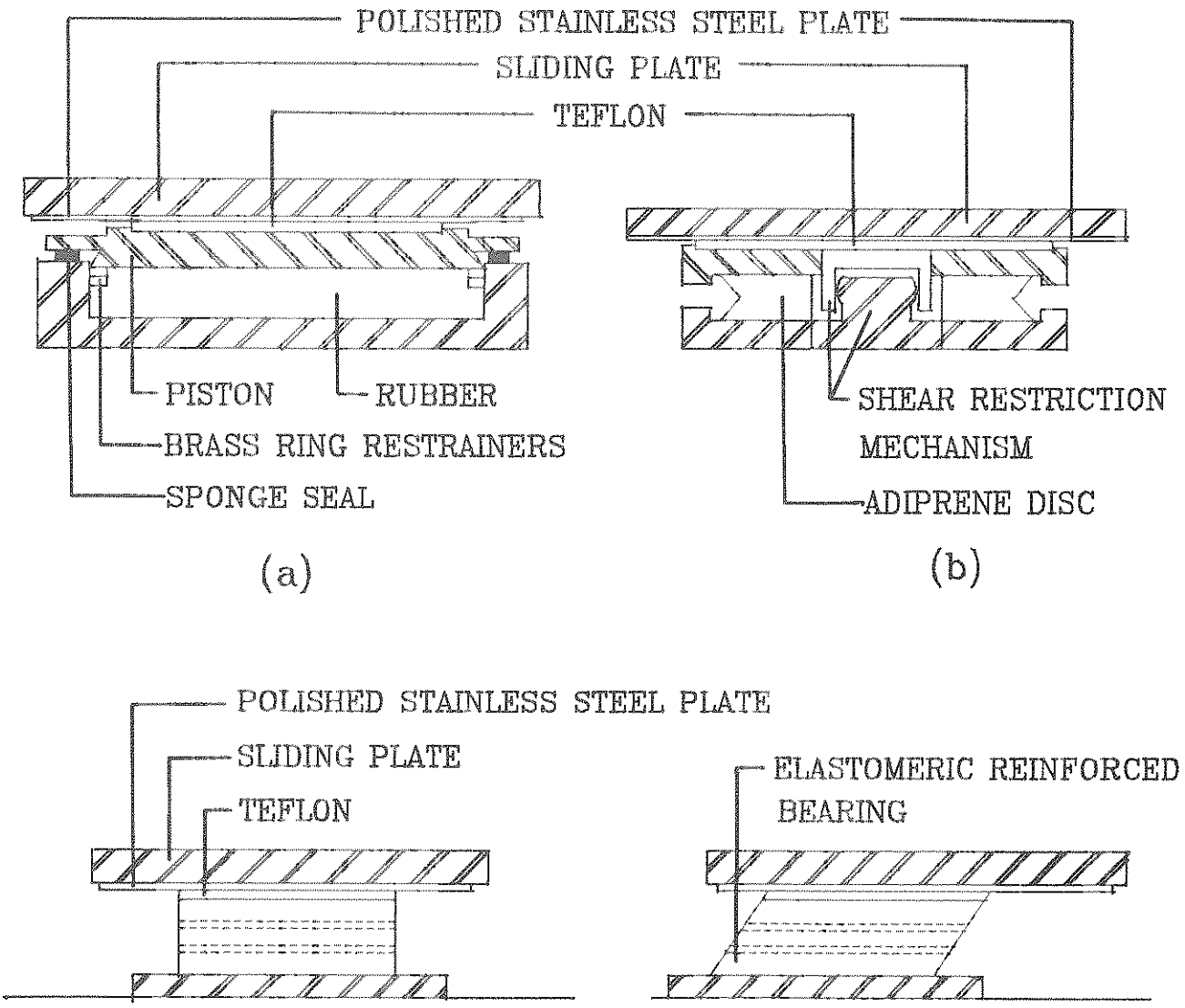

FIGURE 3-1 (a) Pot; (b) Disc; and (c) TFE-Elastomeric Bearings

Specifications for sliding Teflon bearings and specified minimum friction coefficients in bridge applications are summarized in Tables 3-I and 3-II. The specifications reviewed were the AASHTO [1], Standard Specifications of the State of New York [56], California Standard Special Provision [2, 57], Ontario Bridge Design Code [58], Ontario Provincial Standard Specification OPSS 1203 [59], British Standard BS5400 [60] and German DIN 4141, Part 12 [61]. The Ontario Provincial Standard Specification OPSS 1203 does not supersede the Ontario Bridge Design Code but will eventually become part of it when it is revised. The German DIN 4141, Part 12 has not been completed. The information presented in Tables 3-I and 3-II has been extracted from Reference 61. It should be noted that in general, the German procedure for the design of bridge bearings relies on extensive testing of standardized bearings by competent manufacturers and on rigorous quality control checks.

It is apparent in Tables 3-I and 3-II that considerable differences exist between various specifications. In general, the specified type of stainless steel is one of high resistance to corrosion. However, there is substantial variation in the specified roughness of the stainless steel surface. At this point, it is appropriate to briefly discuss specific aspects of surface texture. The subject of surface texture is covered by an ANSI Standard [62]. A comprehensive treatment of surface texture has been presented in Reference 63.

A surface exhibits a combination of three characteristics: roughness, waviness and form error. Roughness represents the irregularities which are inherent in the production process. Waviness is the component of texture upon which roughness is superimposed. Form error is the departure from the intended shape of the surface. The above distinctions are qualitative and are not expressable as a number. In measuring roughness, one has to distinguish between roughness and waviness. This is done by specifying a value of irregularity spacing below which the irregularities represent roughness and above which they become waviness. In practice, this is done by specifying a **cutoff** on the electrical response characteristics of the roughness measuring instrument (electrical filtering). When a cutoff of 0.8 mm is selected, the instrument records only those irregularities having a spacing of 0.8 mm or less. This length is denoted by the symbol B_{max} (termed as meter cutoff or cutoff length). The selection of B_{max} depends on the finishing process and the important characteristics of texture.

The roughness of a surface is assessed from a filtered profile of the surface that is obtained by moving the recording instrument over a certain length. This length is related to B_{max}. The profile is used to obtain a single number that describes roughness. Two well known parameters for assessing roughness are the Arithmetic Average (AA) on Center Line Average (CLA) that is denoted by the symbol R_a and the Root-Mean-Square (RMS) Roughness that is denoted by the symbol R_q.

Table 3-I Specifications for Sliding Teflon Bearings

Specification	Type of Teflon	Type of Stainless Steel	Maximum Surface Roughness μin(μm)	Maximum Bearing Pressure psi (N/mm^2)
AASHTO [1]	Unfilled Filled Woven	ASTM A240 Type 304	20 (0.5) RMS (R_q)	Unfilled Recessed 3500 (24.1) Unfilled not Recessed 2000 (13.8) Filled 3500 (24.1) Woven 3500 (24.1)
Standard Spec. of the State of New York [56]	Unfilled Glass Filled at 15% Carbon Filled at 25% (by weight)	ASTM A167 or ASTM A240, Type 304	Degree No. 8 10 (0.25) RMS (R_q)	Not Specified
California Standard Special Provision [2, 57]	Unfilled	ASTM A240 Type 304	3 (0.076) RMS (R_q) plus Lubrication	Not Specified
Ontario Bridge Design Code [58]	Unfilled and Filled [58]	ASTM A167 Type 304 or Better	10 (0.25) AA or CLA(R_a)	4300 to 6500 (30 to 45)
OPSS 1203 [59]	Unfilled Only with Lubrication [59]			
BS5400 [60]	Unfilled Filled	Grade 316 S16 BS 970, BS1449	6 (0.15) AA or CLA(R_a)	4300 to 6500 (30 to 45)
DIN4141, Part 12 [61]	Unfilled and Possibly Filled	High Quality Pollution Resistant	Unknown. Polishing and Lubrication Required	8700 (60) Under Certain Conditions

Table 3-II Specified Minimum Coefficient of Friction For Teflon Steel-Interfaces in Bridge Applications

Specification	Condition of Interface	Bearing Pressure psi (N/mm^2)		Minimum Coefficient of Friction	
AASHTO [1]	Unfilled or Woven Teflon in contact with stainless steel as specified in Table 1	500 2000 3500	(3.45) (13.8) (24.1)	0.08 0.06 0.04	
	Filled Teflon in contact with stainless steel as specified in Table 1	500 2000 3500	(3.45) (13.8) (24.1)	0.12 0.10 0.08	
Standard Spec. of the State of New York [56]				Measured value shall not exceed 75% of design value	
California Standard Special Provision [2, 57]				Measured breakaway value shall not exceed design value	
Ontario Bridge Design Code [58]	As specified in Table 1	1450 2150 2900 3600 4350 above 4350	(10) (15) (20) (25) (30) (30)	0.06 0.05 0.04 0.03 0.03 0.03 (unfilled)	0.12 0.10 0.08 0.07 0.06 0.06 (filled)
OPSS 1203 [59]	As specified in Table 1 (unfilled with lubrication)	1450 3600 above 3600	(10) (25) (25) interpolation acceptable	0.06 0.03 0.03	
B5 5400 [60]	Unfilled sliding on stainless steel as specified in Table 1 with continuous lubrication	725 1450 2900 4350 above 4350	(5) (10) (20) (30) (30)	0.08 0.06 0.04 0.03 0.03	
	without lubrication and in the absence of test data	725 1450 2900 4350 above 4350	(5) (10) (20) (30) (30)	0.16 0.12 0.08 0.06 0.06	
DIN 4141, Part 12 [61]	Sliding bearings in Germany require product approval by a competent construction authority after extensive testing.				

In both parameters, the quantification of roughness requires the definition of a datum to which measurements are related. This datum is defined as the center line, that is a straight line within the profile such that the sum of the areas enclosed by the profile above the center line equals the sum of those below it. R_a is defined as the arithmetic average value of the departure of the profile from the center line. R_q is the root-mean-square parameter corresponding to R_a. R_a is the most widely used parameter. Conversion of R_a to R_q depends entirely on the shape of the profile. Often the ratio R_a/R_q equal to 1/1.1 is used. This is based on the assumption of sinusoidal profile. In many practical applications, R_a and R_q values are regarded identical. It should be noted that the R_a and R_q values are meaningless unless the meter cutoff (B_{max}) is quoted.

Other roughness parameters which are used in other countries are the maximum peak-to-valley height within one sampling length, R_{ti}, the largest R_{ti} value within the evaluation length (usually five times the sampling length), R_{max} or R_y and the mean value of all R_{ti} values obtained within the evaluation length, R_{tm} or R_z (DIN). All three parameters are obtained from the unfiltered profile of the surface. They are used in Germany and Japan.

The values of roughness listed in Table 3-I vary from 3 to 20μin RMS or AA which is a substantial variation. Only the State of New York specifies how stainless steel should be polished. It specifies a degree of No. 8 that is the most reflective finish that can be produced by common commercial means (mirror finish).

The minimum coefficient of friction specified by various specifications (Table 3-II) also exhibit a substantial variation. Consider, for example, the case of unfilled Teflon sliding against stainless steel without lubrication at a pressure of about 3,500 psi. AASHTO specifies a coefficient of friction of 0.04, the Ontario Code specifies 0.03 and BS5400 specifies 0.07. The differences are substantial when considering that AASHTO specifies a roughness value that is about three times more than that of BS5400. A three-fold increase in roughness may result in a three-fold or more increase in friction [3]. This example illustrates the limitations of our understanding of the behavior of sliding Teflon bearings.

As discussed earlier, all of the theoretical studies on the behavior of sliding isolation systems have used Coulomb's model of friction in which the coefficient of friction was either parametrically varied or selected from available data. Of particular interest are the material specifications and frictional properties of Teflon-steel interfaces in the known application of the TASS system.

The Technology Research Center of Taisei Corporation, Japan, was under construction in June 1988 when one of the authors visited the construction site. The structure is a reinforced concrete four-story building which weighs 2200 tons (see Figure 3-2a). The isolation system consists of eight TFE-elastomeric bearings (Figure 3-2b) and eight Neoprene horizontal springs (Figure

FIGURE 3-2a Technology Research Center of Taisei Corporation Under Construction in June 1988

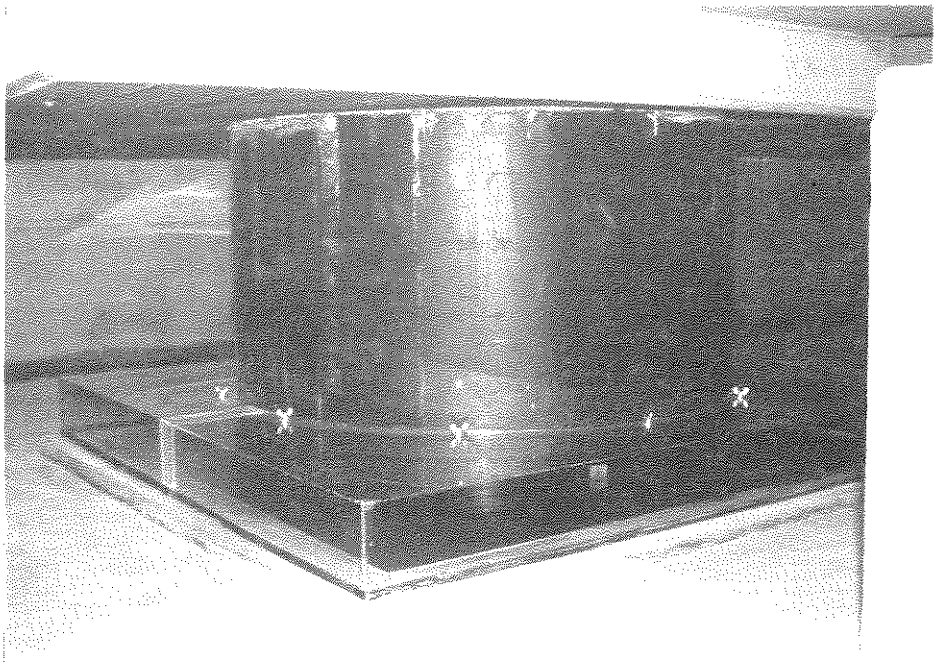

FIGURE 3-2b TFE-Elastomeric Bearing

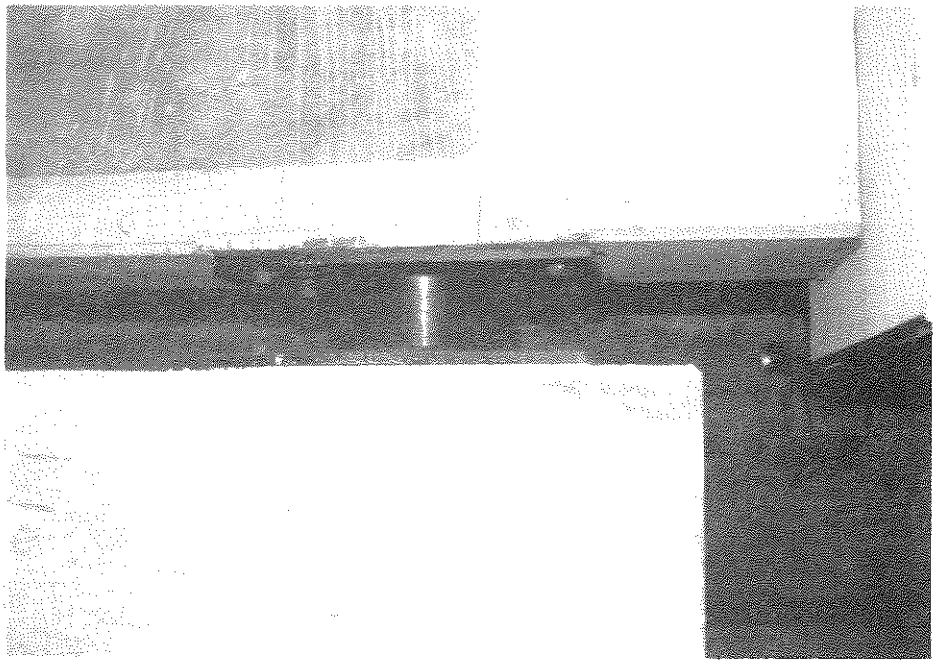

FIGURE 3-2c Neoprene Spring

3-2c). The average pressure on the sliding bearings is about 1000 psi (6.5N/mm^2). This is a low value for Teflon-steel interfaces but normal for the elastomeric part of the bearing that supports the Teflon-steel interface.

Tests on Teflon-steel interfaces were conducted at sliding velocities of 2 to 8 in/sec. The Teflon was filled (unknown composition) and the surface roughness was 2μm in the R_{max} or R_z scale (from personal communication at the site, Reference 17). This corresponds to about 0.05 to 0.5μm in the R_a scale (AA). At about 3,500 psi pressure (25N/mm^2), the recorded coefficient of friction was 0.075 for velocities between 2 and 8 in/sec (this was probably the sliding rather than the breakaway value). The same interface exhibited a friction coefficient of 0.05 at about 7000 psi pressure and about 0.12 at about 1800 psi pressure. These values were recorded at a velocity of 4 in/sec. The results agree quite well with the results for glass filled Teflon at 15% by weight composition. It could not be determined whether Taisei conducted tests at velocities below 2 in/sec. As it will be shown later, the coefficient of friction drops substantially at lower velocities.

SECTION 4
EXPERIMENTAL WORK

This report has demonstrated that a comprehensive set of experimental results on the frictional properties of Teflon-steel interfaces under conditions of interest in base isolation is lacking. In order to obtain information of practical interest, a series of laboratory experiments were designed and conducted. The specific purpose of these experiments was to establish a database of frictional properties of Teflon-steel interfaces for use in the design of base-isolated structures.

4.1 Materials

The materials used in the experiments were as follows:

1. Unfilled and glass filled Teflon at compositions of 15% and 25% by weight. The material was virgin (not reprocessed) and in sheets of 1/8 inch thickness. It was cut into circular shapes of 10 and 5 inches diameter. Both surfaces were smooth (without recesses). One surface was chemically etched for bonding to steel. They were supplied by manufacturers in the Buffalo area.

2. Stainless steel plates of 12 x 26 inches dimensions and 0.063 inch thickness. The stainless steel conforms to ASTM A-240, type 304 requirements. It was commercially polished to a No. 8 degree. The direction of predominant surface pattern (surface lay) was either parallel or perpendicular to the long dimension of each plate. Surface roughness measurements were obtained with a Surtronic 3P instrument with the cutoff length B_{max} set at 0.8 mm and the traverse length set at 4.5 mm. Several measurements were obtained which systematically gave an R_a value of 0.03μm in the parallel to lay direction and 0.04μm in the perpendicular to lay direction. The stylus tip radius of the instrument was 5μm which may have resulted in an underestimation of the R_a value by about 50% [63]. The use of a 2.5μm radius stylus could have resulted in an underestimation by about 25%. As such, the actual R_a value in both directions is less or equal to 0.07μm. It satisfies the requirements of all specifications listed in Table 3-I.

3. Adhesive material consisting of a two-part formulated epoxy resin. It was supplied by the Teflon manufacturer.

4.2 Testing Apparatus

The testing apparatus is schematically shown in Figure 4-1. A central steel plate of 1/2 inch thickness is faced with stainless steel plates and sandwiched between two Teflon sheets of 10

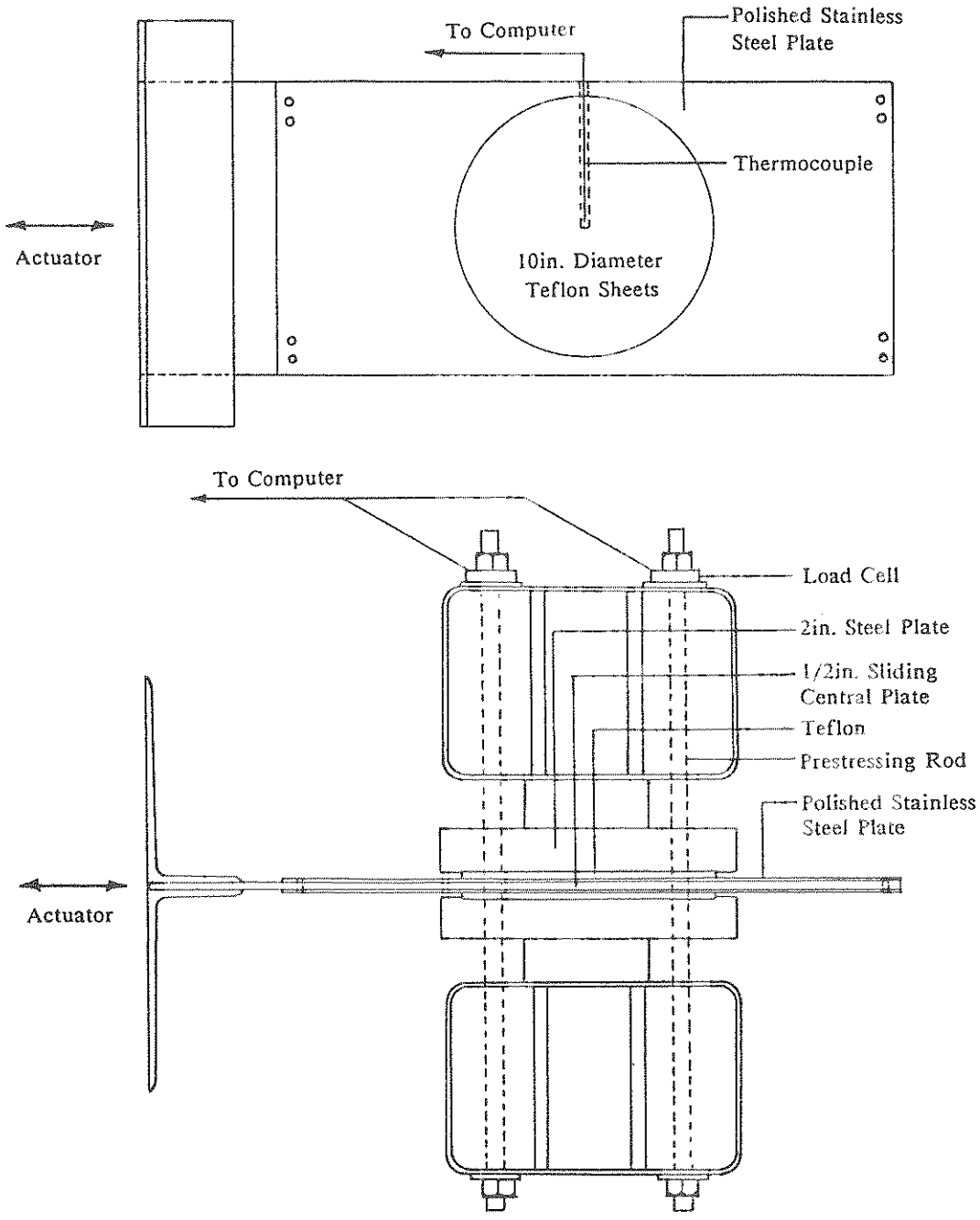

FIGURE 4-1 Testing Arrangement

inch diameter. The Teflon sheets are recessed into a 1/16 inch recess in two heavy 2 inch thick steel plates. The Teflon-steel interface is surrounded by a massive arrangement that prevents any rigid body motion of the two heavy steel plates. The arrangement is compressed by either 4 or 6 prestressing rods. The force in the rods is measured by load cells. This force can safely reach values of more than 60 kips in each rod. The arrangement is attached to the floor and a reaction concrete block while the steel central plate is attached to a 110 kip MTS actuator.

The various parts of the testing apparatus are illustrated in Figure 4-2. Figure 4-2a shows the central steel plate which is faced with polished stainless steel. The degree of finish is evident in the high reflectivity of the plate. Figure 4-2b shows one of the two heavy steel plates with a 10 inch diameter Teflon sheet bonded in the 1/16 inch recess of the plate. The two heavy plates are shown in Figure 4-2c surrounding the steel central plate. The motion restrainers of the heavy plate are visible. Figure 4-2d shows two reinforced heavy tubes that transfer the normal load to the Teflon-steel interface and the prestressing rods for developing the normal force. Figure 4-2e shows the washer load cells for measuring the force in each prestressing rod.

The instrumentation consists of 4 or 6 washer load cells for measuring the force in each prestressing rod, the LVDT and load cell of the actuator, an accelerometer to measure the acceleration of the central steel plate and a thermocouple that was embedded in the central steel plate. It is located 0.063 inch below the interface which allows for reliable measurement of the temperature of the Teflon-steel interface.

An alternative version of the apparatus was used to test 5 inch diameter specimens at very high pressures. The 5 inch diameter specimens were recessed in two steel plates of 10 inch diameter which in turn were placed in the 10 inch diameter recesses of the two heavy steel plates.

A particular characteristic of the test apparatus is the way by which the normal force is developed. Normal force may be maintained for prolonged periods of time which is very important in evaluating any adhesion of the interfaces that may develop over time. At the conclusion of the tests reported herein in May 1988, the arrangement has been prestressed at 160 kips normal force and stored. It will be tested after several months to determine the effect of adhesion on the breakaway coefficient of friction.

4.3 Specimen Preparation and Test Method

The stainless steel plate was attached to its backing plate by bolts at the two ends and along the short dimension of the plate. Initially, the stainless steel plate was bonded and bolted to its backing plate. However, replacing the plate became a problem and bonding was discontinued. In practical applications, the plate is attached by continuous welding.

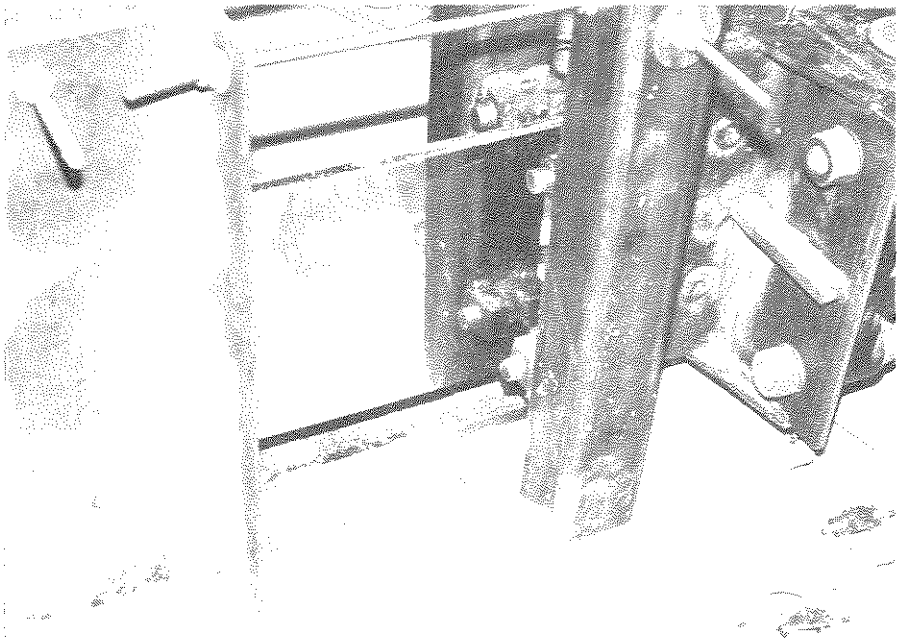

FIGURE 4-2a Central Plate Faced With Polished Stainless Steel

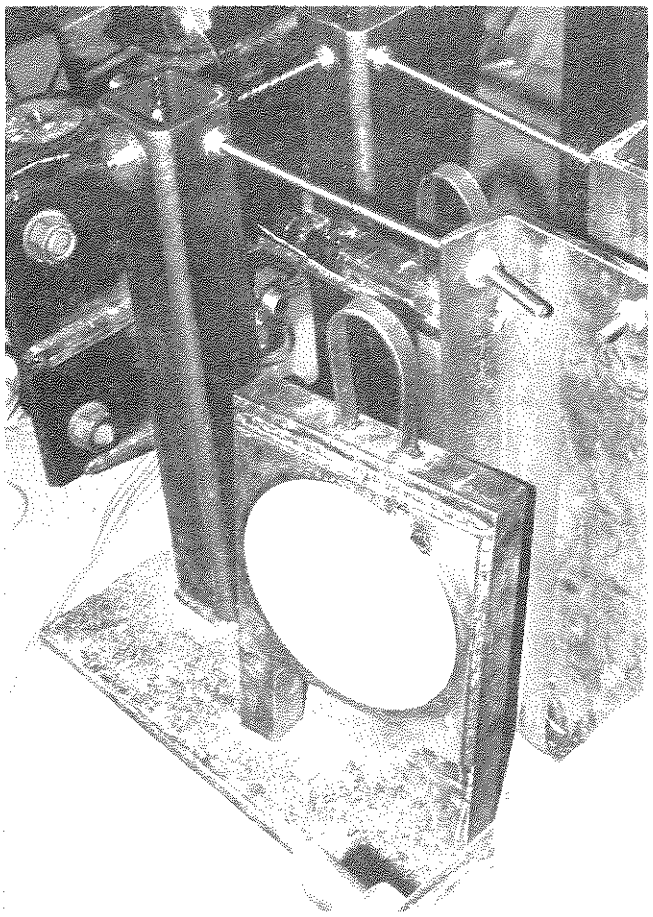

FIGURE 4-2b Teflon Sheet Bonded to Steel Plate

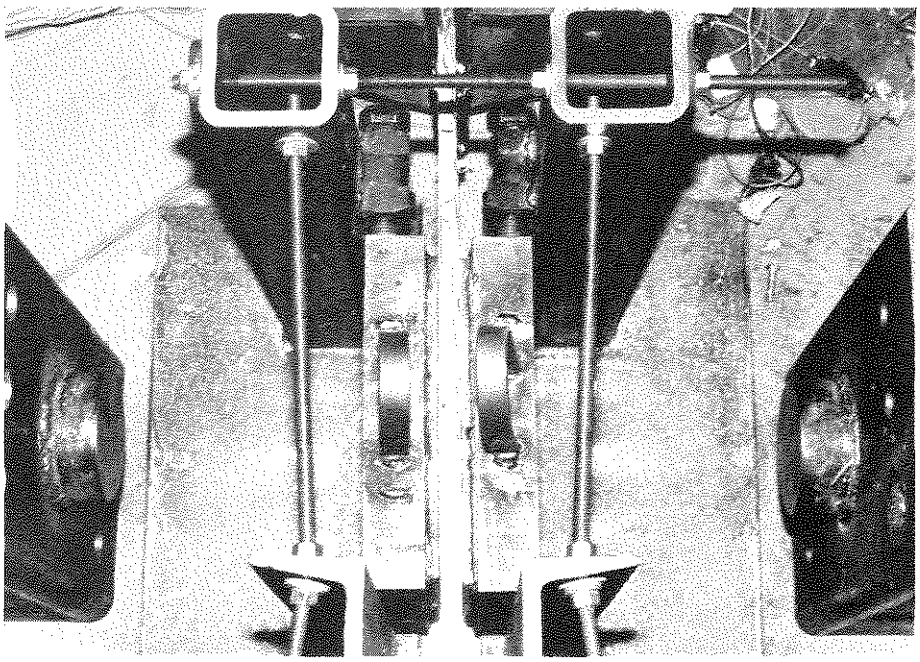

FIGURE 4-2c Teflon-Steel Sandwich

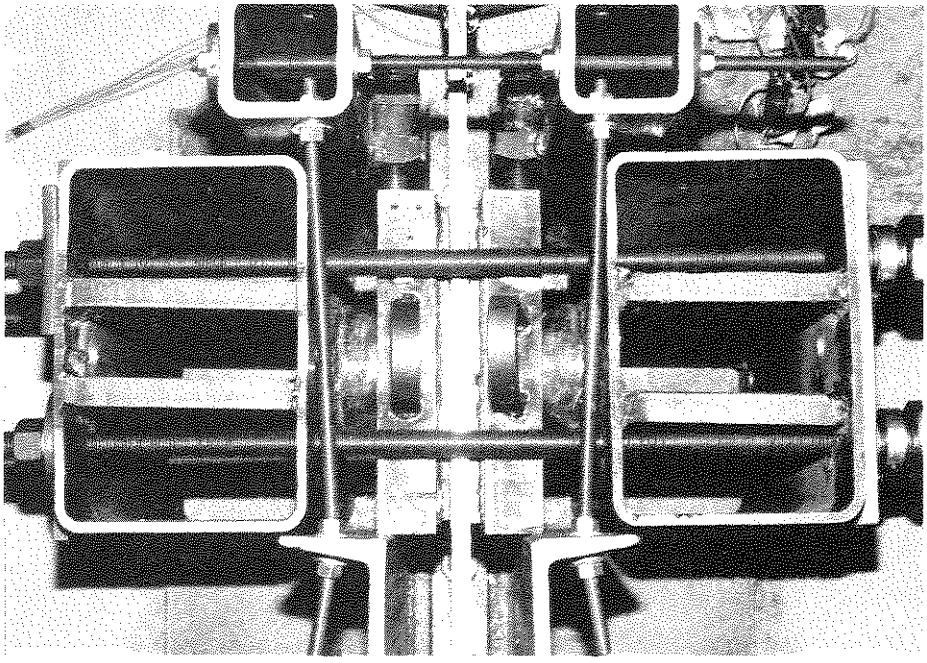

FIGURE 4-2d Complete Arrangement

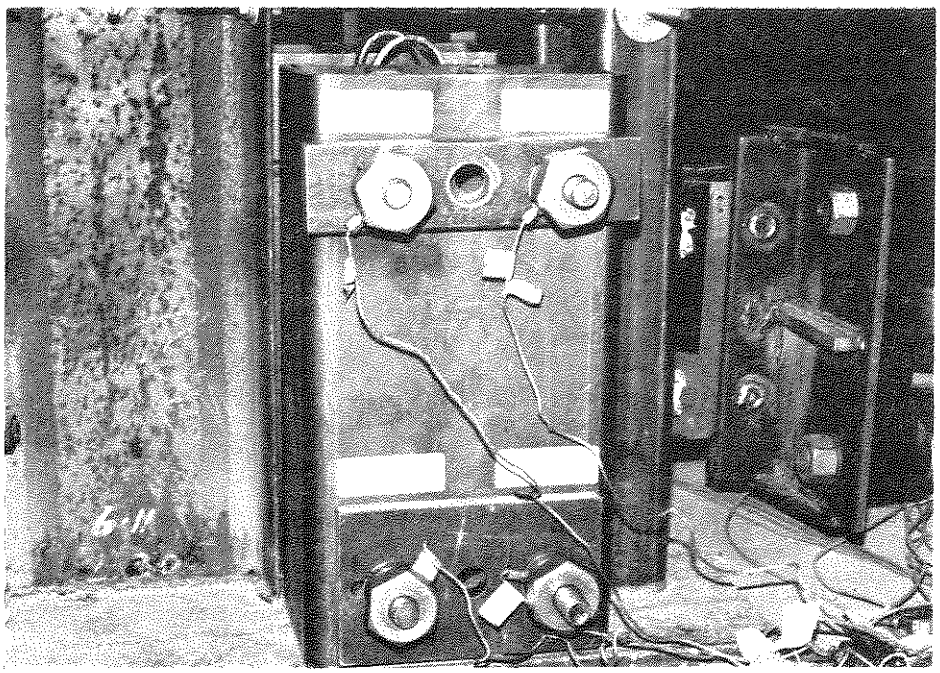

FIGURE 4-2e Washer Load Cells

Bonding of the Teflon sheets within the recesses of the backing heavy steel plate was performed according to the following procedure. The steel plates were thoroughly cleaned, degreased and dried. The epoxy adhesive was prepared and uniformly applied with a spatula on the steel surface. The Teflon sheets were attached to the two steel plates and the whole arrangement was compressed by a hydraulic machine as shown in Figure 4-3, under the test normal load and for about 14 hours (overnight). This resulted in a smooth surface without bubbles.

A set of about 8 tests was conducted each day, all at the same normal load. The Teflon sheets were then removed and fresh ones were attached and compressed overnight. This cycle was continued with only a few interruptions. In these interruptions, the interface was allowed to relax unloaded for about 24 hours before resuming testing.

The tests were conducted according to the following procedure. Motion of the central steel plate was imposed by the actuator and recordings of the force needed to initiate and maintain this motion were made. This is the frictional force from two identical Teflon-steel interfaces. In most of the tests, the motion was sinusoidal with specified amplitude and frequency that resulted in peak velocities of sliding between 0.1 and about 20 in/sec. Furthermore, a number of tests were conducted with constant velocity type of motion (sawtooth displacement). The two types of experiments resulted almost identical results for the same peak velocity of sliding.

There was significant transfer of Teflon flakes to the stainless steel plates as evident in Figure 4-4. The formulation of debris along the sliding path is apparent. Teflon flakes could also be seen on the Teflon sheets. Figure 4-5 shows an unfilled Teflon sheet after testing at 6,500 psi pressure and sinusoidal motion of peak velocity of 19.9 in/sec (test #160). The picture shows the formation of wear debris at the perimeter (top right side). This rather considerable wear was observed after 80 inches of travel at the very high pressure of 6,500 psi. The formation of a thin Teflon film on the stainless steel plate resulted in substantial reduction of the frictional force transmitted through the interface (equivalent to running-in the interface). Furthermore, it was observed that in the case of glass-filled Teflon, very fine steel particles were transferred from the stainless steel plate to the Teflon surface. This resulted in a very smooth, like polished, surface. At the conclusion of each test, the stainless steel plate and Teflon sheet were cleaned to maintain their original condition. The surface of glass-filled Teflon was refinished with a sharp instrument. Furthermore, sufficient time was allowed between experiments for thorough cooling.

Two important observations were made that have significant influence on the recorded frictional force: (a) The frictional force recorded at low sliding velocity following a high velocity test was higher than the original value recorded on a fresh interface, and (b) the frictional force recorded at low bearing pressure following a test at high pressure was higher than the original value.

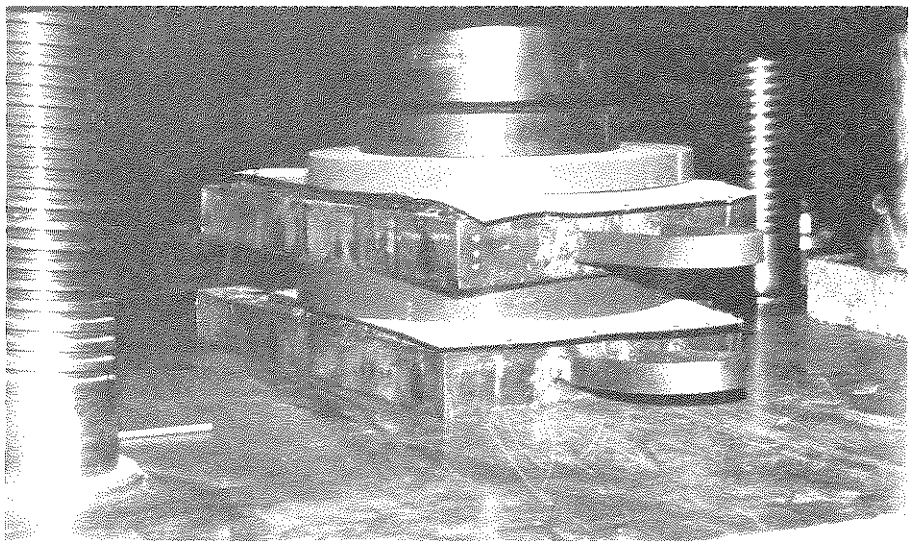

FIGURE 4-3 Teflon Sheets and Backing Plates in Hydraulic Press

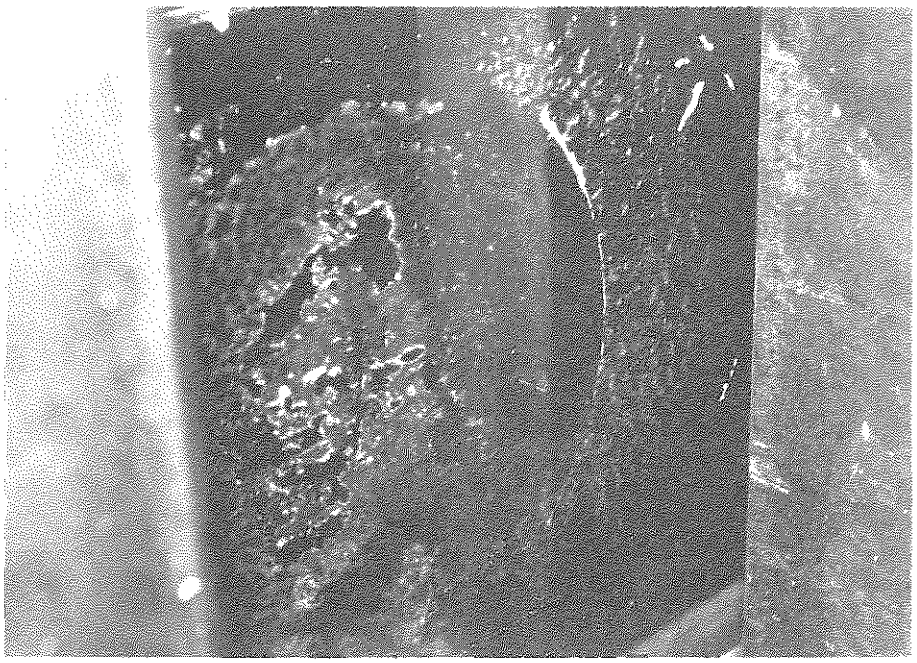

FIGURE 4-4 Teflon Flakes on Slider After a High Velocity Test

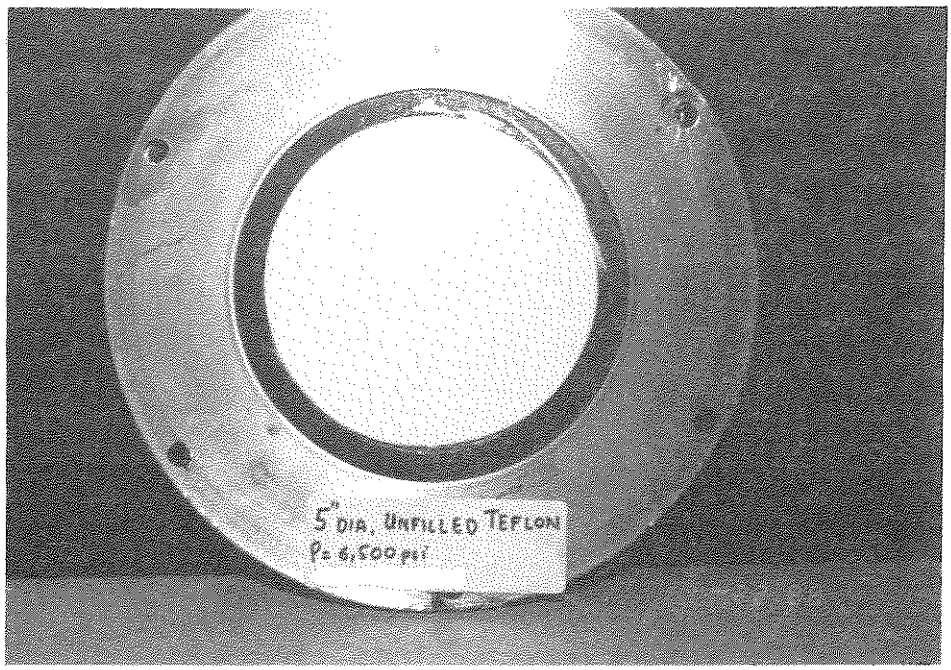

FIGURE 4-5 **Formation of Wear Debris in High Pressure, High Velocity Test. Observe Debris at Upper Right Corner**

An explanation for the first observation which probably applies for both cases was given by Flom and Porile [7]. Frictional heating of the interface may cause degradation of Teflon. Another explanation may be the possibility of orientation of Teflon which may have an effect on its strength properties and surface energy.

Based on these observations, it was decided to use fresh Teflon for each set of tests. These tests were conducted at the same pressure and in increasing order of peak sliding velocity.

4.4 Identification of Experiments

The following notation is used to identify the various conditions of testing:

UF	Unfilled Teflon
15GF	Glass filled Teflon at 15% composition by weight
25GF	Glass filled Teflon at 25% composition by weight
SIN	Sinusoidal test
CV	Constant velocity test
CVR	Constant velocity test with initial build-up
P	Sliding parallel to lay
T	Sliding perpendicular to lay

For example, the designation

UF 80: 2000 PSI: SIN: 0.32HZ: 2": P

identifies the No. 80 test which was conducted on unfilled Teflon at 2,000 psi pressure. Motion was sinusoidal of 2 inch amplitude and 0.32 Hz frequency and in the direction parallel to the lay.

4.5 Results

Tests were conducted at pressures of 1,000, 2,000, 3,000 and 6,500 psi (6.9, 13.8, 20.7, 44.9 N/mm^2) and peak sliding velocity of 0.1 to about 20 in/sec. The direction of sliding was either parallel or perpendicular to the lay. The tests on glass filled Teflon were conducted only with the direction of sliding parallel to the lay. The tests at 1,000, 2,000 and 3,000 psi pressure were conducted with 10 inch diameter specimens while the tests at 6,500 psi pressure were conducted with 5 inch diameter specimens.

Representative frictional force-displacement loops are shown in Figure 4-6 (force from two interfaces). Both tests (No. 80 and 81) were conducted on unfilled Teflon, at 2,000 psi pressure and 2 inch amplitude. The first is a sinusoidal test while the second is a constant velocity test. Different frequencies were used in order to achieve the same peak velocity of 4 in/sec. It is

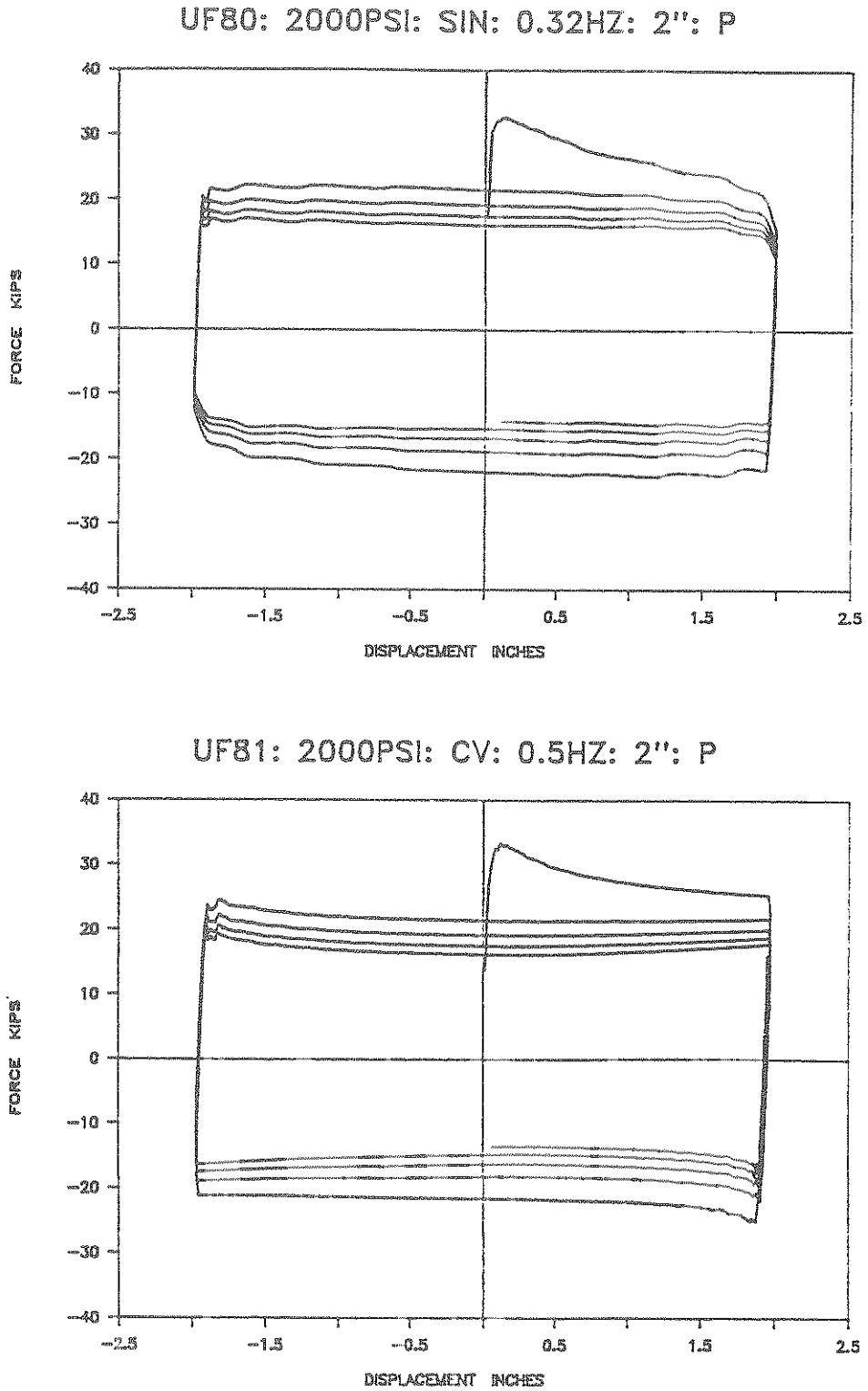

FIGURE 4-6 Frictional Force - Displacement Loop in Sinusoidal and Constant Velocity Tests Conducted at Same Peak Velocity

apparent that the two loops are almost identical. Figure 4-7 shows the input displacement histories in the two tests. Figure 4-8 shows the time histories of the interface temperature and of the total normal force (sum of forces in the four prestressing rods) in test No. 81. The temperature, as in all tests, increases almost linearly with time. The normal force remains practically constant.

The recorded frictional force was used to extract various frictional characteristics of interest. These are defined with reference to Figure 4-9. The frictional force at initiation of sliding upon division by the normal force results in the **coefficient of breakaway friction**, μ_B. This value of the coefficient of friction is also known as static friction. The value of the coefficient of friction at reversal (during reversal of motion a temporary sticking of the interface occurs) is given the symbol μ_R. The value of the coefficient of friction at peak velocity is the **sliding coefficient of friction**, μ_S, which corresponds to this velocity. It is also known as kinetic friction. Subscripts of 1, 3 and 5 are assigned to μ_S, which indicate the cycle at which the coefficient corresponds. There is a continuous drop of the value of sliding (or kinetic) coefficient of friction with increasing number of cycles. Of importance to practical applications are the breakaway and maximum sliding coefficients of friction. The latter usually occurs at the first cycle.

The results are summarized in Table 4-I. This table presents information on the type and conditions of test, materials used, the recorded values of μ_B, μ_{s1}, μ_{s3}, μ_{s5}, and maximum values of μ_R and μ_s. Furthermore, the temperature at the start and end of each test are given. It should be noted that the increase of temperature with time was essentially linear.

The tests are identified by numbers 51 to 213. Frictional force-displacement loops and frictional force histories of these tests are presented in Appendix A. Tests 51 to 60 were preliminary tests that were conducted on improperly bonded Teflon sheets. In this set of tests, the adhesive was not uniformly applied. Rather, it was applied in spots that resulted in uneven distribution of pressure and wear. The average pressure in these tests (normal force divided by true area of contact) was about 1,200 psi. These tests were carried out in order to determine the effect of the acceleration of sliding on the recorded values of friction. In this respect, the tests were useful, however, they were disregarded in the calibration of mathematical models that were developed.

A certain number of comments are included in Table 4-I which warrant further discussion:

1. The actuator in a number of tests at high velocity did not respond to command (unstable operation). In some cases, the problem was significant enough such that certain data had to be disregarded (see Table 4-I).

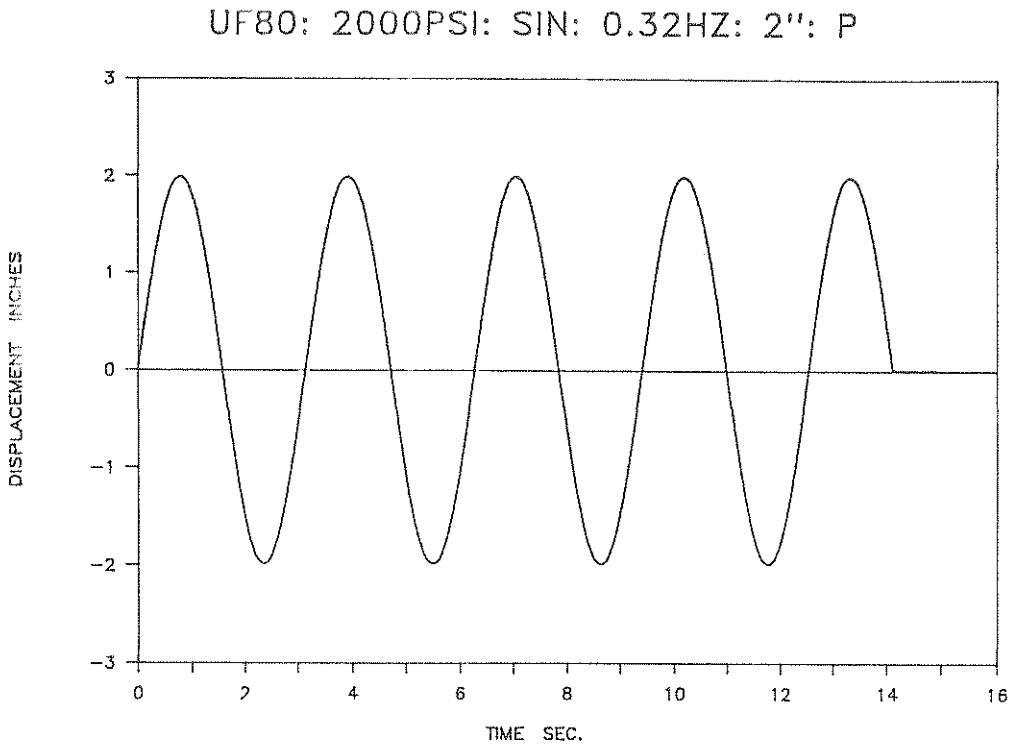

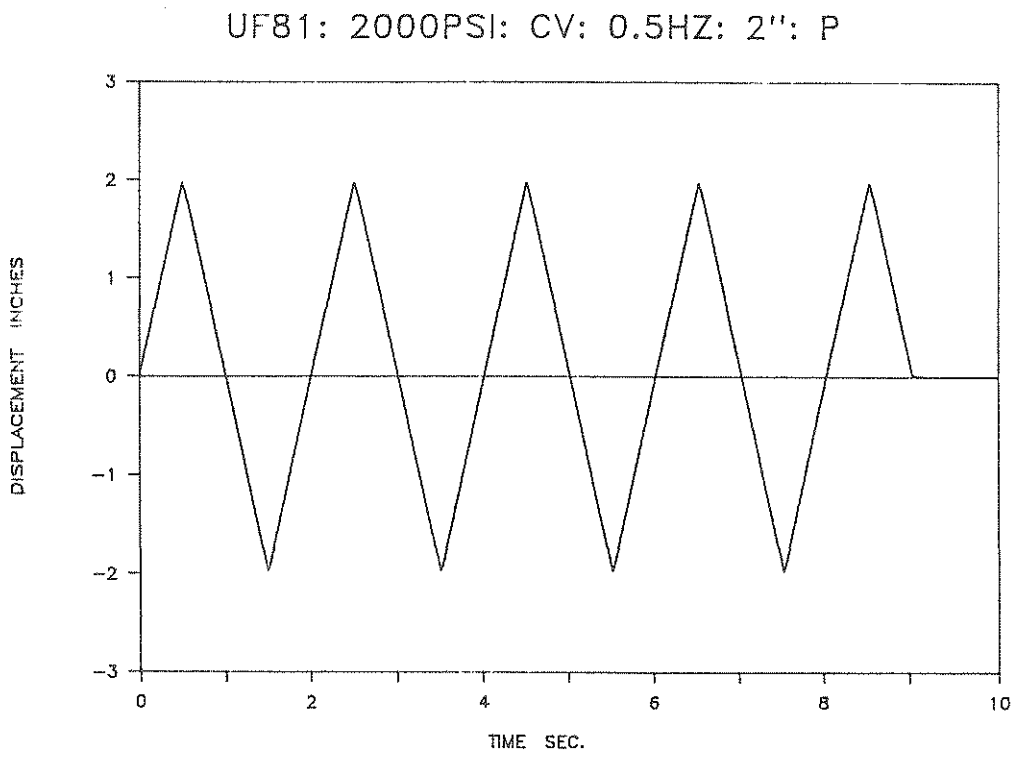

FIGURE 4-7 Input Displacement Histories in Tests No. 80 and 81 (Fig. 4-6)

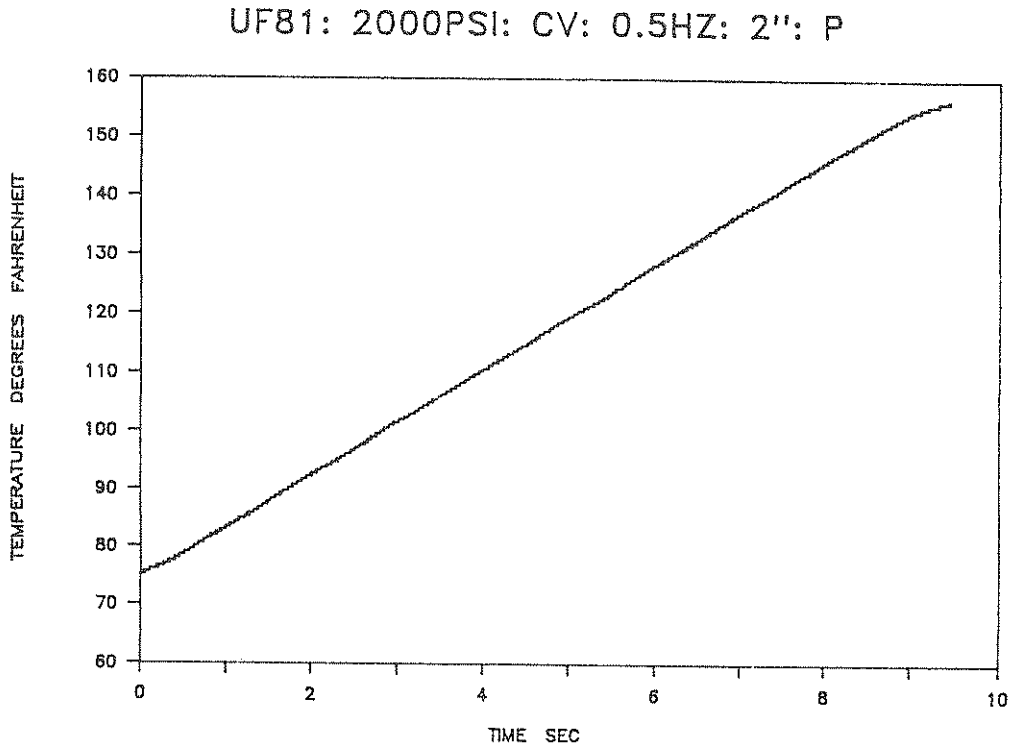

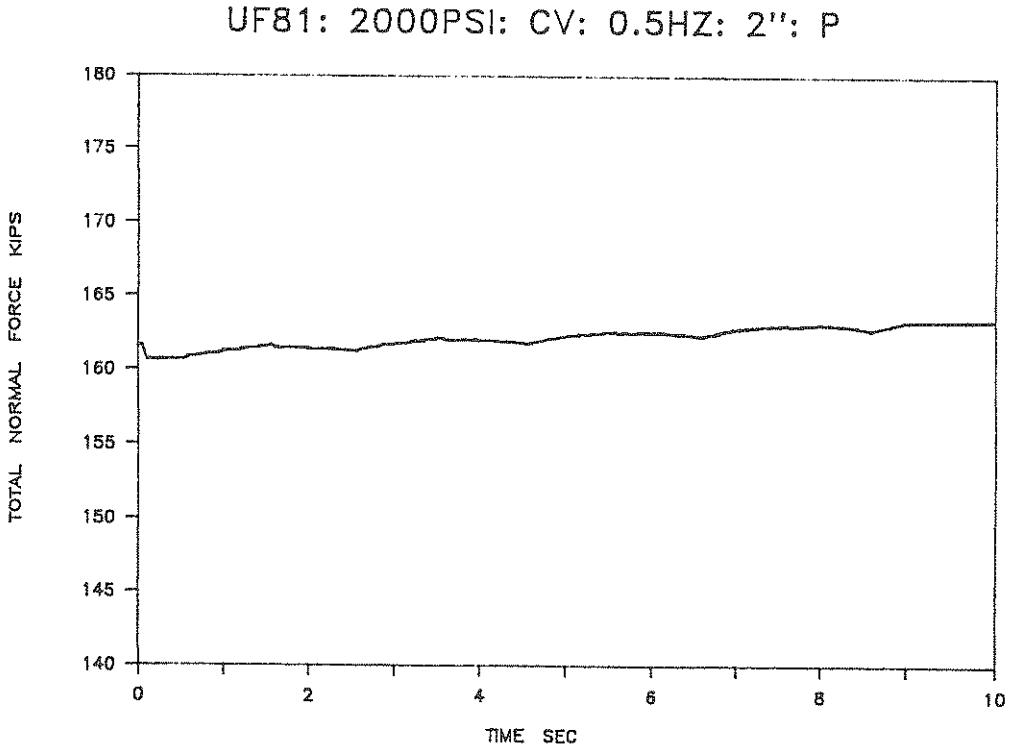

FIGURE 4-8 Recorded Histories of Temperature and Total Normal Force in Test No. 81

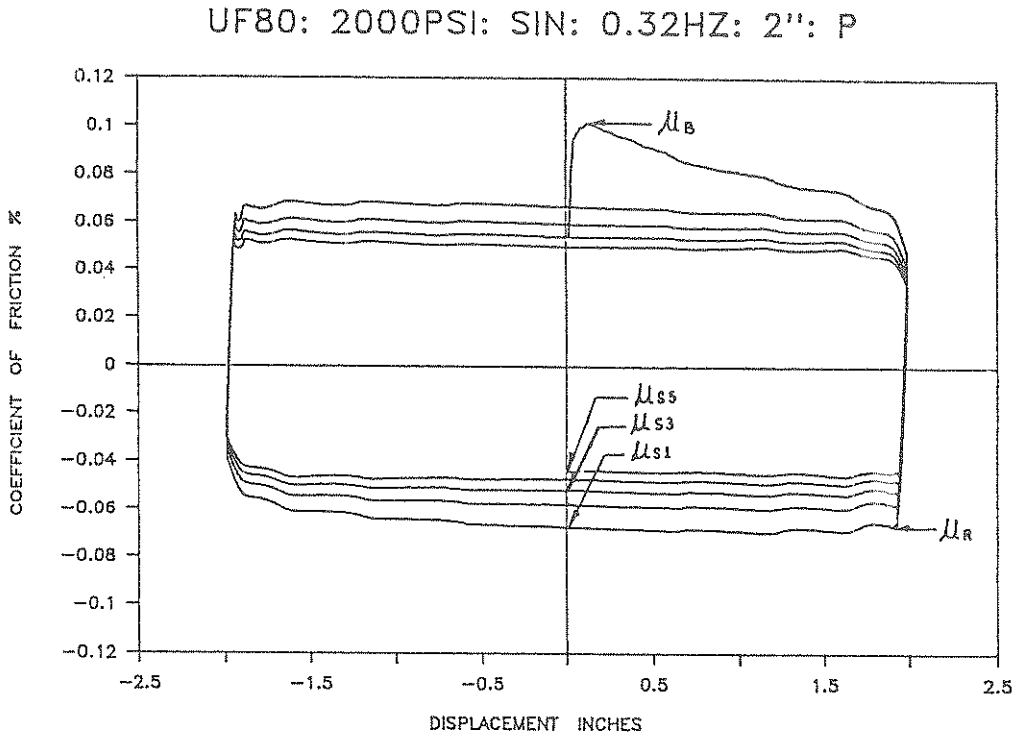

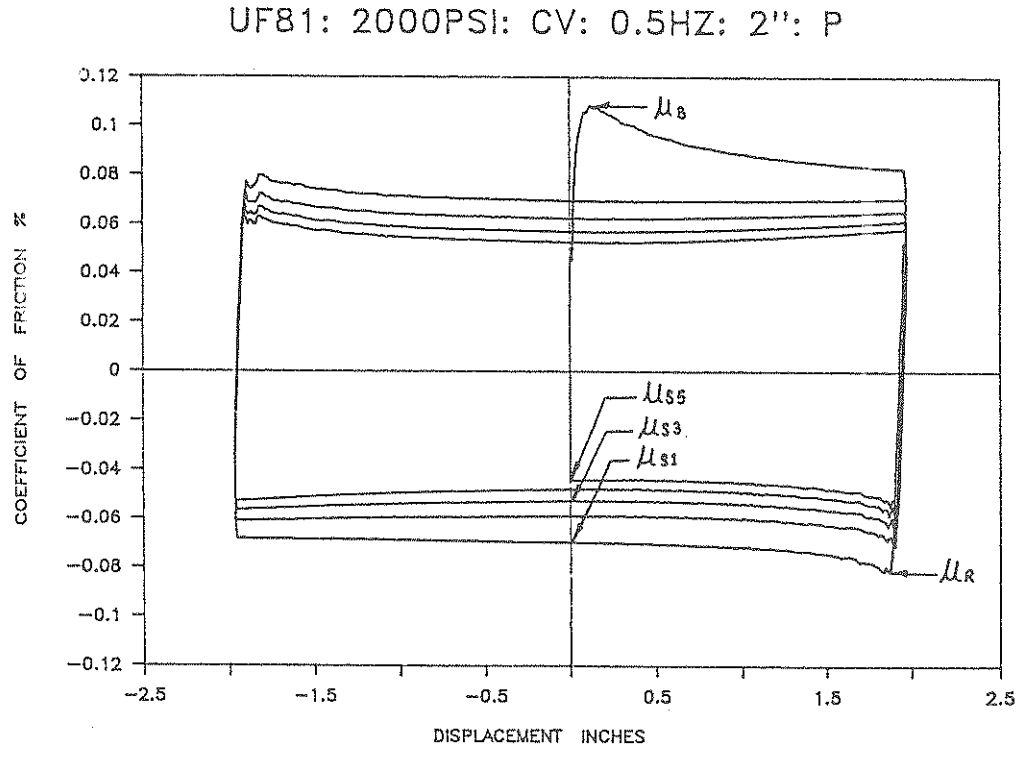

FIGURE 4-9 Definition of Breakaway, Sliding and Reversal Friction

2. In test No. 90, the interface was not cleaned prior to testing, which resulted in very low breakaway friction.

3. In two cases, the actuator moved sideways (tests No. 75 and 96). It was regarded as a minor problem and no data were disregarded. The problem was corrected by fixing the actuator to the floor.

4. In a number of tests, a phenomenon known as stick-slip was observed (tests No. 60, 159, 169, 179, 180, 188, 189 and 198). The recorded frictional force showed a short duration increase that was followed by a rapid fall. It is caused by momentary sticking of the interfaces. This behavior was significant only in high frequency tests (above 1Hz) except in tests No. 159, 169 and 179 which were conducted on 5 inch diameter specimens at 3,000 psi pressure and 0.5 Hz frequency. The possibility of resonance vibration of the oil column in the actuator was eliminated as only the load cell and not the LVDT of the actuator recorded fluctuations. Stick-slip is a quite unpredictable phenomenon.

5. In almost all tests, the recorded frictional force was decreasing with increasing number of cycles which is due to transfer of Teflon to the stainless steel plate. The opposite phenomenon was observed in some tests on glass-filled Teflon. This is attributed to insufficient cleaning of the Teflon surface, which was not restored to its original condition. This is actually an important observation which indicates that by running-in a glass filled Teflon-steel interface (or by polishing the Teflon surface) the breakaway friction may be substantially reduced. It should be noted that the recorded values of friction were of Teflon always restored to its original condition. As such, the presented values of friction must be regarded as high or upper bound values.

6. Recordings of the acceleration of sliding of the central plate were made only for tests No. 51 to 60. The value of amplitude presented in Table 4-I is the one recorded by the LVDT of the actuator. Independent recordings with a sonic displacement transducer were made in preliminary tests. They were identical to that of the LVDT. The value of peak velocity shown in Table 4-I was computed from the recorded amplitude and frequency.

Table 4-I Summary of Experimental Results

Test No.	Date	Time		Test Type	Teflon		Sliding Direction	No. Cycles	Duration (sec)	Total Travel (in)	Comments
		Setup	Start		Type	Diam. (in)					
51	3/3			CV	UF	10	T	5	10	38	Pressure in tests 51 to 60 was approximately 1200 psi
52	3/3			CV	UF	10	T	5	5	18.8	
53	3/3			CV	UF	10	T	5	20	77	
54	3/4			CV	UF	10	T	5	10	76.3	
55	3/4			CVR	UF	10	T	7	15	109	See Appendix for Motion History
56	3/7			S	UF	10	T	5	15	78	
57	3/7			S	UF	10	T	5	12	60	
58	3/7			S	UF	10	T	5	8	40	
59	3/8			CV	UF	10	T	5	10	76.5	
60	3/8			CV	UF	10	T	5	5	37.8	Stick-slip observed

Table 4-I Summary of Experimental Results (Continued)

Test No.	Frequency (Hz)	Amplitude (in)	Peak Velocity (in/s)	μ_B (%)	$\dot{\mu}_R$ max (%)	μ_{S1} (%)	μ_{S3} (%)	μ_{S5} (%)	$\dot{\mu}_S$ max (%)	Temperature Start (°F)	Temperature End (°F)	Recorded Peak Acceleration (g)
51	0.5	1.9	3.8	11.76	10.43/1	11.32	8.98	8.07	11.32/1	68	133	0.34
52	1	0.94	3.76	12.15	11.75/1	12.35	10.34	9.52	12.35/1	69	104	0.30
53	0.25	3.85	3.85	14.20	10.60/1	12.51	8.40	7.10	12.51/1	65	164	0.32
54	0.5	3.81	7.63	10.18	10.18/1	10.18	10.17	9.05	10.18/1	69	167	0.83
55	0.5	3.89	7.78	11.88	10.51/1	----	----	----	10.16/1	69	240	0.81
56	0.32	3.99	7.97	16.25	10.46/1	12.48	10.13	9.20	12.48/1	66	188	0.08
57	0.42	2.99	7.95	14.80	10.77/1	12.10	9.74	8.43	12.10/1	68	170	0.12
58	0.64	1.99	7.96	14.50	10.32/1	12.22	10.79	9.69	12.22/1	71	137	0.19
59	0.5	3.82	7.65	14.38	13.00/1	11.95	9.70	8.37	11.95/1	67	172	0.84
60	1	1.89	7.57	12.83	8.01/1	7.46	7.94	8.06	8.06/5	70	115	0.85

* Index figure is cycle at which maximum was recorded

Table 4-I Summary of Experimental Results (Continued)

Test No.	Date	Time Setup	Time Start	Test Type	Teflon Type	Teflon Diam. (in)	Sliding Direction	No. Cycles	Duration (sec)	Total Travel (in)	Comments
61	3/23	1.20	1.38	SIN	UF	10	P	1	32	2	New S.S. Plate-Fresh TFE
62	3/23	2.05	2.35	SIN	UF	10	P	4	25	16	
63	3/23	2.40	2.50	SIN	UF	10	P	5	16	20	
64	3/23	2.55	3.00	SIN	UF	10	P	5	16	39.6	
65	3/23	3.15	3.30	CV	UF	10	P	5	10	38.2	
66	3/24	3.05	3.10	SIN	UF	10	P	5	16	39.6	Interface relaxed for 24 hrs
67	3/24	3.50	4.00	SIN	UF	10	P	5	16	39.6	
68	3/25	9.20	9.35	SIN	UF	10	P	5	10	35.5	Interface relaxed for 17 hrs
69	3/25	10.07	10.30	SIN	UF	10	P	1	32	2	Test following a higher velocity test
70	3/25	10.50	11.05	SIN	UF	10	P	4	25	16	Test following a higher velocity test
71	3/25	11.30	11.50	SIN	UF	10	P				Data lost
72	3/25	12.50	1.07	SIN	UF	10	P	5	10	39.4	
73	3/25	1.20	1.30	SIN	UF	10	P	5	10	39.2	
74	3/25	1.55	2.09	SIN	UF	10	P	5	8.5	41.4	
75	3/25	2.25	2.29	SIN	UF	10	P	5	8.5	49.1	Actuator moved sidesway
76	3/25	3.05	3.13	SIN	UF	10	P	5	6.5	98.8	Unstable operation
77	3/28	8.40	8.50	SIN	UF	10	P	1	32	2	Fresh TFE
78	3/28	9.38	9.45	SIN	UF	10	P	4	25	12.4	

Table 4-I Summary of Experimental Results (Continued)

Test No.	Frequency (Hz)	Amplitude (in)	Peak Velocity (in/s)	μ_B (%)	$\dot{\mu}_R$ max (%)	μ_{S1} (%)	μ_{S3} (%)	μ_{S5} (%)	$\dot{\mu}_S$ max (%)	Temperature Start (°F)	Temperature End (°F)	Pressure (psi)
61	0.03	0.5	0.1	5.90	2.78/1	2.66	-	-	2.66/1	68	69	1000
62	0.16	1	1	9.75	5.08/3	6.60	7.02	-	6.95/3	68	82	1000
63	0.32	1	2	12.35	8.78/1	10.50	9.55	8.90	10.5/1	68	107	1000
64	0.32	1.98	3.96	16.67	11.17/1	12.10	10	8.72	12.10/1	71	143	1000
65	0.5	1.91	3.82	18.86	13.77/1	12.55	10	8.74	12.55/1	73	154	1000
66	0.32	1.98	3.96	14.03	9.82/1	10.67	8.73	7.64	10.67/1	68	134	1000
67	0.32	1.98	3.96	13.50	9.59/1	9.85	7.77	6.52	9.85/1	70	156	2000
68	0.32	1.97	3.94	10.65	7.74/1	7.90	6.20	5.21	7.90/1	72	164	3000
69	0.03	0.5	0.1	11.25	3.99/1	3.94	-	-	3.94/1	69	71	1000
70	0.16	1	1	11.14	6.23/4	6.74	7.61	-	7.59/4	69	86	1000
71	0.5	2										
72	0.5	1.97	6.19	15.06	11.43/1	11.90	10	9.27	11.90/1	72	127	1000
73	0.5	2.97	9.35	16.35	11.54/1	11.74	9.53	-	11.74/1	79	149	1000
74	0.6	3	11.30	17.60	12.0/1	11.82	9.88	-	11.82/1	82	145	1000
75	0.6	3.96	15.08	17.75	12.26/1	11.93	10.10	-	11.93/1	84	172	1000
76	0.8	4.94	25.13	19.51	12.15/1	11.59	9.30	8.41	11.59/1	85	152	1000
77	0.03	0.5	0.1	4.09	1.91/1	1.75	-	-	1.75/1	69	71	2000
78	0.16	1	1	7.33	6.25/1	6.07	5.50	-	6.07/1	70	84	2000

* Index figure is cycle at which maximum was recorded

Table 4-I Summary of Experimental Results (Continued)

Test No.	Date	Time Setup	Time Start	Test Type	Teflon Type	Teflon Diam. (in)	Sliding Direction	No. Cycles	Duration (sec)	Total Travel (in)	Comments
79	3/28	11.06	11.20	SIN	UF	10	P	5	16	14	
80	3/29	1.50	2.10	SIN	UF	10	P	5	16	36	Interface relaxed for 24 hrs
81	3/29	2.35	2.40	CV	UF	10	P	5	10	35.5	
82	3/29	2.55	3.02	SIN	UF	10	P	5	10	36	
83	3/29	3.25	3.30	SIN	UF	10	P	5	10	54	
84	3/29-30	3.50	8.45	SIN	UF	10	P	5	10	54	Pressure on 17 hrs
85	3/30	9.00	9.15	CV	UF	10	P	5	6.5	52.2	
86	3/30	9.30	9.50	SIN	UF	10	P	5	8.5	72	
87	3/30	10.20	10.50	SIN	UF	10	P				Low oil pressure
88	3/30	11.20	11.25	SIN	UF	10	P	5	6.5	77.4	Unstable operation
89	3/31	10.30	10.40	SIN	UF	10	P	1	32	1	Fresh TFE
90	3/31	10.45	11.05	SIN	UF	10	P	4	25	13	Interface not cleaned
91	4/1	9.10	9.20	SIN	UF	10	P	5	16	20	
92	4/1	9.53	10.00	SIN	UF	10	P	5	16	40	
93	4/1	10.25	10.45	CV	UF	10	P	5	10	39.2	
94	4/1	11.10	11.17	SIN	UF	10	P	5	10	40	
95	4/1	11.35	11.45	SIN	UF	10	P	5	10	60	
96	4/1	12.05	12.15	CV	UF	10	P	5	6.5	58.2	Actuator moved sidesway

Table 4-I Summary of Experimental Results (Continued)

Test No.	Frequency (Hz)	Amplitude (in)	Peak Velocity (in/s)	μ_B (%)	$\dot{\mu}_R$ max (%)	μ_{S1} (%)	μ_{S3} (%)	μ_{S5} (%)	$\dot{\mu}_S$ max (%)	Temperature Start (°F)	Temperature End (°F)	Pressure (psi)
79	0.32	1	2	8.91	6.89/1	7.27	6.17	3.21	7.27/1	73	120	2000
80	0.32	2	4	10.12	6.69/1	6.96	5.37	4.49	6.96/1	71	156	2000
81	0.5	1.97	3.94	10.33	7.76/1	6.89	5.27	4.69	6.89/1	74	150	2000
82	0.5	2	6.28	11.37	7.24/1	7.44	5.52	4.67	7.44/1	77	166	2000
83	0.5	3	9.43	12.43	7.58/1	7.50	5.41	4.47	7.50/1	78	190	2000
84	0.5	3	9.43	14.20	8.64/1	8.56	5.81	4.70	8.56/1	74	189	2000
85	0.78	2.90	9.12	13.61	8.74/1	7.92	5.44	4.49	7.92/1	79	179	2000
86	0.6	4	15.08	15.80	9.09/1	9.09	6.29	5.24	9.09/1	79	198	2000
87	0.8											
88	0.8	4.30	21.61	17.35	10.58/1					85	201	2000
89	0.03	0.5	0.1	5.52	1.74/1	1.51	- - - -	- - - -	1.51/1	72	73	3000
90	0.16	1	1	4.74	5.01/2	5.38	5.41	- - - -	5.38/1	72	109	3000
91	0.32	1	2	7.40	5.78/1	6.30	5.29	4.73	6.30/1	74	134	3000
92	0.32	2	4	8.04	6.34/1	6.77	5.00	4.19	6.77/1	76	187	3000
93	0.5	1.96	3.92	8.65	7.45/1	6.68	5.08	4.28	6.68/1	78	180	3000
94	0.5	2	6.28	9.60	6.86/1	7.03	5.12	4.34	7.03/1	80	187	3000
95	0.5	3	9.43	10.32	7.12/1	7.27	5.11	4.21	7.27/1	83	220	3000
96	0.78	2.91	9.14	10.17	8.11/1	7.32	5.19	4.34	7.32/1	87	181	3000

Table 4-I Summary of Experimental Results (Continued)

Test No.	Date	Time Setup	Time Start	Test Type	Teflon Type	Teflon Diam. (in)	Sliding Direction	No. Cycles	Duration (sec)	Total Travel (in)	Comments
97	4/1	2.15	2.20	SIN	UF	10	P	5	8.5	71.5	
98	4/1	2.45	2.52	SIN	UF	10	P	5	6.5	77.1	Unstable Operation
99	4/4	9.45	9.50	SIN	15GF	10	P	1	32	2	Fresh TFE
100	4/4	10.08	10.17	SIN	15GF	10	P	4	25	16	
101	4/4	10.35	10.42	SIN	15GF	10	P	5	16	20	
102	4/4	11.10	11.20	SIN	15GF	10	P	5	16	40	
103	4/4	11.50	11.58	CV	15GF	10	P	5	10	39.4	
104	4/4	1.30	1.40	SIN	15GF	10	P	5	10	40	
105	4/4	2.05	2.15	SIN	15GF	10	P	5	10	60	
106	4/4	2.40	2.50	SIN	15GF	10	P	5	8.5	80	
107	4/4	3.10	3.20	SIN	15GF	10	P	5	6.5	91	Unstable Operation
108	4/5	2.50	3.03	SIN	15GF	10	P	1	32	2	Fresh TFE
109	4/5	3.25	3.33	SIN	15GF	10	P	4	25	16	
110	4/6	9.05	9.15	SIN	15GF	10	P	5	16	20	
111	4/6	9.50	10.05	SIN	15GF	10	P	5	16	39.6	
112	4/6	10.50	11.02	CV	15GF	10	P	5	10	39.2	
113	4/6	11.35	11.45	SIN	15GF	10	P	5	10	40	
114	4/6	1.30	1.40	SIN	15GF	10	P	5	10	59.6	

Table 4-I Summary of Experimental Results (Continued)

Test No.	Frequency (Hz)	Amplitude (in)	Peak Velocity (in/s)	μ_B (%)	μ_R max (%)	μ_{S1} (%)	μ_{S3} (%)	μ_{S5} (%)	μ_S max (%)	Temperature Start (°F)	Temperature End (°F)	Pressure (psi)
97	0.6	3.97	14.97	11.69	7.92/1	8.02	5.43	4.69	8.02/1	80	212	3000
98	0.8	4.28	21.51	11.98	7.87/1	7.06	-	-	7.06/1	87	226	3000
99	0.03	0.5	0.1	8.34	4.64/1	4.01	-	-	4.01/1	71	72	1000
100	0.16	1	1	10.65	7.87/4	7.60	-	-	9.09/4	71	107	1000
101	0.32	1	2	11.93	9.75/1	11.29	-	-	11.29/1	73	130	1000
102	0.32	2	4	13.11	12.02/1	13.68	-	-	13.68/1	74	170	1000
103	0.5	1.97	3.94	14.50	13.65/1	13.51	-	-	13.51/1	75	159	1000
104	0.5	2	6.28	17.76	13.65/1	15.11	12.67	11.27	15.11/1	75	166	1000
105	0.5	3	9.43	17.95	14.28/1	14.61	12.30	10.81	14.61/1	78	188	1000
106	0.6	4	15.08	19.54	13.58/1	14.35	11.56	10.06	14.35/1	80	210	1000
107	0.8	4.55	22.88	20.23	15.40/1	14.41	-	-	14.41/1	83	220	1000
108	0.03	0.5	0.1	5.80	4.64/1	4.28	-	-	4.28/1	77	80	2000
109	0.16	1	1	7.03	6.94/1	7.57	7.39	-	7.57/1	77	117	2000
110	0.32	1	2	8.25	7.56/1	8.60	8.37	7.73	8.60/1	78	112	2000
111	0.32	1.98	3.96	10.88	8.67/1	9.36	7.41	6.43	9.36/1	79	176	2000
112	0.5	1.96	3.92	10.91	10.13/1	9.14	7.39	6.42	9.14/1	81	178	2000
113	0.5	2.0	6.28	11.67	9.34/1	9.80	7.61	6.69	9.80/1	83	178	2000
114	0.5	2.98	9.36	12.03	9.51/1	10.08	7.59	6.55	10.08/1	82	189	2000

Table 4-I Summary of Experimental Results (Continued)

Test No.	Date	Time Setup	Time Start	Test Type	Teflon Type	Teflon Diam. (in)	Sliding Direction	No. Cycles	Duration (sec)	Total Travel (in)	Comments
115	4/6	2.05	2.15	SIN	15GF	10	P	5	8.5	79.4	
116	4/6	2.30	2.38	SIN	15GF	10	P	5	6.5	79.4	
117	4/7	9.40	9.55	SIN	15GF	10	P	1	32	2	Fresh TFE
118	4/7	11.05	11.10	SIN	15GF	10	P	4	25	16	
119	4/7	11.35	11.45	SIN	15GF	10	P	5	16	20	
120	4/7	12.05	12.10	SIN	15GF	10	P	5	16	40	
121	4/7	12.55	1.03	CV	15GF	10	P	5	10	39.2	
122	4/7	1.25	1.31	SIN	15GF	10	P	5	10	40	
123	4/7	1.54	2.00	SIN	15GF	10	P	5	10	59.6	
124	4/7	2.30	2.45	SIN	15GF	10	P	5	6.5	79.2	Unstable Operation
125	4/8	9.05	9.15	SIN	25GF	10	P	1	32	2	Fresh TFE
126	4/8	9.30	9.35	SIN	25GF	10	P	4	25	16	
127	4/8	9.55	10.03	SIN	25GF	10	P	5	16	20	
128	4/8	10.15	10.20	SIN	25GF	10	P	5	16	40	
129	4/8	10.40	10.50	CV	25GF	10	P	5	10	39.2	
130	4/8	11.10	11.15	SIN	25GF	10	P	5	10	40	
131	4/8	1.10	1.17	SIN	25GF	10	P	5	10	59.6	
132	4/8	1.35	1.45	SIN	25GF	10	P	5	8.5	79.4	

Table 4-I Summary of Experimental Results (Continued)

Test No.	Frequency (Hz)	Amplitude (in)	Peak Velocity (in/s)	μ_B (%)	μ_R max (%)	μ_{S1} (%)	μ_{S3} (%)	μ_{S5} (%)	μ_S max (%)	Temperature Start (°F)	Temperature End (°F)	Pressure (psi)
115	0.6	3.97	14.97	12.71	9.97/1	10.03	7.42	6.36	10.03/1	85	207	2000
116	0.8	3.97	19.96	13.05	9.92/1	9.96	7.54	6.55	9.96/1	90	208	2000
117	0.03	0.5	0.1	5.83	4.78/1	4.32	-	-	4.32/1	78	82	3000
118	0.16	1	1	6.98	6.19/1	6.63	6.44	-	6.63/1	78	130	3000
119	0.32	1	2	7.76	6.62/1	7.53	6.78	6.10	7.53/1	80	137	3000
120	0.32	2	4	9.18	7.46/1	7.72	6.02	5.16	7.72/1	82	184	3000
121	0.5	1.96	3.92	9.82	8.62/1	8.01	6.22	5.28	8.01/1	83	178	3000
122	0.5	2	6.28	10.46	7.96/1	8.49	6.41	5.56	8.49/1	86	175	3000
123	0.5	2.98	9.36	11.15	8.33/1	8.49	6.24	5.35	8.49/1	88	206	3000
124	0.8	3.86	19.40	11.67	8.19/1	8.21	-	-	8.21/1	89	231	3000
125	0.03	0.5	0.1	8.12	7.28/1	5.76	-	-	5.76/1	76	78	1000
126	0.16	1	1	9.36	9.30/1	9.42	10.15	-	10.15/3	76	102	1000
127	0.32	1	2	11.78	10.02/1	11.23	11.32	11.09	11.46/2	77	112	1000
128	0.32	2	4	13.62	10.40/1	12.31	11.46	10.76	12.31/1	79	136	1000
129	0.5	1.96	3.92	12.96	12.30/1	11.71	10.61	9.80	11.71/1	81	138	1000
130	0.5	2	6.28	15.06	12.45/1	13.44	11.61	10.86	13.44/1	84	138	1000
131	0.5	2.98	9.36	15.02	12.42/1	12.84	11.26	10.40	12.84/1	80	160	1000
132	0.6	3.97	14.97	16.88	12.81/1	13.12	10.88	9.75	13.12/1	85	168	1000

Table 4-I Summary of Experimental Results (Continued)

Test No.	Date	Time Setup	Time Start	Test Type	Teflon Type	Teflon Diam. (in)	Sliding Direction	No. Cycles	Duration (sec)	Total Travel (in)	Comments
133	4/8	2.05	2.15	SIN	25GF	10	P	5	6.5	79.2	
134	4/11	9.05	9.10	SIN	25GF	10	P	1	32	2	Fresh TFE
135	4/11	10.10	10.20	SIN	25GF	10	P	4	25	16	
136	4/11	10.55	11.00	SIN	25GF	10	P	5	16	20	
137	4/11	11.35	11.40	SIN	25GF	10	P	5	16	40	
138	4/11	12.05	12.10	CV	25GF	10	P	5	10	39.2	
139	4/11	1.20	1.30	SIN	25GF	10	P	5	10	40	
140	4/11	2.10	2.15	SIN	25GF	10	P	5	10		Test discontinued
141	4/12	2.05	2.10	SIN	25GF	10	P	5	10	60	
142	4/12	2.50	3.00	SIN	25GF	10	P	5	6.5	78.8	
143	4/13	9.30	9.35	SIN	25GF	10	P	1	32	2	Fresh TFE
144	4/13	10.15	10.28	SIN	25GF	10	P	4	25	16	Thermocouple removed for repair
145	4/13	11.15	11.25	SIN	25GF	10	P	5	16	20	
146	4/13	11.50	11.55	SIN	25GF	10	P	5	16	40	
147	4/13	12.15	12.23	CV	25GF	10	P	5	10	39.2	
148	4/13	1.35	1.45	SIN	25GF	10	P	5	10	39.6	
149	4/13	2.20	2.25	SIN	25GF	10	P	5	10	59.6	
150	4/13	2.55	3.00	SIN	25GF	10	P	5	6.5	78	

Table 4-I Summary of Experimental Results (Continued)

Test No.	Frequency (Hz)	Amplitude (in)	Peak Velocity (in/s)	μ_B (%)	μ_B^* max (%)	μ_{st} (%)	μ_{sd} (%)	μ_{ss} (%)	μ_S^* max (%)	Temperature Start (°F)	Temperature End (°F)	Pressure (psi)
133	0.8	3.96	19.91	17.48	13.18/1	13.42	11.83	10.79	13.42/1	87	178	1000
134	0.03	0.5	0.1	6.70	5.76/1	4.87	-	-	4.87/1	76	78	2000
135	0.16	1	1	7.31	7.97/1	7.71	8.79	-	8.79/3	76	99	2000
136	0.32	1	2	9.35	8.37/1	9.47	9.47	9.03	9.63/2	78	108	2000
137	0.32	2	4	11.59	9.93/1	10.64	9.03	8.15	10.64/1	81	146	2000
138	0.5	1.96	3.92	11.23	11.08/1	10.13	9.05	8.41	10.13/1	82	147	2000
139	0.5	2	6.28	12.53	10.53/1	11.00	9.32	8.70	11.00/1	82	148	2000
140	0.5	-	-	-	-	-	-	-	-	-	-	2000
141	0.5	3	9.43	14.52	11.75/1	11.64	9.66	8.57	11.64/1	78	206	2000
142	0.8	3.94	19.80	12.66	10.72/1	11.06	9.33	8.25	11.06/1	83	252	2000
143	0.03	0.5	0.1	6.53	4.80/1	4.22	-	-	4.22/1	75	79	3000
144	0.16	1	1	6.19	5.23/3	5.06	5.50	-	5.50/3	-	-	3000
145	0.32	1	2	7.76	5.60/3	5.86	6.24	6.14	6.24/3	-	-	3000
146	0.32	2	4	8.52	7.14/1	8.00	7.39	6.75	8.00/1	-	-	3000
147	0.5	1.96	3.92	9.65	9.18/1	8.40	7.32	6.60	8.60/1	-	-	3000
148	0.5	1.98	6.22	10.99	9.47/1	9.80	7.88	7.10	9.80/1	-	-	3000
149	0.5	2.98	9.36	10.95	9.26/1	9.42	7.47	6.42	9.42/1	-	-	3000
150	0.8	3.90	19.60	12.12	9.39/1	9.32	6.78	5.68	9.32/1	-	-	3000

Table 4-I Summary of Experimental Results (Continued)

Test No.	Date	Time Setup	Time Start	Test Type	Teflon Type	Teflon Diam. (in)	Sliding Direction	No. Cycles	Duration (sec)	Total Travel (in)	Comments
151	4/14	9.30	9.38	SIN	UF	5	P	1	32	2	Fresh TFE
152	4/14	10.05	10.10	SIN	UF	5	P	4	25	16	
153	4/14	10.30	10.35	SIN	UF	5	P	5	16	20	
154	4/14	11.05	11.10	SIN	UF	5	P	5	16	40	
155	4/14	11.40	11.45	CV	UF	5	P	5	10	39.4	Thermocouple repaired
156	4/14	12.05	12.15	SIN	UF	5	P	5	16	40	
157	4/14	1.30	1.35	SIN	UF	5	P	5	10	40	
158	4/14	2.00	2.10	SIN	UF	5	P	5	10	59.6	
159	4/14	2.30	2.35	SIN	UF	5	P	5	10	59.6	Stick-slip observed
160	4/14	2.50	2.55	SIN	UF	5	P	5	6.5	79.2	
161	4/15	9.30	9.35	SIN	15GF	5	P	1	32	2	Fresh TFE
162	4/15	10.05	10.10	SIN	15GF	5	P	4	25	16	
163	4/15	10.40	10.45	SIN	15GF	5	P	5	16	20	
164	4/15	11.10	11.15	SIN	15GF	5	P	5	16	40	
165	4/15	11.40	11.45	CV	15GF	5	P	5	10	39.2	
166	4/15	1.25	1.38	SIN	15GF	5	P	5	16	40	
167	4/15	1.55	2.00	SIN	15GF	5	P	5	10	40	
168	4/15	2.25	2.30	SIN	15GF	5	P	5	10	59.6	

Table 4-I Summary of Experimental Results (Continued)

Test No.	Frequency (Hz)	Amplitude (in)	Peak Velocity (in/s)	μ_B (%)	μ_R^* max (%)	μ_{S1} (%)	μ_{S3} (%)	μ_{S5} (%)	μ_S^* max (%)	Temperature Start (°F)	Temperature End (°F)	Pressure (psi)
151	0.03	0.5	0.1	3.76	1.01/1	0.87	-	-	0.87/1	-	-	6500
152	0.16	1	1	4.70	1.47/3	1.89	2.14	-	2.14/3	-	-	6500
153	0.32	1	2	4.12	2.86/1	3.65	3.52	3.27	3.65/1	-	-	6500
154	0.32	2	4	6.80	3.77/1	4.88	3.81	3.25	4.88/1	-	-	6500
155	0.5	1.97	3.94	6.75	5.43/1	4.97	3.72	3.19	4.97/1	77	164	6500
156	0.32	2	4	8.31	5.54/1	7.34	6.76	6.06	7.34/1	78	145	3000
157	0.5	2	6.28	7.48	4.73/1	5.54	4.48	3.89	5.54/1	77	168	6500
158	0.5	2.98	9.36	8.37	5.29/1	5.72	4.55	3.99	5.72/1	79	191	6500
159	0.5	2.98	9.36	12.59	5.42/1	7.47	5.98	5.46	7.47/1	83	184	3000
160	0.8	3.96	19.91	9.28	3.64/1	5.36	3.48	3.07	5.36/1	84	208	6500
161	0.03	0.5	0.1	4.67	2.40/1	2.15	-	-	2.15/1	74	77	6500
162	0.16	1	1	5.47	2.27/1	2.77	3.03	-	3.03/3	74	106	6500
163	0.32	1	2	6.23	2.68/1	4.69	4.06	3.67	4.69/1	74	145	6500
164	0.32	2	4	6.66	3.17/1	5.44	4.35	3.84	5.44/1	75	183	6500
165	0.5	1.96	3.92	6.73	5.22/1	5.11	4.23	3.75	5.11/1	77	180	6500
166	0.32	2	4	9.79	5.48/1	7.30	5.88	5.35	7.30/1	75	176	3000
167	0.5	2	6.28	8.47	5.37/1	5.79	4.47	3.95	5.79/1	77	199	6500
168	0.5	2.98	9.36	8.27	5.03/1	5.19	4.01	3.56	5.19/1	78	221	6500

Table 4-I Summary of Experimental Results (Continued)

Test No.	Date	Time Setup	Time Start	Test Type	Teflon Type	Teflon Diam. (in)	Sliding Direction	No. Cycles	Duration (sec)	Total Travel (in)	Comments
169	4/15	2.50	2.55	SIN	15GF	5	P	5	10	79.6	Stick-slip observed
170	4/15	3.10	3.15	SIN	15GF	5	P	5	6.5	79.4	
171	4/18	9.10	9.30	SIN	25GF	5	P	1	32	2	Fresh TFE
172	4/18	9.55	10.00	SIN	25GF	5	P	4	25	16	
173	4/18	10.30	10.40	SIN	25GF	5	P	5	16	20	
174	4/18	11.05	11.10	SIN	25GF	5	P	5	16	40	
175	4/18	11.45	11.50	CV	25GF	5	P	5	10	39.2	
176	4/18	1.10	1.15	SIN	25GF	5	P	5	16	39.6	
177	4/18	1.45	1.50	SIN	25GF	5	P	5	10	39.6	
178	4/18	2.30	2.35	SIN	25GF	5	P	5	10	60	
179	4/18	3.10	3.15	SIN	25GF	5	P	5	10	60	Stick-slip observed
180	4/18	3.35	3.40	SIN	25GF	5	P	5	6.5	79.2	Stick-slip observed
181	4/19	9.55	10.00	SIN	UF	5	T	1	32	2	New S.S. Plate- Fresh TFE
182	4/19	10.15	10.20	SIN	UF	5	T	4	25	16	
183	4/19	10.45	10.50	SIN	UF	5	T	5	16	20	
184	4/19	11.30	11.35	SIN	UF	5	T	5	16	40	
185	4/19	11.55	12.00	CV	UF	5	T	5	10	39.6	
186	4/19	1.10	1.15	SIN	UF	5	T	5	10	39.6	

Table 4-I (Summary of Experimental Results (Continued)

Test No.	Frequency (Hz)	Amplitude (in)	Peak Velocity (in/s)	μ_B (%)	$\dot{\mu}_R$ max (%)	μ_{S1} (%)	μ_{S3} (%)	μ_{S5} (%)	$\dot{\mu}_S$ max (%)	Temperature Start (°F)	Temperature End (°F)	Pressure (psi)
169	0.5	2.98	9.36	11.89	7.43/1	7.71	6.54	5.94	7.71/1	82	206	3000
170	0.8	3.97	19.96	9.97	5.34/1	5.27	3.91	3.46	5.27/1	83	236	6500
171	0.03	0.5	0.1	5.75	3.29/1	3.19	-	-	3.19/1	70	75	6500
172	0.16	1	1	6.65	4.35/1	5.56	5.35	-	5.68/2	70	118	6500
173	0.32	1	2	7.27	5.12/1	5.87	4.97	4.29	5.87/1	72	149	6500
174	0.32	2	4	8.03	5.65/1	5.97	4.80	4.25	5.97/1	73	190	6500
175	0.5	1.96	3.92	8.39	5.91/1	5.89	4.49	3.91	5.89/1	74	196	6500
176	0.32	1.98	3.96	9.63	7.62/1	8.64	7.37	6.60	8.64/1	73	180	3000
177	0.5	1.98	6.22	9.30	5.89/1	6.59	5.15	4.56	6.59/1	75	208	6500
178	0.5	3	9.43	8.33	5.10/1	5.41	4.16	3.61	5.41/1	75	243	6500
179	0.5	3	9.43	13.27	6.17/1	6.53	5.13	4.61	6.53/1	77	211	3000
180	0.8	3.96	19.91	10.37	4.97/1	5.37	3.78	3.26	5.37/1	78	248	6500
181	0.03	0.5	0.1	3.50	1.13/1	1.11	-	-	1.11/1	71	73	6500
182	0.16	1	1	5.05	2.85/2	3.22	3.20	-	3.25/2	71	111	6500
183	0.32	1	2	5.22	3.52/1	4.11	3.74	3.45	4.11/1	72	128	6500
184	0.32	2	4	7.17	3.47/1	4.87	3.76	3.23	4.87/1	73	161	6500
185	0.5	1.98	3.96	7.27	4.96/1	4.51	3.42	2.90	4.51/1	76	164	6500
186	0.5	1.98	6.22	7.57	3.82/1	4.52	3.08	2.59	4.52/1	74	168	6500

Table 4-I (Summary of Experimental Results (Continued)

Test No.	Date	Time Setup	Time Start	Test Type	Teflon Type	Teflon Diam. (in)	Sliding Direction	No. Cycles	Duration (sec)	Total Travel (in)	Comments
187	4/19	1.45	1.50	SIN	UF	5	T	5	10	59.6	
188	4/19	2.10	2.15	SIN	UF	5	T	5	5	29.2	Stick-slip observed
189	4/19	2.40	2.45	SIN	UF	5	T	5	2.5	14.4	Significant stick-slip
190	4/19	3.10	3.15	SIN	UF	5	T	5	6.5	79.2	
191	4/20	9.30	9.40	SIN	UF	10	T	1	32	2	Fresh TFE
192	4/20	10.10	10.15	SIN	UF	10	T	5	25	16	
193	4/20	10.40	10.45	SIN	UF	10	T	5	16	20	
194	4/20	11.15	11.20	SIN	UF	10	T	5	16	40	
195	4/20	11.50	11.55	SIN	UF	10	T	5	10	40	
196	4/20	1.40	1.47	SIN	UF	10	T	5	10		Data Lost
197	4/20	2.20	2.25	SIN	UF	10	T	5	5	29.6	
198	4/20	2.45	2.50	SIN	UF	10	T	5	2.5	14.4	Stick-slip observed
199	4/20	3.15	3.20	SIN	UF	10	T	5	6.5	79.2	
200	4/21	9.30	9.35	SIN	UF	10	T	1	32	2	Fresh TFE
201	4/21	10.15	10.20	SIN	UF	10	T	4	25	16	
202	4/21	10.45	10.50	SIN	UF	10	T	5	16	20	
203	4/21	11.15	11.20	SIN	UF	10	T	5	16	40	
204	4/21	11.45	11.50	SIN	UF	10	T	5	10	40	

Table 4-I (Summary of Experimental Results (Continued)

Test No.	Frequency (Hz)	Amplitude (in)	Peak Velocity (in/s)	μ_B (%)	$\dot{\mu}_R$ max (%)	μ_{S1} (%)	μ_{S3} (%)	μ_{S5} (%)	$\dot{\mu}_S$ max (%)	Temperature Start (°F)	Temperature End (°F)	Pressure (psi)
187	0.5	2.98	9.36	8.71	4.00/1	4.66	3.46	2.88	4.66/1	75	185	6500
188	1	1.46	9.17	9.31	5.32/1	5.48	3.93	3.40	5.48/1	79	156	6500
189	2	0.72	9.05	10.30	6.48/1	6.41	4.73	4.22	6.41/1	77	121	6500
190	0.8	3.96	19.91	10.53	5.61/1	5.64	3.63	3.18	5.64/1	76	178	6500
191	0.03	0.5	0.1	7.16	2.67/1	2.39	-	-	2.39/1	68	69	1000
192	0.16	1	1	9.70	3.80/4	5.51	6.33	-	6.35/4	68	85	1000
193	0.32	1	2	11.89	8.83/1	10.27	10.13	9.62	10.27/1	69	106	1000
194	0.32	2	4	13.85	10.54/1	11.75	10.10	9.03	11.75/1	71	141	1000
195	0.5	2	6.28	17.72	9.93/1	13.93	9.06	7.94	13.93/1	73	144	1000
196	0.5											
197	1	1.48	9.30	17.28	13.73/1	14.15	11.78	10.79	14.15/1	76	121	1000
198	2	0.72	9.05	18.17	13.58/1	15.17	12.60	11.56	15.17/1	77	96	1000
199	0.8	3.96	19.91	20.68	13.08/1	13.89	10.70	9.31	13.89/1	76	94	1000
200	0.03	0.5	0.1	7.49	2.22/1	1.72	-	-	1.72/1	68	69	2000
201	0.16	1	1	8.23	6.23/3	6.11	6.89	-	6.89/1	69	86	2000
202	0.32	1	2	10.27	8.31/1	9.07	8.07	7.42	9.07/1	71	103	2000
203	0.32	2	4	11.95	9.25/1	9.63	7.85	6.87	9.63/1	72	140	2000
204	0.5	2	6.28	13.24	9.97/1	10.32	8.20	7.22	10.32/1	74	138	2000

Table 4-I (Summary of Experimental Results (Continued)

Test No.	Date	Time		Test Type	Teflon		Sliding Direction	No. Cycles	Duration (sec)	Total Travel (in)	Comments
		Setup	Start		Type	Diam. (in)					
205	4/21	2.20	2.25	SIN	UF	10	T	5	10	59.6	
206	4/21	3.00	3.05	SIN	UF	10	T	5	6.5	76.8	Unstable Operation
207	4/22	9.30	9.35	SIN	UF	10	T	1	32	2	Fresh TFE
208	4/22	10.05	10.10	SIN	UF	10	T	4	25	16	
209	4/22	10.30	10.35	SIN	UF	10	T	5	16	20	
210	4/22	11.05	11.10	SIN	UF	10	T	5	16	40	
211	4/22	11.50	11.55	SIN	UF	10	T	5	10	39.6	
212	4/22	1.30	1.40	SIN	UF	10	T	5	10	59.6	
213	4/22	2.10	2.15	SIN	UF	10	T	5	6.5	74.8	Unstable Operation

Table 4-I (Summary of Experimental Results (Continued)

Test No.	Frequency (Hz)	Amplitude (in)	Peak Velocity (in/s)	μ_B (%)	$\dot{\mu}_R$ max (%)	μ_{S1} (%)	μ_{S3} (%)	μ_{S5} (%)	$\dot{\mu}_S$ max (%)	Temperature Start (°F)	Temperature End (°F)	Pressure (psi)
205	0.5	2.98	9.36	14.28	10.34/1	10.52	8.09	6.95	10.52/1	73	171	2000
206	0.8	3.84	19.32	16.54	10.92/1	10.65	8.04	6.79	10.65/1	79	215	2000
207	0.03	0.5	0.1	4.55	2.42/1	3.00	-	-	3.00/1	69	72	3000
208	0.16	1	1	6.61	4.93/1	5.78	5.22	-	5.78/1	70	107	3000
209	0.32	1	2	8.15	6.36/1	6.81	5.70	5.14	6.81/1	73	121	3000
210	0.32	2	4	9.94	6.94/1	7.43	5.64	4.72	7.43/1	74	176	3000
211	0.5	1.98	6.22	10.97	7.61/1	7.96	5.91	4.97	7.96/1	76	168	3000
212	0.5	2.98	9.36	11.58	8.00/1	8.30	5.81	4.71	8.30/1	75	194	3000
213	0.8	3.74	18.78	12.88	8.24/1	7.79			7.79/1	82	223	3000

SECTION 5
INTERPRETATION OF RESULTS

5.1 Theoretical Considerations

Bowden and Tabor [64] have presented fundamental studies on the nature of friction of metals and polymers. There are many types of strength of bond that is formed at the contact interface of two materials. Teflon exhibits a type of interfacial bonding that is unique. Sliding in Teflon occurs truly at the interface and this is attributed to the smooth molecular profile of Teflon [65].

The question of practical interest is if friction of Teflon interfaces may be predicted by theoretical considerations. Theories exist that explain aspects of the frictional behavior of Teflon. These aspects of behavior are the low coefficient friction, the decrease of friction with increasing pressure and the increase of friction with velocity. The low coefficient of friction of Teflon at low velocities is caused by the formation of a very thin film of highly crystalline Teflon on the mating surface. This film has a high degree of molecular orientation [66, 67]. In tests conducted at low velocity (see in Appendix A tests No. 69, 77, 89 and 151), a substantial difference between the breakaway value of friction and the sliding (or kinetic) value was observed. Initially, the interface adhesion is relatively strong. When it is overcome, a thin film of Teflon develops on the slider and friction drops dramatically. In these tests, the ratio μ_B to μ_{smax} was between 2.3 and 4.3. At high velocities, the mechanism is different. Teflon is transferred to the mating surface in the form of large fragments (see Figure 4-4) which gives rise to higher friction.

The decrease of the coefficient of friction with increases in pressure may be explained using the elastic and plastic deformation theories [64]. Under elastic deformations of Teflon, the true area of contact may be given by

$$A = kW^n \tag{5-1}$$

in which W is the normal load and k is a constant that depends on the form of surface and its elastic constants. n is a constant taking values of 2/3 to 1. The case n = 2/3 is derived when considering a surface covered with spherical asperities. If each spherical asperity is considered having smaller spherical asperities, n takes the value 8/9. Continuing like this (what Bowden and Tabor call as small fleas and lesser fleas) a value of n equal to unity is recovered.

At loads at which the deformations of Teflon are plastic, the true area of contact is given by

$$A = W/p \tag{5-2}$$

in which p is the compressive yield strength of Teflon. The frictional force during sliding is given by

$$F = sW \tag{5-3}$$

in which s is the shear strength of the interface. The coefficient of friction is given by

$$\mu = F/W \tag{5-4}$$

which results in the following expressions

$$\mu = ksW^{1-n} \tag{5-5}$$

for elastic deformation and

$$\mu = s/p \tag{5-6}$$

for plastic deformation. Equation 5-5 explains the reduction of the coefficient of friction with increasing loads; while equations 5-2 and 5-6 suggest the existence of a limiting value of pressure beyond which the coefficient of friction remains constant. This value of pressure should be equal to the compressive yield strength of Teflon. This value is about equal to 1500 psi at normal temperatures (Reference 6 based on ASTM D-690-80 standard). Values of the limiting pressure beyond which friction is constant have been reported in the literature. They vary from about 1,500 psi [41] to 7250 psi [10]. This substantial variation in the reported value of limiting pressure may be attributed to the following:

1. The influence of size and type of specimen (recessed and confined) on the yield strength, and

2. The difference between true area of contact, A, and geometrical cross-sectional area, A_o. In general, A is less than or equal to A_o. Reported values of pressure are with respect to area A_o.

5.2 Effect of Type of Test

Most of the conducted tests were with sinusoidal motion. In this type of motion, both the sliding velocity and acceleration vary with time. It has been expected and confirmed in these tests that acceleration has only a minor effect on the measured coefficient of friction; velocity being the most influential parameter.

Constant velocity test (cyclic sawtooth displacement) is another test that is appropriate for measuring the friction of Teflon-steel interfaces. Presumably in a constant velocity test, the acceleration is zero and, therefore, it appears to be a more appropriate test than a sinusoidal one because the results cannot be masked by the influence of acceleration. This is not exactly true

because the acceleration at the start and at every reversal in a cyclic constant velocity test is markedly different than zero. The reader is referred to Appendix A in which acceleration records in tests No. 51 to 60 are presented. It is reasonable to assume that the observed substantial acceleration impulse at the start of the experiment will have some influence on the breakaway value of friction. On the other hand, both types of test (sinusoidal and constant velocity) should yield the same coefficient of sliding friction at peak velocity. It should be noted that in both tests the peak velocity occurs at a time at which acceleration is zero.

A number of tests was conducted to investigate the effect of type of tests on the recorded values of friction. Sinusoidal and constant velocity tests were conducted with the same amplitude but different frequency in order to yield the same velocity. A summary of the obtained results is presented in Table 5-I. It is evident in this table that the type of test has an insignificant effect on the recorded value of maximum sliding coefficient of friction. There is some effect on the breakaway of coefficient of friction, which is minor.

5.3 Effect of Specimen Size

Our tests were conducted on 10 inch diameter specimens at 1,000, 2,000 and 3,000 psi pressure and on 5 inch diameter specimens at 6,500 psi pressure. Six tests were conducted at 3,000 psi pressure on 5 inch specimen in order to determine the effect of specimen size. Table 5-II summarizes the results of these tests. The agreement between results with 5 and 10 inch diameter specimens is fairly good except in the three cases where significant stick-slip was observed (No. 159, 169, 179). In the studies of Taylor [10], the effect of specimen size has been shown to be minimal. The size effect in our studies appears to be more than what was found by Taylor. Velocity may have had an effect.

5.4 Effect of Acceleration

Tests 56 to 60 were conducted at the same peak velocity (values between 7.57 and 7.97 in/sec) but different amplitude, frequency and even type of test. The peak acceleration in these tests varied between 0.08 and 0.85 g. This is the value recorded after the initial acceleration impulse. This impulse had a value of 0.43 g in the sinusoidal tests and 0.85 g in the constant velocity tests. Other than test No. 60, in which stick-slip was observed, the tests yielded values of μ_B and μ_{smax} that compare very well. This is illustrated in Figure 5-1. Clearly, the effect of acceleration is minimal.

5.5 Effect of Frequency

As discussed earlier, the phenomenon known as stick-slip was observed in some high frequency tests (usually at 1 Hz and above). The difference between a high frequency and a low frequency test conducted at the same velocity is in the time needed to complete a cycle (eg. tests No. 59 and

Table 5-I Effect of Type of Test

Test No.	Conditions	Pressure (psi)	Test Type	Freq. (Hz)	Amplit. (in)	Peak Velocity (in/s)	μ_B (%)	μ_s max (%)	Comments
64	UF, P	1000	SIN	0.32	1.98	3.96	16.67	12.10	
65	UF, P	1000	CV	0.5	1.91	3.82	18.86	12.55	
80	UF, P	2000	SIN	0.32	2	4	10.12	6.96	
81	UF, P	2000	CV	0.5	1.97	3.94	10.33	6.89	
83	UF, P	2000	SIN	0.5	3	9.43	12.43	7.50	
85	UF, P	2000	CV	0.78	2.90	9.12	13.61	7.92	minor stick-slip
92	UF, P	3000	SIN	0.32	2	4	8.04	6.77	
93	UF, P	3000	CV	0.5	1.96	3.92	8.65	6.68	
95	UF, P	3000	SIN	0.5	3	9.43	10.32	7.27	
96	UF, P	3000	CV	0.78	2.91	9.14	10.17	7.32	
102	15GF, P	1000	SIN	0.32	2	4	13.11	13.68	
103	15GF, P	1000	CV	0.5	1.97	3.94	14.50	13.51	
111	15GF, P	2000	SIN	0.32	1.98	3.96	10.88	9.36	
112	15GF, P	2000	CV	0.5	1.96	3.92	10.91	9.14	
120	15GF, P	3000	SIN	0.32	2	4	9.18	7.72	
121	15GF, P	3000	CV	0.5	1.96	3.92	9.82	8.01	
128	25GF, P	1000	SIN	0.32	2	4	13.62	12.31	
129	25GF, P	1000	CV	0.5	1.96	3.92	12.96	11.71	Absence of breakaway, insufficient cleaning
137	25GF, P	2000	SIN	0.32	2	4	11.59	10.64	
138	25GF, P	2000	CV	0.5	1.96	3.92	11.23	10.13	
146	25GF, P	3000	SIN	0.32	2	4	8.52	8.00	Absence of breakaway, Insufficient cleaning
147	25GF, P	3000	CV	0.5	1.96	3.92	9.65	8.40	
154	UF, P	6500	SIN	0.32	2	4	6.80	4.88	
155	UF, P	6500	CV	0.5	1.97	3.94	6.75	4.97	
164	15GF, P	6500	SIN	0.32	2	4	6.66	5.44	
165	15GF, P	6500	CV	0.5	1.96	3.92	6.73	5.11	
174	25GF, P	6500	SIN	0.32	2	4	8.03	5.97	
175	25GF, P	6500	CV	0.5	1.97	3.94	8.39	5.89	
184	UF, T	6500	SIN	0.32	2	4	7.17	4.87	
185	UF, T	6500	CV	0.5	1.98	3.96	7.27	4.51	

Table 5-II Effect of Specimen Size (Pressure is 3,000 psi)

Test No.	Conditions	Diam. (in)	Freq. (Hz)	Amplit. (in)	Peak Velocity (in/s)	μ_B (%)	μ_s max (%)	Comments
92	UF, P, SIN	10	0.32	2	4	8.04	6.77	
156	UF, P, SIN	5	0.32	2	4	8.31	7.34	
95	UF, P, SIN	10	0.5	3	9.43	10.32	7.27	
159	UF, P, SIN	5	0.5	2.98	9.36	12.59	7.47	Stick-slip
120	15GF, P, SIN	10	0.32	2	4	9.18	7.72	
166	15GF, P, SIN	5	0.32	2	4	9.79	7.30	
123	15GF, P, SIN	10	0.5	2.98	9.36	11.15	8.49	
169	15GF, P, SIN	5	0.5	2.98	9.36	11.89	7.71	Stick-slip
146	25GF, P, SIN	10	0.32	2	4	8.52	8.00	
176	25GF, P, SIN	5	0.32	1.98	3.96	9.63	8.64	
149	25GF, P, SIN	10	0.5	2.98	9.36	10.95	9.42	
179	25GF, P, SIN	5	0.5	3	9.43	13.27	6.53	Significant stick-slip

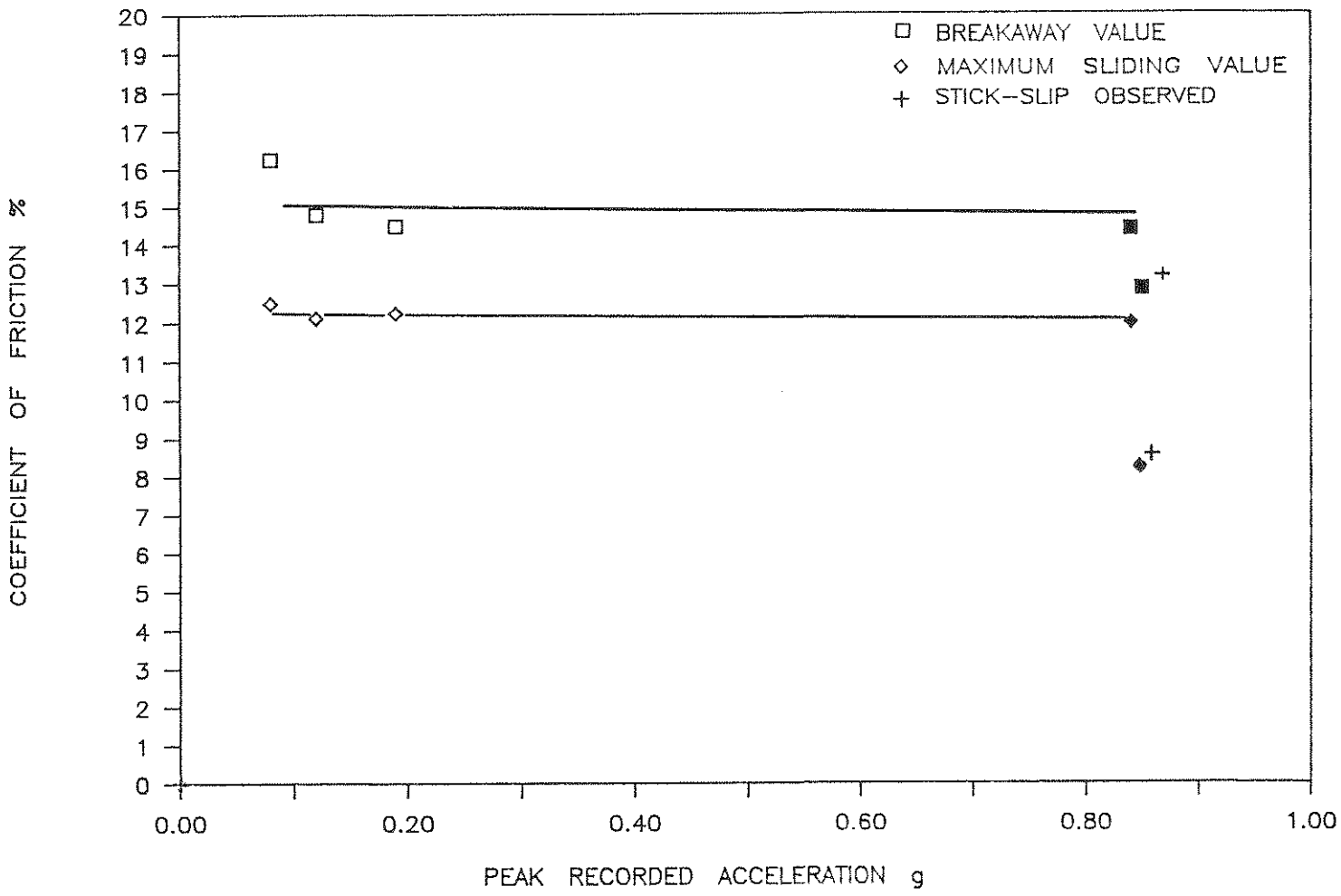

FIGURE 5-1 Effect of Acceleration on Breakaway and Maximum Sliding Coefficient of Friction

60). In each cycle, the Teflon-steel interface goes through two momentary phases of sticking when the displacement direction is reversed. This may have an effect on the initiation of stick-slip. Furthermore, there is a possibility that the frequency beyond which stick-slip occurs is related to the dynamic characteristics of the test apparatus rather than the interface characteristics.

In the cases in which stick-slip does not occur, frequency should not have any significant effect. Tests No. 51 to 53 were conducted at the same velocity (about 3.8 in/sec) and the recorded peak acceleration was about 0.32 g in all three tests. Frequency was 0.5, 1 and 0.25 Hz, respectively. The maximum sliding coefficients of friction in the three tests compare well. The breakaway value in test No. 53 appears to be higher than the other two tests. The initial condition of the interface might have been different in this test. In general, the frequency of test does not have any significant effect on the results provided that is not high enough to induce stick-slip.

5.6 Effect of Velocity

It is apparent from the results of Table 4-I that the coefficient of friction increases rapidly with sliding velocity up to a certain value of velocity beyond which it remains almost constant.

We first focus on the sliding (or kinetic) coefficient of friction. Figures 5-2 through 5-5 show the variation of μ_{smax} with velocity in the four groups of tests (UF, P; 15GF, P; 25GF, P; UF, T). The value of friction at very low velocity (0.1 in/sec) is between 0.01 and 0.03 for unfilled Teflon and between 0.02 and 0.06 for glass-filled Teflon. At high velocities, the value of friction is in both cases between 0.06 and 0.14, depending on the bearing pressure. The velocity at which maximum friction occurs (sliding value) is between 4 and 8 in/sec. Above this value, sliding velocity has relatively little effect. The difference between minimum and maximum value of sliding friction is larger at low bearing pressure. For example, in the case of unfilled Teflon with sliding parallel to lay (Figure 5-2) the minimum value is 0.027 and the maximum is about 0.12. Such a four-fold increase is substantial and indicates the significant deviation of the frictional behavior of these interfaces from Coulomb's theory.

The breakaway value of the coefficient of friction is examined next. This value appears to be substantially larger than the sliding value. The authors believe that the significance of the breakaway value at high velocities of sliding has been overstated (eg. Reference 13). Under laboratory conditions, a Teflon-steel interface may be subjected to high initial velocities that are associated with an impulse of acceleration (see Appendix A, tests No. 56, 57, 58). In the field, however, such conditions are very unlikely or impossible. **Sliding initiates (breakaway) at essentially zero velocity.** This condition also occurs at each reversal of motion, as during reversal, the interface undergoes a momentary sticking. There is, however, a difference between the two cases because the latter case occurs after some transfer of Teflon to the slider, which tends to reduce friction.

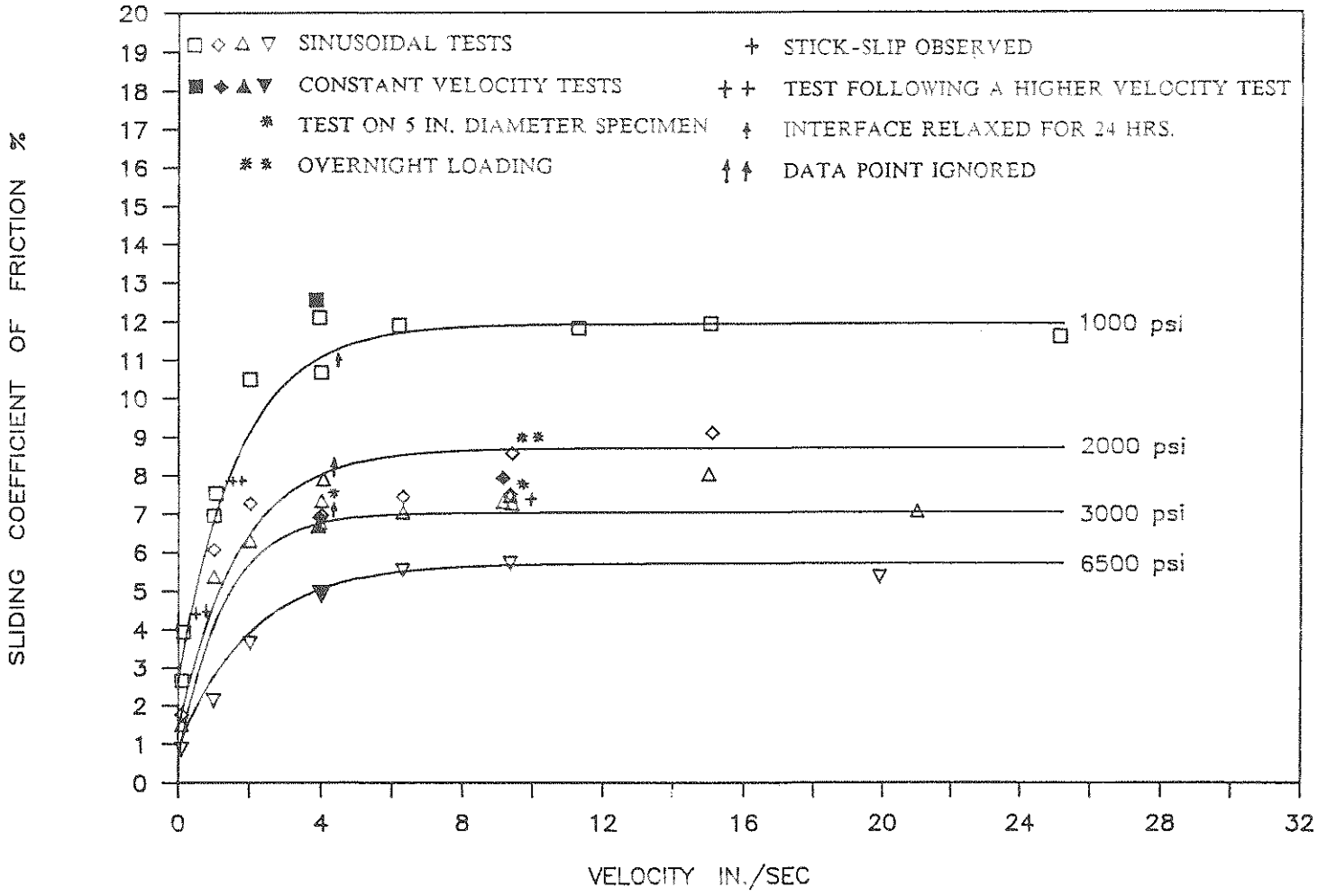

FIGURE 5-2 Variation of Maximum Sliding Coefficient of Friction With Velocity of Unfilled Teflon Sliding Parallel to Lay

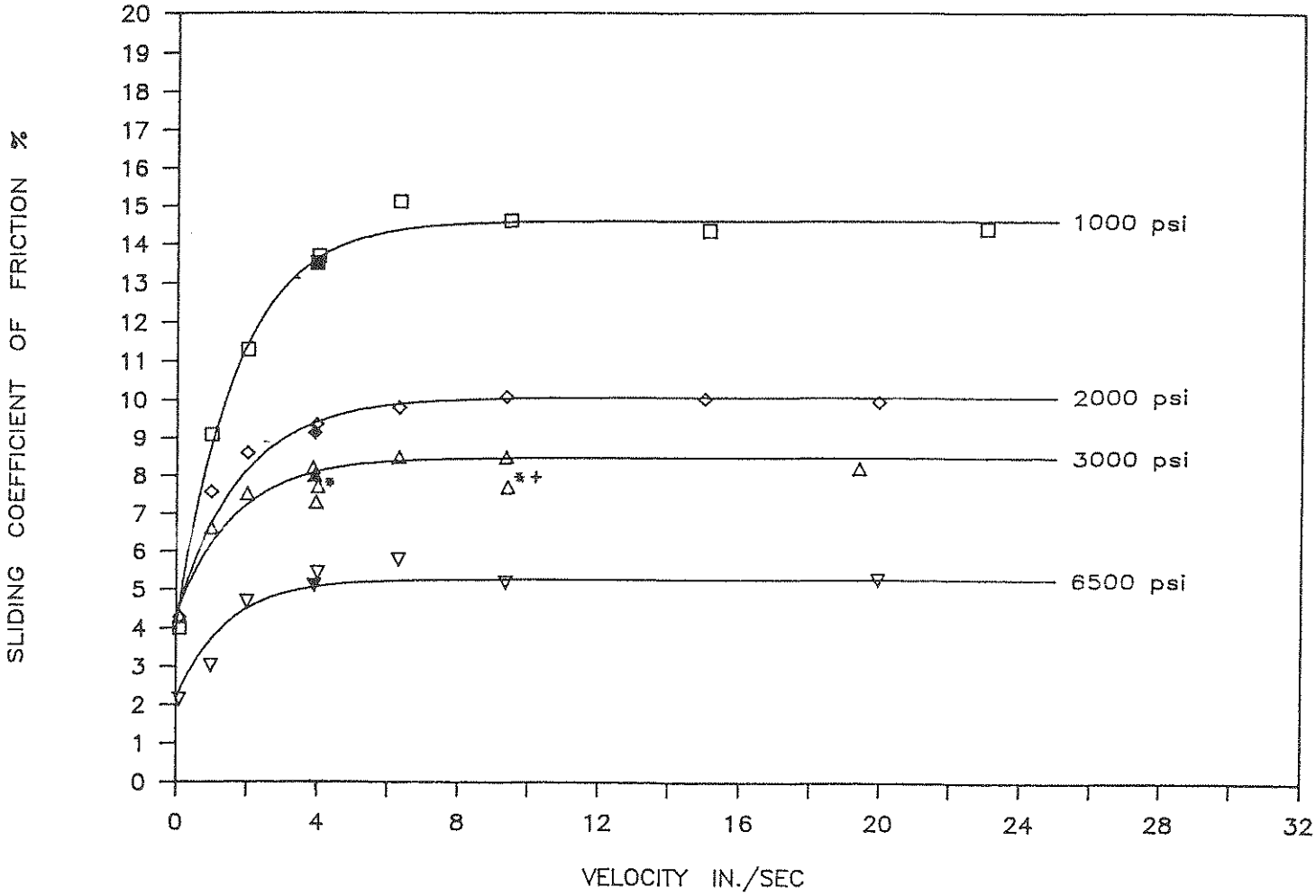

FIGURE 5-3 Variation of Maximum Sliding Coefficient of Friction With Velocity of Glass-Filled Teflon at 15% Sliding Parallel to Lay

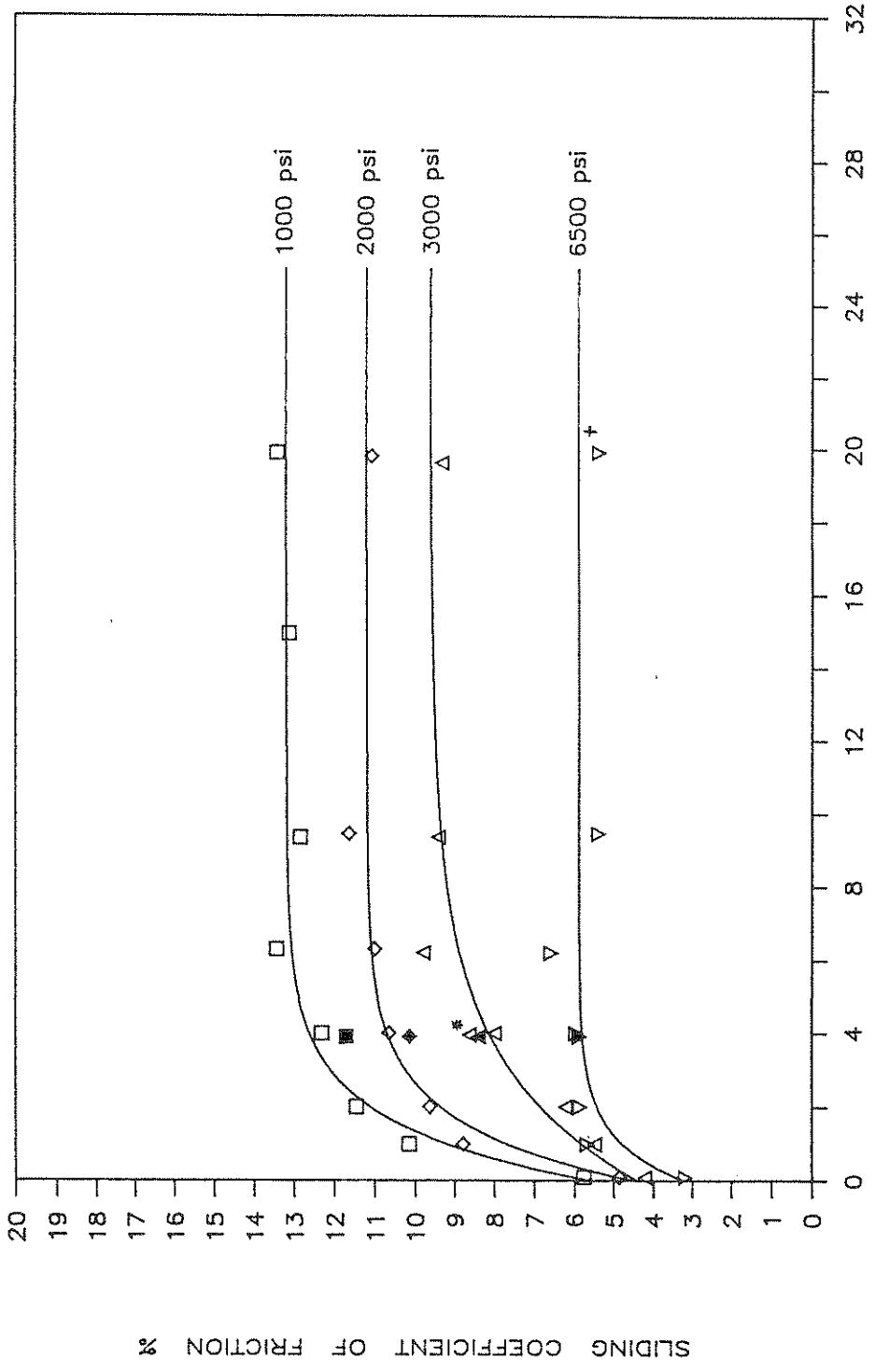

FIGURE 5-4 Variation of Maximum Sliding Coefficient of Friction With Velocity of Glass-Filled Teflon at 25% Sliding Parallel to Lay

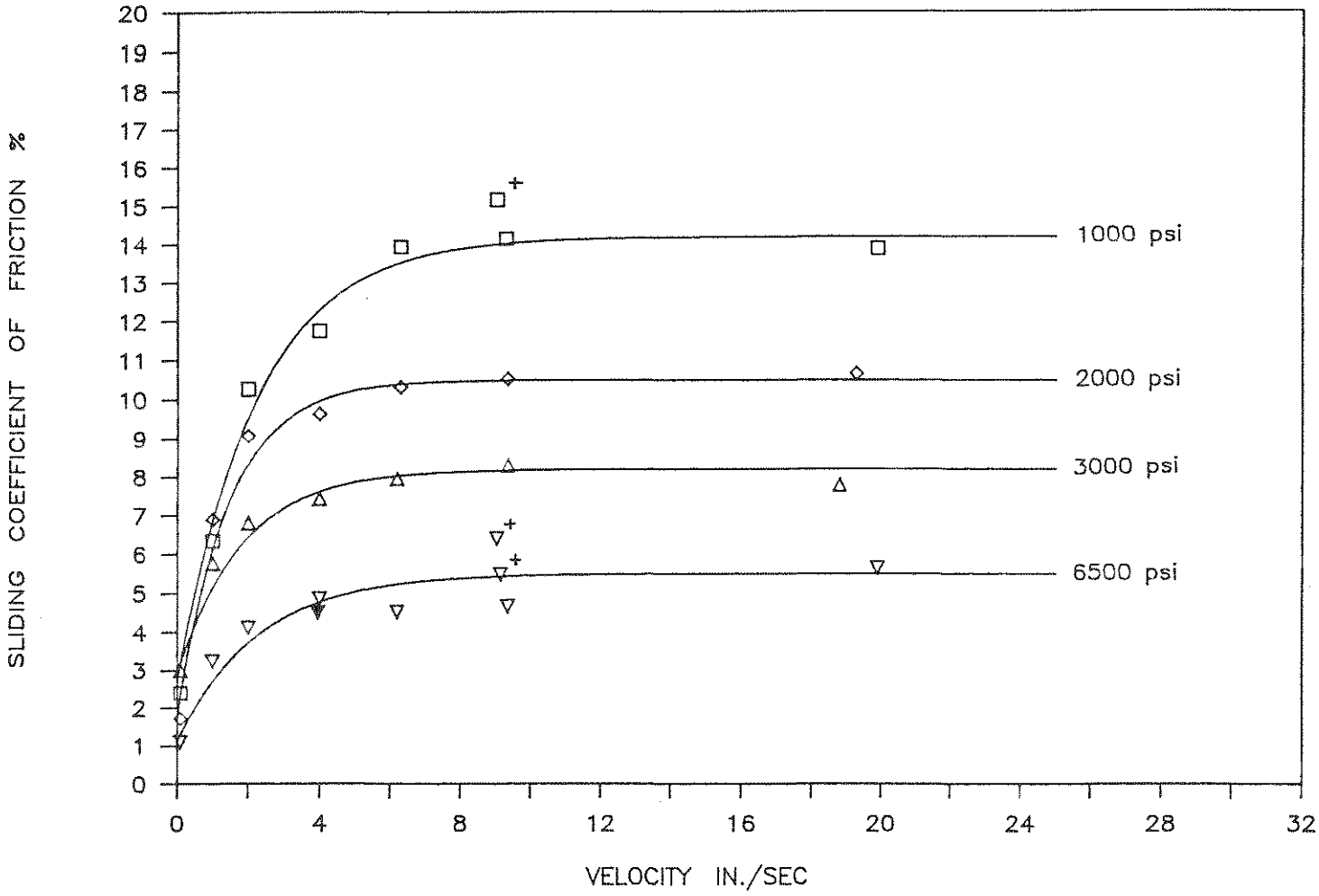

FIGURE 5-5 Variation of Maximum Sliding Coefficient of Friction With Velocity of Unfilled Teflon Sliding Perpendicular to Lay

The authors assert that only the breakaway value of friction at very low velocity is of interest. This value dictates if sliding or not will occur. When sliding occurs, the frictional resistance of the interface is characterized by the value of μ_{smax}, which depends on velocity. After momentary sticking at motion reversals, the interface exhibits a value of friction that may be conservatively taken to be equal to the breakaway value at very low velocity (eg. μ_B at 0.1 in/sec velocity). Alternatively, the increase in friction after this momentary sticking may be disregarded.

5.7 Effect of Pressure

Figures 5-6 to 5-9 show the variation of the recorded sliding coefficient of friction, μ_{smax}, with pressure for unfilled and glass-filled Teflon at velocities of 0.1, 1, 4 and above 10 in/sec. As expected, the coefficient of friction reduces with increasing pressure. The pressure at which levelling off occurs depends on the sliding velocity. This limit value of pressure increases with increasing velocity of sliding. At velocity of 0.1 in/sec, it is about 5000 psi. At velocities exceeding 10 in/sec, it appears to be larger than 6,500 psi. Furthermore, the rate of reduction of the sliding coefficient of friction with increasing pressure depends strongly on the sliding velocity. This rate is larger at a high velocity of sliding.

Figure 5-10 shows the variation of the breakaway value of the coefficient of friction with pressure at a velocity of 0.1 in/sec. In this case, levelling off occurs at a pressure of about 5000 psi. The trend is similar to that for the sliding coefficient of friction at sliding velocity of 0.1 in/sec.

There is one inconsistency in the data depicted in Figure 5-7. The recorded value of μ_{smax} at 0.1 in/sec velocity and pressure of 3,000 psi (test No. 207) appears to be twice as much as expected. In this test, the ratio of the breakaway to sliding value was much lower than in all other tests conducted at the same velocity (0.1 in/sec) on unfilled Teflon.

5.8 Effect of Surface Finish

Measurements of the surface roughness of the stainless steel plate in the two directions of parallel to lay (P) and perpendicular to lay (T) have shown that the roughness in the "T" direction was about 30% more than in the "P" direction. This is a small difference. The recorded values of friction in the latter case are less than in the former case (see Figures 5-2 and 5-5 to 5-7). The difference diminishes at 6,500 psi pressure. At the pressure of 1,000 psi, the recorded friction in the "P" direction is about 15% less than that in the "T" direction.

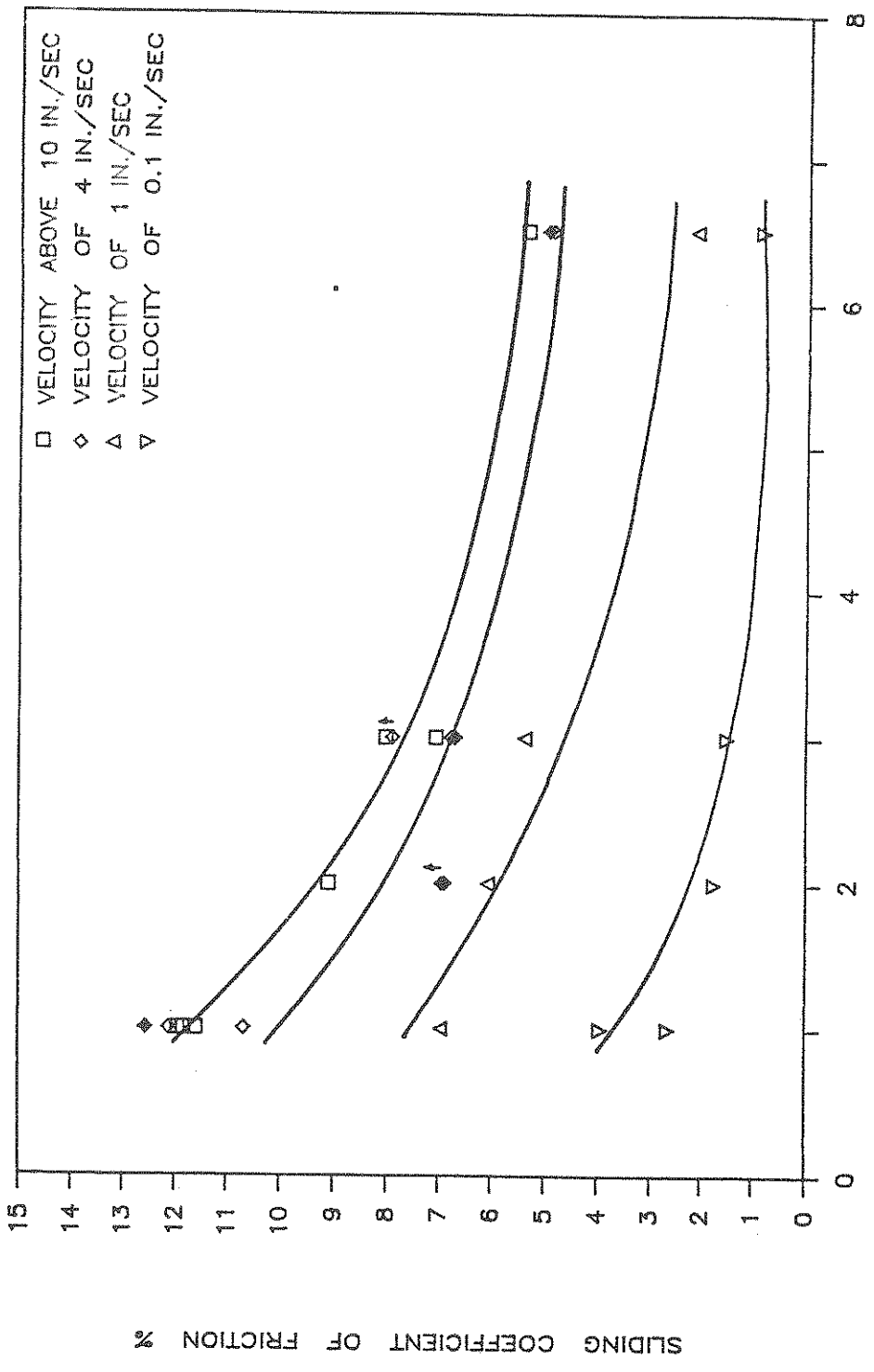

FIGURE 5-6 Effect of Bearing Pressure on Maximum Sliding Coefficient of Friction of Unfilled Teflon Sliding Parallel to Lay

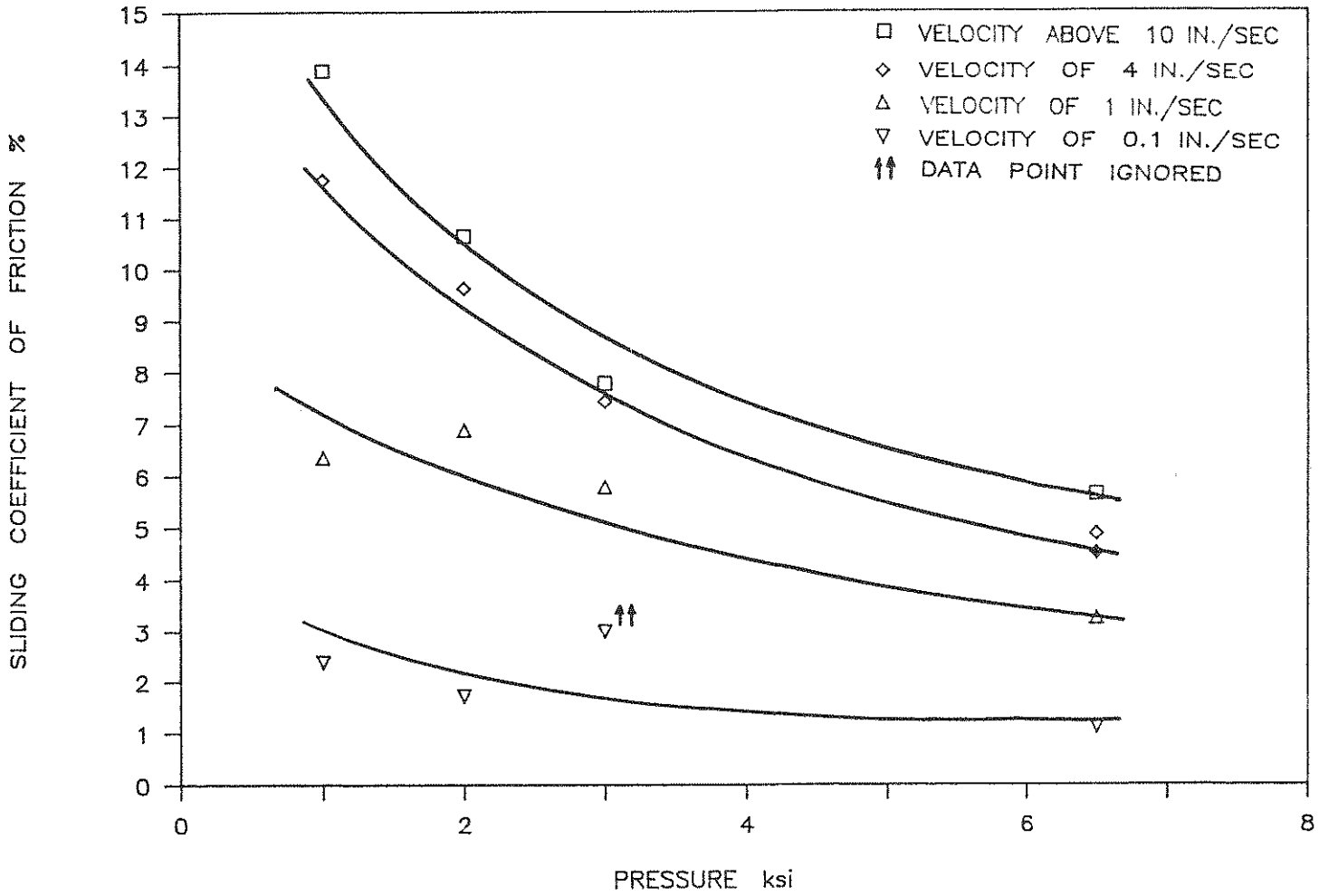

FIGURE 5-7 Effect of Bearing Pressure on Maximum Sliding Coefficient of Friction of Unfilled Teflon Sliding Perpendicular to Lay

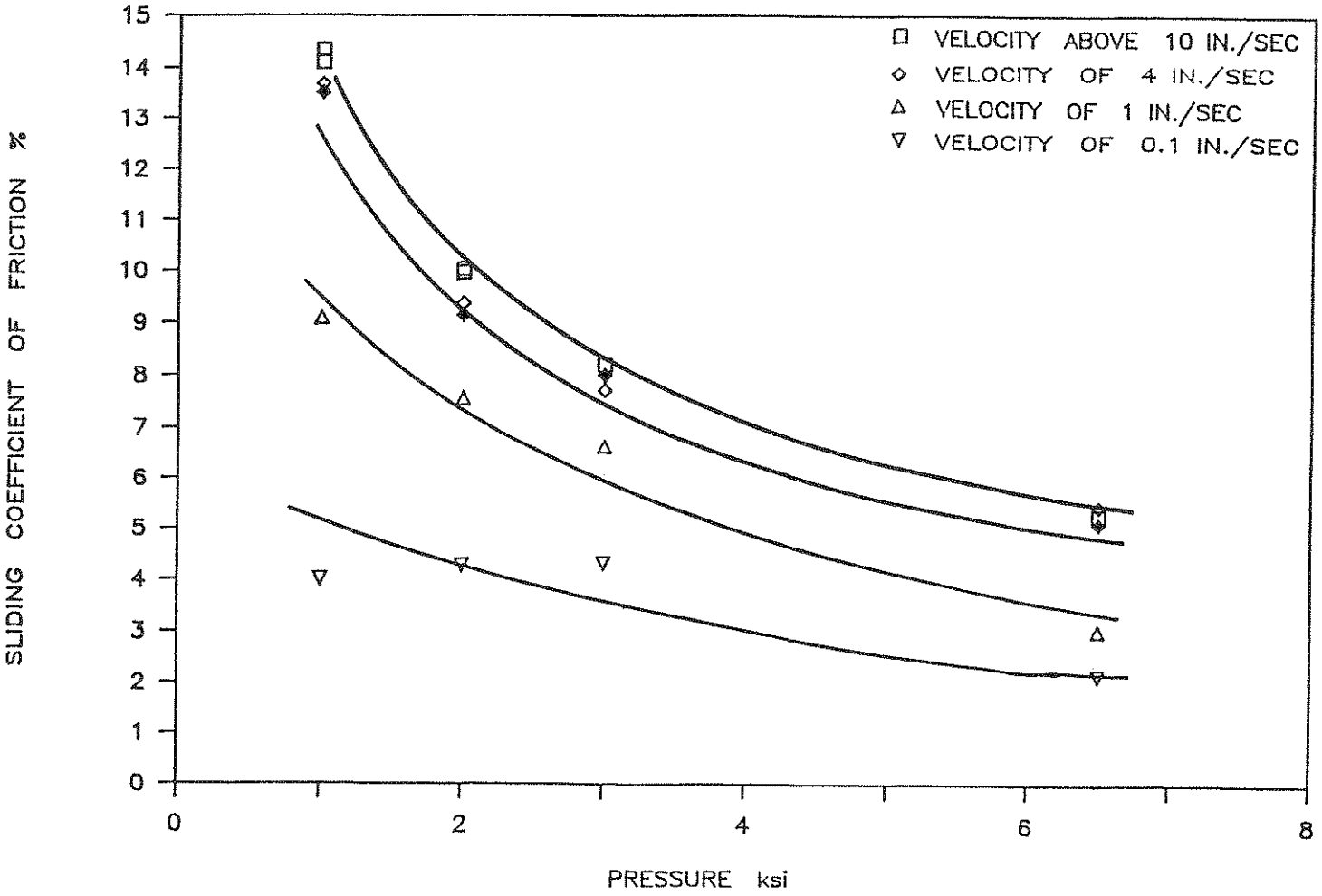

FIGURE 5-8 Effect of Bearing Pressure on Maximum Sliding Coefficient of Friction of Glass-Filled Teflon at 15% Sliding Parallel to Lay

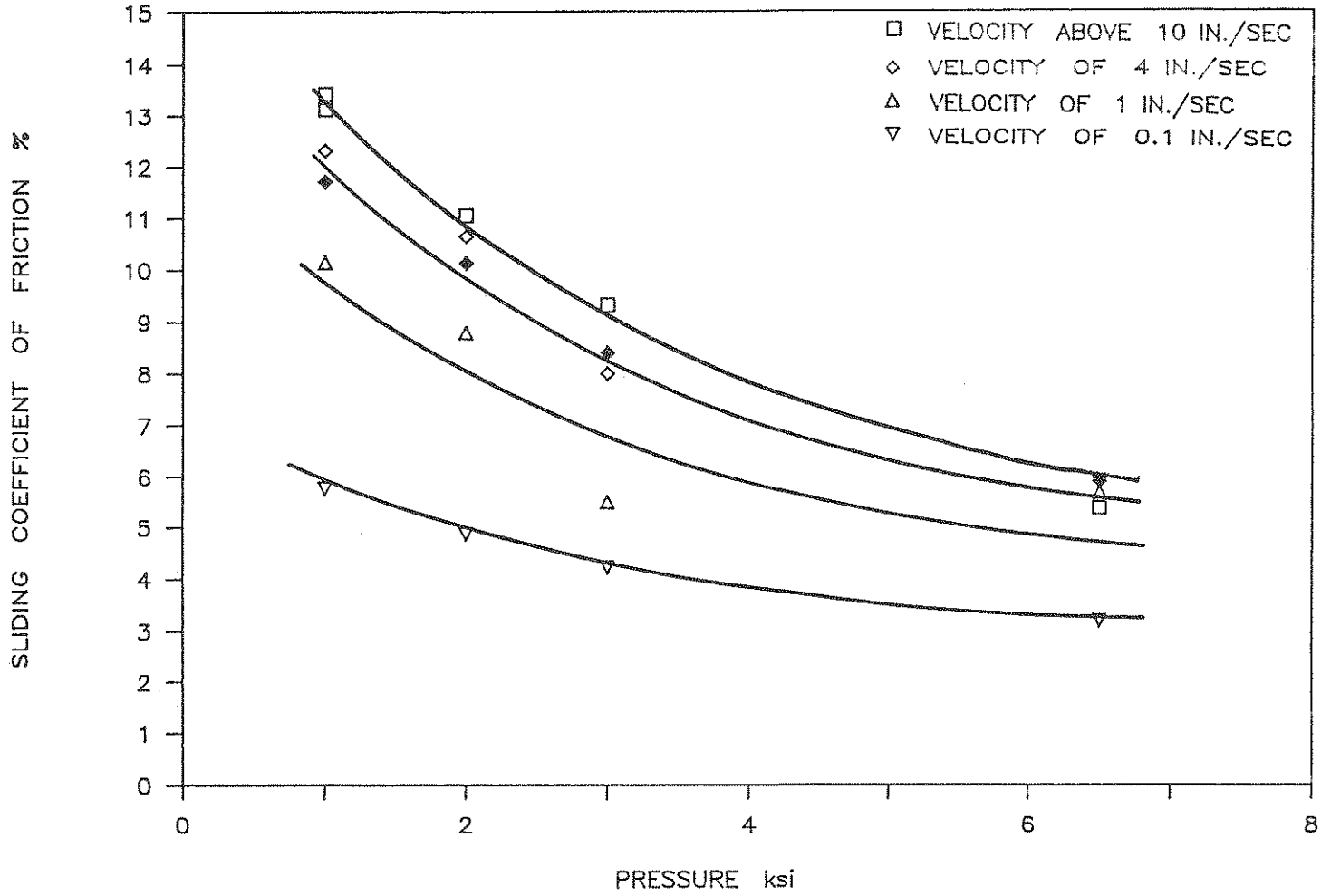

FIGURE 5-9 Effect of Bearing Pressure on Maximum Sliding Coefficient of Friction of Glass-Filled Teflon at 25% Sliding Parallel to Lay

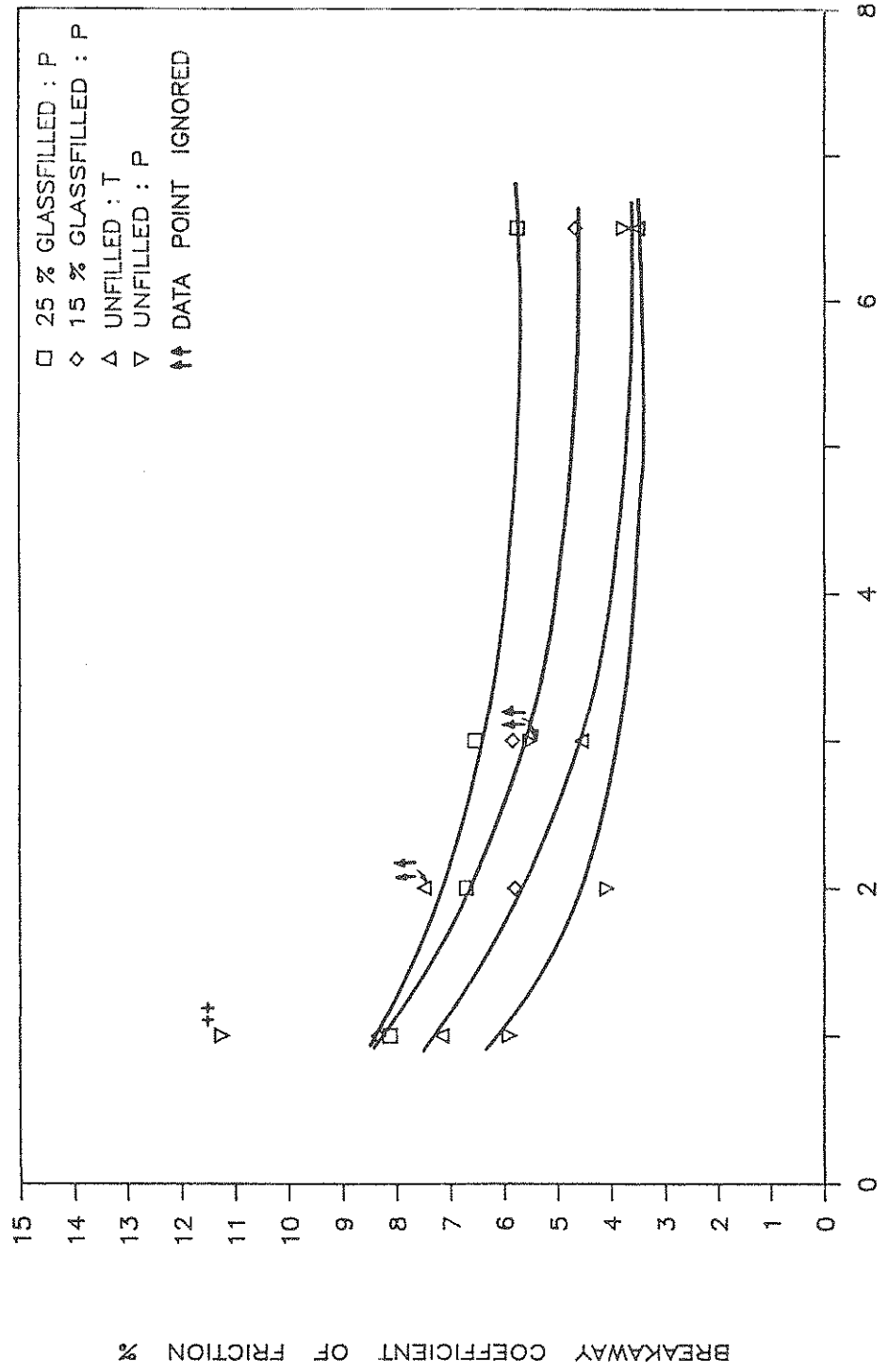

FIGURE 5-10 Effect of Bearing Pressure on Breakaway Coefficient of Friction at Very Slow Velocity (0.1 in./sec.)

5.9 Effect of Type of Teflon

The addition of glass filler to Teflon results in an increase in breakaway and sliding coefficient of friction that appears to be related to the quantity of filler and bearing pressure. At a pressure of 6,500 psi, the coefficient of friction is practically unaffected by the amount of filler. At lower pressures, glass filled Teflon exhibits higher friction than unfilled Teflon. The difference appears to increase with decreasing pressure.

The amount of glass filler has a rather complicated effect on friction. At a pressure of 1,000 psi, friction of 15% glass filled Teflon is higher than that of 25% glass filled. The opposite is observed at higher pressures.

5.10 Comparison With Other Studies

Comparison of experimental data obtained by different researchers is important but difficult because in many cases, the conditions under which the tests are conducted are inadequately reported. One cannot ignore the influence a laboratory test method may have on the recorded data.

One of the earliest studies of Teflon-steel interfaces was reported by Thompson et al [9]. The apparatus used in the Thompson studies has been described in the Introduction. Tests were conducted on unfilled Teflon sliding against stainless steel of an R_q value (RMS) of 2μin (0.05μm) and velocity of about 0.1 in/sec. The conditions appear to be very close to those in our tests conducted with the direction of sliding parallel to the lay. Table 5-III compares the two sets of data. The comparison is very good.

Taylor's [10] experiments were conducted on interfaces that have been run-in previously at high pressure. Only one test has been conducted on fresh unfilled Teflon mating with stainless steel of R_a roughness of 0.025 to 0.05μm. At a very low speed (0.0008 in/sec) and pressure of 5,000 psi, the recorded value of breakaway coefficient of friction was 0.028. Interpolating our results, a value of 0.04 to 0.045 at a velocity of 0.1 in/sec is obtained. The two values compare favorably when considering that the roughness in these tests was about twice that in Taylor's experiments (velocity may had an influence as well).

Tyler's study [13] is certainly the most interesting one as it has been carried out at conditions of interest in base isolation. Tyler did not take measurements of the stainless steel surface roughness but rather assumed that is in the range of 0.05 to 0.15μm in the R_a scale (mirror finish). The tests were conducted at different frequencies and amplitudes than the tests in this study. Furthermore, Tyler concentrated on the breakaway value of the coefficient of friction which appears to be sensitive to the interface condition at the start of each experiment.

Table 5-III Comparison of Sliding Coefficient of Friction in Thompson's Tests [9] and Our Tests

Pressure (psi)	Coefficient of Friction at 0.1 in/sec	
	Thompson	Ours (μ_{smax})
1000	0.022	0.027
2000	0.017	0.017
3000	0.016	0.015

A comparison of some data from this study to those obtained by Tyler is presented in Table 5-IV. Only pressure and peak velocity are shown in the table, which are the most influential parameters. Data from this study has been compiled from the data obtained in the parallel and perpendicular to lay direction of sliding. The two sets of data compare quite well.

Table 5-IV Comparison of Breakaway Coefficient of Friction in Tyler's Tests [13] and Our Tests

Tyler			Ours		
Pressure* (psi)	Peak Velocity** (in/sec)	μ_B	Pressure (psi)	Peak Velocity (in/sec)	μ_B
1100	3.74	0.135	1000	~4	0.136-0.188
1100	14.76	0.178	1000	15	0.178
1100	14.76	0.176[t]			
2100	5.33	0.129	2000	4-6.28	0.101-0.132
2100	8.90	0.105	2000	~9.4	0.124-0.143
2100	14.76	0.119	2000	~9.4	0.142[t]
2100	14.76	0.155[tt]	2000	15	0.158
3300	2.50	0.070	3000	2	0.074-0.078
3300	14.76	0.116	3000	14.97	0.117

t Loaded Overnight

tt Loaded for 2 1/4 hours

* Approximate Value

** Calculated from Frequency and Stroke

SECTION 6
MATHEMATICAL MODELING

It has been known and further demonstrated in this experimental study that Teflon-steel interfaces do not behave according to Coulomb's law of friction. The dependency of the coefficient of friction on the sliding velocity and bearing pressure is significant enough to warrant consideration of these factors on the dynamic response of sliding isolation systems.

The coefficient of sliding friction at sliding velocity $\dot{u}$ may be approximated by the following equation:

$$\mu_s = f_{max} - Df \exp(-a|\dot{u}|) \tag{6-1}$$

in which f_{max} is the coefficient of friction at large velocity of sliding (after levelling off) and Df is the difference between f_{max} and the sliding value at very low velocity. Furthermore, a is a constant for given bearing pressure and condition of interface. Table 6-I presents values of f_{max}, Df and a for various conditions of Teflon-steel interface and pressure that resulted in the solid line curves in Figure 5-2 to 5-5. It is apparent that Equation 6-1 reproduces with good accuracy the results of experiments.

For dynamic analysis of sliding isolation systems, Equation 6-1 may be used to adjust the coefficient of friction according to the value of the sliding velocity. The incorporation of breakaway and reversal friction may be done by adjustment of μ_s to a higher value (by a factor of 2 to 3) at initiation of sliding. Furthermore, the effect of fluctuations in the bearing pressure may be incorporated by continuously adjusting the values of f_{max}, Df and a (use of interpolation in this case is necessary). Fluctuations in the bearing pressure are caused by the vertical component of ground motion and by overturning moments in slender systems.

6.1 Modified Coulomb Model

The analysis of motion with friction in a single plane direction is relatively easy. This kind of motion arises in symmetric structural systems with the ground motion consisting of components lying in a vertical plane. The analysis of this kind of motion has been the subject of numerous investigations [42-44, 49, 68]. All these studies utilized Coulomb's model of friction.

When the frictional interface consists of Teflon bearings, the analysis may be performed by the procedures presented in References 42-44, 49 and 68 with the frictional force, F_f, described by the following equation:

$$F_f = \mu_s W \mathrm{sgn}(\dot{u}) \tag{6-2}$$

Table 6-I Constants f_{max}, D_f and a

Type of Teflon	Pressure (psi)	Sliding Direction	f_{max} (%)	D_f (%)	a (sec/in)
UF	1000	P	11.93	9.27	0.60
UF	2000	P	8.70	6.95	0.60
UF	3000	P	7.03	5.52	0.80
UF	6500	P	5.72	4.85	0.50
15GF	1000	P	14.61	10.60	0.60
15GF	2000	P	10.08	5.80	0.55
15GF	3000	P	8.49	4.17	0.60
15GF	6500	P	5.27	3.12	0.70
25GF	1000	P	13.20	7.66	0.65
25GF	2000	P	11.20	6.33	0.65
25GF	3000	P	9.60	5.20	0.32
25GF	6500	P	5.89	2.70	0.90
UF	1000	T	14.20	11.81	0.45
UF	2000	T	10.50	8.78	0.70
UF	3000	T	8.20	5.30	0.55
UF	6500	T	5.50	4.39	0.45

in which W is the weight of the system above the level of the bearings and μ_s is given by Equation 6-1. In this case, $\dot{u}$ is the velocity of the basemat of the isolated structure relative to the foundation slab. Equation 6-2 is, of course, valid during sliding of the interface. The transition from sticked to sliding mode of motion and vice versa is controlled by stick-slip conditions as described in References 42-44, 49 and 68. This model is referred to as the **Modified Coulomb Model.**

6.2 Modified Viscoplasticity Model

There are certain complications that arise in the use of the Modified Coulomb Model. The most important one arises in the use of the model for the analysis of systems with multiple support motion and in systems in which each Teflon bearing undergoes different motion than other bearings. This situation occurs in bridges in which Teflon bearings are placed on top of flexible piers. Situations like this require the use of multiple stick-slip conditions which control the transition from one mode of motion to another. Each one of these modes of motion is governed by different equations of motion.

A model that accounts for sticking and sliding by itself is presented herein. It is based on principles of the theory of viscoplasticity and it will be referred to as the **Modified Viscoplasticity Model**. This model is based on the following equation which was originally proposed by Bouc [69] and subsequently extended and used by Wen and co-workers [70, 71] in random vibration studies of hysteretic systems:

$$Y\dot{Z} + \gamma|\dot{u}|Z|Z|^{n-1} + \beta\dot{u}|Z|^{n} - A\dot{u} = 0 \tag{6-3}$$

in which $\dot{u}$ stands for the velocity, Z is a hysteretic dimensionless quantity and β, γ, A and η are dimensionless constants. Furthermore, Y represents a displacement quantity. Constantinou and Adnane [72] have shown that when A=1 and $\beta + \gamma = 1$, the model of Equation 6-3 collapses to a model of viscoplasticity that was proposed by Ozdemir [73]. In this case, Y represents the yield displacement while η controls the mode of transition into the inelastic range. The model exhibits a rate dependency which reduces with increases in the value of exponent η and/or increases in the ductility ratio.

The frictional force is given by

$$F_f = \mu_s ZW \tag{6-4}$$

which is essentially identical to Equation (6-2). It should be noted that during sliding (yielding), Z takes values of ± 1. During sticking (elastic behavior), the absolute value of Z is less than unity. The conditions of separation and reattachment are accounted for by Equation 6-3.

A problem with the viscoplasticity model is its inability to reproduce truly rigid-plastic behavior. However, Teflon-steel interfaces undergo some very small elastic displacement before sliding. This elastic displacement, that is apparent in the hysteresis loops in Appendix A, is partially elastic deformation of Teflon and partially elastic deformation of the stainless steel plate. Appropriate values for the yield displacement, Y, are in the neighborhood of 0.005 inches. With such low yield displacement, the resulting ductility ratio (max. displacement to yield displacement) is very large. As such, the model exhibits an insignificant rate dependency and the value $\eta=2$ together with $\beta=0.1$ and $\gamma=0.9$ produces hysteresis loops that are in good accord with experimental results.

Figure 6-1 presents hysteresis loops produced by the viscoplasticity model of Equations 6-1, 6-3 and 6-4. The results in this figure were produced by numerically simulating experiments No. 62 and 75 (see Appendix A). These tests were conducted on unfilled Teflon, in the parallel to lay direction and at 1,000 psi pressure. Apart from the regions around breakaway and reversal of motion, the model reproduces well the experimental results. The incorporation of breakaway and reversal friction in this model is currently under investigation.

The two models, modified Coulomb and modified viscoplasticity, are compared in the following simple example. A rigid mass is assumed to be supported on Teflon-steel interfaces at a bearing pressure of 2,000 psi (conditions UF and P). The mass is excited by ground motion which consists of the first 10 secs of the S00E component of the 1940 El Centro earthquake. Figure 6-2 presents time histories of the sliding displacement, U, and total acceleration, $\ddot{U}_t$, of the mass. The agreement between the results of the two models is very good. Of interest is to note the small difference in the total acceleration at the start of the motion and in the interval of 6 to 8 secs. During these intervals, the system responds in the sticked mode. In the modified viscoplasticity model, sticking is accounted for by very small amplitude vibration in the elastic range. This explains the small difference in the responses as calculated by the two models. Suppression of this elastic vibration may be accomplished by introduction of viscous damping that acts only in the elastic range of response of the viscoplasticity model.

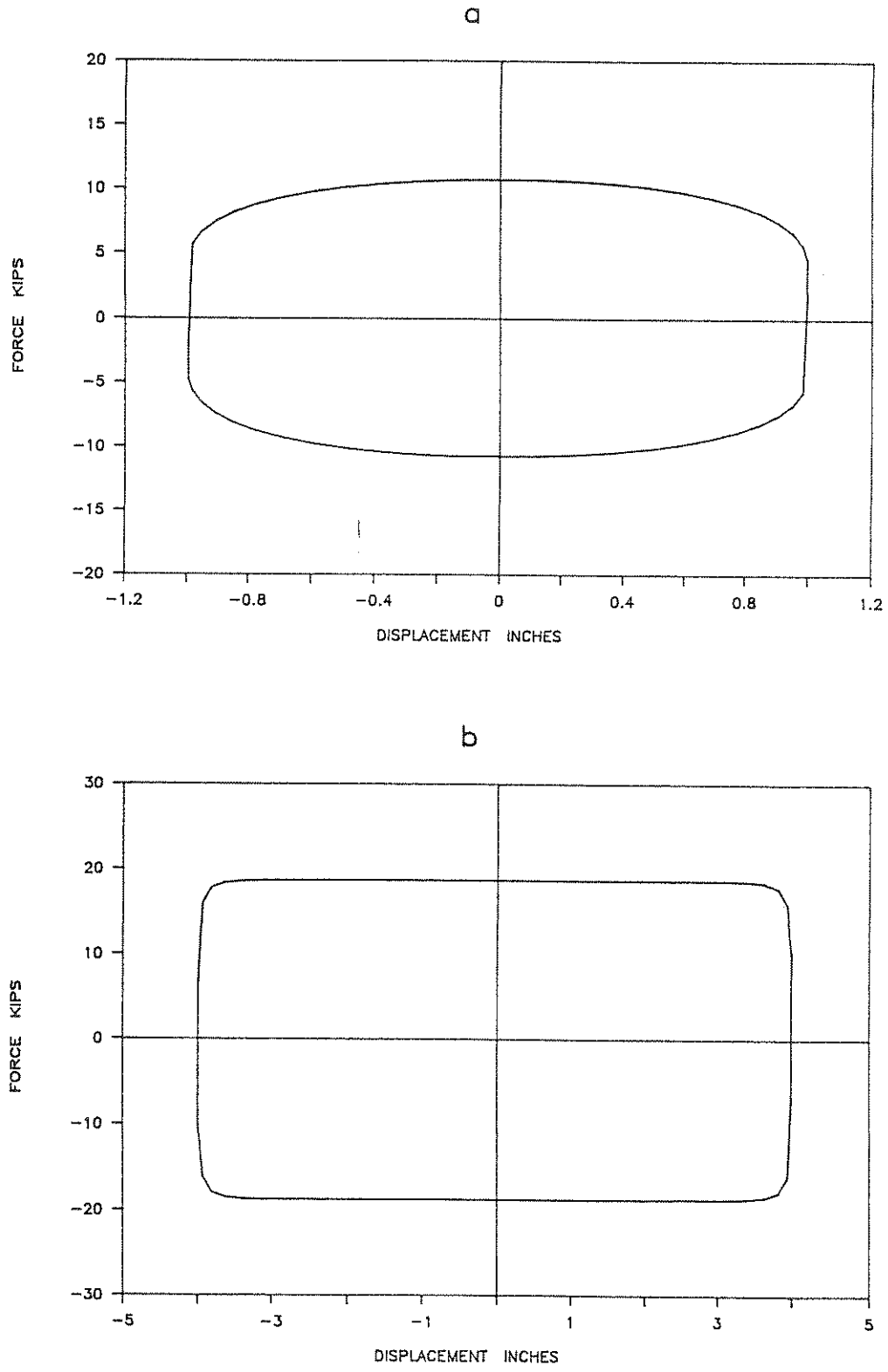

FIGURE 6-1 Numerical Simulation of Experiments (a) No. 62 and (b) No. 75

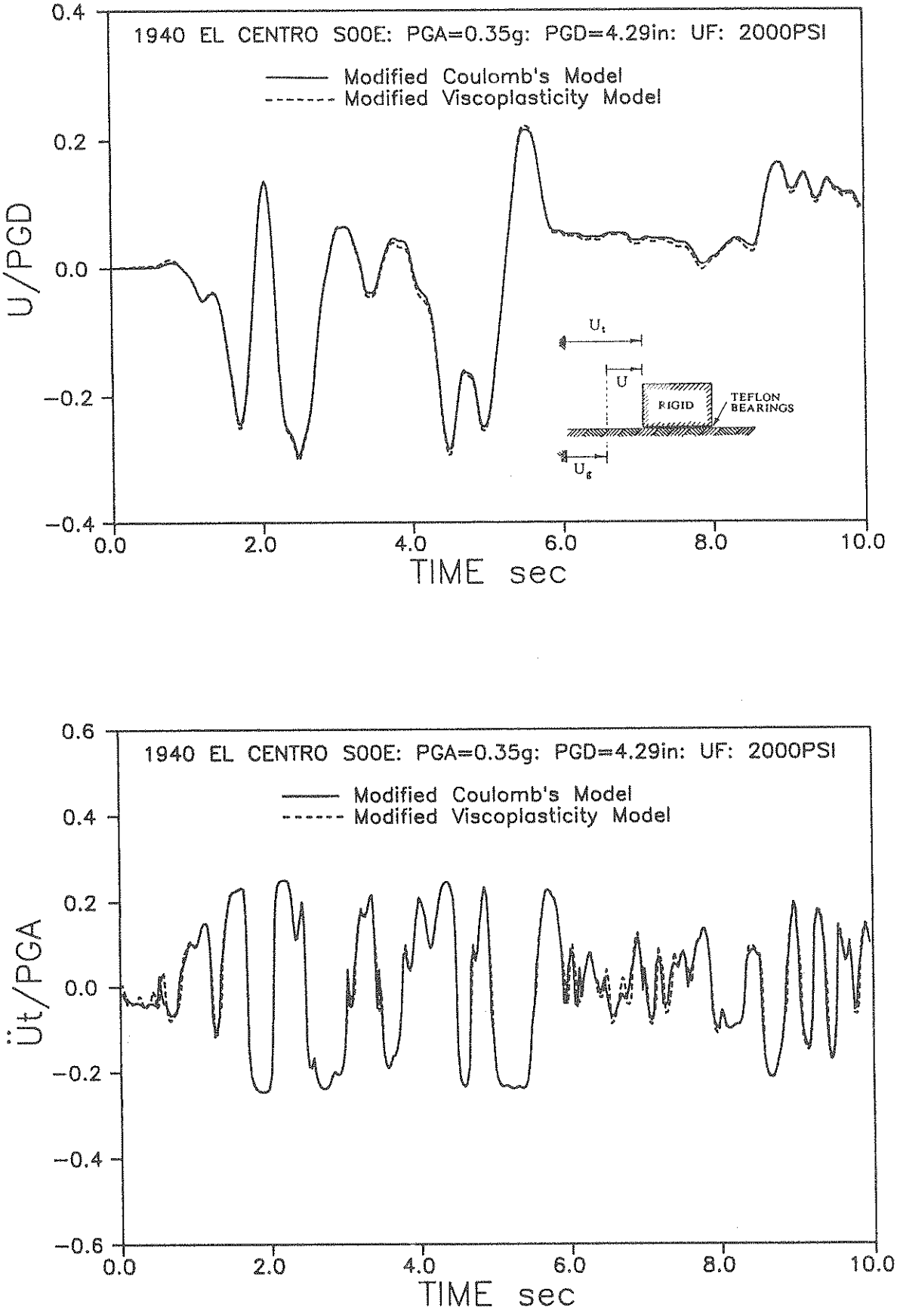

FIGURE 6-2 Time Histories of Displacement and Total Acceleration of Rigid Mass as Computed by Modified Coulomb and Modified Viscoplasticity Models

SECTION 7
APPLICATION OF RESULTS

In this section, the proposed model of friction of Teflon-steel interfaces is applied in the analysis of base-isolated structures that incorporate such interfaces together with centering force devices.

7.1 Comparison of Proposed Model to Coulomb's Model

The implications of using Coulomb's model of friction in the analysis of structures supported by Teflon bearings are demonstrated with the following example. A rigid structure is considered supported on Teflon bearings at a pressure of 1,000 psi. The conditions at the interface are, those of unfilled Teflon with the sliding direction parallel to the lay. The ground is excited by sinusoidal acceleration of amplitude $\ddot{U}_{go}$ and circular frequency w. Figure 7-1 shows the sliding displacement, U, and total acceleration, $\ddot{U}_t$, time histories of the rigid structure when $\ddot{U}_{go}$=0.05g and w=π rad/sec. The solid line represents the exact response when accounting for the variation of the coefficient of friction with the velocity. The dashed lines show the response when using Coulomb's model with constant friction which takes either the minimum value (at zero velocity) or the maximum value (at high velocity) or an average value. In this case of "weak" excitation, the use of Coulomb's model with an average value of the friction coefficient results in responses that are close to exact.

Figure 7-2 shows the response of the rigid structure when the amplitude $\ddot{U}_{go}$ is increased to 0.25 g. In this case of "strong" excitation, the use of Coulomb's model with the maximum value of friction results in responses that are close to exact.

Finally, Figure 7-3 shows the response of the structure when excited with the S00E component of the El Centro earthquake. The use of Coulomb's model with maximum friction predicts the peak total acceleration quite accurately. The actual time history of the acceleration, however, is very different in the two models. Higher frequency content in the case of Coulomb's model with maximum friction is apparent in Figure 7-3d. This is apparently a consequence of more stick-slip tendencies in Coulomb's model. The displacement response (Figure 7-3a) is different in the four models. The Coulomb's model with maximum friction predicts a displacement response that approximates the exact one but with considerably more sticking.

The preceding example illustrates the significance of the variation of the friction force with velocity. The use of the constant friction Coulomb model may result in a useful estimation of the peak response only if an appropriate value of the coefficient of friction is used. This value depends on the resulting sliding velocity at the isolation interface, which itself depends on the characteristics of the structural system and of the excitation. Postulation of this velocity is certainly very difficult.

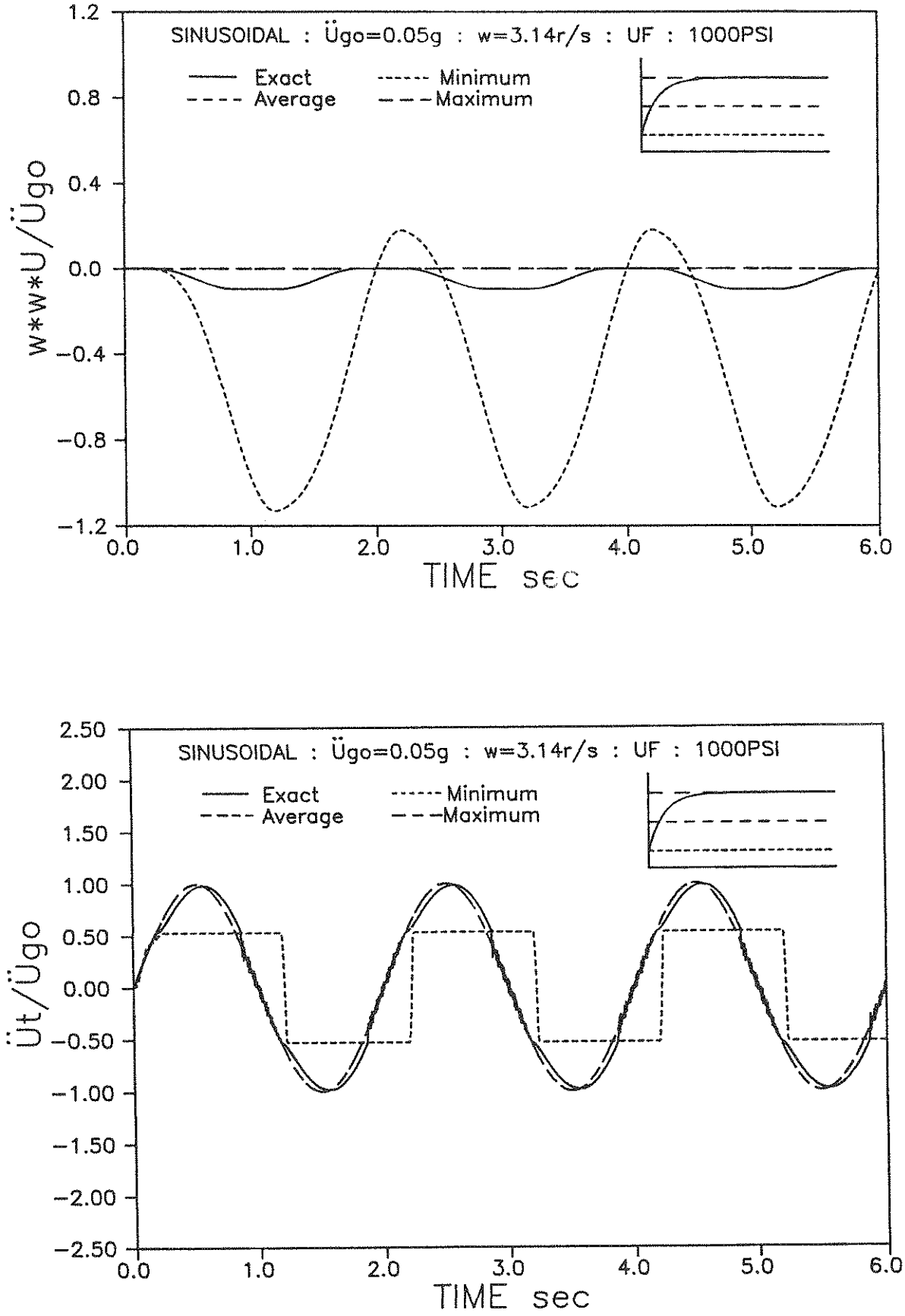

FIGURE 7-1 Comparison of Response of Rigid Mass as Computed by Proposed Model (Exact) and Coulomb's Model in the Case of "Weak" Harmonic Excitation

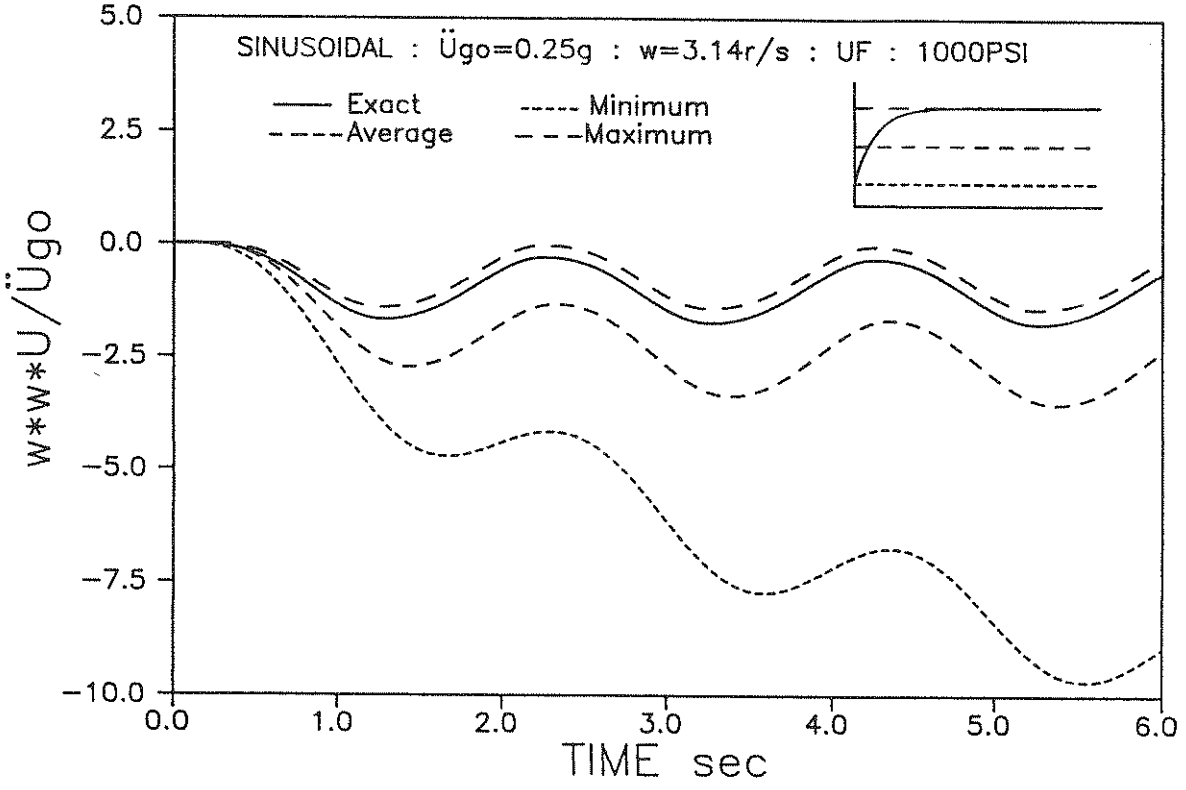

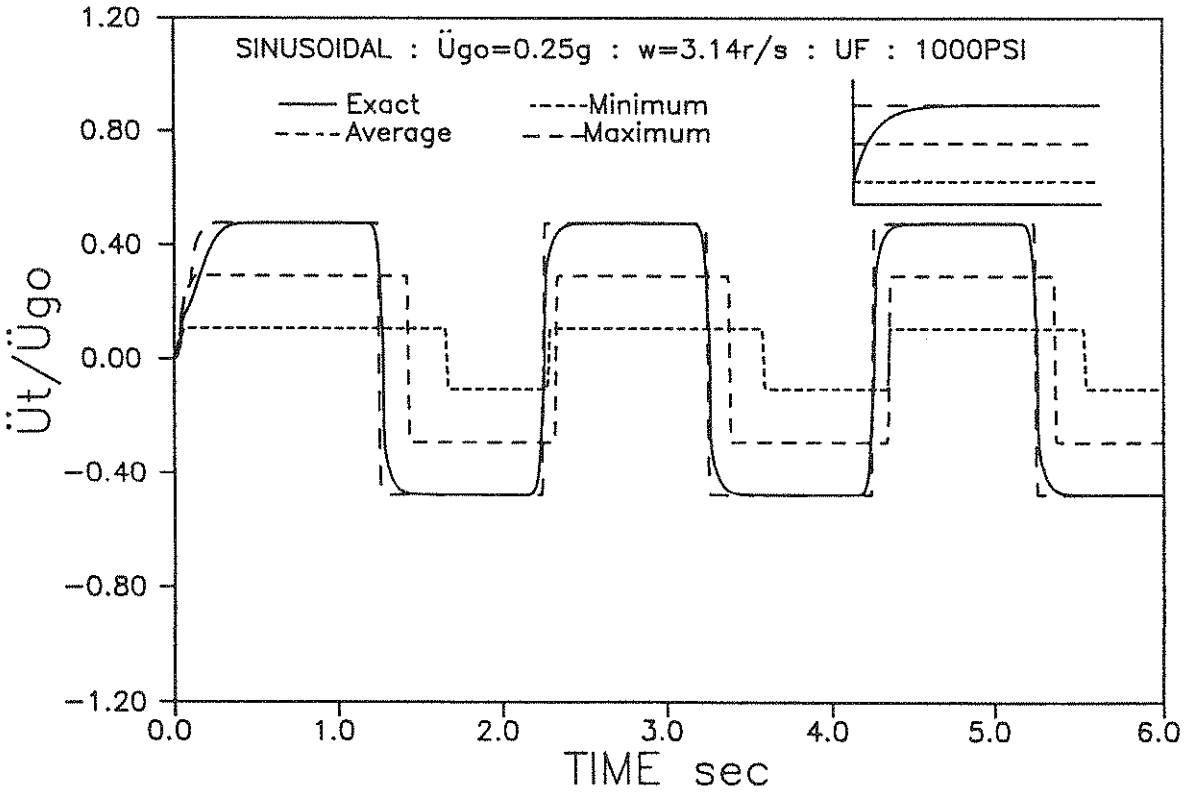

FIGURE 7-2 Comparison of Response of Rigid Mass as Computed by Proposed Model (Exact) and Coulomb's Model in the Case of "Strong" Harmonic Excitation

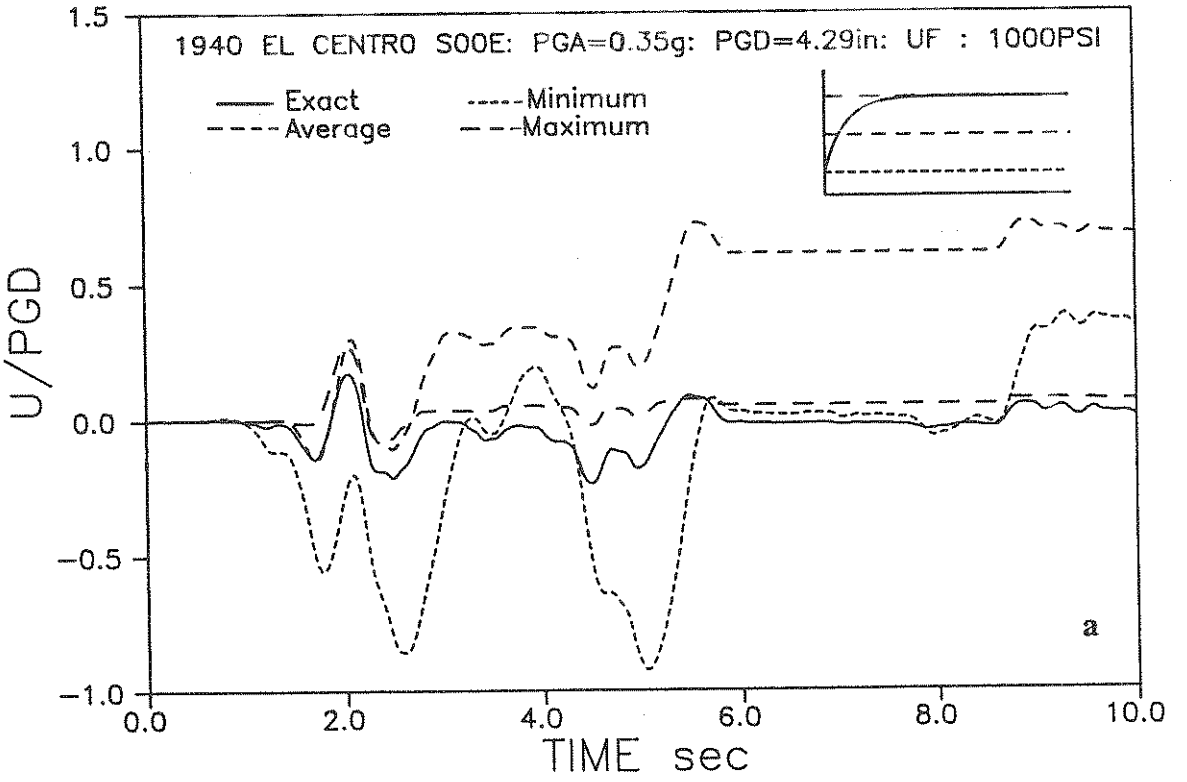

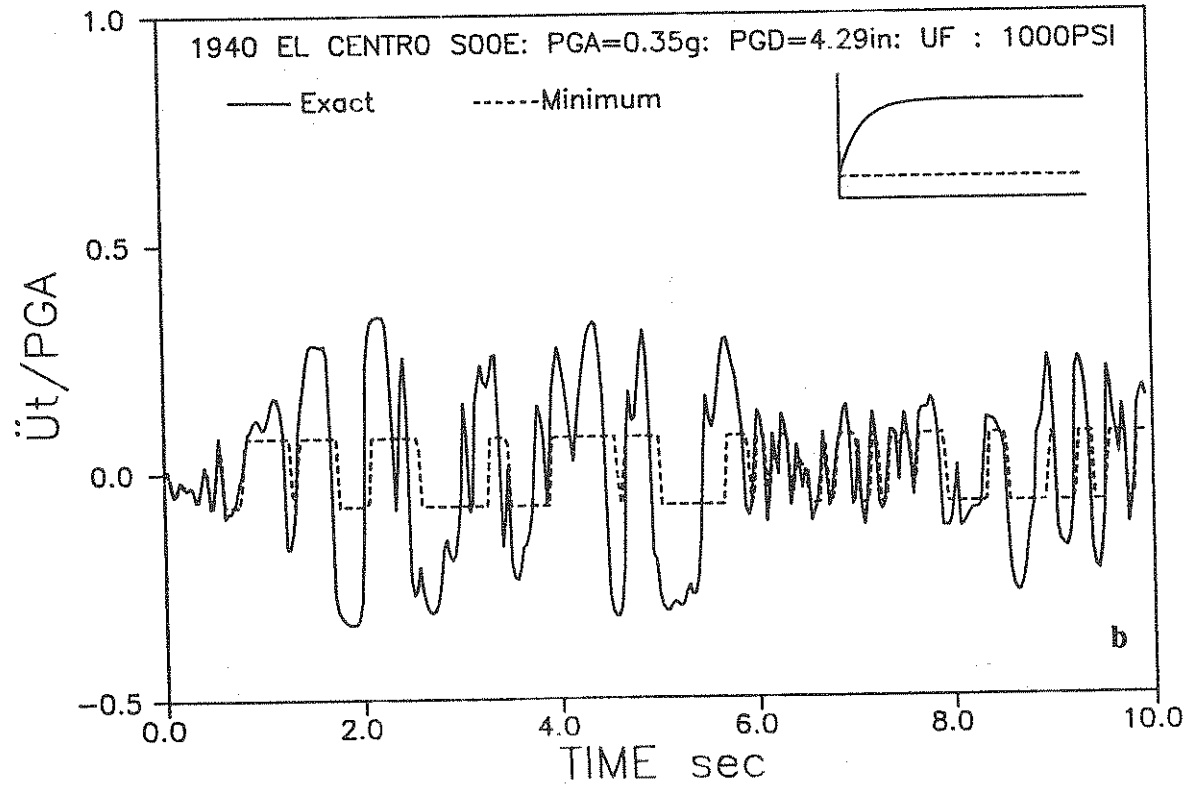

FIGURE 7-3 Comparison of Response of Rigid Mass Excited by El Centro as Computed by Proposed Model (Exact) and Coulomb's Model

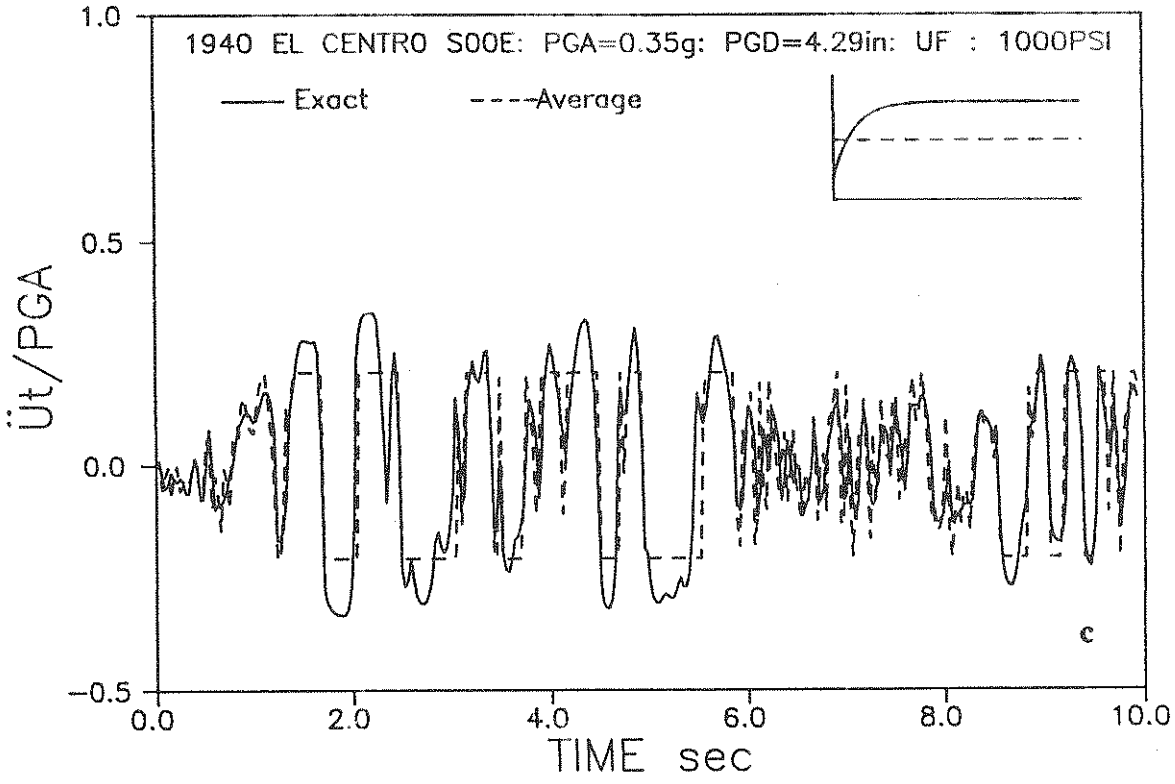

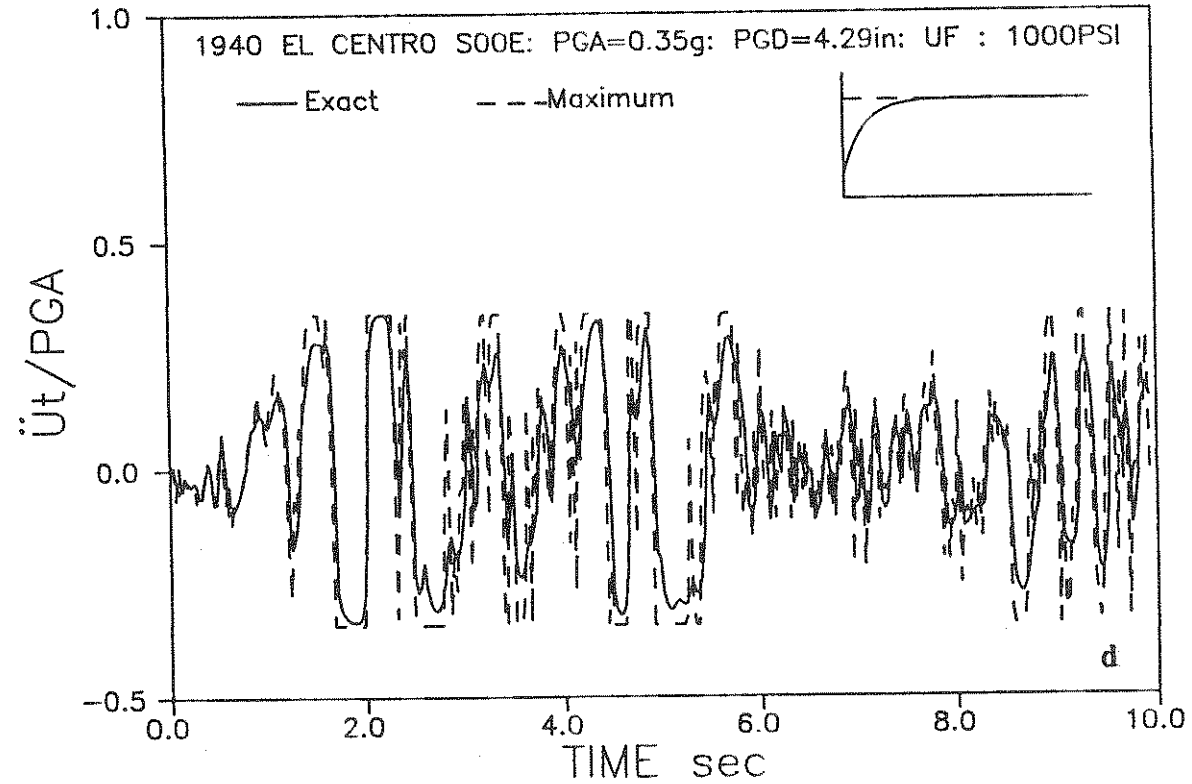

FIGURE 7-3 Comparison of Response of Rigid Mass Excited by El Centro as Computed by Proposed Model (Exact) and Coulomb's Model, (Continued)

7.2 Analysis of Base-Isolated Structures Incorporating Teflon Bearings and Centering Force Devices

The earthquake response of a simple structure consisting of either 3 or 6 stories is now considered. The structure is supported by a sliding isolation system that incorporates Teflon sliding bearings and rubber springs. The sliding bearings are made of unfilled Teflon and bearing pressure is assumed to be the same for all bearings at 1,000, 2,000 or 3,000 psi. The rubber springs do not carry any vertical load (eg. Ikonomou and TASS system) and provide a total horizontal stiffness K_b. The rigid body period of the system is defined as

$$T_b = 2\pi \left(\frac{W}{gK_b} \right)^{1/2} \tag{7-1}$$

in which W is the weight of the structure. Furthermore, the rubber springs provide an equivalent viscous damping factor in the rigid body of vibration equal to 0.05. Damping in the superstructure is assumed to be 2% of critical.

Spectra of the basemat displacement and base shear, normalized respectively by the peak ground displacement and weight, are presented in Figures 7-4 and 7-5 for the El Centro input. Values of T_b vary between 0.2 and 4 secs. The solid line represents the response of a linear isolation system with the same period T_b but with a viscous damping factor of 0.10. It represents a high damping rubber isolation system. All three sliding isolation systems have a basemat displacement that is substantially lower than that of the elastomeric isolation system. Base shear is slightly larger in the sliding systems (appropriate values of T_b for sliding systems are larger than 3 secs). Still, however, the base shear coefficient is about 0.2 for which a structure may remain elastic. When comparing the elastomeric isolation system with T_b=2 secs and the sliding systems with T_b=4 secs (these are easily realizable values), the sliding systems show a clear superiority. Base shears are about the same but the displacement is less in the sliding systems by a factor of about 3.

Figures 7-6 and 7-7 present the response of the system when subjected to N90W component of the Mexico City earthquake of 1985. This earthquake has a predominant period at about 2.5 secs. Clearly, in this case, the sliding systems show substantially lower response, both in the displacement and base shear, than the elastomeric isolation system. Furthermore, a comparison of Figures 7-4 and 7-5 to Figures 7-6 and 7-7 confirms the low sensitivity of sliding isolation systems to the frequency content of excitation.

It is evident in Figures 7-4 to 7-7 that a sliding isolation system designed for a bearing pressure of 1000 psi will undergo a lower basemat displacement than either sliding systems designed at

higher pressure or elastomeric systems. This is apparently due to higher friction in low pressure Teflon bearings. As a consequence of this higher friction, it would be expected that base shear in low pressure sliding isolation systems is higher than in high pressure sliding systems. Figures 7-4 to 7-7 provide evidence to the contrary. Around resonance areas (values of T_b close to predominant earthquake period), low pressure sliding isolation systems have a base shear coefficient that is lower than the corresponding coefficient in higher pressure systems.

The behavior is similar to that of a viscously damped harmonically excited single-degree-of freedom system of which the base shear decreases with increasing damping factor in the resonance region (excitation frequency to natural frequency less than $\sqrt{2}$). It may be concluded that sliding isolation systems exhibit a behavior that resembles that of highly damped linear systems. The authors caution the reader to avoid generalization of this statement. Replacement of a frictional system with an equivalent viscous system may not be possible. The preceding observation suggests that the use of low pressure Teflon bearings in sliding isolation systems may be preferable.

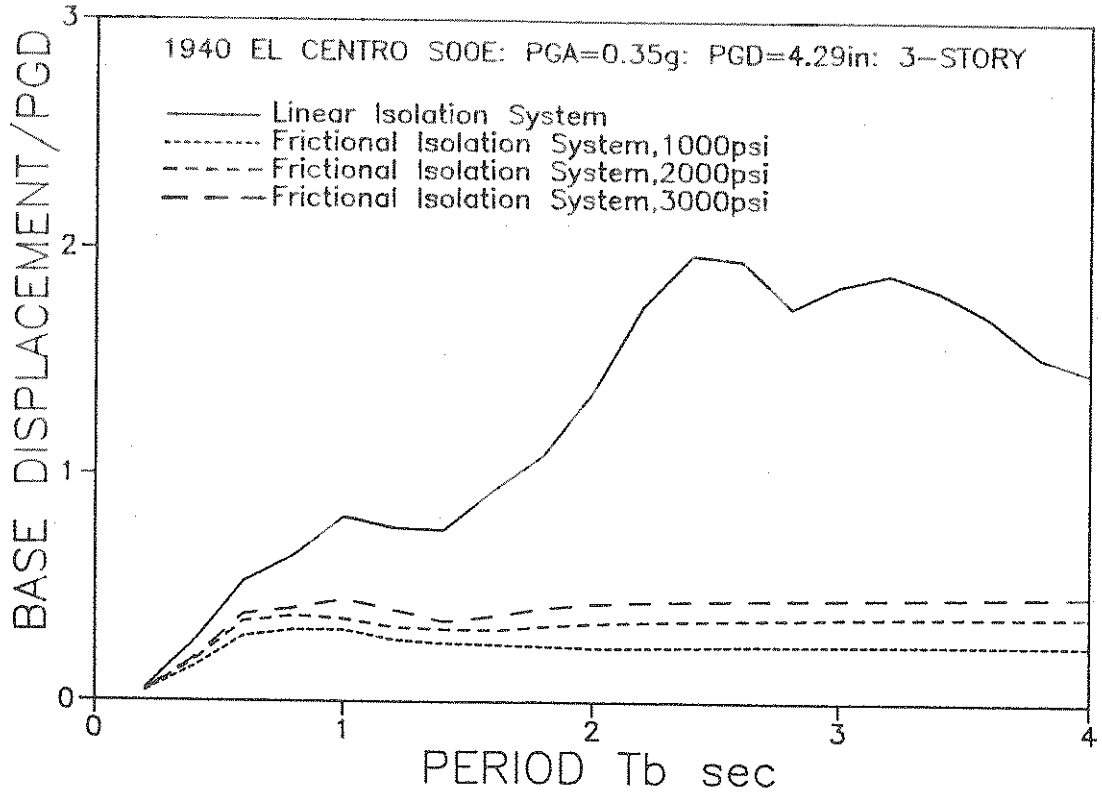

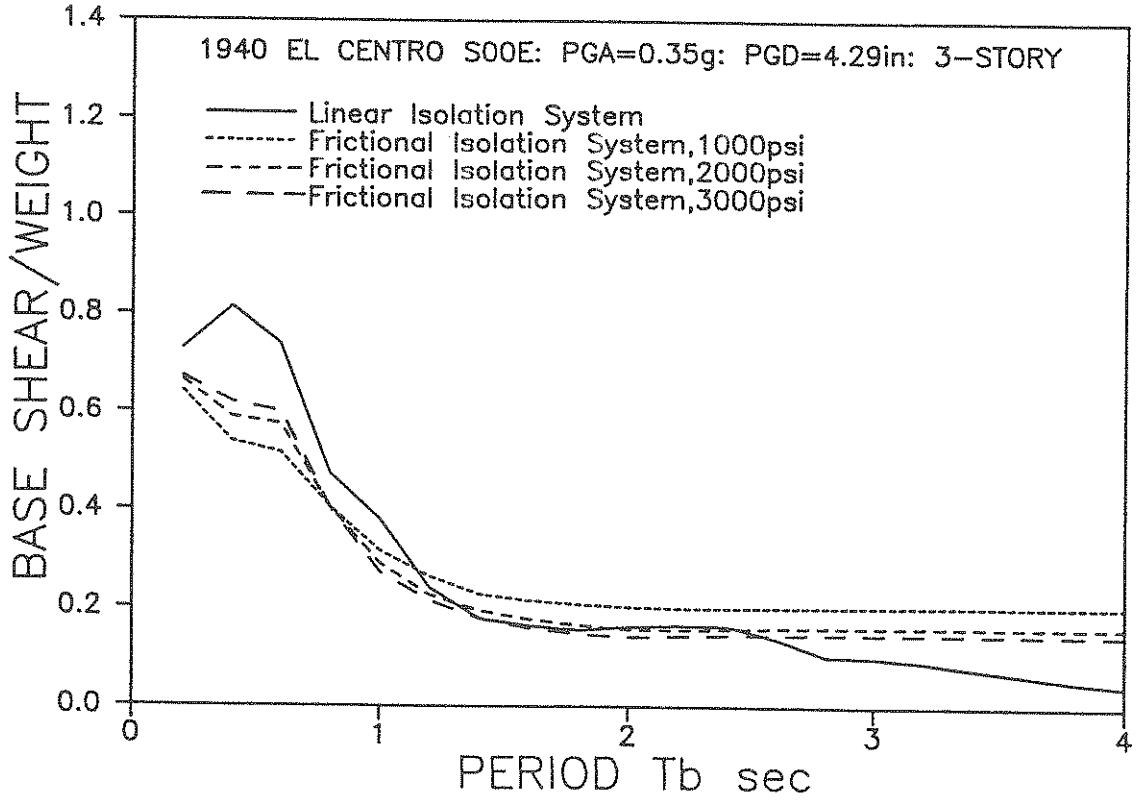

FIGURE 7-4 Spectra of Basemat Displacement and Base Shear of 3-Story Isolated Structure Subjected to El Centro Earthquake

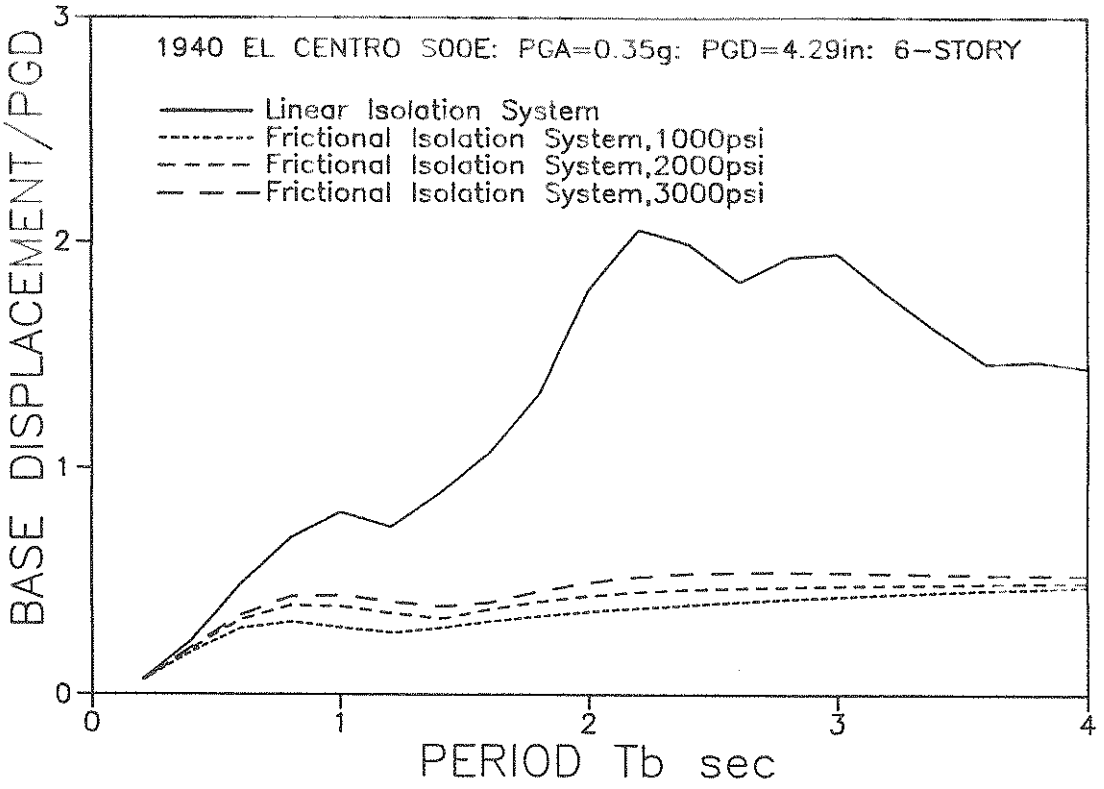

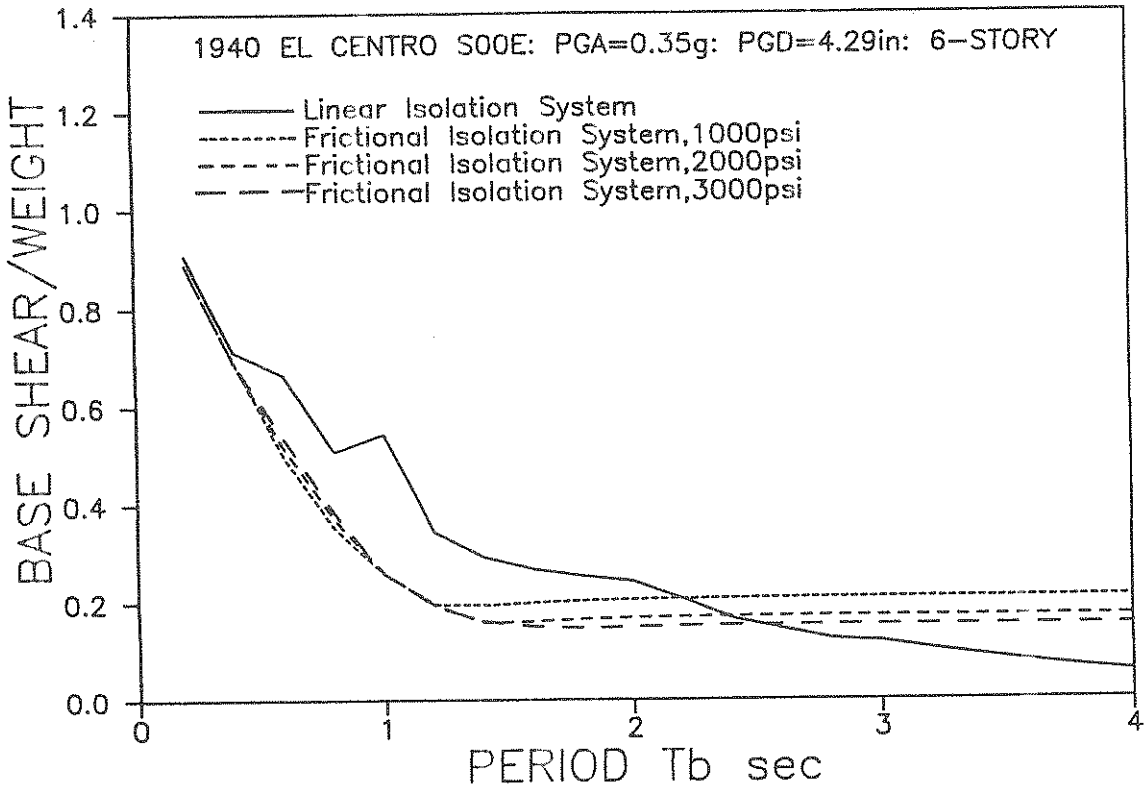

FIGURE 7-5 Spectra of Basemat Displacement and Base Shear of 6-Story Isolated Structure Subjected to El Centro Earthquake

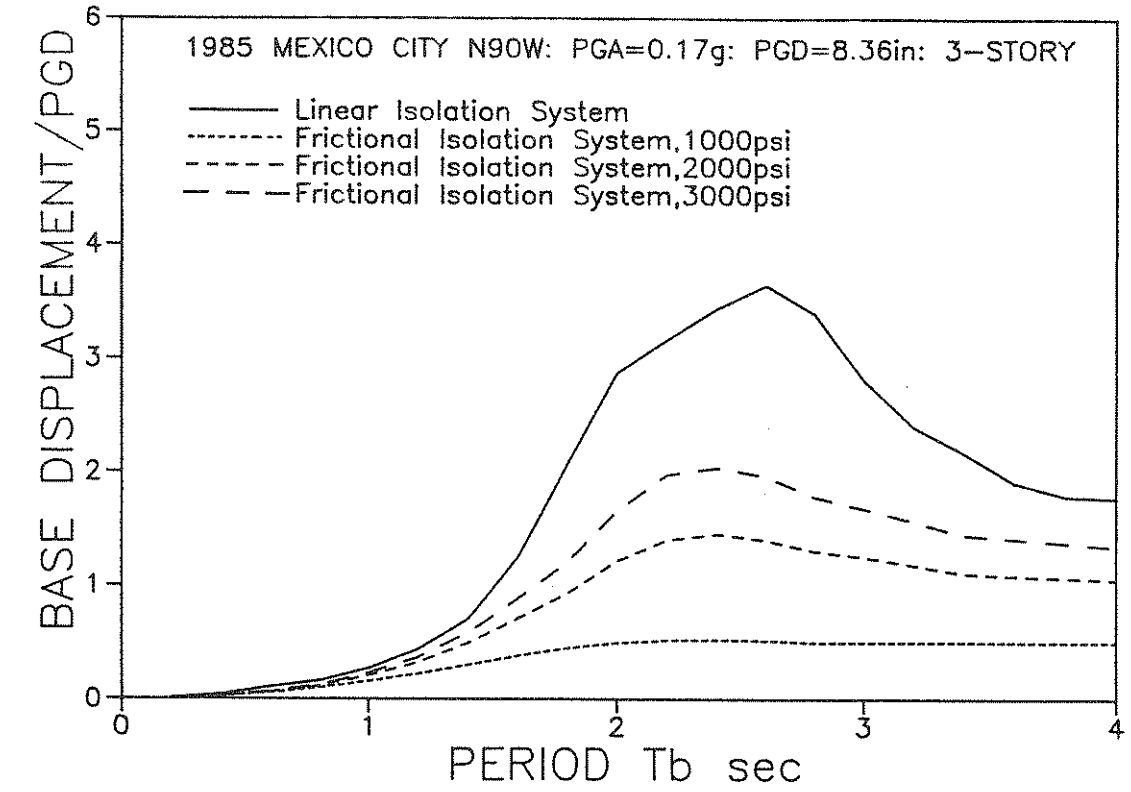

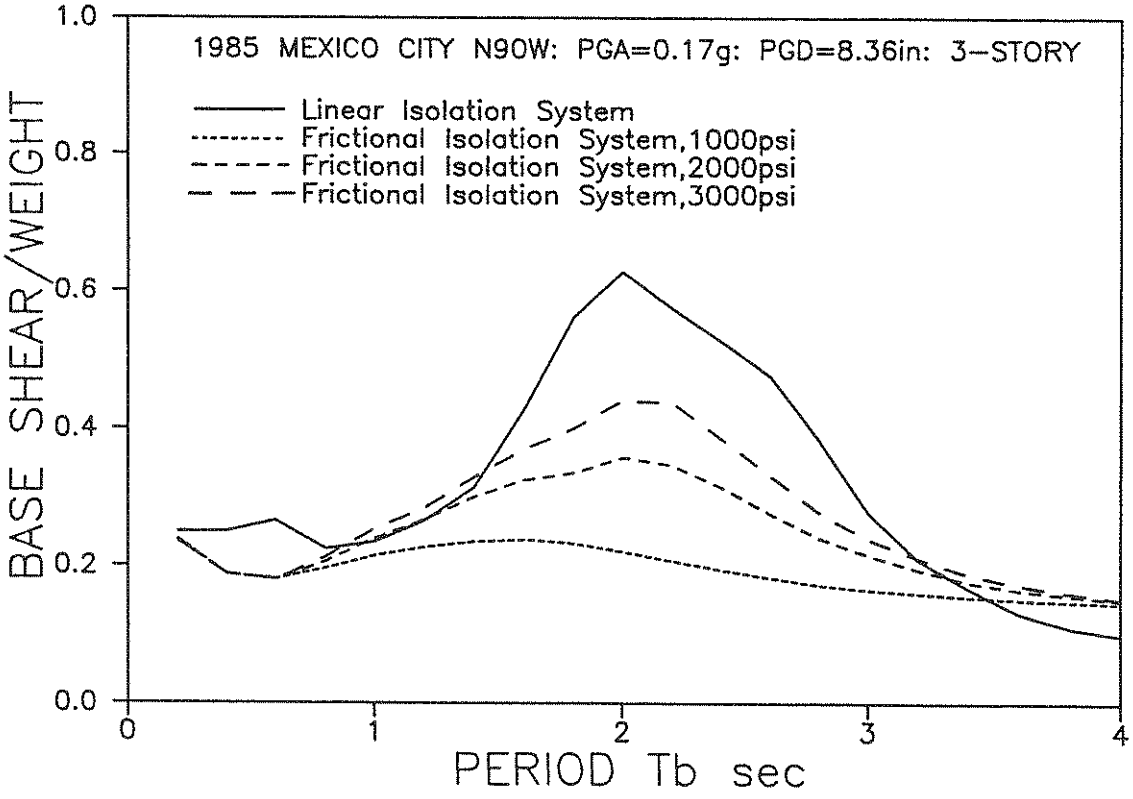

FIGURE 7-6 Spectra of Basemat Displacement and Base Shear of 3-Story Isolated Structure Subjected to Mexico City Earthquake

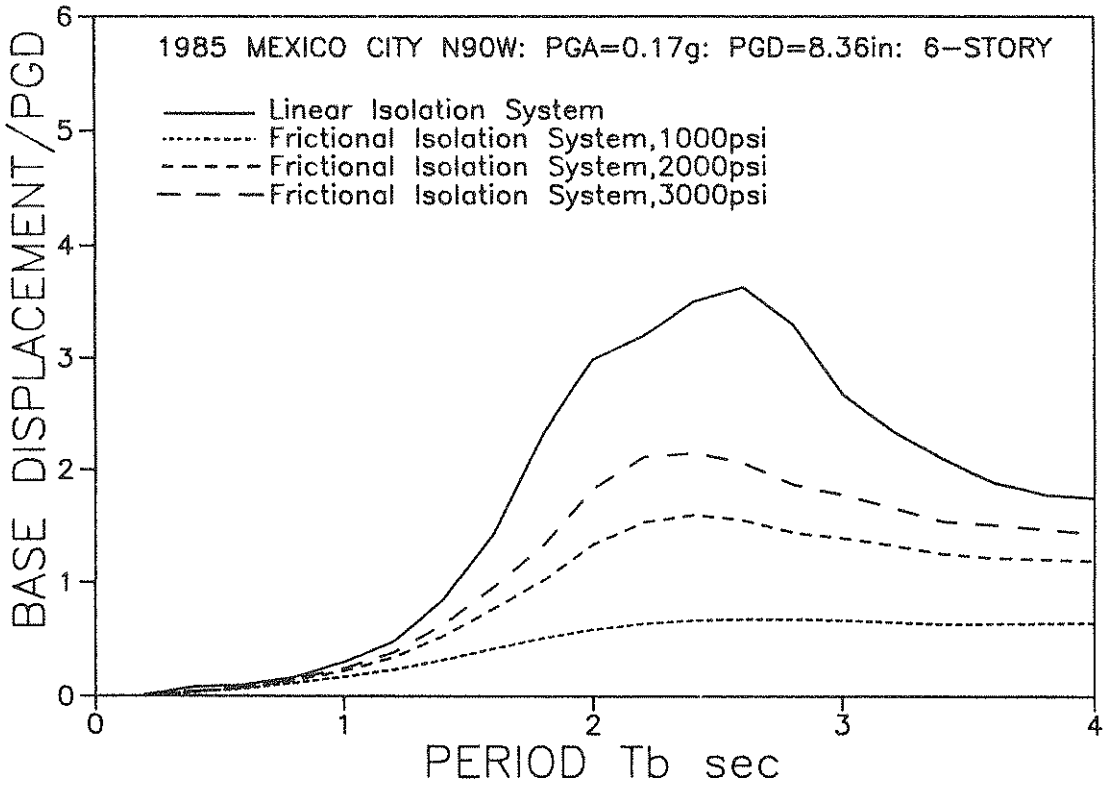

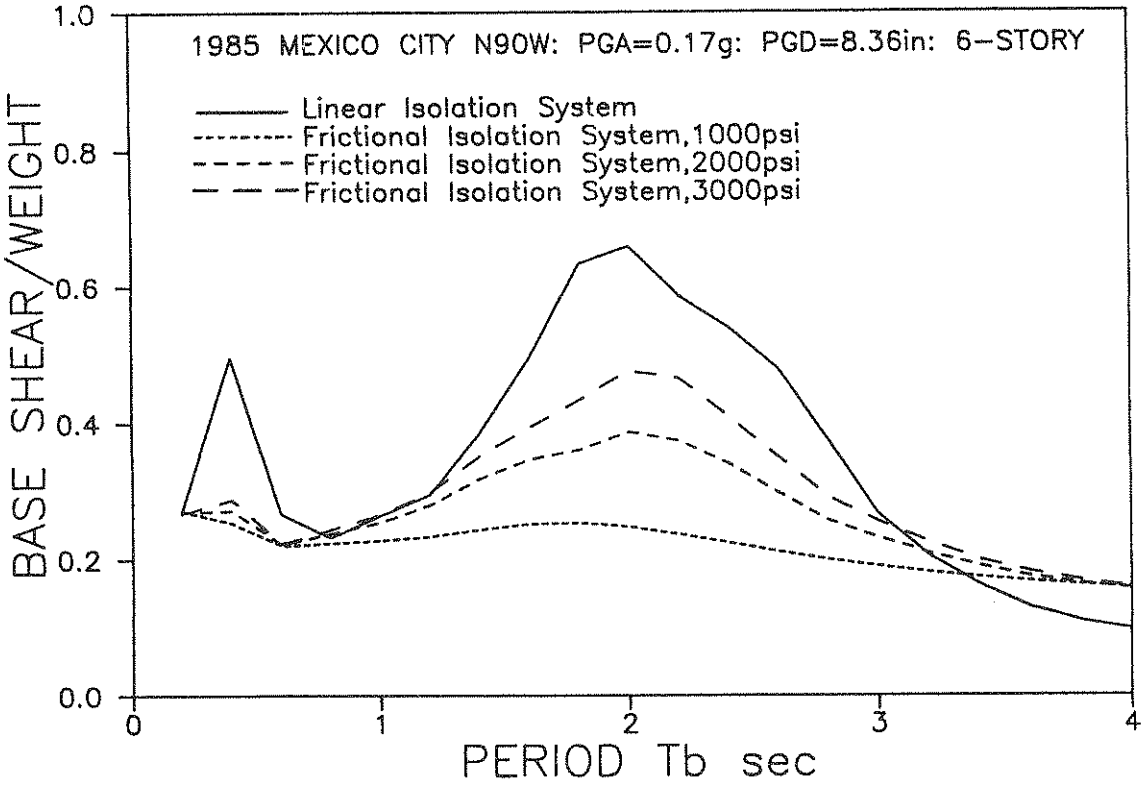

FIGURE 7-7 Spectra of Basemat Displacement and Base Shear of 6-Story Isolated Structure Subjected to Mexico City Earthquake

SECTION 8
CONCLUSIONS

A number of tests (total of 164) were conducted on unfilled and glass-filled Teflon in contact with polished stainless steel at bearing pressure of 1,000, 2,000, 3,000 and 6,500 psi and sliding velocity of 0.1 to about 20 in/sec. The effects on friction of pressure, velocity, acceleration, type and condition of interface and type of test were investigated. The following conclusions have been derived.

1. The type of test (sinusoidal or sawtooth displacement input) has an insignificant effect on the value of the sliding coefficient of friction. Only a minor effect on the recorded value of breakaway friction was observed.

2. The effect of relative acceleration at the sliding interface is not important.

3. Sliding velocity has an important effect on the coefficient of sliding friction. Friction increases rapidly with increasing velocity up to a certain value of velocity beyond which it remains constant. This value of velocity is between 4 and 8 in/sec. The lower limit applies for interfaces at high pressure and the upper limit applies for interfaces at low pressure.

4. Friction decreases with increasing bearing pressure. The rate of reduction depends strongly on the sliding velocity. It is greatest at high velocity. The value of pressure beyond which friction is independent of pressure is about 5,000 psi at 0.1 in/sec velocity and more than 6,500 psi at velocities exceeding 10 in/sec.

5. Friction of unfilled Teflon is lower than friction of glass-filled Teflon under identical conditions of testing. The difference appears to reduce with increasing pressure and it almost diminishes at the pressure of 6,500 psi.

6. The friction of glass-filled Teflon at 15% by weight composition was lower than that of glass filled at 25% composition at pressures exceeding 2000 psi. The opposite was observed at the pressure of 1,000 psi. Differences were not substantial.

7. For sliding parallel to lay, friction of unfilled Teflon was slightly less than when sliding was perpendicular to lay. The surface roughness of stainless steel in the latter case was about 30% more than in the former case (0.04μm versus 0.03μm R_a). The difference in the recorded value of friction showed a reduction with increasing pressure and diminished at the pressure of 6,500 psi.

8. The recorded values of breakaway and sliding coefficient of friction appear to compare well with data reported by other investigators.

9. Mathematical models of friction have been developed and shown to be capable of reproducing the behavior observed in the laboratory.

10. Application of these mathematical models in the analysis of sliding isolation systems has shown that the use of Teflon bearings at low bearing pressure may be advantageous over the use of bearings at high pressure.

SECTION 9
REFERENCES

1. American Association of State Highway and Transportation Officials, "Standard Specifications for Highway Bridges," 13th Edition, Washington D.C., 1983.

2. California Standard Special Provision, "Sliding Bearings."

3. Long, J.E., "Bearings in Structural Engineering," Butterworths & Co. Ltd., John Wiley & Sons Inc., 1974.

4. E.I. du Pont de Nemours & Co., "The How's and Why's of Friction for Teflon Resins," Reprint no. 19 from J. Teflon.

5. E.I. du Pont de Nemours & Co., "Selecting the Right Teflon TFE Compound," Reprint no. 47 from J. Teflon.

6. E.I. du Pont de Nemours & Co., "Teflon: Mechanical Design Data," Wilmington, DE, 1981.

7. Flom, D.G. and Porile, N.T., "Friction of Teflon Sliding on Teflon," J. Applied Physics, 26, 1088-1092, 1955.

8. Constantinou, M.C., Caccese, J. and Harris, H.G., "Frictional Characteristics of Teflon-Steel Interfaces under Dynamic Conditions," Earthquake Engineering and Structural Dynamics, 15, 751-759, 1987.

9. Thompson, J.B., Turrell, G.C. and Sandt, B.W.," The Sliding Friction of Teflon," SPE Journal, 13-14, April 1955.

10. Taylor, M.E., "PTFE in Highway Bridge Bearings," TRRL Report LR49, Transport and Road Research Laboratory, Department of the Environment, Crowthorne, Berkshire (U.K.), 1982.

11. Campbell, T.I. and Kong, W.L., "TFE Sliding Surfaces in Bridge Bearings," Report ME-87-06, Ontario Ministry of Transportation and Communications, Ontario, July 1987.

12. Long, J.E., "The Performance of PTFE in Bridge Bearings," Civil Engineering and Public Works Review, 64, 459-462, May 1969.

13. Tyler, R.G., "Dynamic Tests on PTFE Sliding Layers Under Earthquake Conditions," Bull. New Zealand National Society for Earthquake Engineering, 10, 3, 129-138, 1977.

14. Buckle, I.G., "Development and Application of Base Isolation and Passive Energy Dissipation," Proc. of ATC-17 Seminar on Base Isolation and Passive Energy Dissipation, San Francisco, California, 153-174, 1986.

15. Kelly, J.M., "Aseismic Base Isolation: Review and Bibliography," Soil Dynamics and Earthquake Engineering, 5, 3, 202-216, 1986.

16. Stevenson, A. and Price, A.R., "A Case Study of Elastomeric Bridge Bearings After 20 Years Service," 2nd World Congress on Joints and Bearings, ACI-SP-94, 1, 113-136, 1986.

17. Constantinou, M.C., "Overview of Base Isolation Study Tour of Japan," Report to the National Center for Earthquake Engineering Research, Buffalo, New York, June 1988.

18. Kelly, J.M. and Hodder, S.B., "Experimental Study of Lead and Elastomeric Dampers for Base Isolation Systems in Laminated Neoprene Bearings," Bulletin of the New Zealand National Society for Earthquake Engineering, 15, 2, 53-67, 1982.

19. Kelly, J.M. and Buckle, I.G., "Shake Table Studies of Base Isolated Bridge Superstructures," Proc. 2nd Joint U.S. - New Zealand Workshop on Seismic Resistance of Highway Bridges, ATC-12-1, 251-257, 1985.

20. Built, S.M., "Lead Rubber Dissipators for the Base Isolation of Bridge Structures," School of Engineering Report No. 289, Department of Civil Engineering, University of Auckland, Auckland, New Zealand, Aug. 1982.

21. Tyler, R.G. and Robinson, W.H., "Tests on Lead-Rubber Bearings," Proc. 2nd Joint U.S. - New Zealand Workshop on Seismic Resistance of Highway Bridges, ATC-12-1, 217-221, 1985.

22. Buckle, I.G., "New Developments in Energy Dissipators for Bridges," Proc. 2nd Joint U.S. - New Zealand Workshop on Seismic Resistance of Highway Bridges, ATC-12-1, 223-229, 1985.

23. Way, D., and Lew, M., "Design and Analysis of a High-Damping-Rubber Isolation System," Proc. of ATC-17 Seminar on Base Isolation and Passive Energy Dissipation, San Francisco, California, 83-92, 1986.

24. Derham, C.J., Kelly, J.M. and Thomas, A.G., "Nonlinear Natural Rubber Bearings for Seismic Isolation," Nuclear Engineering and Design, 84, 417-428, 1985.

25. Kelly, J.M. and Beucke, K.E., "A Friction Damped Base Isolation System with Fail-Safe Characteristics," Earthquake Engineering and Structural Dynamics, 11, 33-56, 1983.

26. Delfosse, G.C., "Full Earthquake Protection Through Base Isolation System," 7th World Conference on Earthquake Engineering, Istanbul, Turkey, 8, 61, 1980.

27. Delfosse, G.C. and Delfosse, P.G., "Earthquake Protectection of a Building Containing Radioactive Waste by Means of Base Isolation System," 8th World Conference on Earthquake Engineering, San Francisco, 5, 1047-1054, 1984.

28. Delfosse, G.C., "Construction and Testing of an Experimental Dwelling-House on Rubber Bearings," 2nd World Congress on Joints and Bearings, ACI-SP-94, 1, 223-232, 1986.

29. Staudacher, K., "Protection for Structures in Extreme Earthquakes: Full Base Isolation (3-D) by the Swiss Seismafloat System," Nuclear Engineering and Design, 84, 343-357, 1985.

30. Wolf, J.P. and Obernhuber, P., "Effects of Horizontally Propagating Waves on the Response of Structures with a Soft First Story," Earthquake Engineering and Structural Dynamics, 9, 1-21, 1981.

31. Simo, J.C. and Kelly, J.M., "The Analysis of Multilayer Elastomeric Bearings," ASME Journal of Applied Mechanics, 51, 256-262, 1984.

32. Buckle, I.G. and Kelly, J.M., "Properties of Slender Elastomeric Isolation Bearings During Shake Table Studies of a Large-Scale Model Bridge Deck," 2nd World Congress on Joints and Bearings, ACI-SP-94, 1, 247-269, 1986.

33. Pan, T. and Kelly, J.M., "Seismic Response of Torsionally Coupled Base Isolated Structures," Earthquake Engineering and Structural Dynamics, 11, 749-770, 1983.

34. Pan, T.C. and Kelly, J.M., "Seismic Response of Base-Isolated Structures with Vertical-Rocking Coupling," Earthquake Engineering and Structural Dynamics, 12, 681-702, 1984.

35. Constantinou, M.C. and Kneifati, M.C., "Dynamics of Soil-Base-Isolated-Structure Systems," Journal of Structural Engineering, ASCE, 114, 1, 211-221, 1988.

36. Constantinou, M.C., "A Simplified Analysis Procedure for Base-Isolated Structures on Flexible Foundation," Earthquake Engineering and Structural Dynamics, 15, 963-983, 1987.

37. Constantinou, M.C. and Kneifati, M.C., "Dynamics of Soil-Base-Isolated-Structure Systems: Nonlinear Systems," Report to NSF, Drexel University, 1987.

38. Siddiqui, F.M.A. and Constantinou, M.C., "Simplified Analysis Method of Multistory Base-Isolated Structures on Viscoelastic Halfspace," Earthquake Engineering and Structural Dynamics, to appear in 1989.

39. Su, L., Ahmadi, G. and Tadjbakhsh, I.G., "A Comparitive Study of Base Isolation Systems," Report No. MIE-150, Clarkson University, 1987.

40. Plichon, C. and Jolivet F., "Aseismic Foundation Systems for Nuclear Power Plants," Proceedings of SMIRT Conference, Paper No. C 190/78, 1978.

41. TFE Expansion Bearings for Highway Bridges, Report FHWA-IL-PR71, Illinois Department of Transportation, 1977.

42. Mostaghel, N. and Tanbakuchi, J., "Response of Sliding Structures to Earthquake Support Motion," Earthquake Engineering and Structural Dynamics, 11, 729-748, 1983.

43. Ahmadi, G. and Mostaghel, N., "On Dynamics of a Structure With a Frictional Foundation," Journal de Mecanique Theorique et Appliquee, 3, 2, 271-285, 1984.

44. Younis, C.J. and Tadjbakhsh, I.G., "Response of a Sliding Rigid Structure to Base Excitation," ASCE Journal of Engineering Mechanics, 110, 3, 417-431, March, 1984.

45. Constantinou, M.C., Gazetas, G. and Tadjbakhsh, I.G., "Stochastic Seismic Sliding of Rigid Mass Supported Through Non-Symmetric Friction," Earthquake Engineering and Structural Dynamics, 12, 6, 777-794, 1984.

46. Caspe, M.S. and Reinhorn, A.M., "The Earthquake Barrier. A Solution for Adding Ductility to Otherwise Brittle Buildings," Proceedings of ATC-17 Seminar on Base Isolation and Passive Energy Dissipation, San Francisco, CA, 331-342, 1986.

47. Ikonomou, A.S., "Alexisismon Isolation Engineering for Nuclear Power Plants," Nuclear Engineering and Design, 85, 201-216, 1985.

48. Nagashima, I., Kawamura, S., Kitazawa, K. and Hisano, M., "Study on a Base Isolation System," Proc. 3rd Conference on Soil Dynamics and Earthquake Engineering, Princeton University, June 1987.

49. Mostaghel, N. and Khodaverdian, M., "Dynamics of Resilient-Friction Base Isolator (R-FBI)," Earthquake Engineering and Structural Dynamics, 15, 379-390, 1987.

50. Watson Bowman Acme Corp., "Wabo-Fyfe Earthquake Protection System," Amherst, NY 1981.

51. Watson Bowman Acme Corp., "Wabo-Fyfe High Load Structural Bearing," Amherst, NY 1983.

52. Huffman, G.K., "Full Base Isolation for Earthquake Protection by Helical Springs and Viscodampers," Nuclear Engineering and Design, 84, 331-338, 1985.

53. Hadjian, A.H. and Tseng, W.S., "A Comparative Evaluation of Passive Seismic Isolation Schemes," Proc. ATC-17 Seminar on Base Isolation and Passive Energy Dissipation, San Francisco, California, 291-304, 1986.

54. Standard Association of New Zealand, "New Zealand Standard 3101: Code of Practice for the Design of Concrete Structures," Part 1, 1982.

55. Structural Engineering Association of Northern California, "Draft on Seismic Isolation Design Requirements," 1986.

56. New York State Department of Transportation, "Standard Specifications: Construction and Materials," January 1985.

57. Jensen, T., "Caltrans Elastomeric/TFE Bearing, "Western Bridge Engineers' Seminar, Sacramento, CA, October 1987.

58. "Ontario Highway Bridge Design Code," Ministry of Transportation and Communications, Second Edition, 1983.

59. OPSS 1203, "Material Specification for Bearings-Rotational and Sliding Surface," Ontario Provincial Standard Specification, Draft for Comments, January 1987.

60. British Standards Institution, "BS 5400, Sections 9.1 and 9.2: Steel, Concrete and Composite Bridges, Bridge Bearings," 1983.

61. Eggert, H., "Standardization of Bridge Bearings: A Report on German Standards and a Proposal for an International Standard," 2nd World Congress on Joints and Bearings, ACI-SP-94, 2, 543-550, 1985.

62. "ANSI/ASME, B46.1-1985: Surface Texture (Surface Roughness, Waviness, and Lay)," 1985.

63. Dagnall, H., "Exploring Surface Texture," Rank Taylor Hobson, England, 1988.

64. Bowden, F.P. and Tabor, D., "The Friction and Lubrication of Solids," Oxford, Clavendon Press, 1964.

65. Tabor, D., "Friction - The Present State of Our Understanding," Journal of Lubrication Technology, ASME, 103, 169-178, 1981.

66. Makinson, K.R. and Tabor, D., "The Friction and Transfer of Polytetrafluoroethylene," Proceedings of Royal Society of London, Series A, 281, 49-61, 1964.

67. Steijn, R.P., "The Sliding Surface of PTFE," Wear, 12, (3), 1968.

68. Tadjbakhsh, I. and Lin, B.C., "Effect of Vertical Motion on Friction-Driven Isolation Systems," Earthquake Engineering and Structural Dynamics, 14, 609-622, 1986.

69. Bouc, R., "Modele Mathematique d'Hysteresis," Acustica, 24, 16-25, 1971.

70. Wen, Y.K., "Approximate Method for Nonlinear Random Vibration," J. Engineering Mechanics Division, ASCE, 101 (EM4), 389-401, 1975.

71. Wen, Y.K., "Method of Random Vibration of Hysteretic Systems," J. Engineering Mechanics Division, ASCE, 102 (EM2), 249-263, 1976.

72. Constantinou, M.C. and Adnane, M.A., "Dynamics of Soil-Based-Isolated-Structure Systems: Evaluation of Two Models for Yielding Systems," Report to NSF, Dept. of Civil Engineering, Drexel University, Sept. 1987.

73. Ozdemir, H., "Nonlinear Transient Dynamic Analysis of Yielding Structures," Ph.D. Thesis, University of California, Berkeley, 1976.

APPENDIX A

EXPERIMENTAL RESULTS

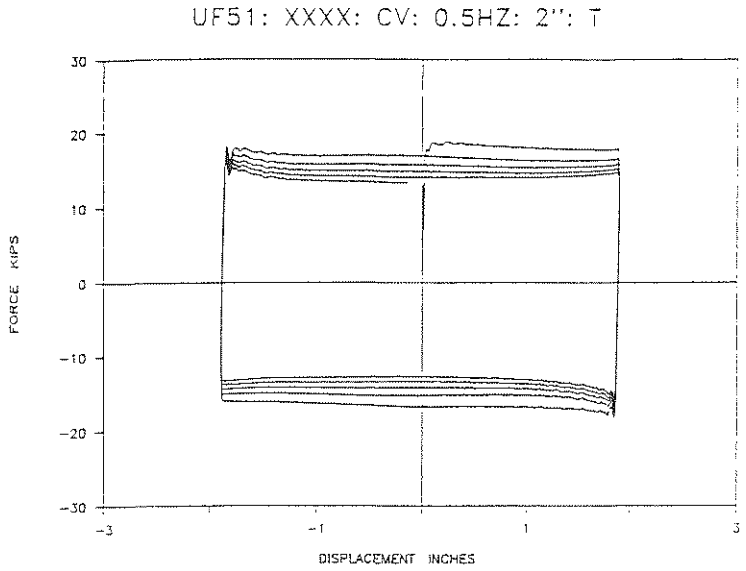
UF51: XXXX: CV: 0.5HZ: 2": T
FORCE KIPS
DISPLACEMENT INCHES

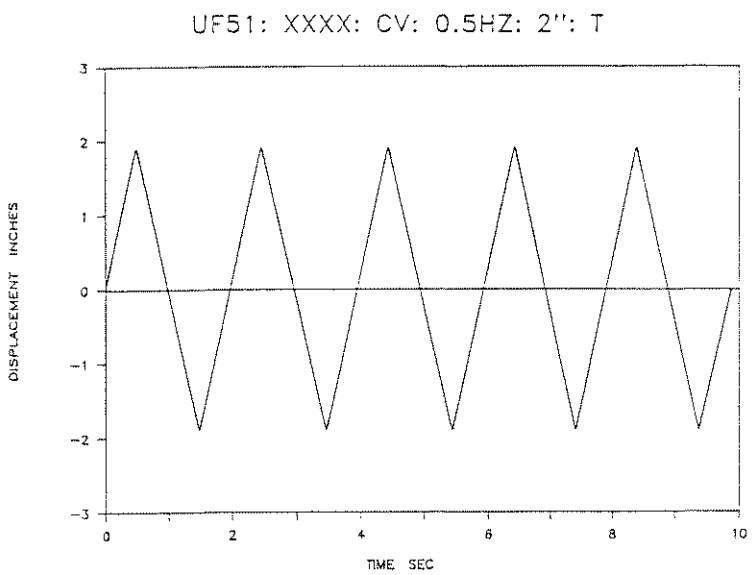
UF51: XXXX: CV: 0.5HZ: 2": T
DISPLACEMENT INCHES
TIME SEC

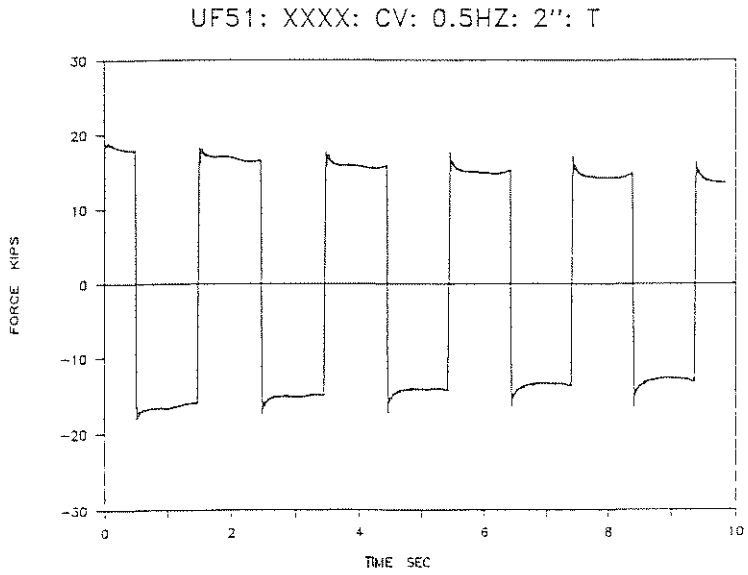
UF51: XXXX: CV: 0.5HZ: 2": T
FORCE KIPS
TIME SEC

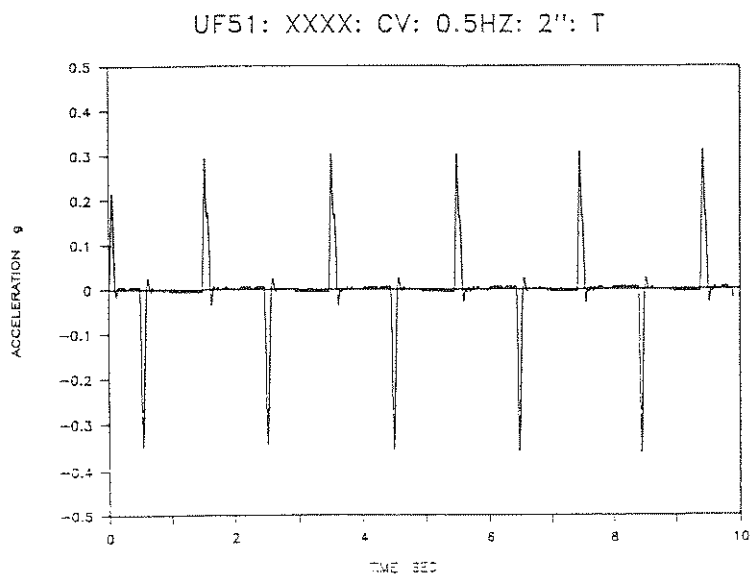
UF51: XXXX: CV: 0.5HZ: 2": T
ACCELERATION g
TIME SEC

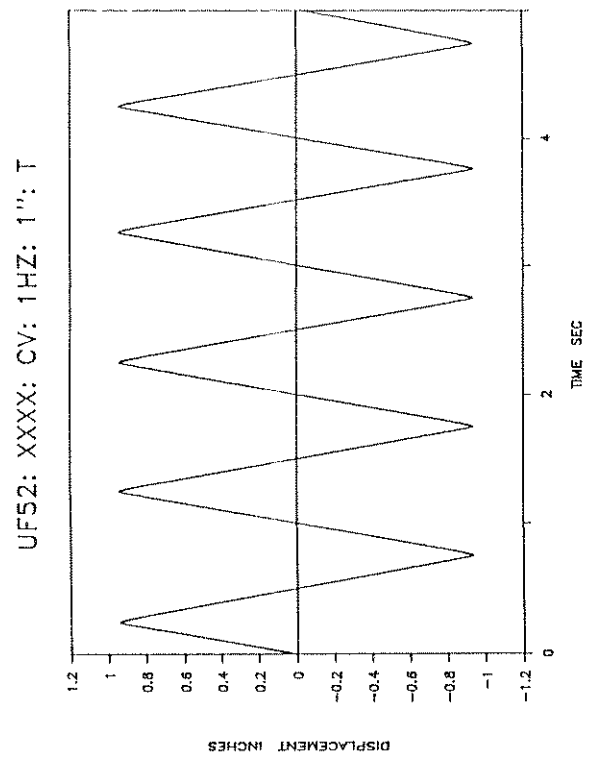
UF52: XXXX: CV: 1HZ: 1": T
DISPLACEMENT INCHES
TIME SEC

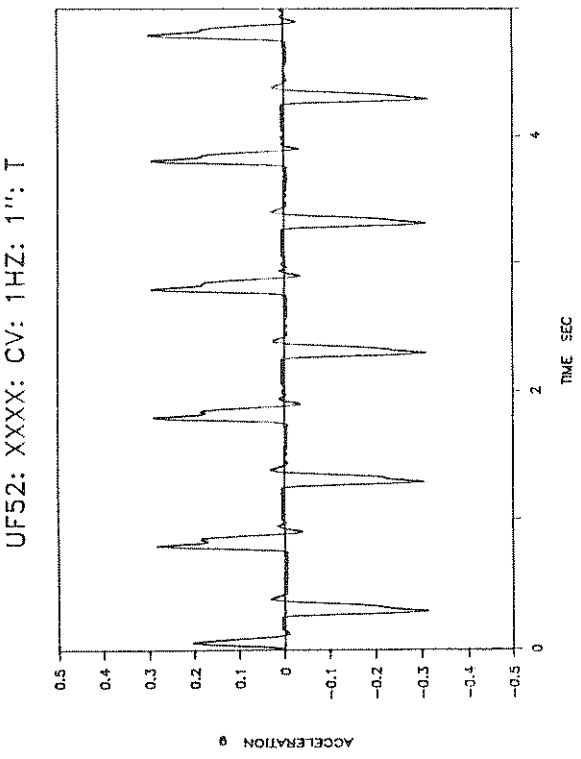
UF52: XXXX: CV: 1HZ: 1": T
ACCELERATION g
TIME SEC

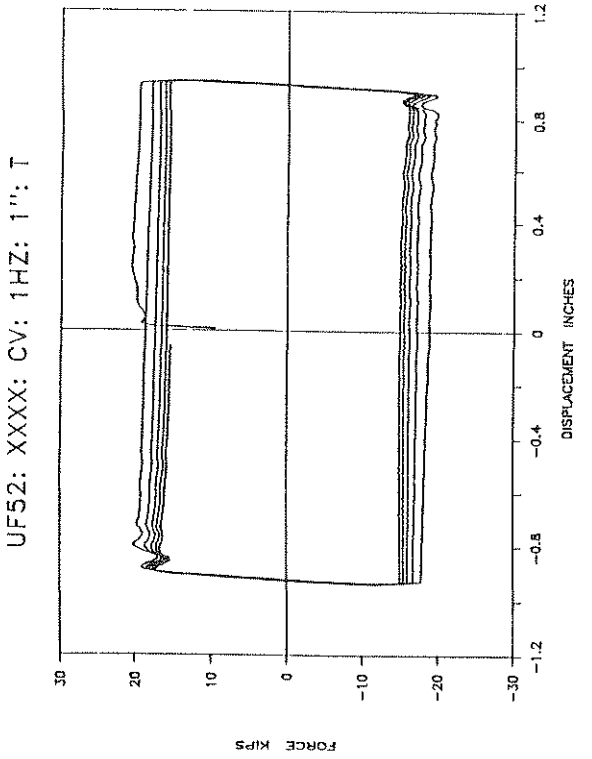
UF52: XXXX: CV: 1HZ: 1": T
FORCE KIPS
DISPLACEMENT INCHES

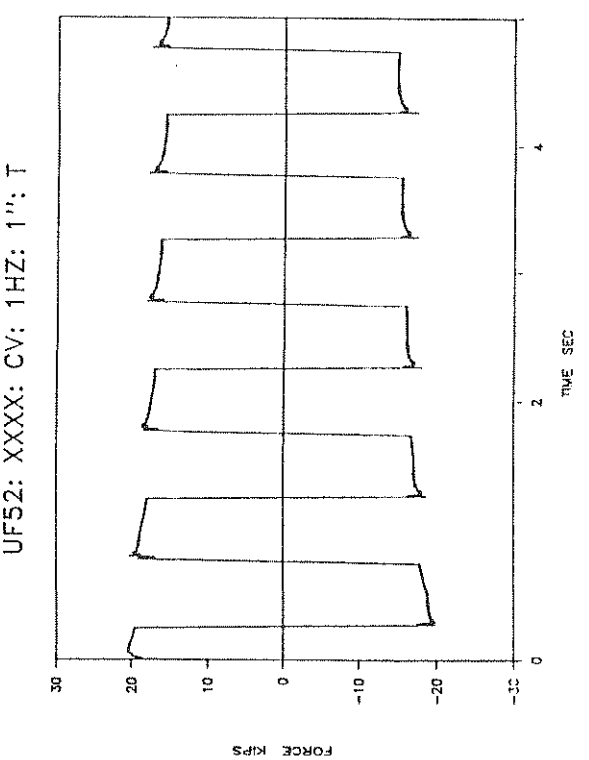
UF52: XXXX: CV: 1HZ: 1": T
FORCE KIPS
TIME SEC

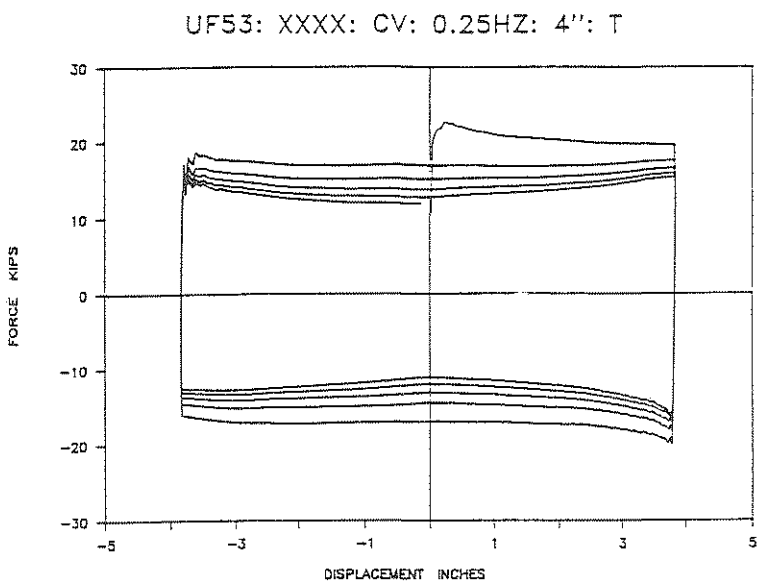
UF53: XXXX: CV: 0.25HZ: 4": T
FORCE KIPS
DISPLACEMENT INCHES

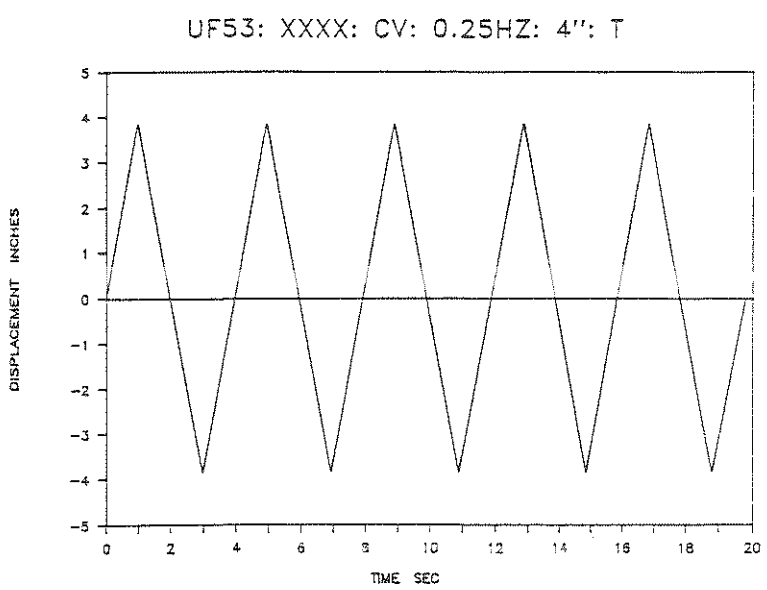
UF53: XXXX: CV: 0.25HZ: 4": T
DISPLACEMENT INCHES
TIME SEC

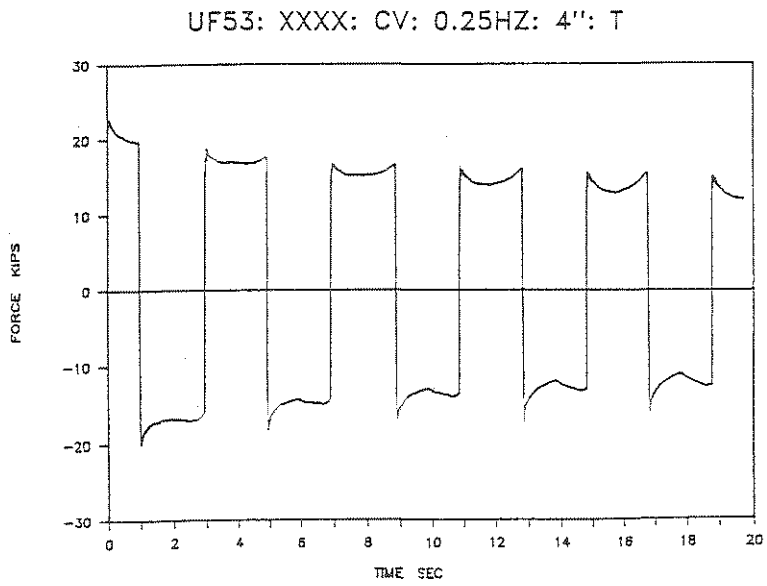
UF53: XXXX: CV: 0.25HZ: 4": T
FORCE KIPS
TIME SEC

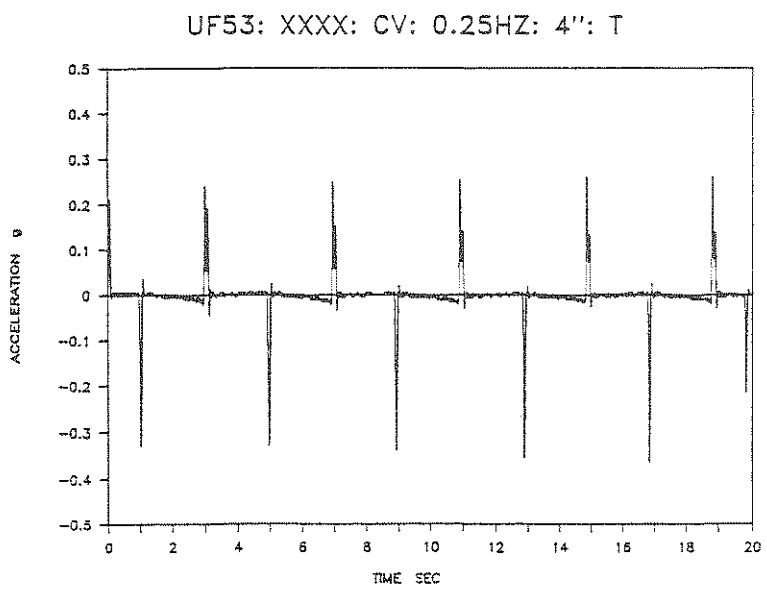
UF53: XXXX: CV: 0.25HZ: 4": T
ACCELERATION g
TIME SEC

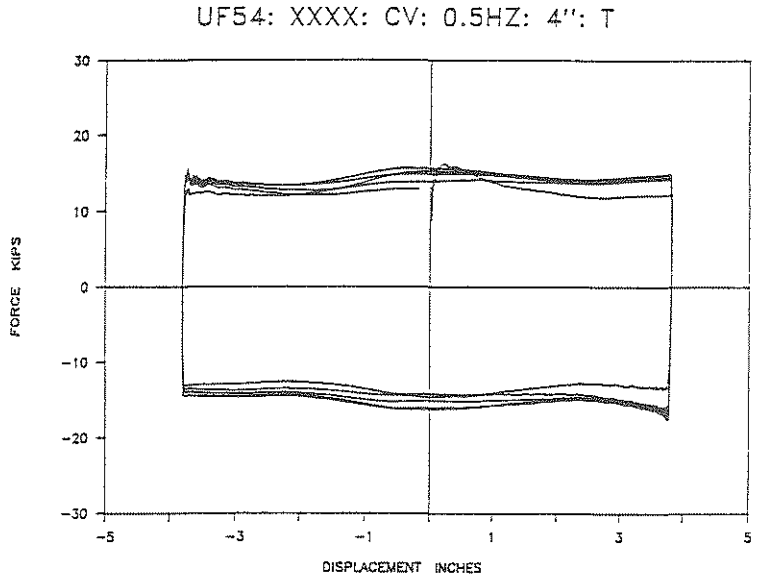
UF54: XXXX: CV: 0.5HZ: 4": T
FORCE KIPS
DISPLACEMENT INCHES

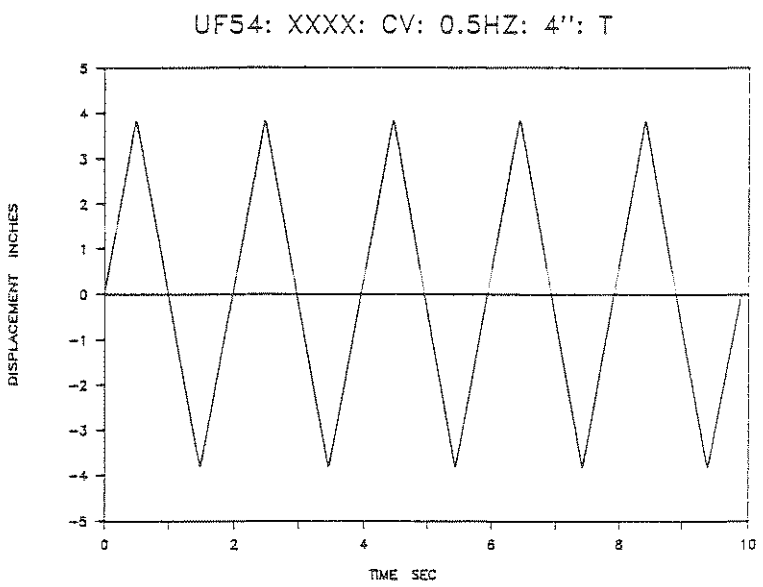
UF54: XXXX: CV: 0.5HZ: 4": T
DISPLACEMENT INCHES
TIME SEC

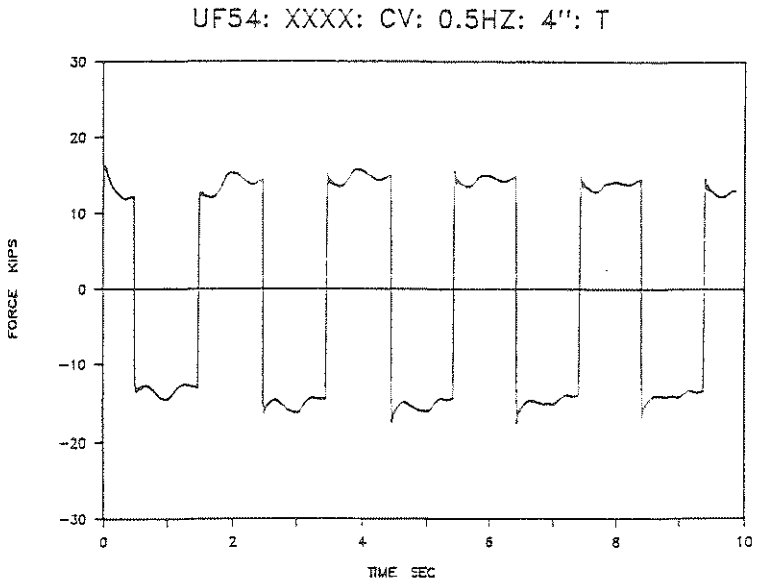
UF54: XXXX: CV: 0.5HZ: 4": T
FORCE KIPS
TIME SEC

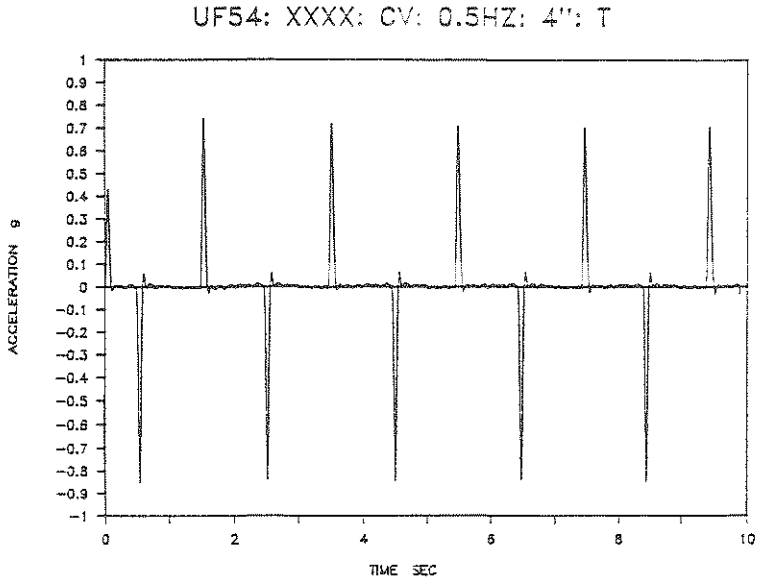
UF54: XXXX: CV: 0.5HZ: 4": T
ACCELERATION g
TIME SEC

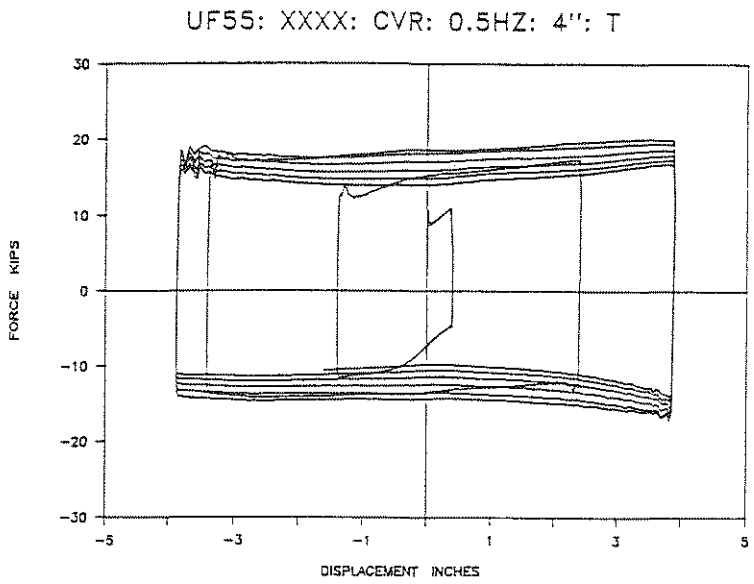
UF55: XXXX: CVR: 0.5HZ: 4": T
FORCE KIPS
DISPLACEMENT INCHES

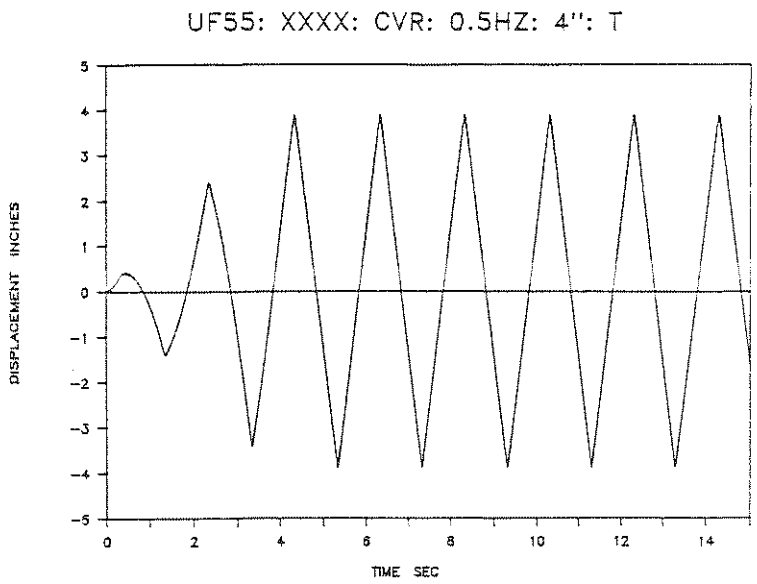
UF55: XXXX: CVR: 0.5HZ: 4": T
DISPLACEMENT INCHES
TIME SEC

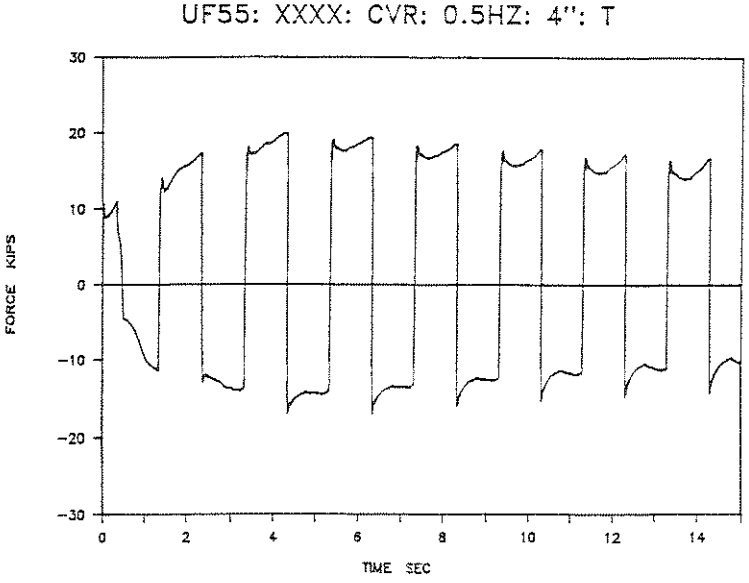
UF55: XXXX: CVR: 0.5HZ: 4": T
FORCE KIPS
TIME SEC

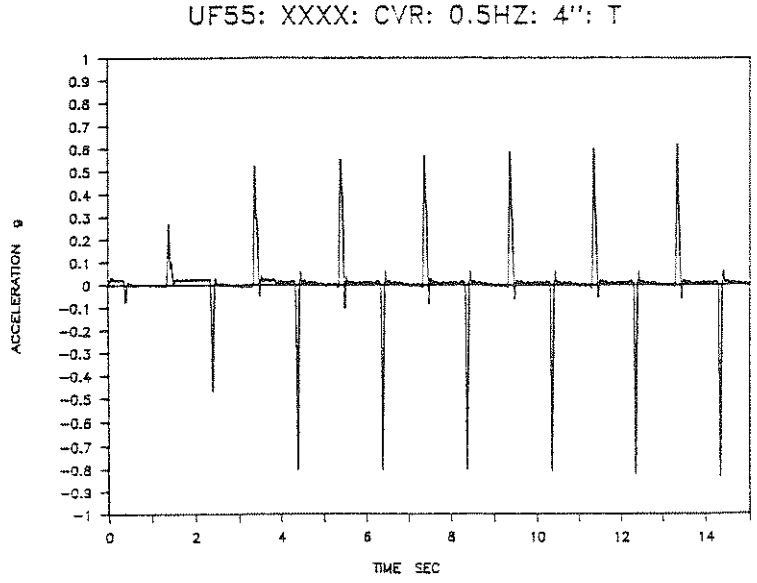
UF55: XXXX: CVR: 0.5HZ: 4": T
ACCELERATION g
TIME SEC

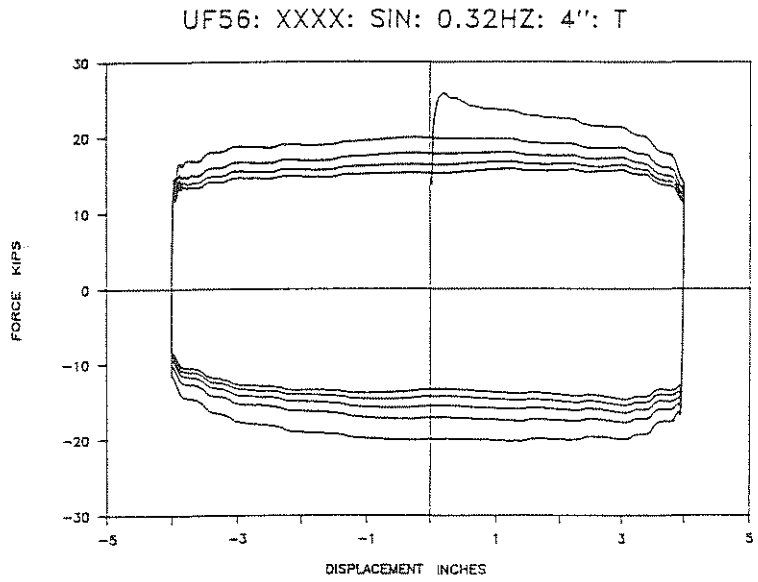
UF56: XXXX: SIN: 0.32HZ: 4": T
FORCE KIPS
DISPLACEMENT INCHES

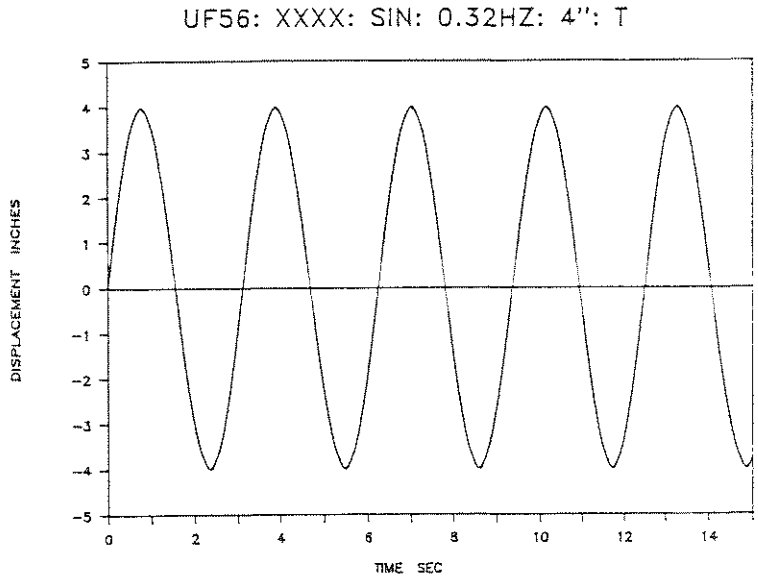
UF56: XXXX: SIN: 0.32HZ: 4": T
DISPLACEMENT INCHES
TIME SEC

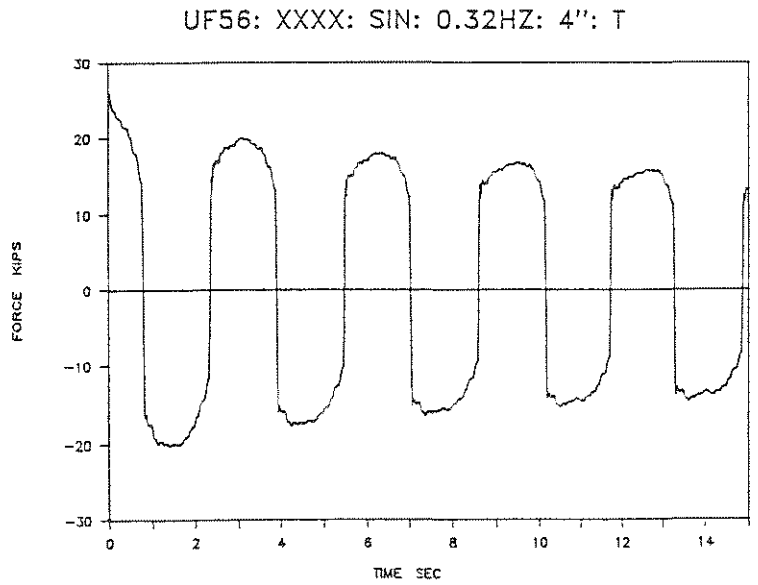
UF56: XXXX: SIN: 0.32HZ: 4": T
FORCE KIPS
TIME SEC

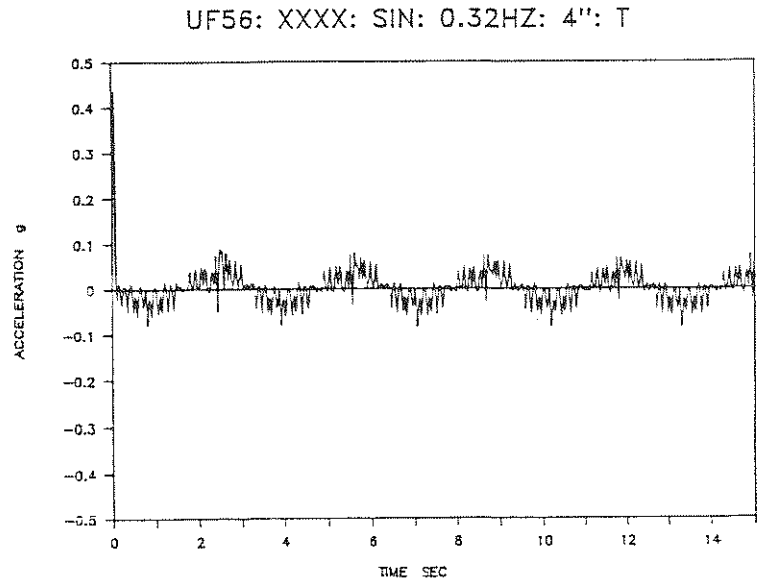
UF56: XXXX: SIN: 0.32HZ: 4": T
ACCELERATION g
TIME SEC

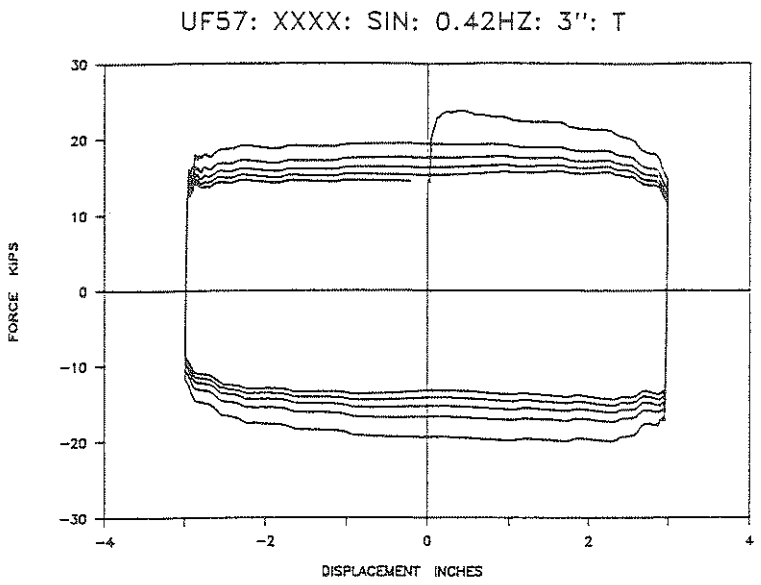
UF57: XXXX: SIN: 0.42HZ: 3": T
FORCE KIPS
DISPLACEMENT INCHES

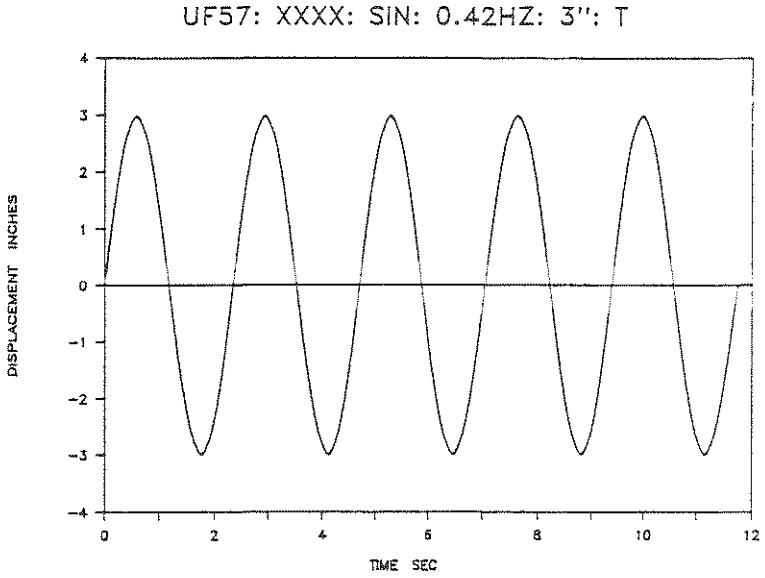
UF57: XXXX: SIN: 0.42HZ: 3": T
DISPLACEMENT INCHES
TIME SEC

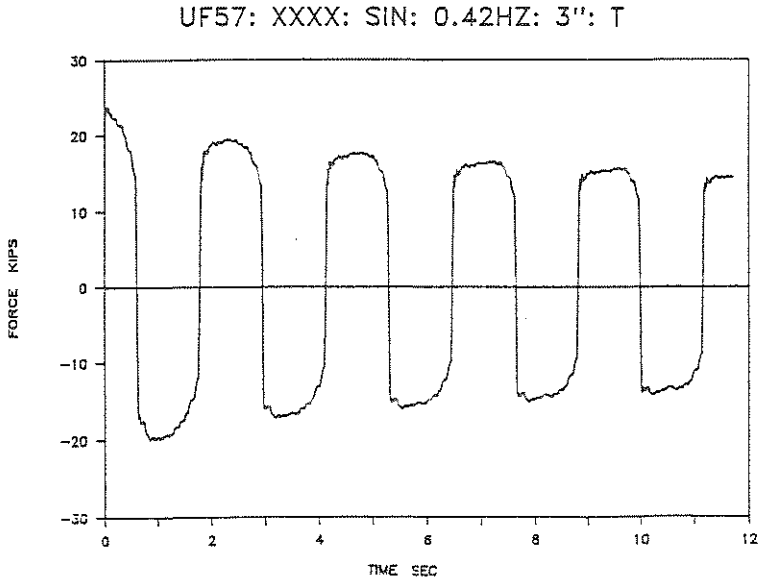
UF57: XXXX: SIN: 0.42HZ: 3": T
FORCE KIPS
TIME SEC

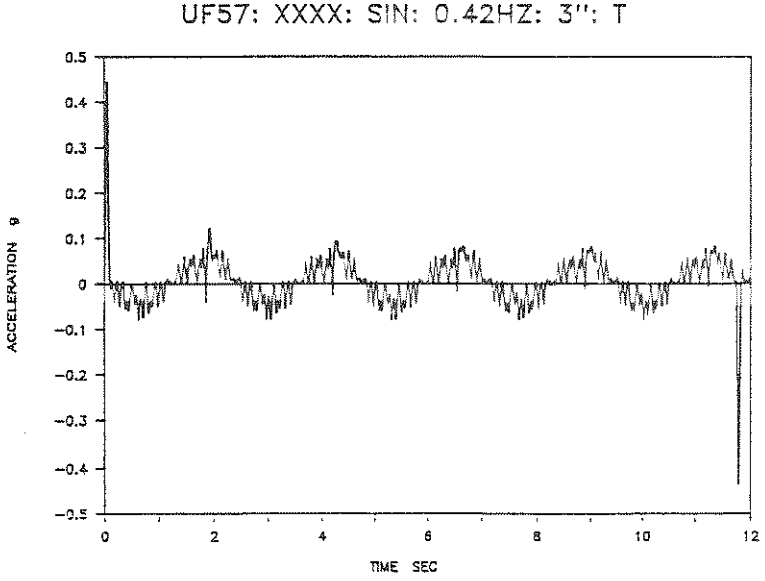
UF57: XXXX: SIN: 0.42HZ: 3": T
ACCELERATION g
TIME SEC

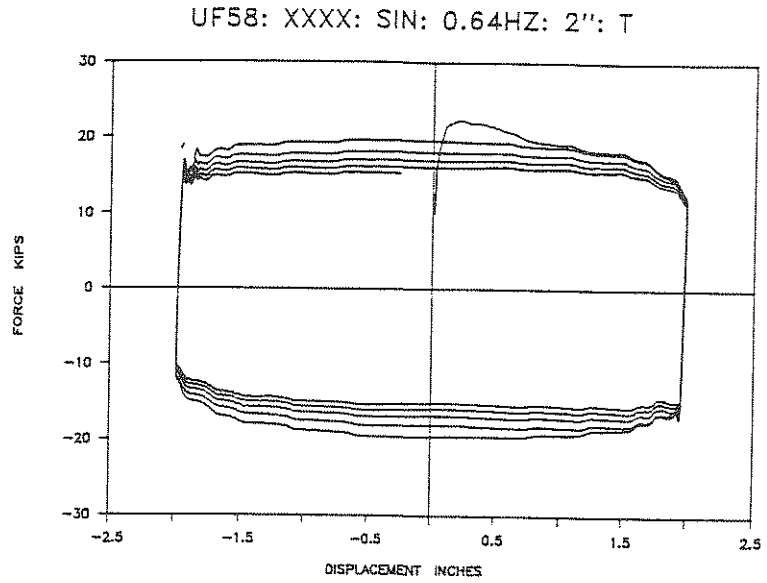
UF58: XXXX: SIN: 0.64HZ: 2": T
FORCE KIPS
DISPLACEMENT INCHES
30
20
10
0
-10
-20
-30
-2.5
-1.5
-0.5
0.5
1.5
2.5

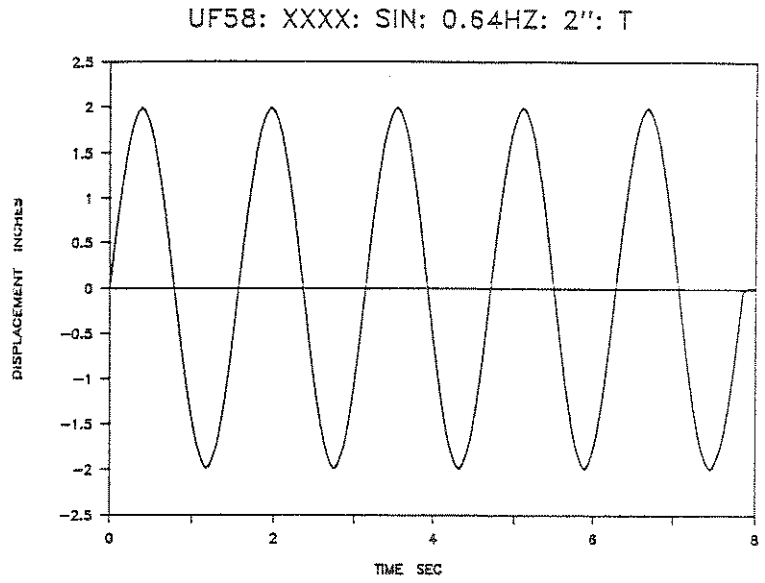
UF58: XXXX: SIN: 0.64HZ: 2": T
DISPLACEMENT INCHES
TIME SEC
2.5
2
1.5
1
0.5
0
-0.5
-1
-1.5
-2
-2.5
0
2
4
6
8

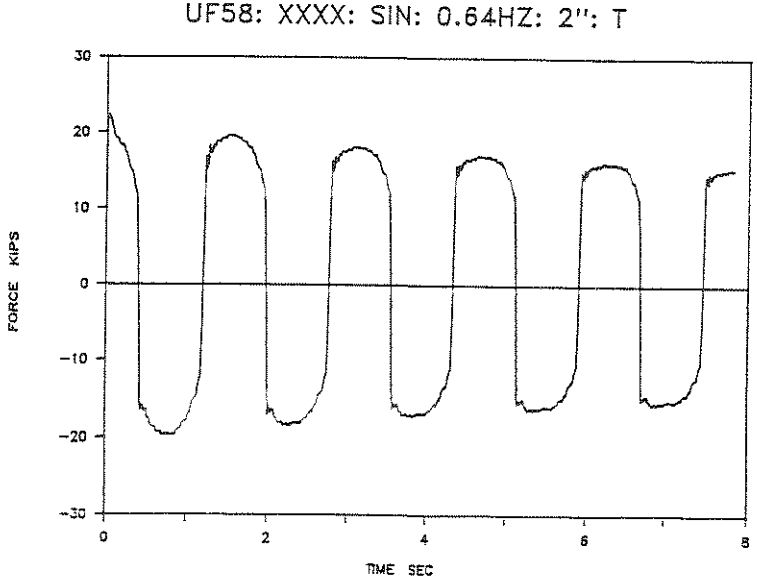
UF58: XXXX: SIN: 0.64HZ: 2": T
FORCE KIPS
TIME SEC
30
20
10
0
-10
-20
-30
0
2
4
6
8

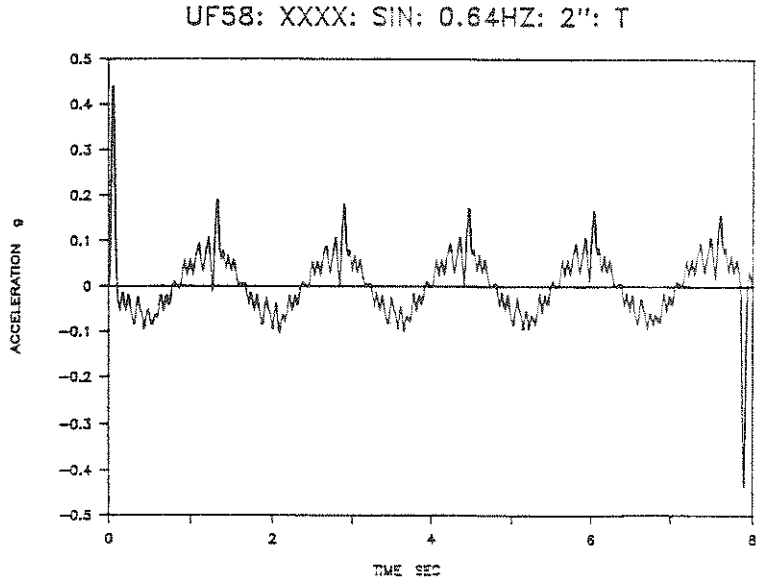
UF58: XXXX: SIN: 0.64HZ: 2": T
ACCELERATION g
TIME SEC
0.5
0.4
0.3
0.2
0.1
0
-0.1
-0.2
-0.3
-0.4
-0.5
0
2
4
6
8

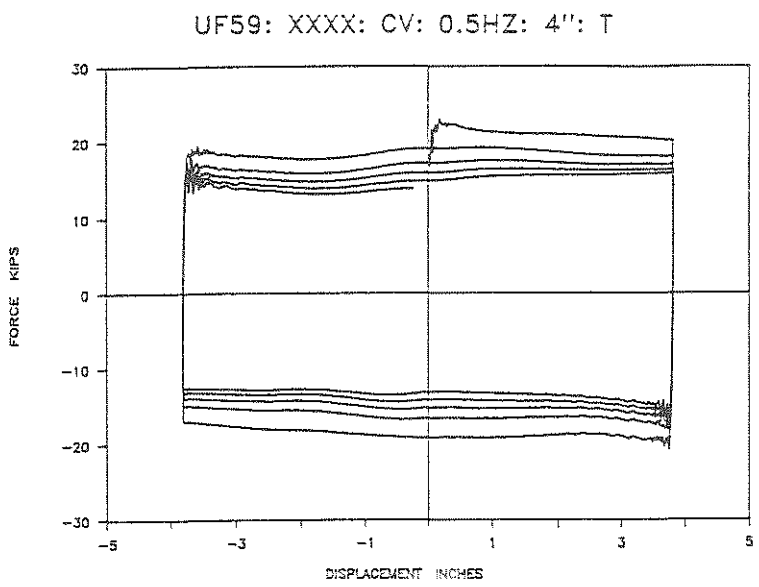
UF59: XXXX: CV: 0.5HZ: 4": T
FORCE KIPS
DISPLACEMENT INCHES

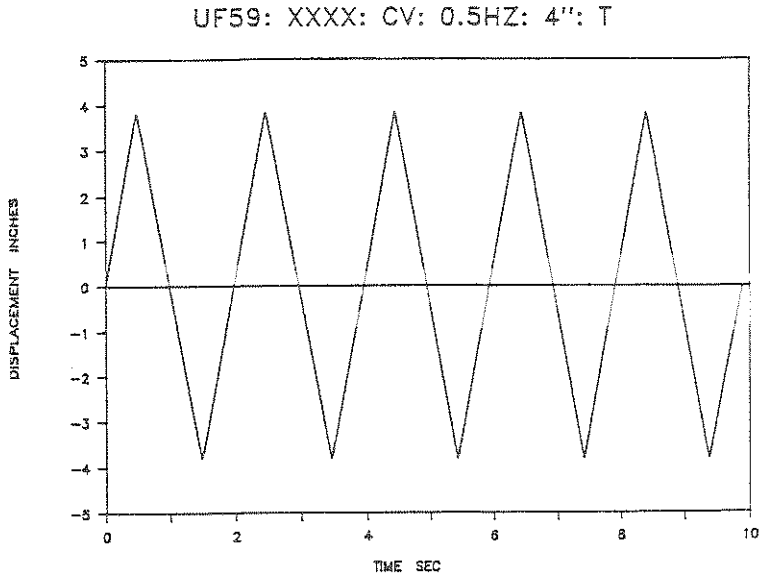
UF59: XXXX: CV: 0.5HZ: 4": T
DISPLACEMENT INCHES
TIME SEC

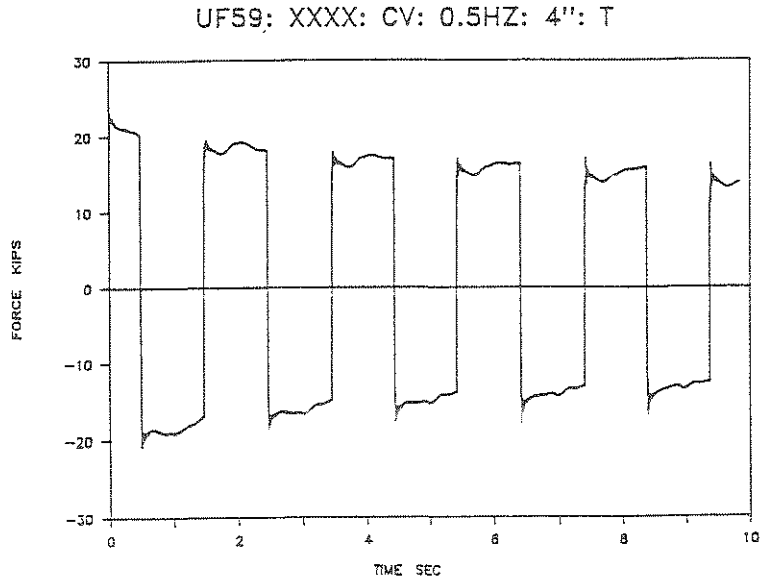
UF59: XXXX: CV: 0.5HZ: 4": T
FORCE KIPS
TIME SEC

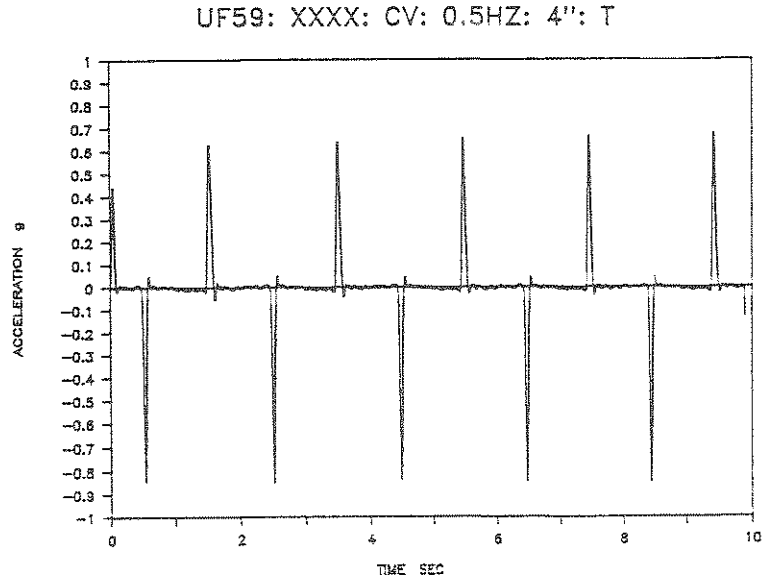
UF59: XXXX: CV: 0.5HZ: 4": T
ACCELERATION g
TIME SEC

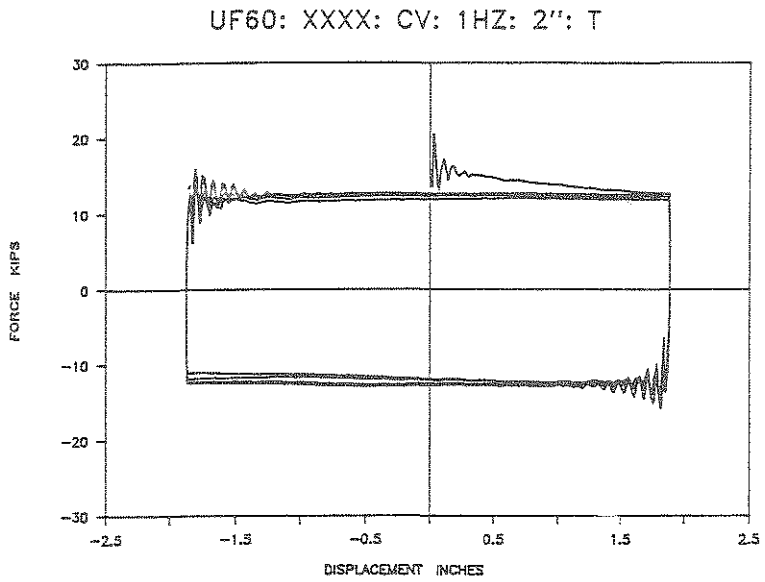
UF60: XXXX: CV: 1HZ: 2": T
FORCE KIPS
DISPLACEMENT INCHES
30
20
10
0
-10
-20
-30
-2.5
-1.5
-0.5
0.5
1.5
2.5

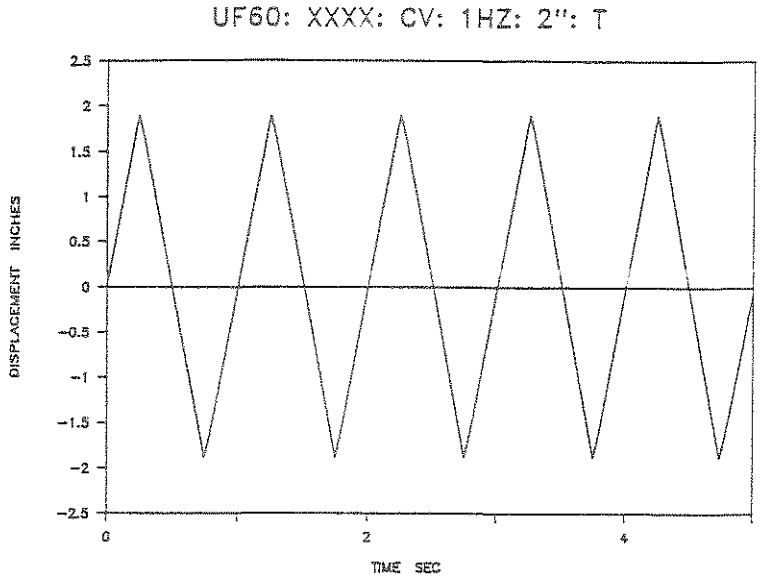
UF60: XXXX: CV: 1HZ: 2": T
DISPLACEMENT INCHES
TIME SEC
2.5
2
1.5
1
0.5
0
-0.5
-1
-1.5
-2
-2.5
0
2
4

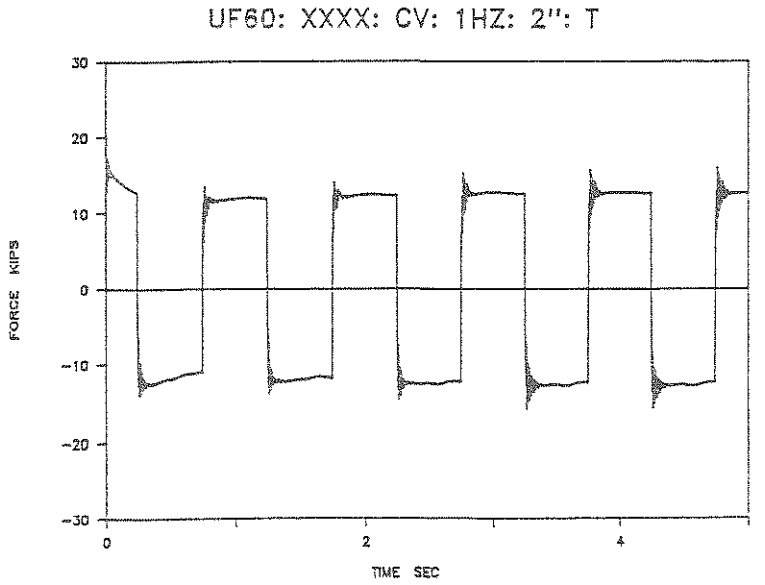
UF60: XXXX: CV: 1HZ: 2": T
FORCE KIPS
TIME SEC
30
20
10
0
-10
-20
-30
0
2
4

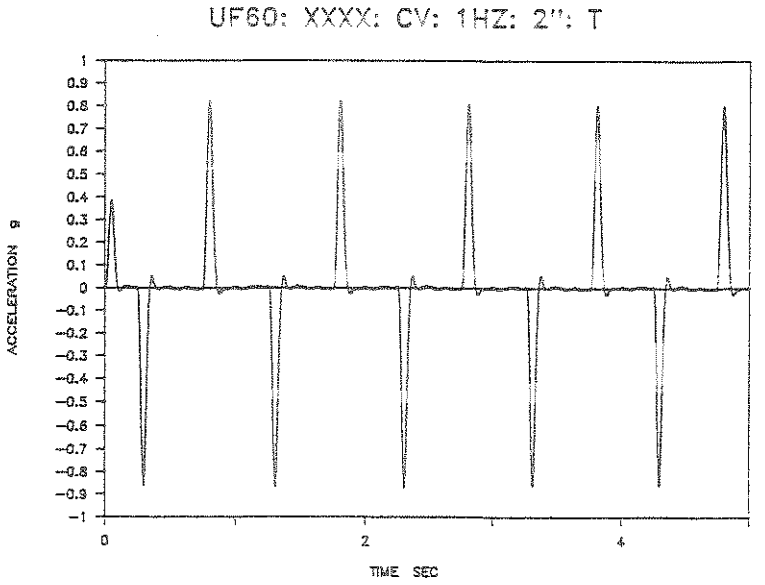
UF60: XXXX: CV: 1HZ: 2": T
ACCELERATION g
TIME SEC
1
0.9
0.8
0.7
0.6
0.5
0.4
0.3
0.2
0.1
0
-0.1
-0.2
-0.3
-0.4
-0.5
-0.6
-0.7
-0.8
-0.9
-1
0
2
4

UF61: 1000PSI: SIN: 0.03HZ: 0.5": P

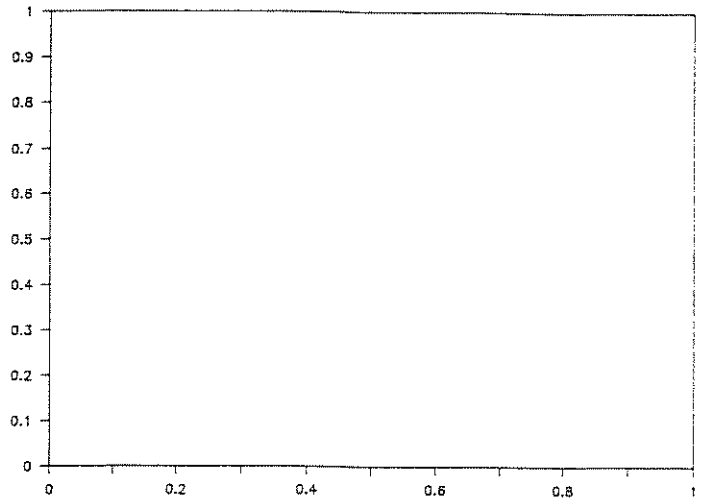

UF62: 1000PSI: SIN: 0.16HZ: 1": P

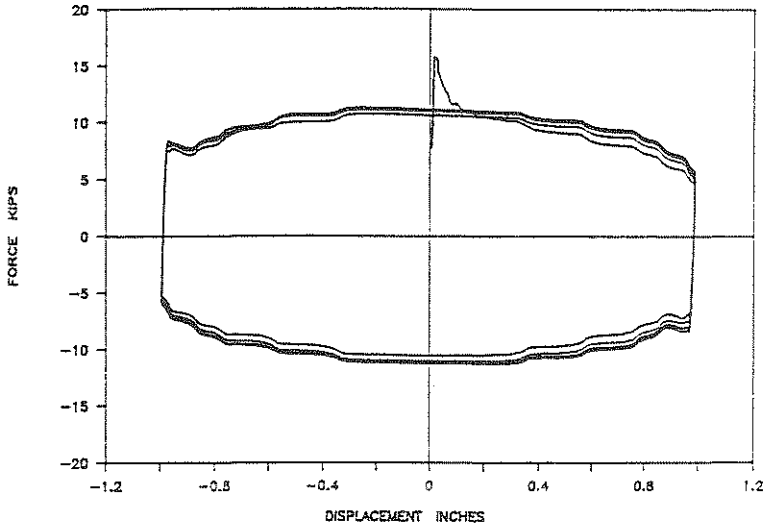

UNABLE TO RECOVER TEST DATA

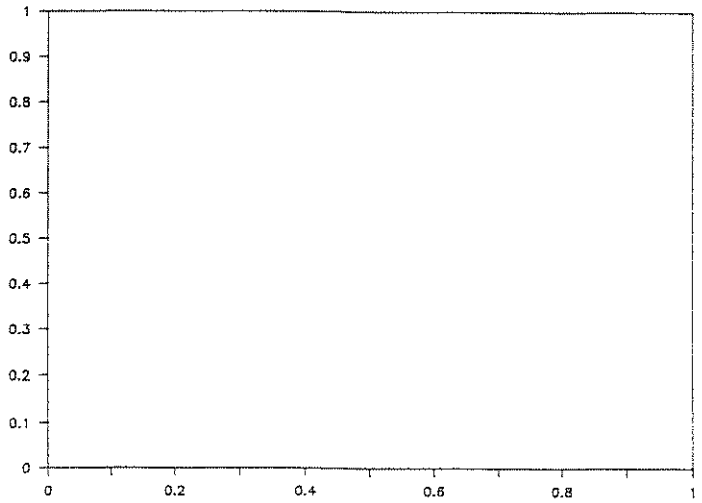

UF62: 1000PSI: SIN: 0.16HZ: 1": P

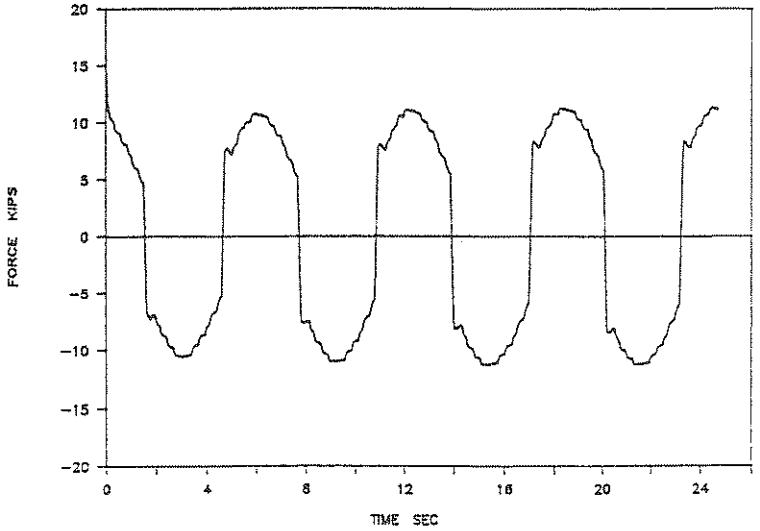

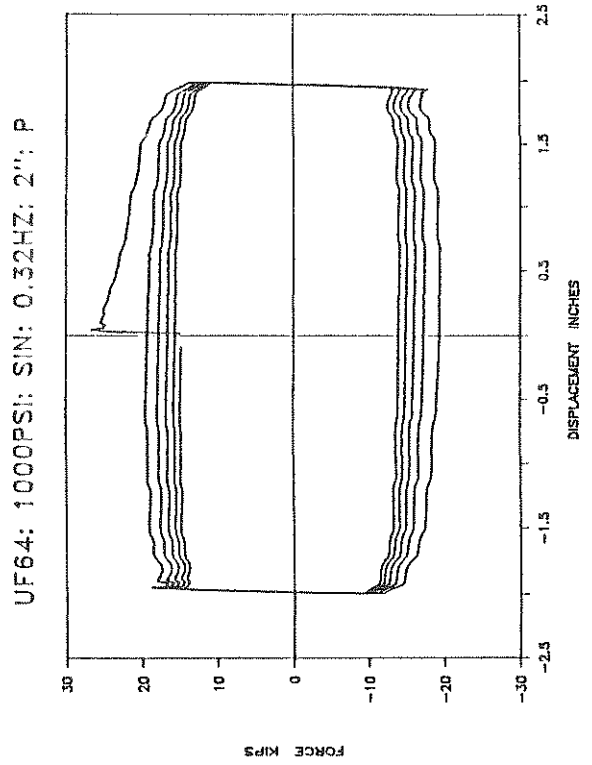
UF64: 1000PSI: SIN: 0.32HZ: 2": P
FORCE KIPS
DISPLACEMENT INCHES

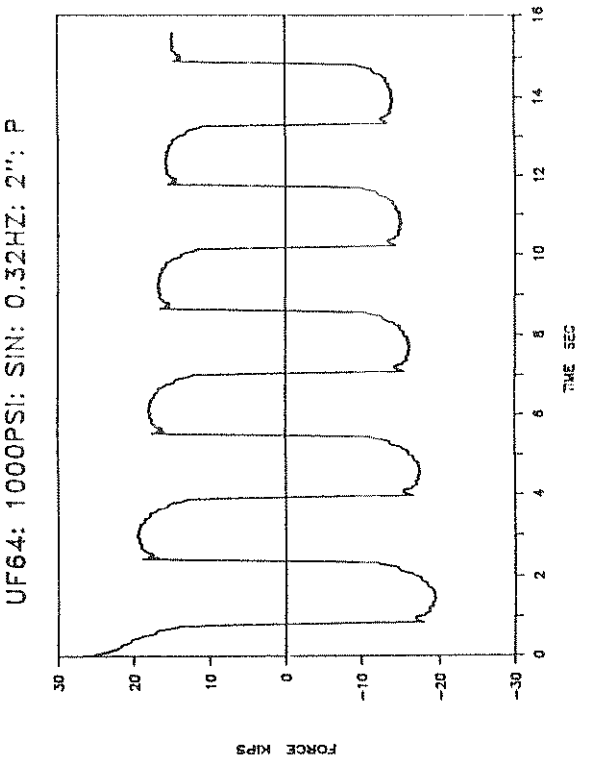
UF64: 1000PSI: SIN: 0.32HZ: 2": P
FORCE KIPS
TIME SEC

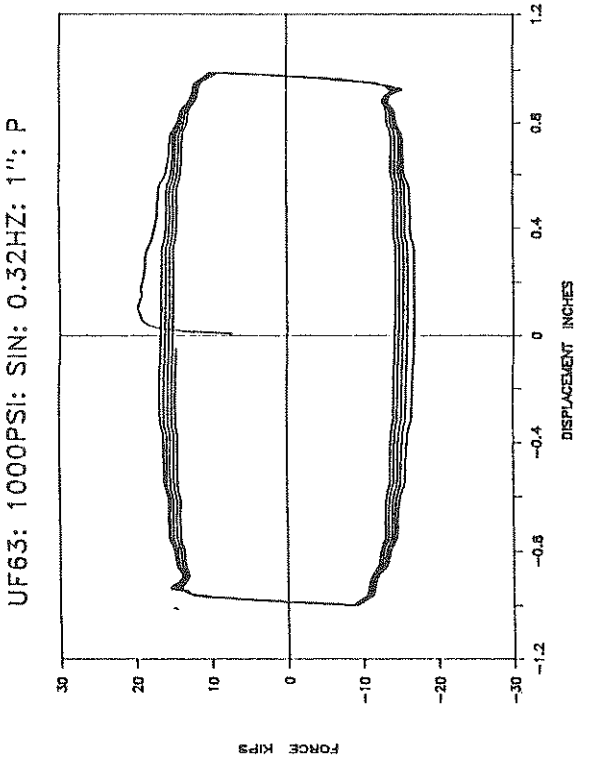
UF63: 1000PSI: SIN: 0.32HZ: 1": P
FORCE KIPS
DISPLACEMENT INCHES

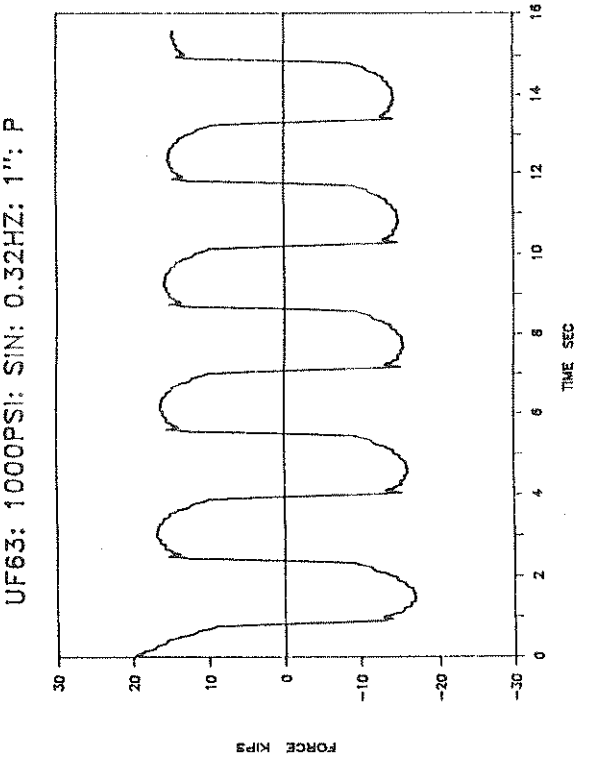
UF63: 1000PSI: SIN: 0.32HZ: 1": P
FORCE KIPS
TIME SEC

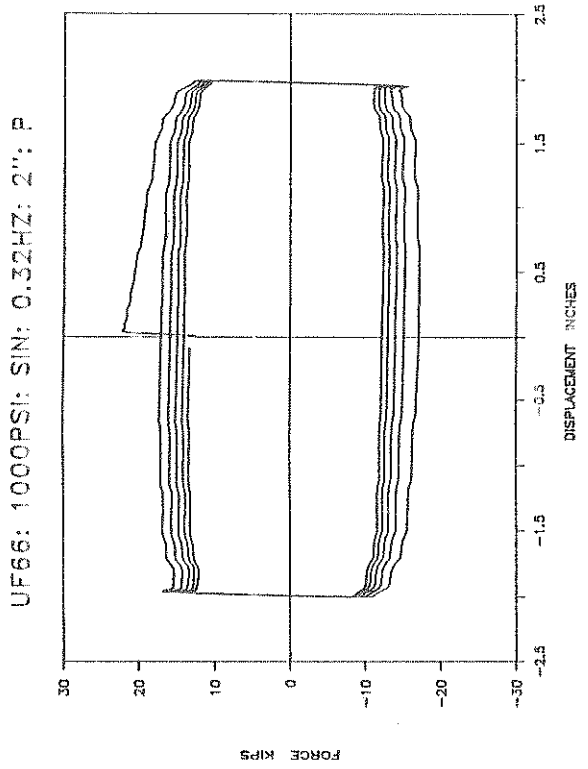
UF66: 1000PSI: SIN: 0.32HZ: 2": P
FORCE KIPS
DISPLACEMENT INCHES

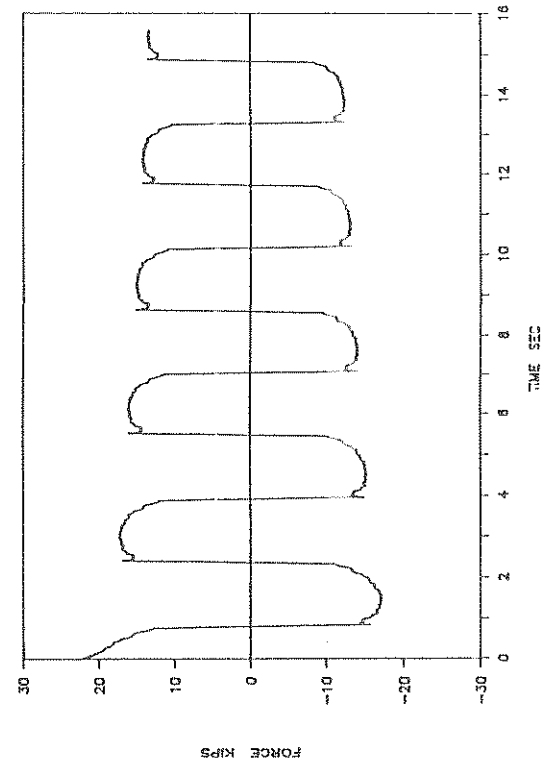
UF66: 1000PSI: SIN: 0.32HZ: 2": P
FORCE KIPS
TIME SEC

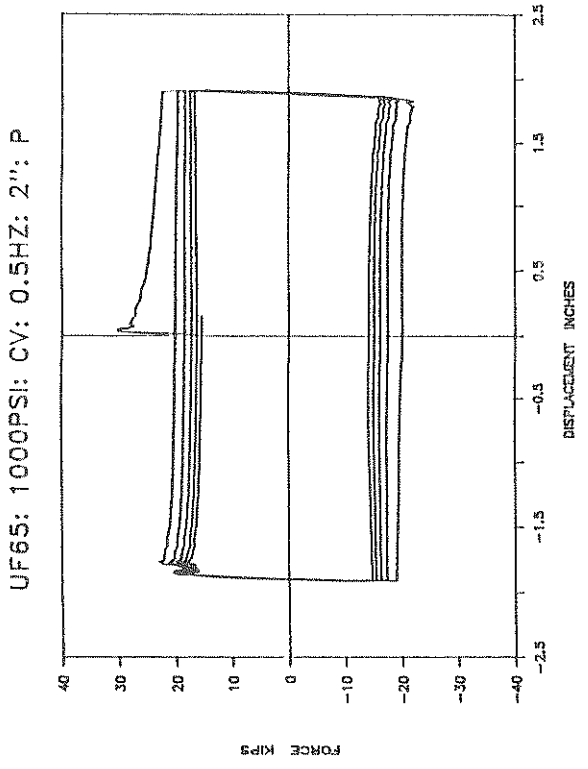
UF65: 1000PSI: CV: 0.5HZ: 2": P
FORCE KIPS
DISPLACEMENT INCHES

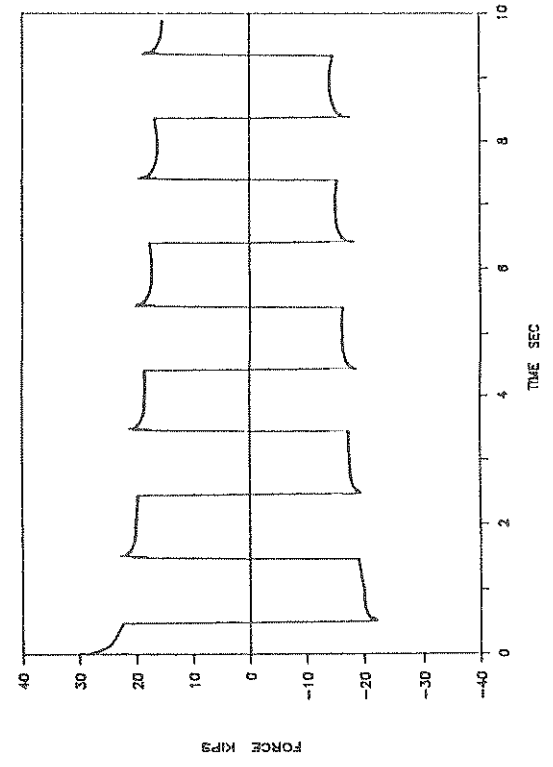
UF65: 1000PSI: CV: 0.5HZ: 2": P
FORCE KIPS
TIME SEC

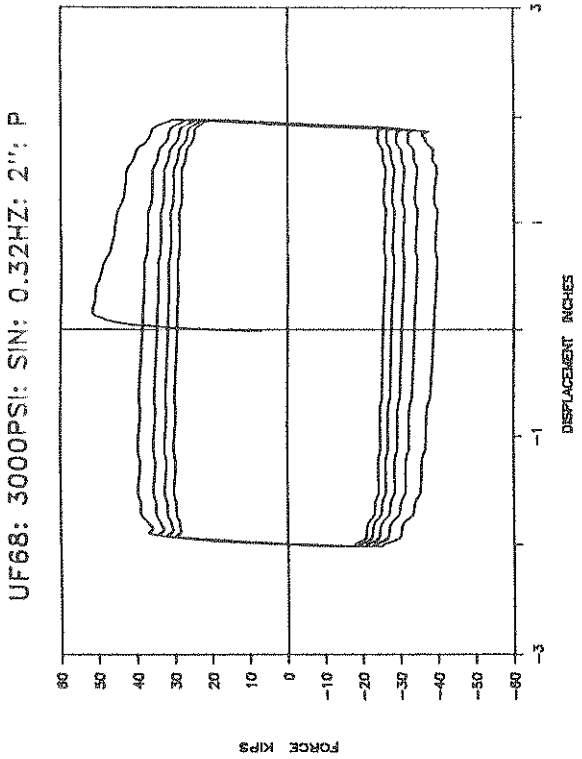
UF68: 3000PSI: SIN: 0.32HZ: 2": P
FORCE KIPS
DISPLACEMENT INCHES

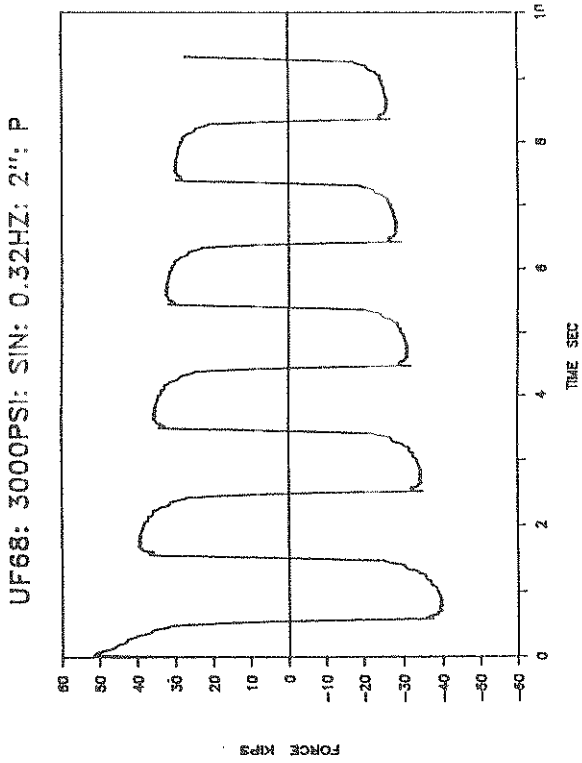
UF68: 3000PSI: SIN: 0.32HZ: 2": P
FORCE KIPS
TIME SEC

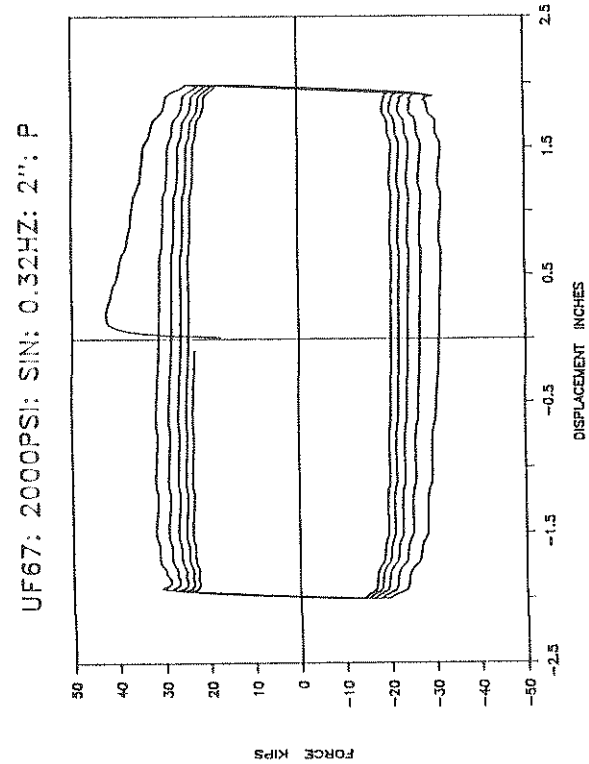
UF67: 2000PSI: SIN: 0.32HZ: 2": P
FORCE KIPS
DISPLACEMENT INCHES

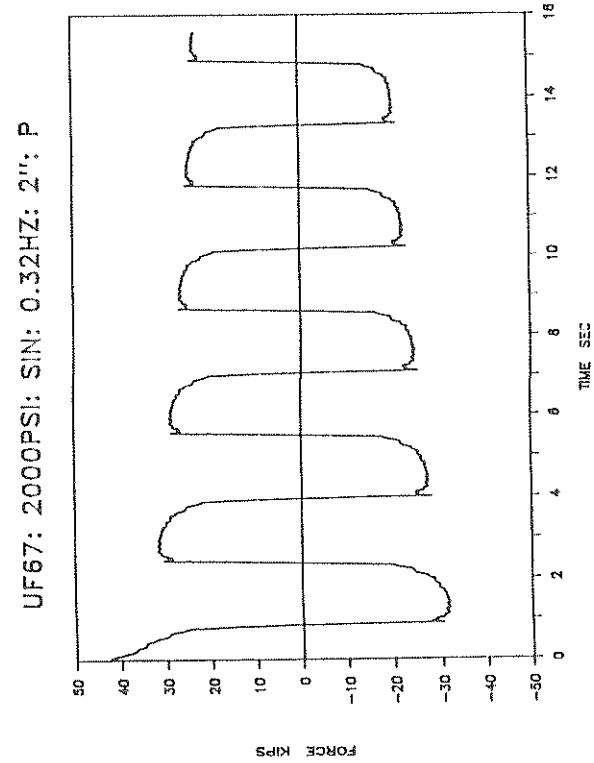
UF67: 2000PSI: SIN: 0.32HZ: 2": P
FORCE KIPS
TIME SEC

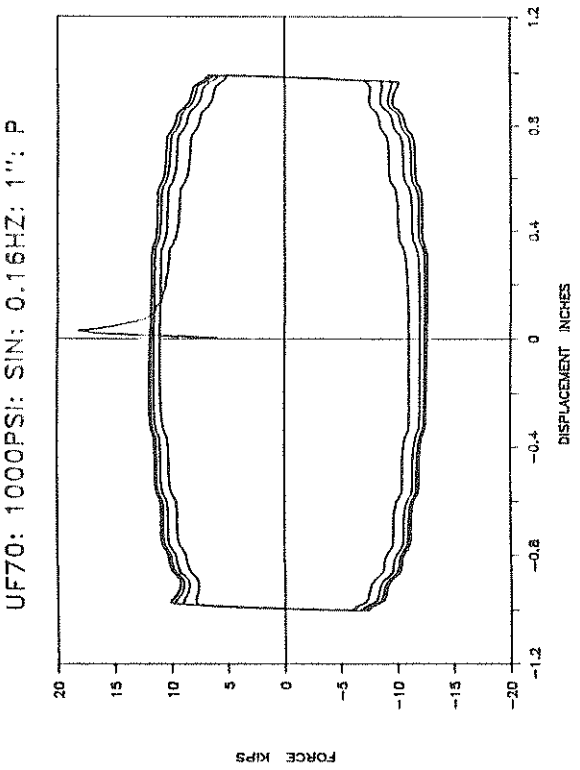
UF70: 1000PSI: SIN: 0.16HZ: 1": P
FORCE KIPS
DISPLACEMENT INCHES

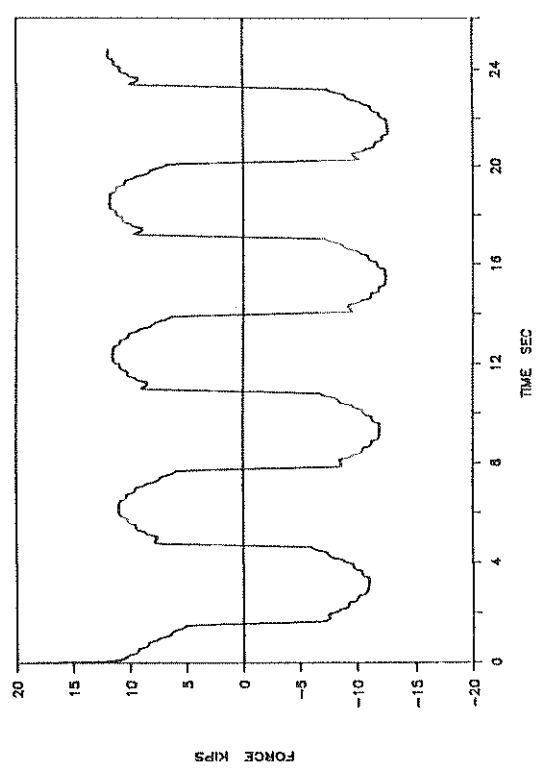
UF70: 1000PSI: SIN: 0.16HZ: 1": P
FORCE KIPS
TIME SEC

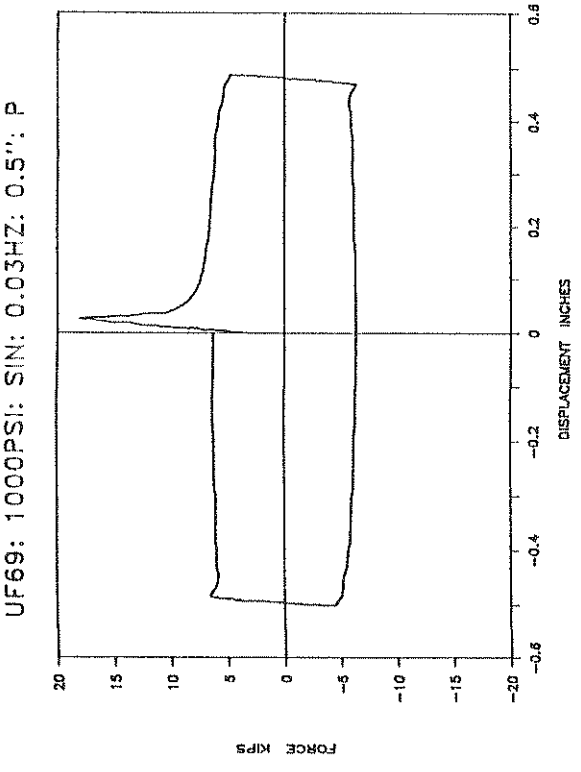
UF69: 1000PSI: SIN: 0.03HZ: 0.5": P
FORCE KIPS
DISPLACEMENT INCHES

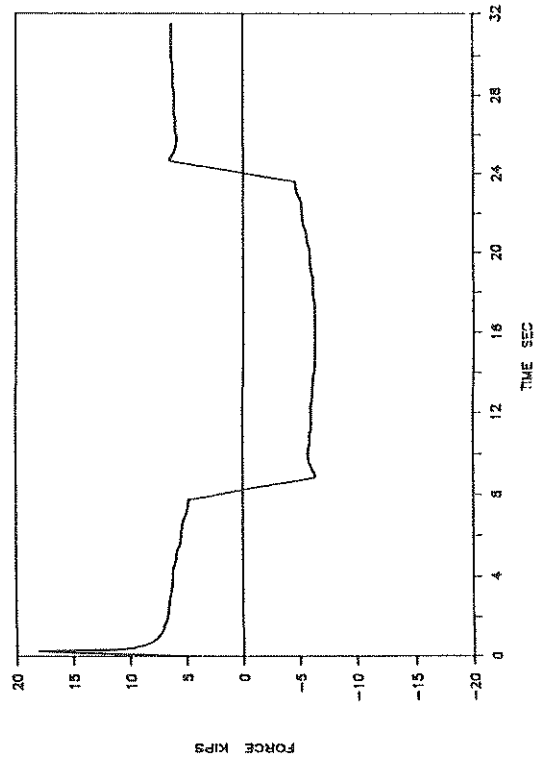
UF69: 1000PSI: SIN: 0.03HZ: 0.5": P
FORCE KIPS
TIME SEC

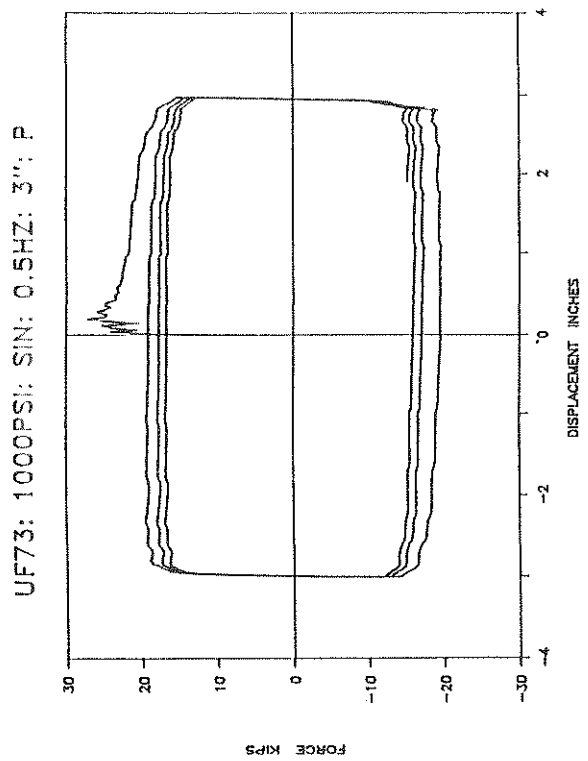
UF73: 1000PSI: SIN: 0.5HZ: 3": P
FORCE KIPS
DISPLACEMENT INCHES

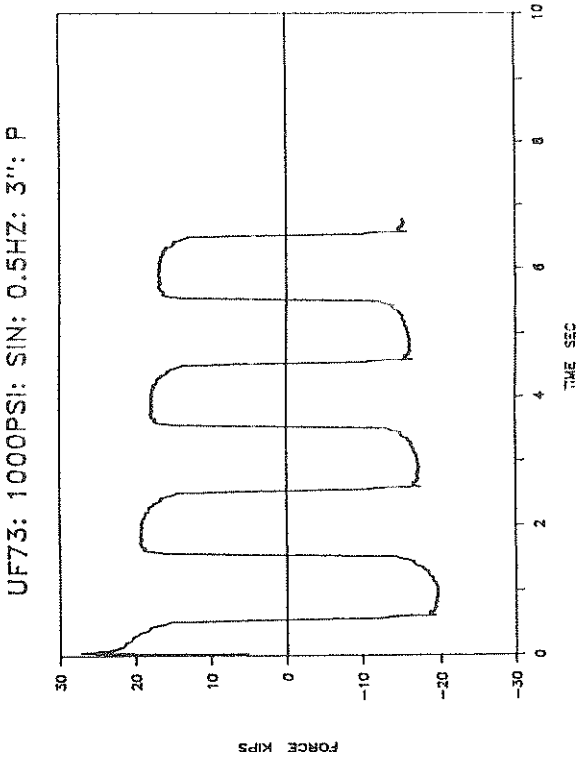
UF73: 1000PSI: SIN: 0.5HZ: 3": P
FORCE KIPS
TIME SEC

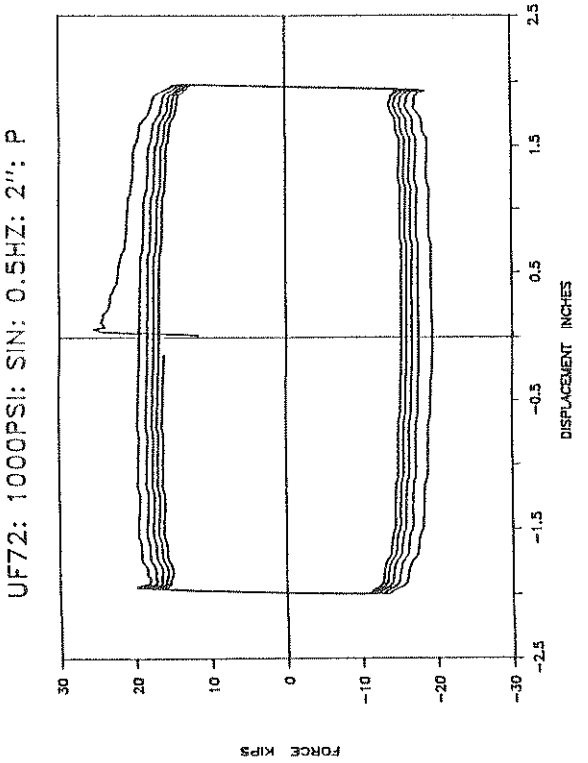
UF72: 1000PSI: SIN: 0.5HZ: 2": P
FORCE KIPS
DISPLACEMENT INCHES

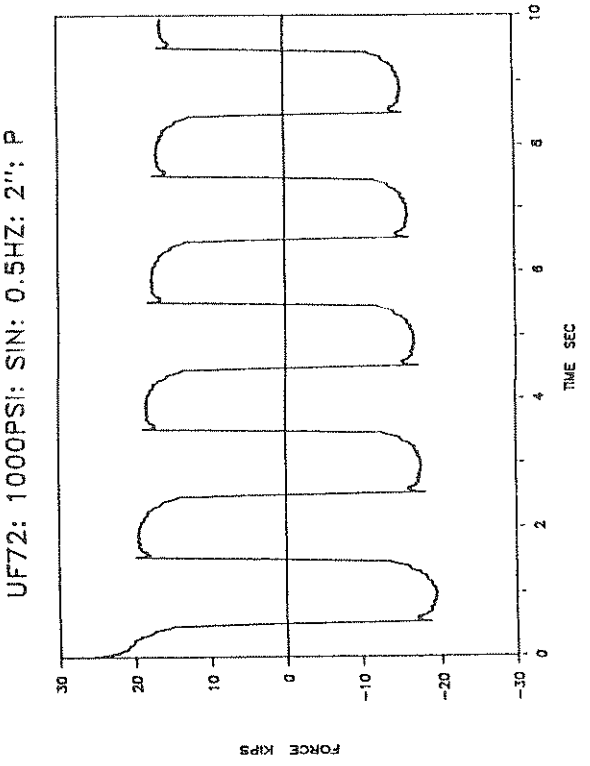
UF72: 1000PSI: SIN: 0.5HZ: 2": P
FORCE KIPS
TIME SEC

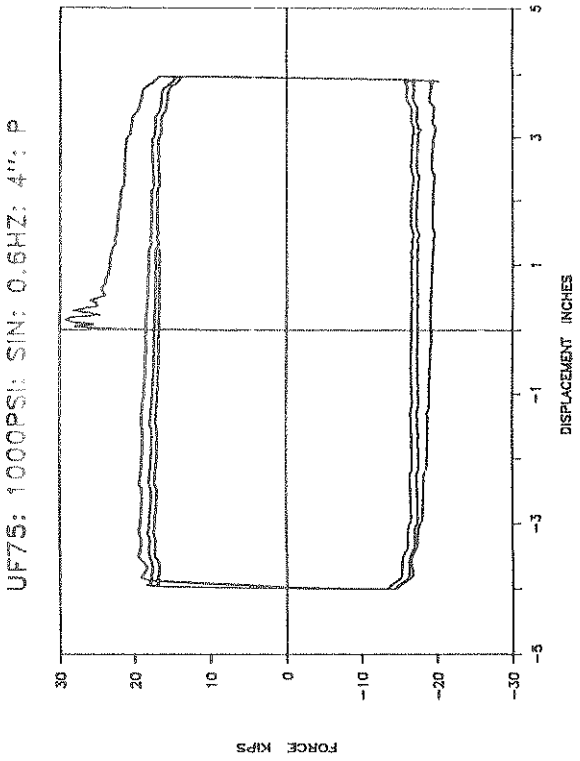
UF75: 1000PSI: SIN: 0.6HZ: 4": P
FORCE KIPS
DISPLACEMENT INCHES

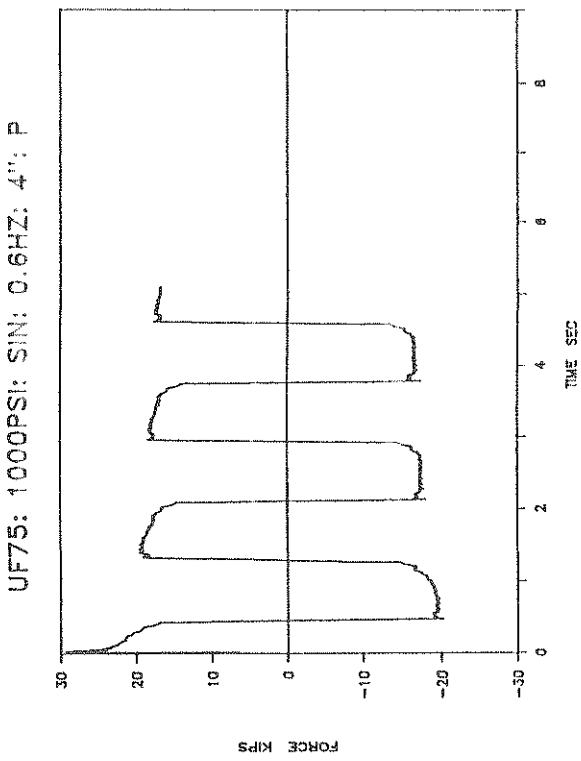
UF75: 1000PSI: SIN: 0.6HZ: 4": P
FORCE KIPS
TIME SEC

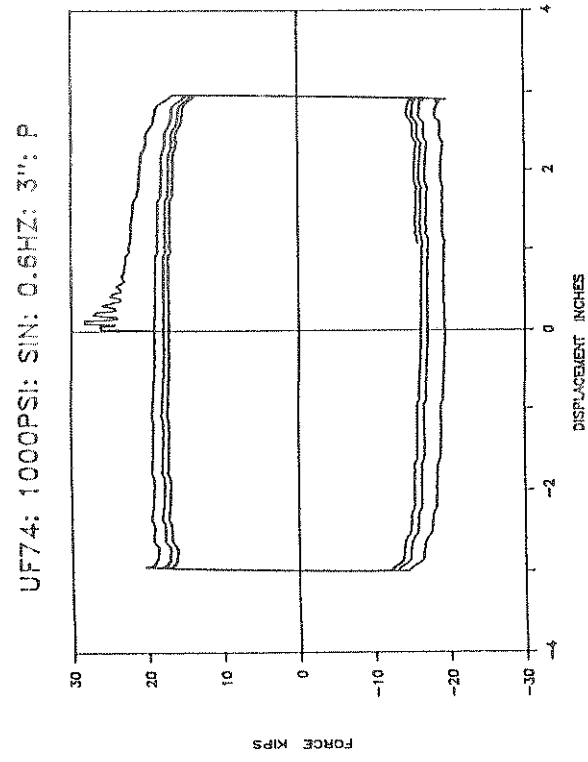
UF74: 1000PSI: SIN: 0.6HZ: 3": P
FORCE KIPS
DISPLACEMENT INCHES

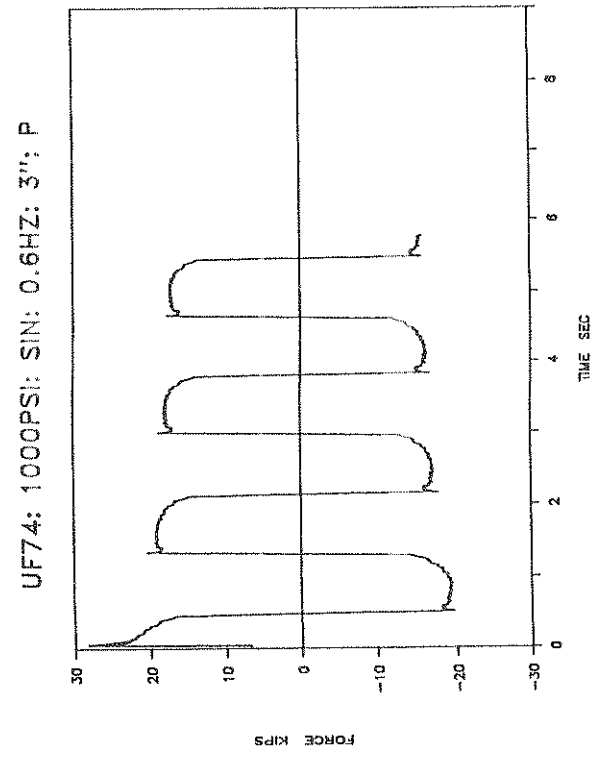
UF74: 1000PSI: SIN: 0.6HZ: 3": P
FORCE KIPS
TIME SEC

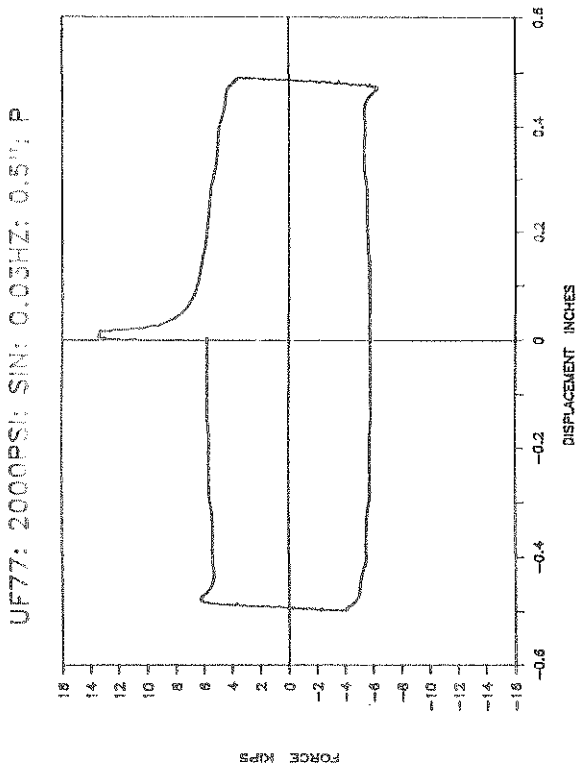
UF77: 2000PSI: SIN: 0.03HZ: 0.5": P
FORCE KIPS
DISPLACEMENT INCHES

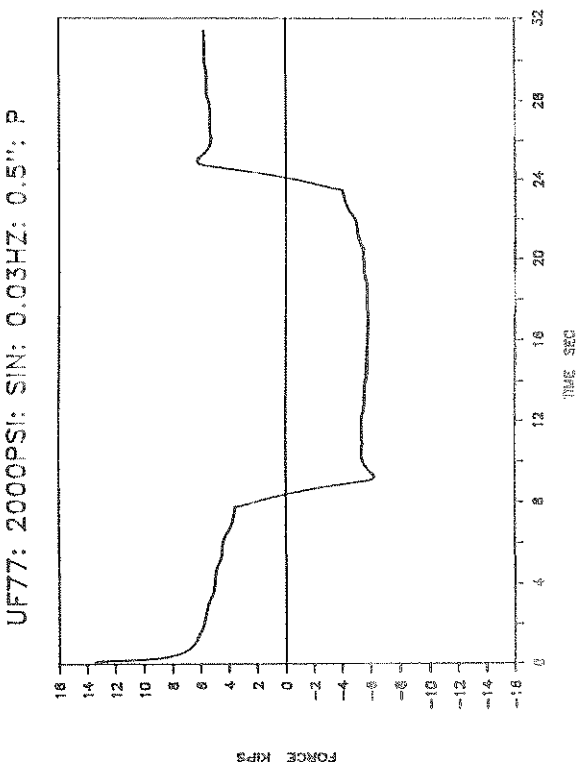
UF77: 2000PSI: SIN: 0.03HZ: 0.5": P
FORCE KIPS
TIME SEC

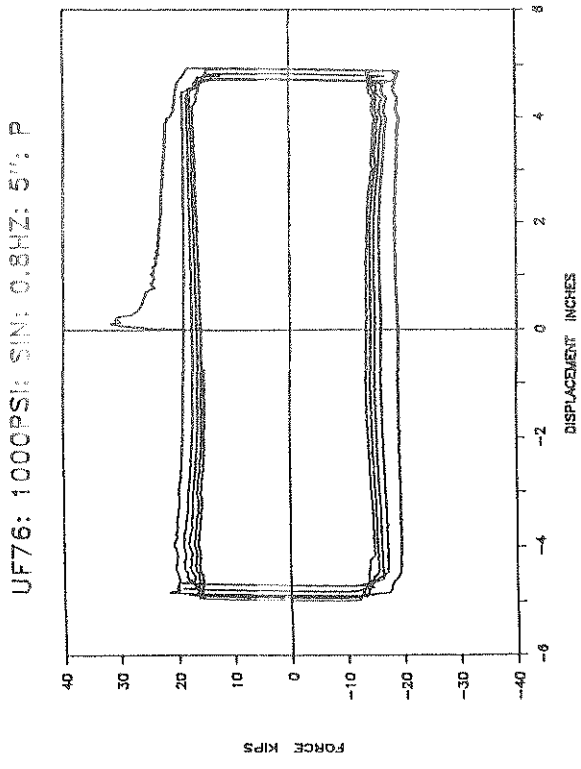
UF76: 1000PSI: SIN: 0.8HZ: 5": P
FORCE KIPS
DISPLACEMENT INCHES

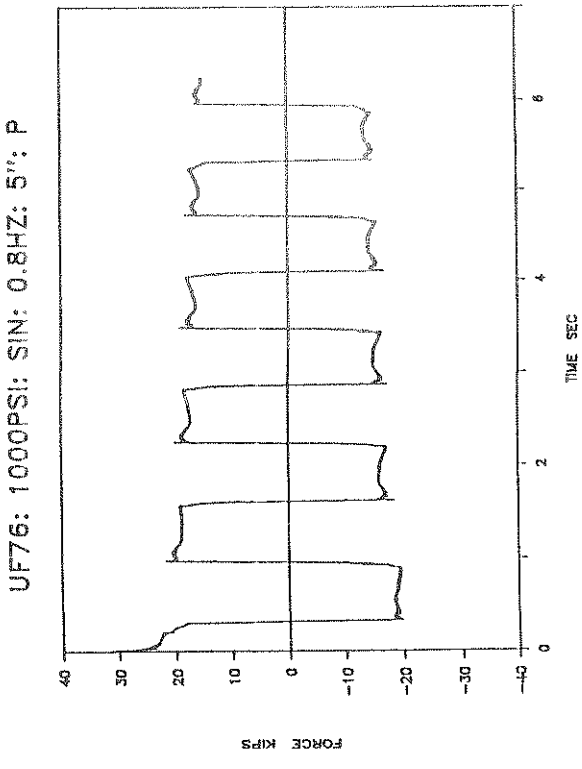
UF76: 1000PSI: SIN: 0.8HZ: 5": P
FORCE KIPS
TIME SEC

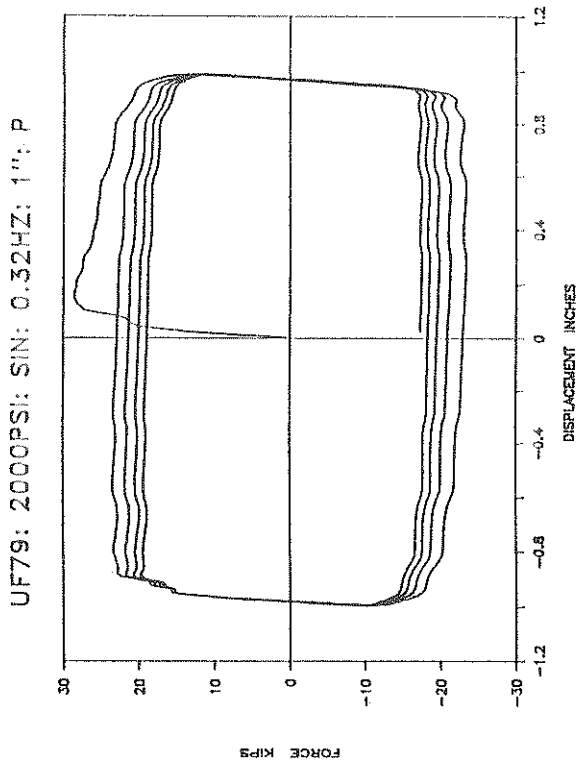
UF79: 2000PSI: SIN: 0.32HZ: 1": P
FORCE KIPS
DISPLACEMENT INCHES

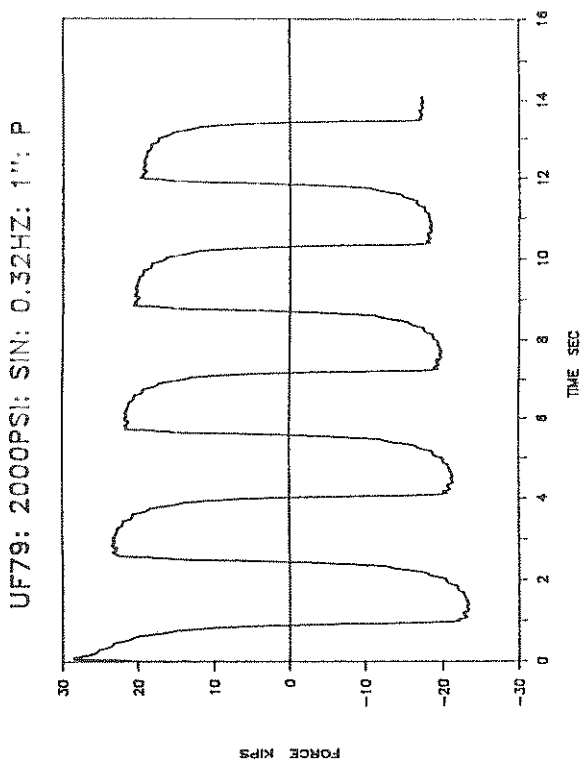
UF79: 2000PSI: SIN: 0.32HZ: 1": P
FORCE KIPS
TIME SEC

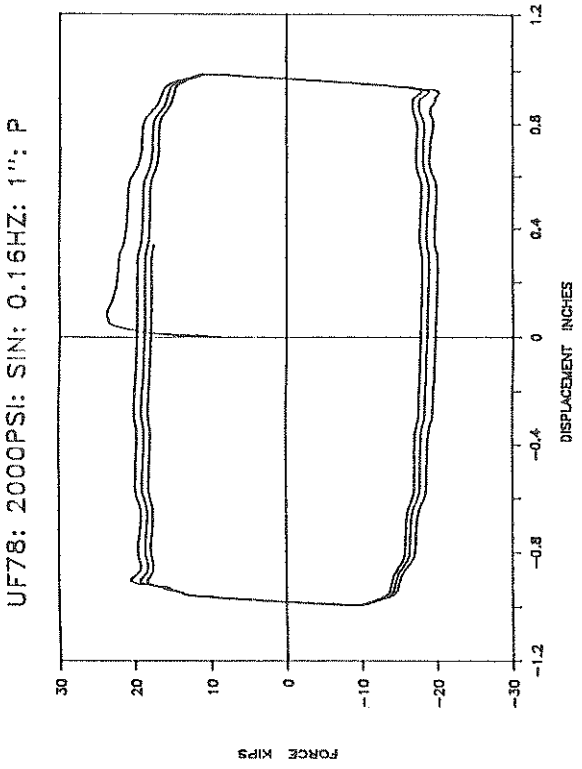
UF78: 2000PSI: SIN: 0.16HZ: 1": P
FORCE KIPS
DISPLACEMENT INCHES

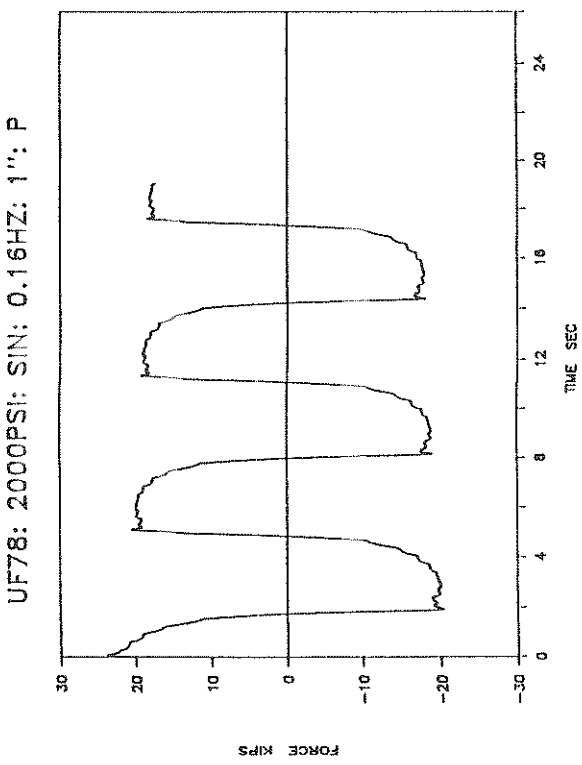
UF78: 2000PSI: SIN: 0.16HZ: 1": P
FORCE KIPS
TIME SEC

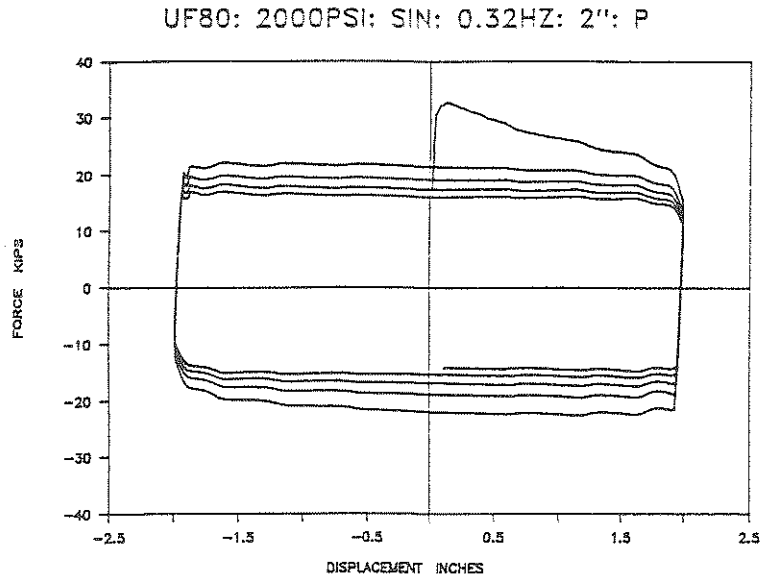
UF80: 2000PSI: SIN: 0.32HZ: 2": P
FORCE KIPS
DISPLACEMENT INCHES

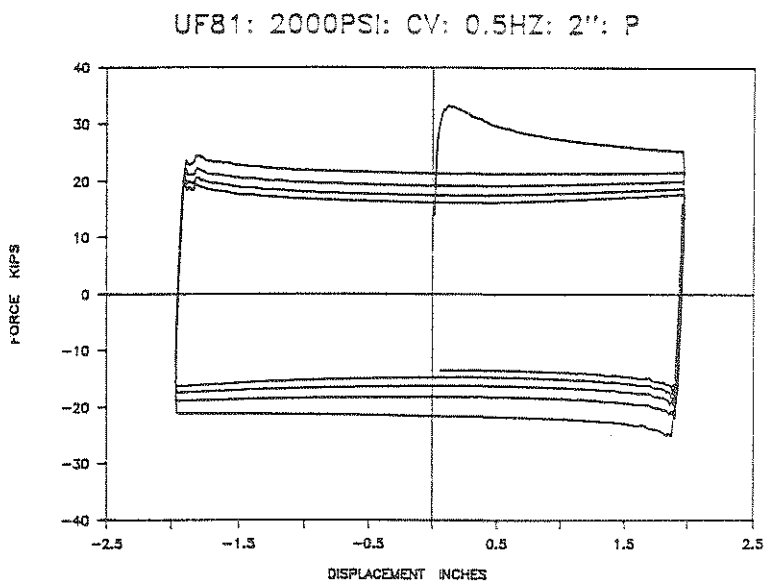
UF81: 2000PSI: CV: 0.5HZ: 2": P
FORCE KIPS
DISPLACEMENT INCHES

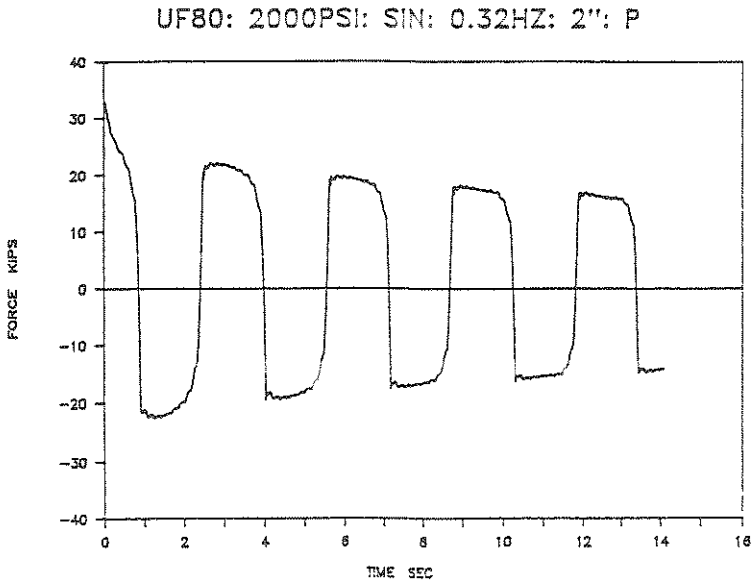
UF80: 2000PSI: SIN: 0.32HZ: 2": P
FORCE KIPS
TIME SEC

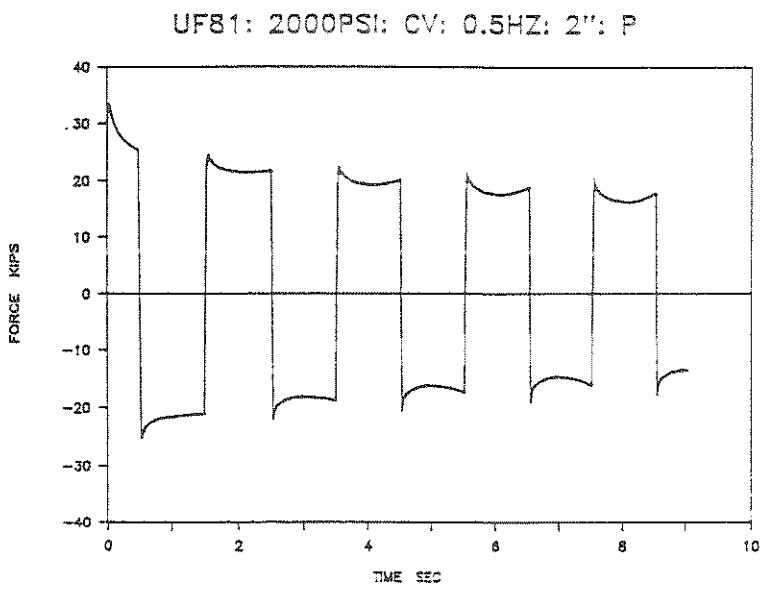
UF81: 2000PSI: CV: 0.5HZ: 2": P
FORCE KIPS
TIME SEC

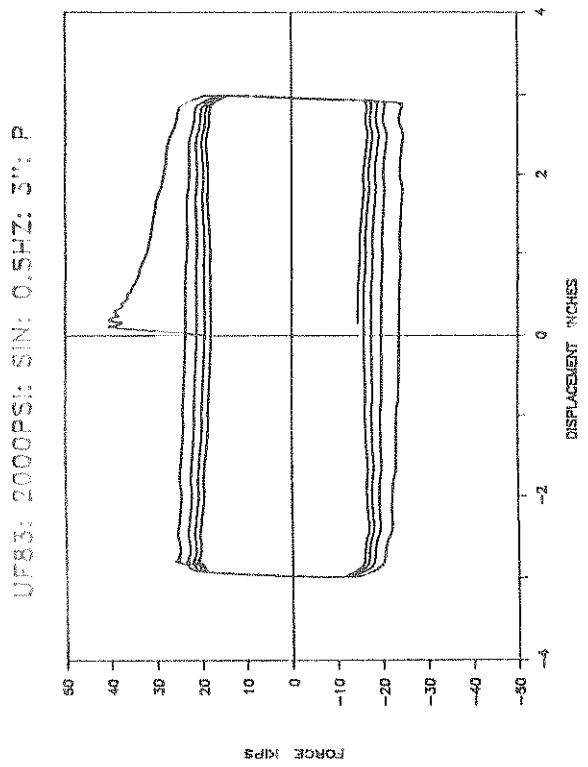
UF83: 2000PSI: SIN: 0.5HZ: 3": P
FORCE KIPS
DISPLACEMENT INCHES

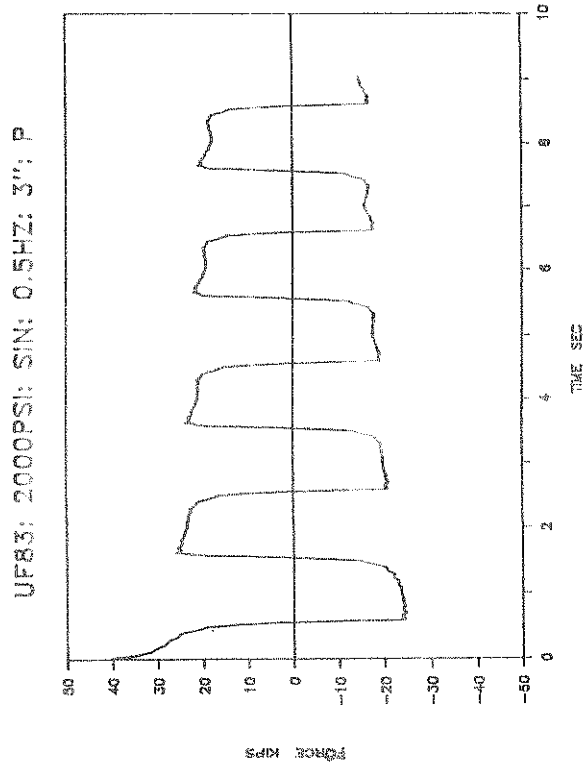
UF83: 2000PSI: SIN: 0.5HZ: 3": P
FORCE KIPS
TIME SEC

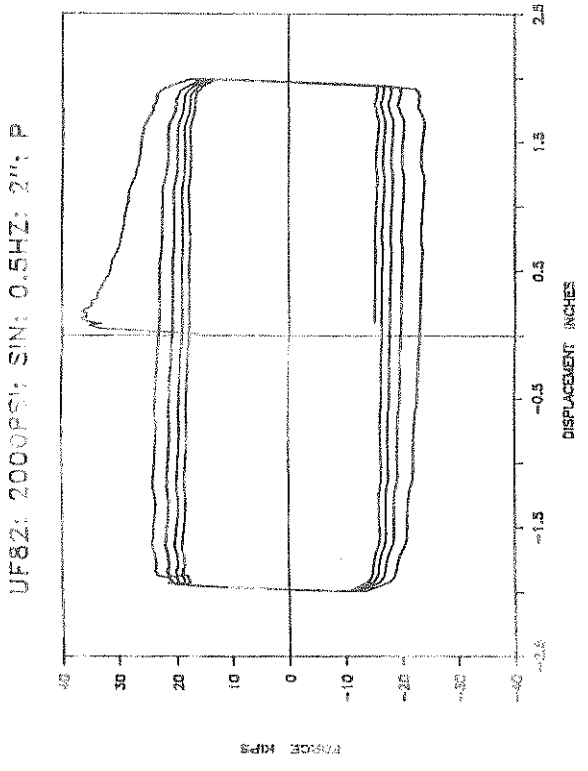
UF82: 2000PSI: SIN: 0.5HZ: 2": P
FORCE KIPS
DISPLACEMENT INCHES

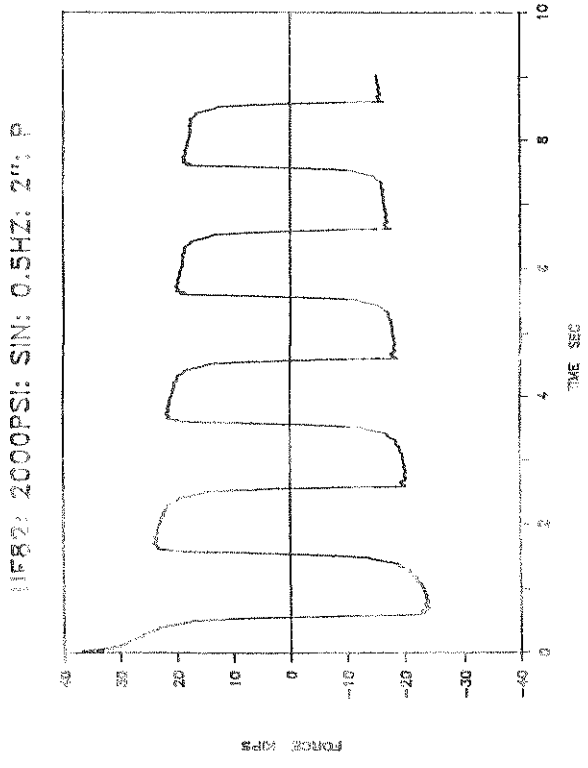
UF82: 2000PSI: SIN: 0.5HZ: 2": P
FORCE KIPS
TIME SEC

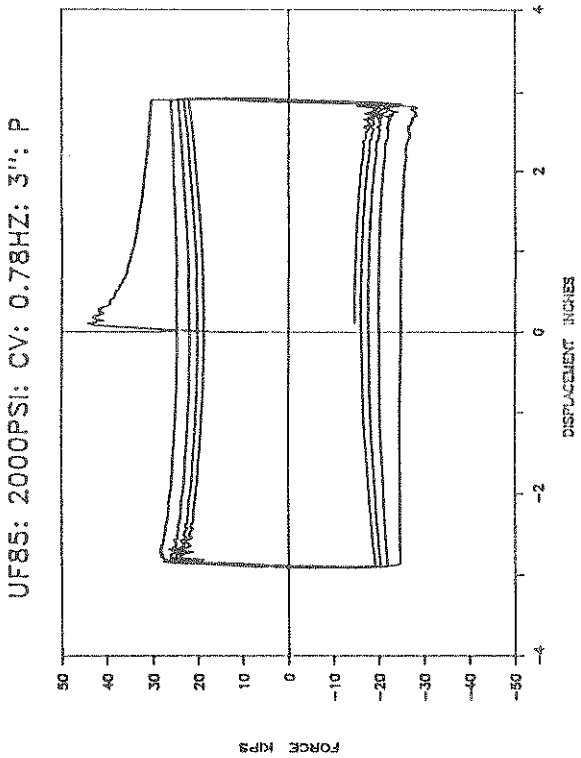
UF85: 2000PSI: CV: 0.78HZ: 3": P
FORCE KIPS
DISPLACEMENT INCHES

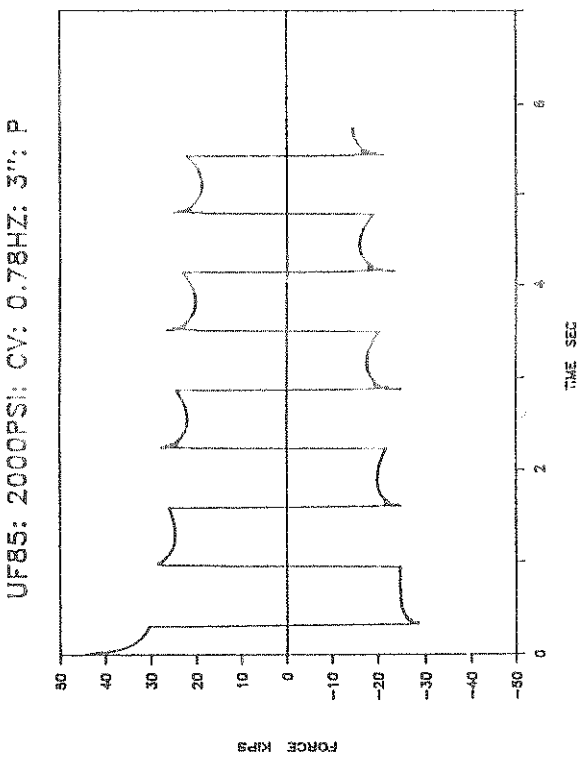
UF85: 2000PSI: CV: 0.78HZ: 3": P
FORCE KIPS
TIME SEC

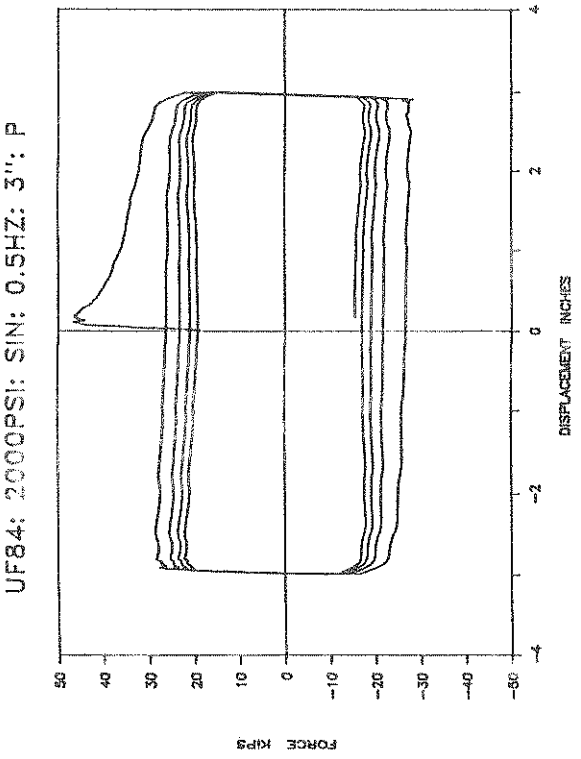
UF84: 2000PSI: SIN: 0.5HZ: 3": P
FORCE KIPS
DISPLACEMENT INCHES

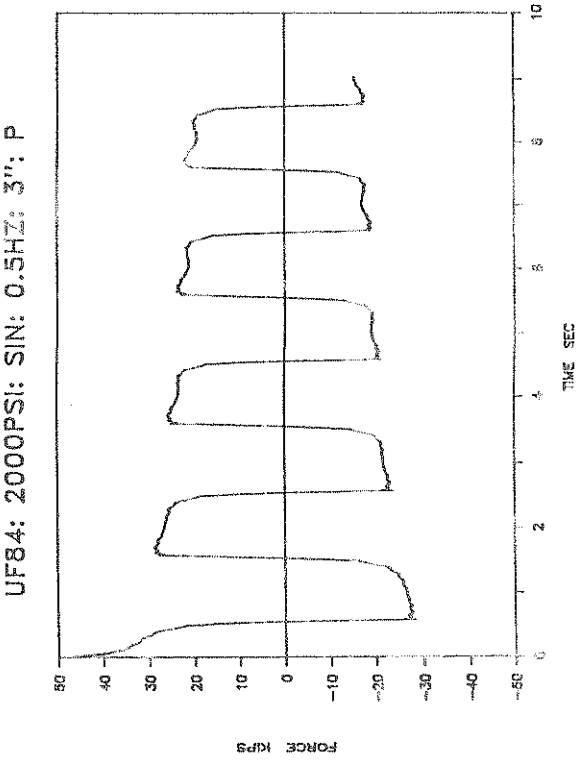
UF84: 2000PSI: SIN: 0.5HZ: 3": P
FORCE KIPS
TIME SEC

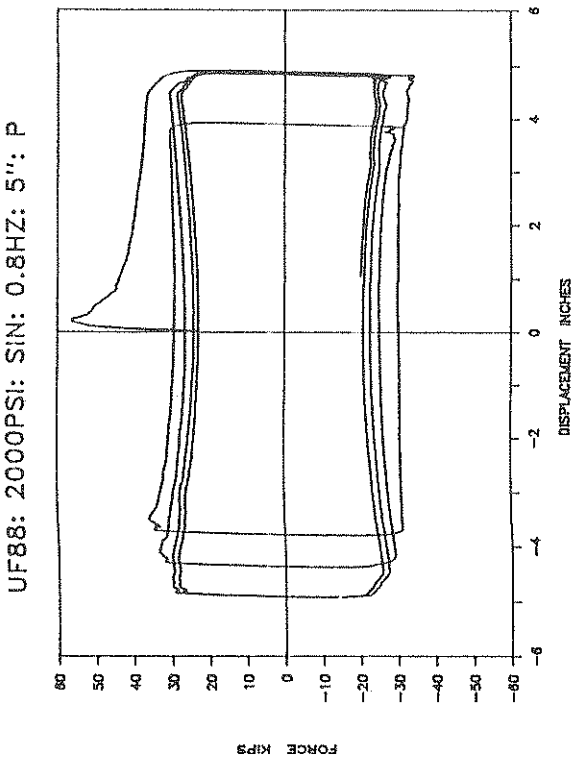
UF88: 2000PSI: SIN: 0.8HZ: 5": P
FORCE KIPS
DISPLACEMENT INCHES

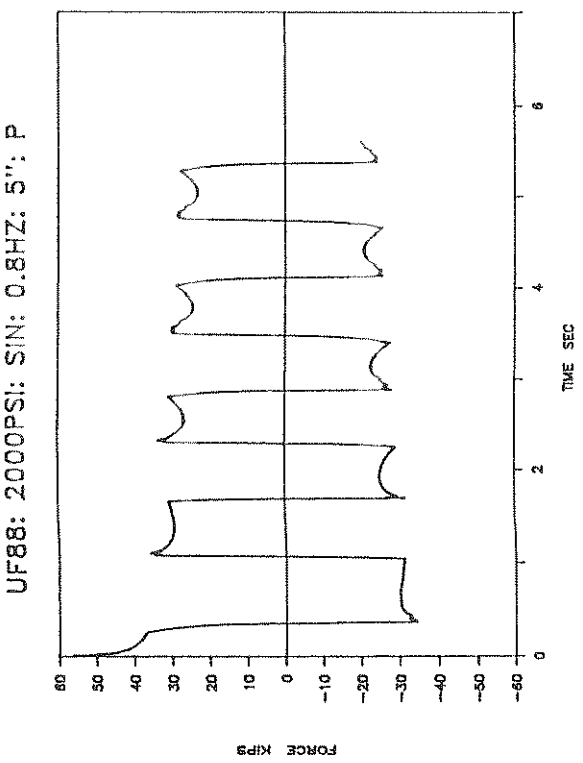
UF88: 2000PSI: SIN: 0.8HZ: 5": P
FORCE KIPS
TIME SEC

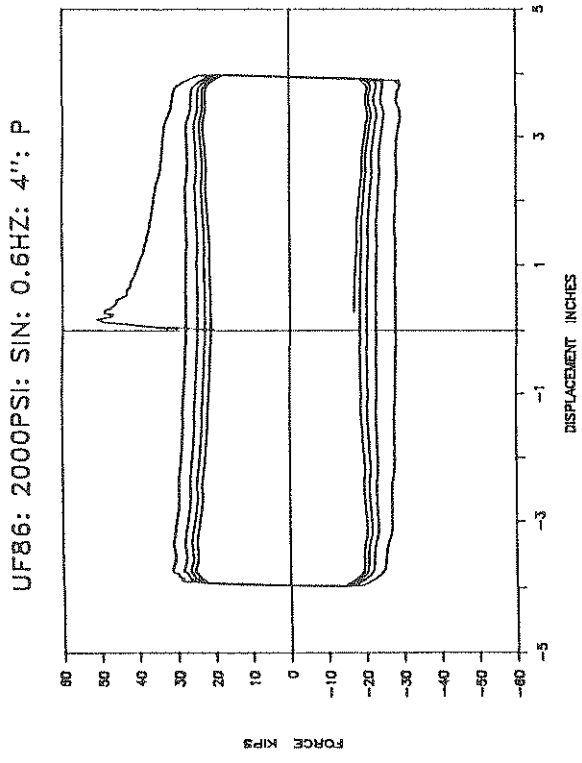
UF86: 2000PSI: SIN: 0.6HZ: 4": P
FORCE KIPS
DISPLACEMENT INCHES

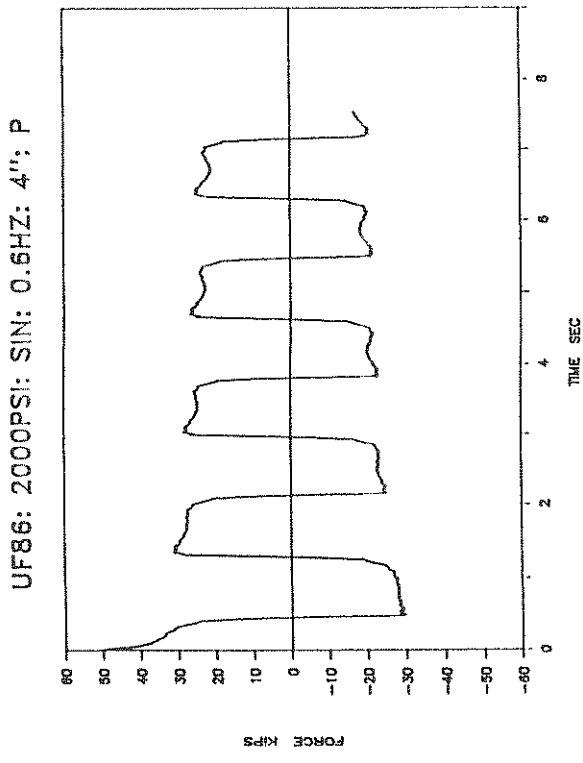
UF86: 2000PSI: SIN: 0.6HZ: 4": P
FORCE KIPS
TIME SEC

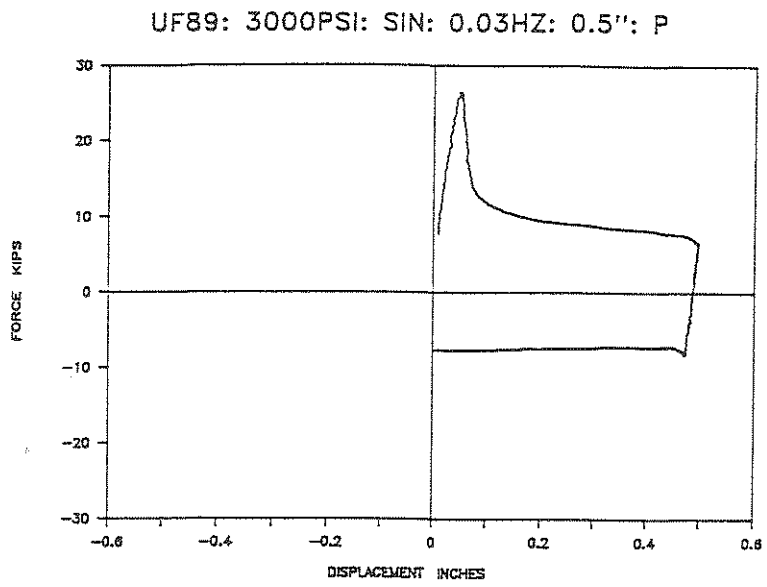
UF89: 3000PSI: SIN: 0.03HZ: 0.5": P
FORCE KIPS
DISPLACEMENT INCHES
30
20
10
0
-10
-20
-30
-0.6
-0.4
-0.2
0
0.2
0.4
0.6

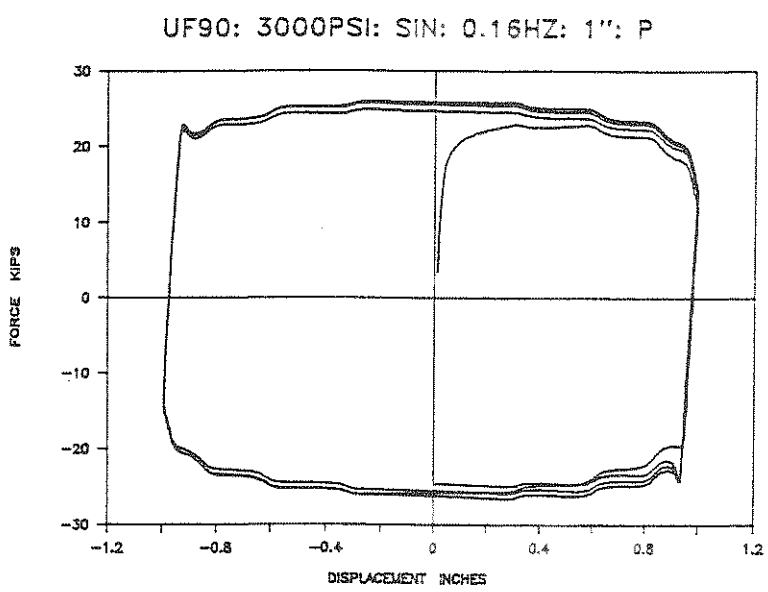
UF90: 3000PSI: SIN: 0.16HZ: 1": P
FORCE KIPS
DISPLACEMENT INCHES
30
20
10
0
-10
-20
-30
-1.2
-0.8
-0.4
0
0.4
0.8
1.2

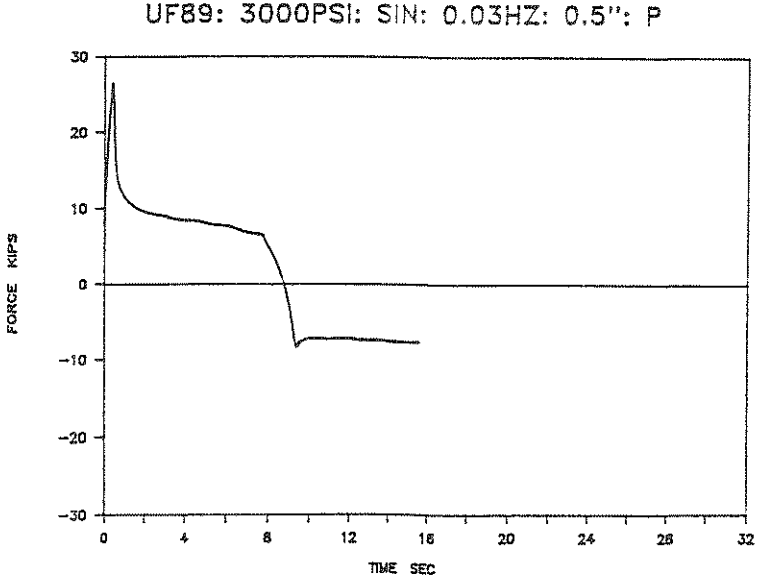
UF89: 3000PSI: SIN: 0.03HZ: 0.5": P
FORCE KIPS
TIME SEC
30
20
10
0
-10
-20
-30
0
4
8
12
16
20
24
28
32

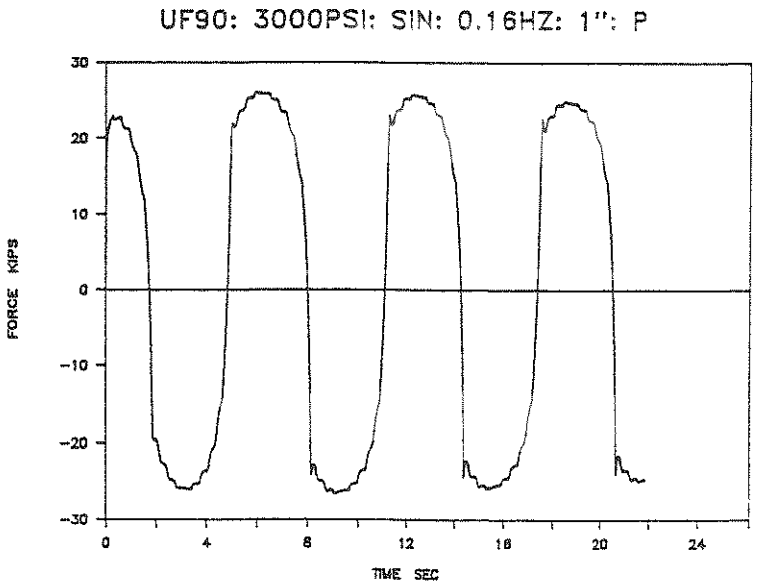
UF90: 3000PSI: SIN: 0.16HZ: 1": P
FORCE KIPS
TIME SEC
30
20
10
0
-10
-20
-30
0
4
8
12
16
20
24

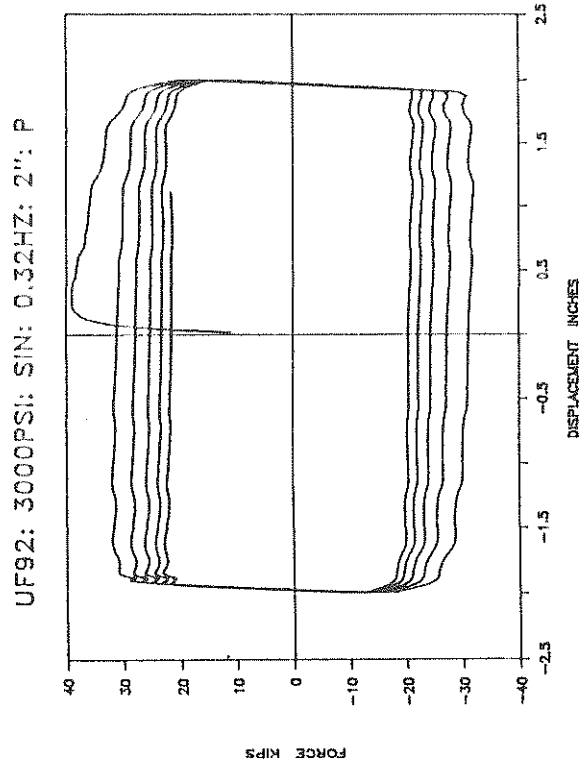
UF92: 3000PSI: SIN: 0.32HZ: 2": P
FORCE KIPS
DISPLACEMENT INCHES

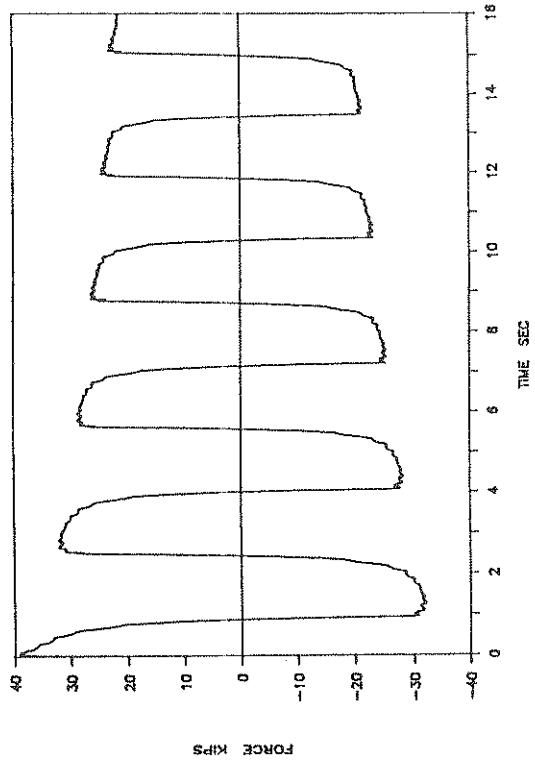
UF92: 3000PSI: SIN: 0.32HZ: 2": P
FORCE KIPS
TIME SEC

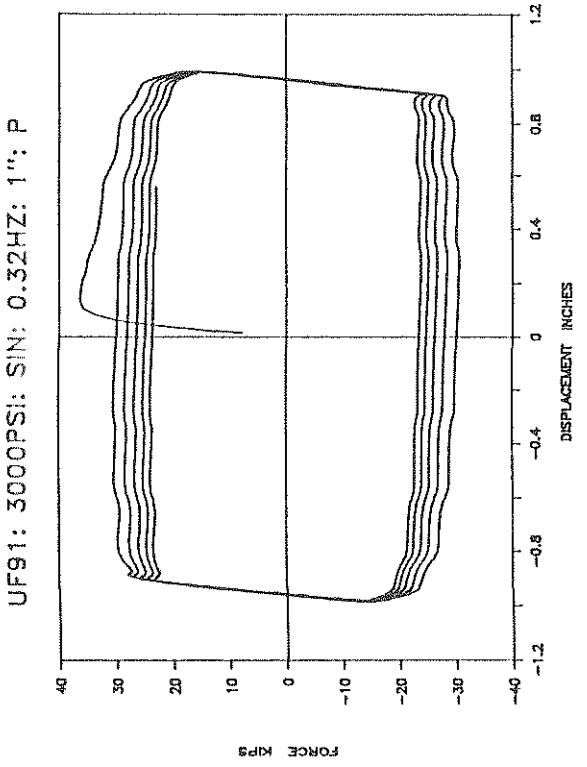
UF91: 3000PSI: SIN: 0.32HZ: 1": P
FORCE KIPS
DISPLACEMENT INCHES

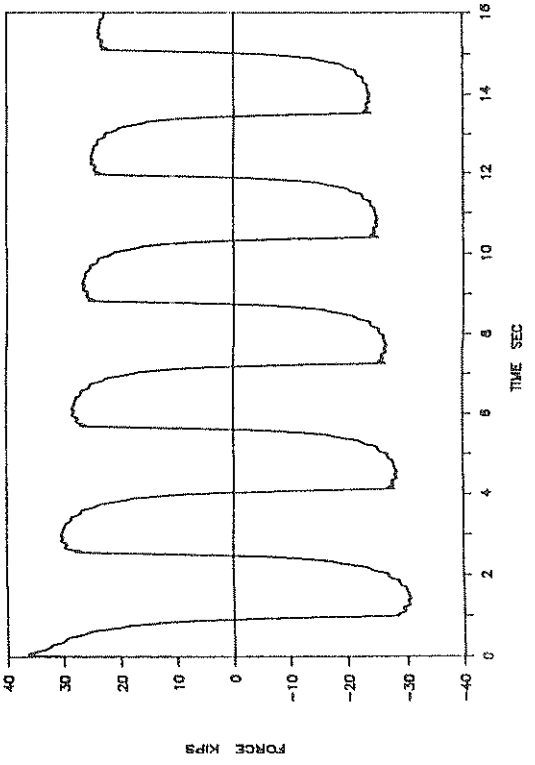
UF91: 3000PSI: SIN: 0.32HZ: 1": P
FORCE KIPS
TIME SEC

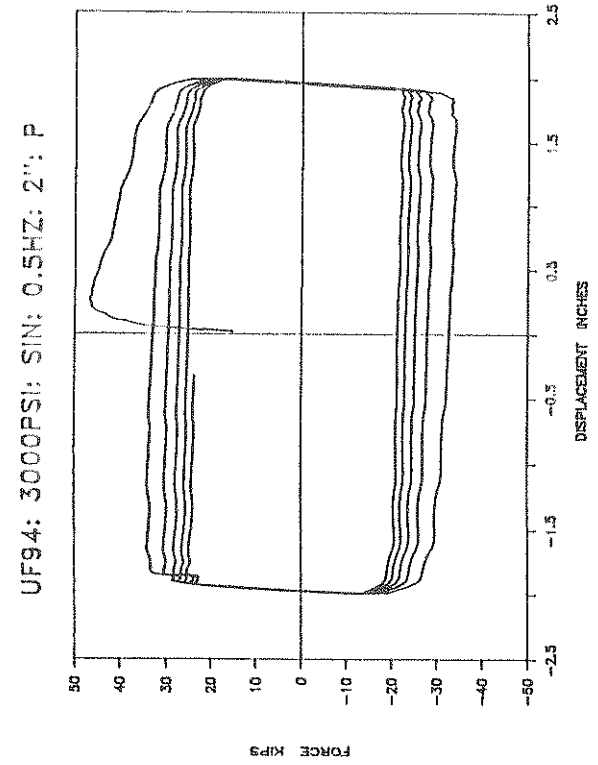
UF94: 3000PSI: SIN: 0.5HZ: 2": P
FORCE KIPS
DISPLACEMENT INCHES

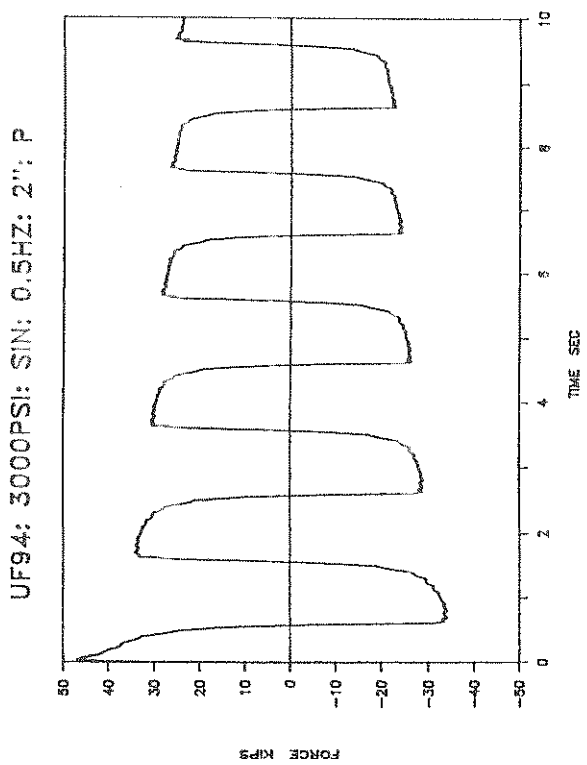
UF94: 3000PSI: SIN: 0.5HZ: 2": P
FORCE KIPS
TIME SEC

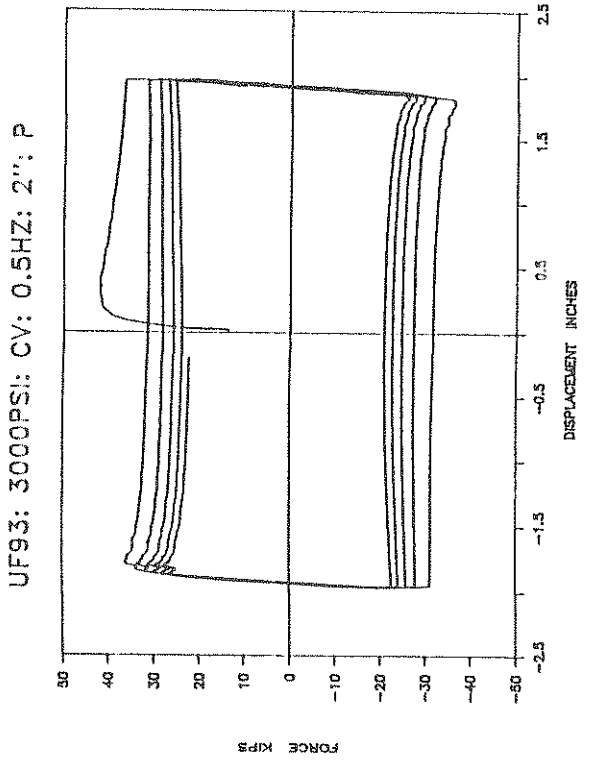
UF93: 3000PSI: CV: 0.5HZ: 2": P
FORCE KIPS
DISPLACEMENT INCHES

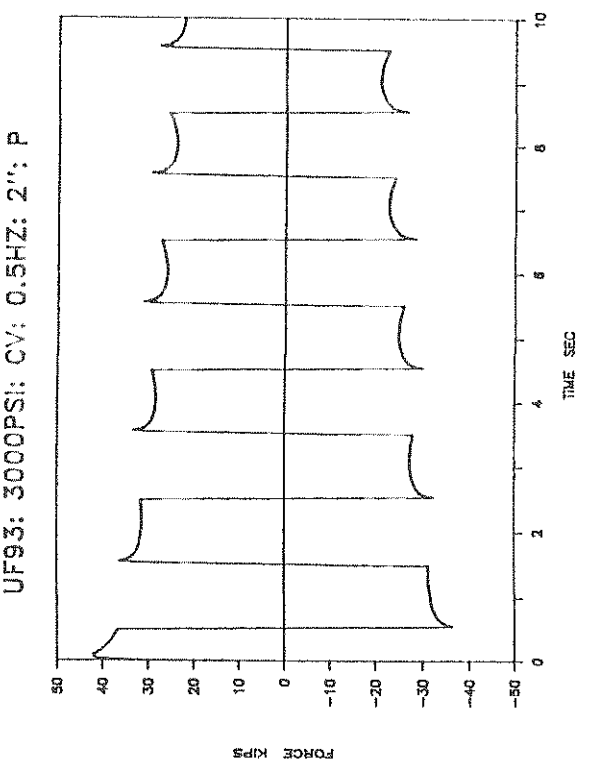
UF93: 3000PSI: CV: 0.5HZ: 2": P
FORCE KIPS
TIME SEC

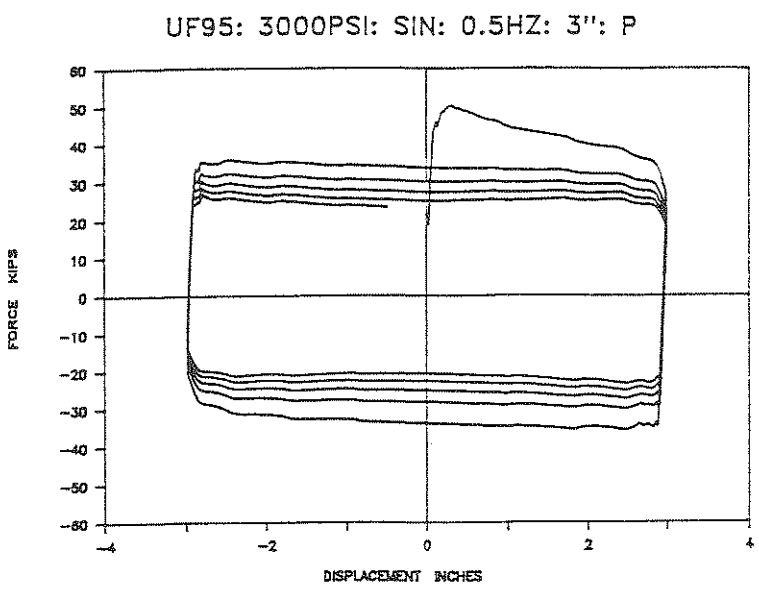
UF95: 3000PSI: SIN: 0.5HZ: 3": P
FORCE KIPS
DISPLACEMENT INCHES

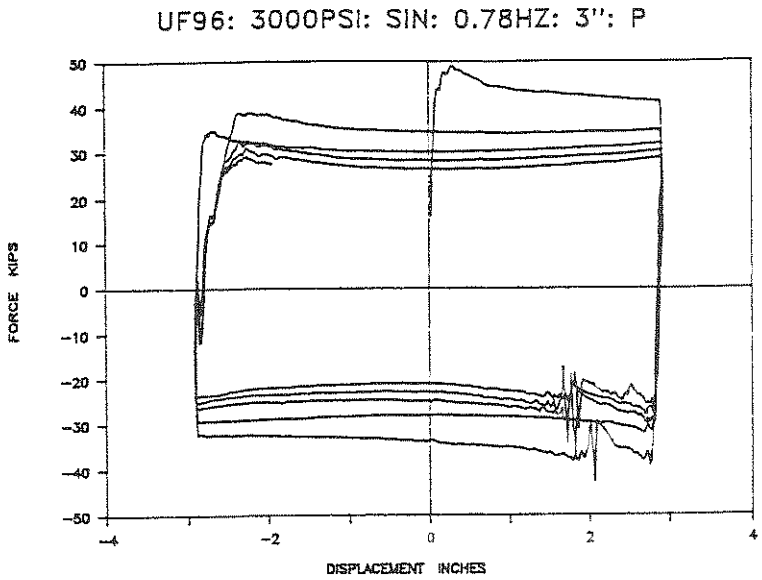
UF96: 3000PSI: SIN: 0.78HZ: 3": P
FORCE KIPS
DISPLACEMENT INCHES

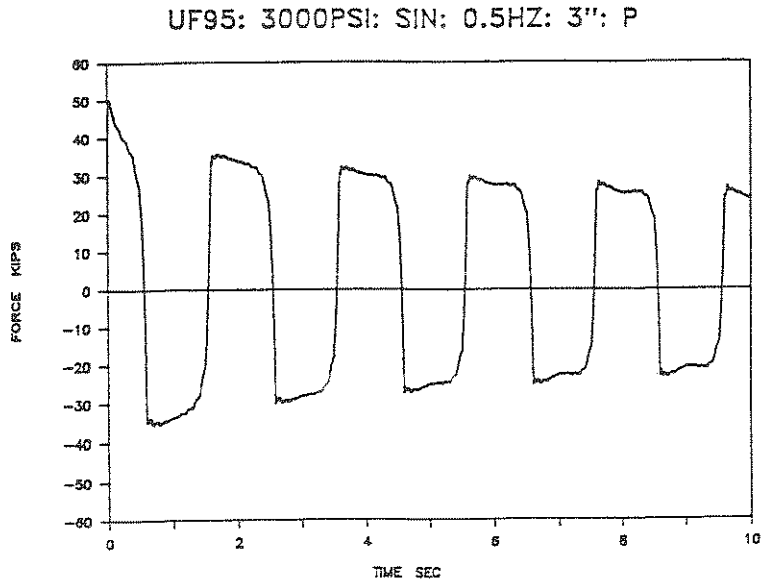
UF95: 3000PSI: SIN: 0.5HZ: 3": P
FORCE KIPS
TIME SEC

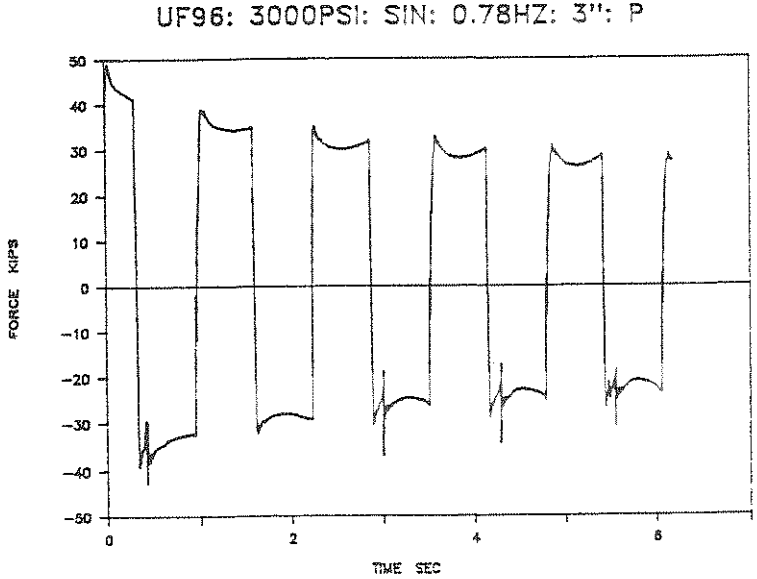
UF96: 3000PSI: SIN: 0.78HZ: 3": P
FORCE KIPS
TIME SEC

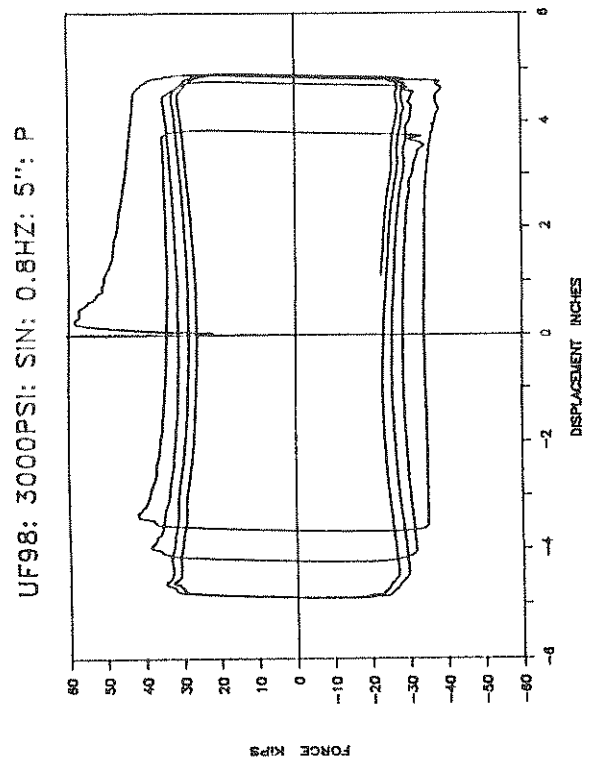
UF98: 3000PSI: SIN: 0.8HZ: 5": P
FORCE KIPS
DISPLACEMENT INCHES

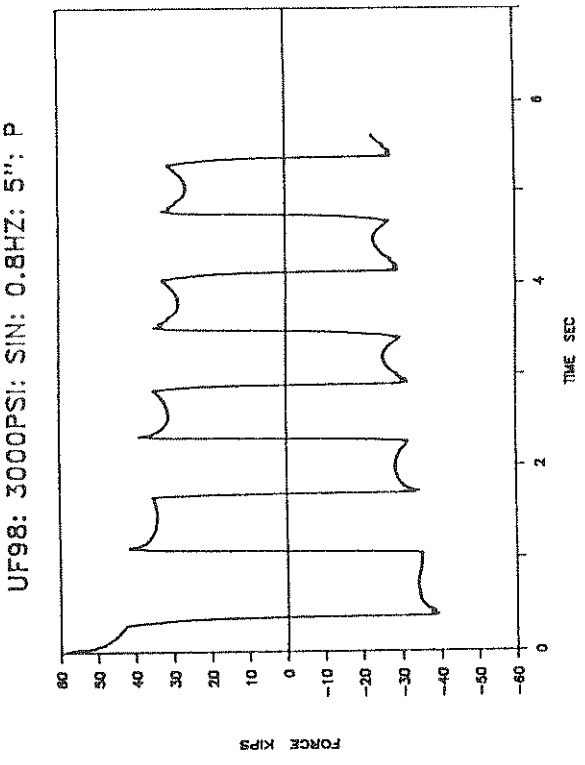
UF98: 3000PSI: SIN: 0.8HZ: 5": P
FORCE KIPS
TIME SEC

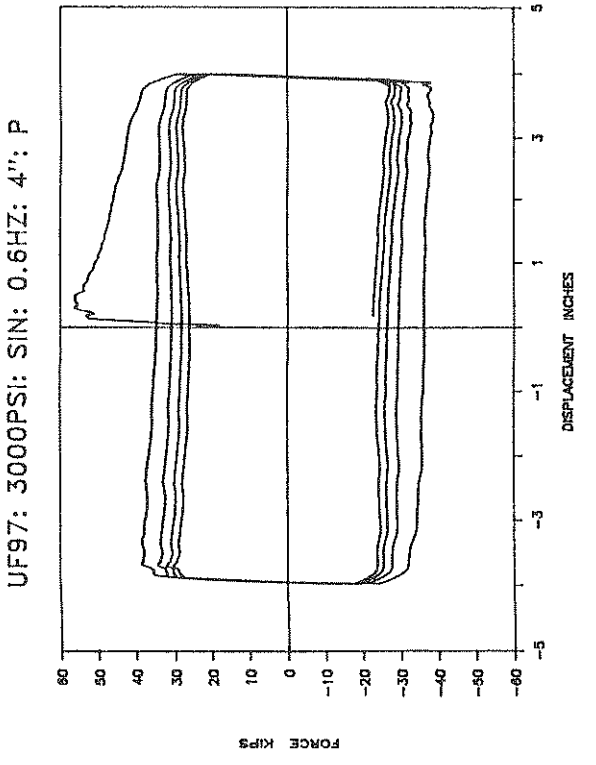
UF97: 3000PSI: SIN: 0.6HZ: 4": P
FORCE KIPS
DISPLACEMENT INCHES

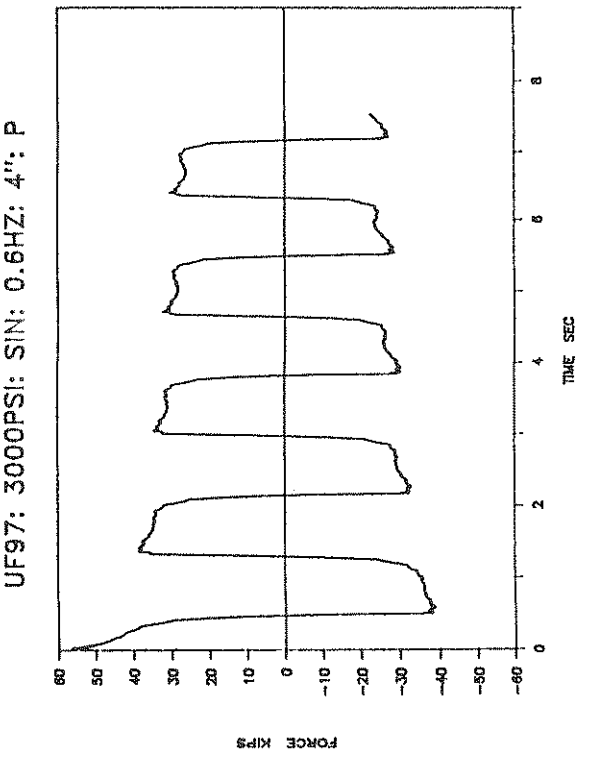
UF97: 3000PSI: SIN: 0.6HZ: 4": P
FORCE KIPS
TIME SEC

15GF99: 1000PSI: SIN: 0.03HZ: 0.5": P

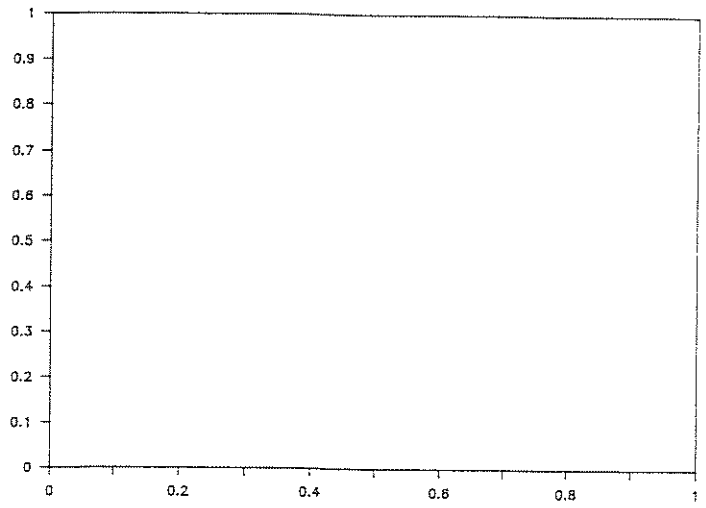

15GF100: 1000PSI: SIN: 0.16HZ: 1": P

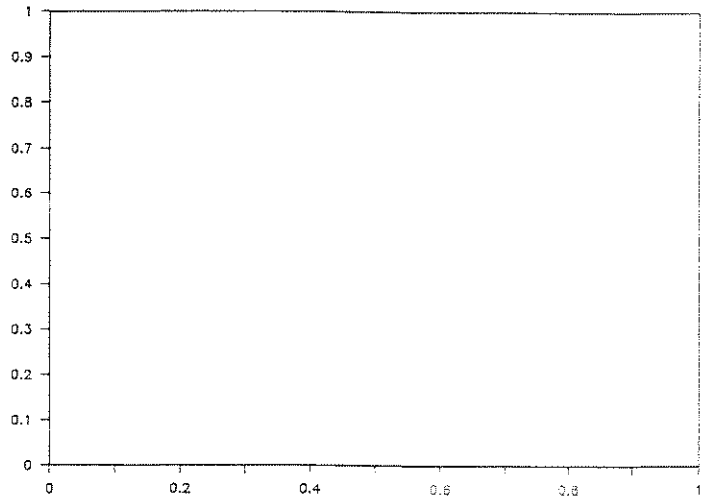

UNABLE TO RECOVER TEST DATA

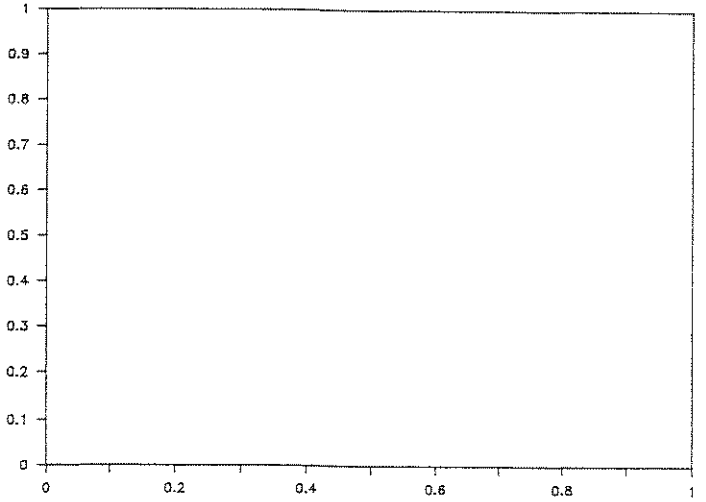

UNABLE TO RECOVER TEST DATA

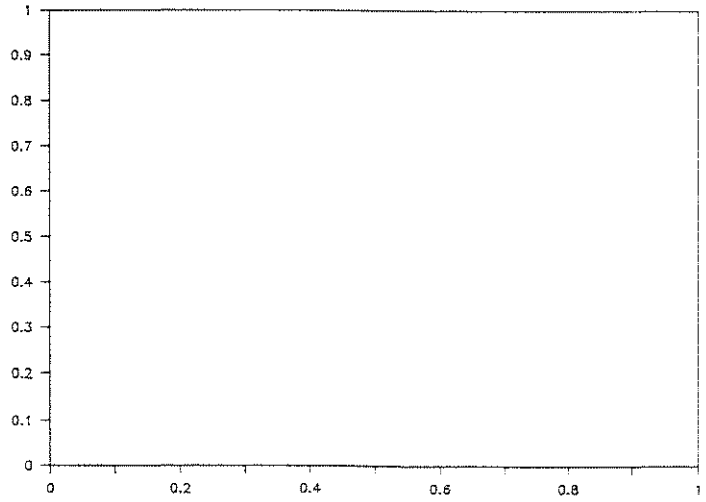

15GF101: 1000PSI: SIN: 0.32HZ: 1": P

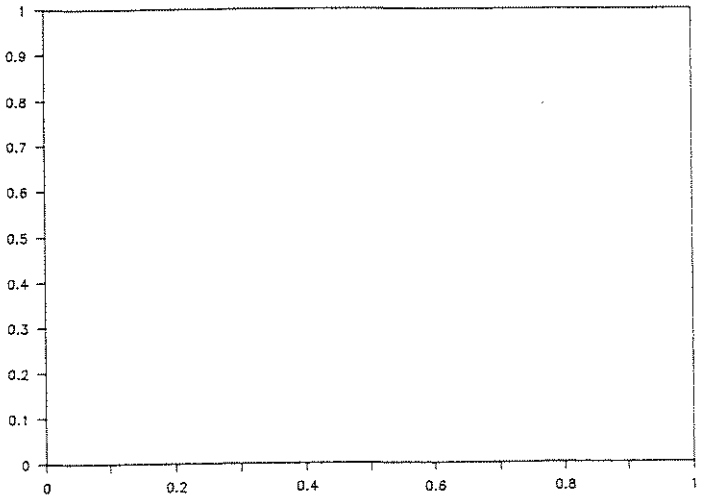

15GF102: 1000PSI: SIN: 0.32HZ: 2": P

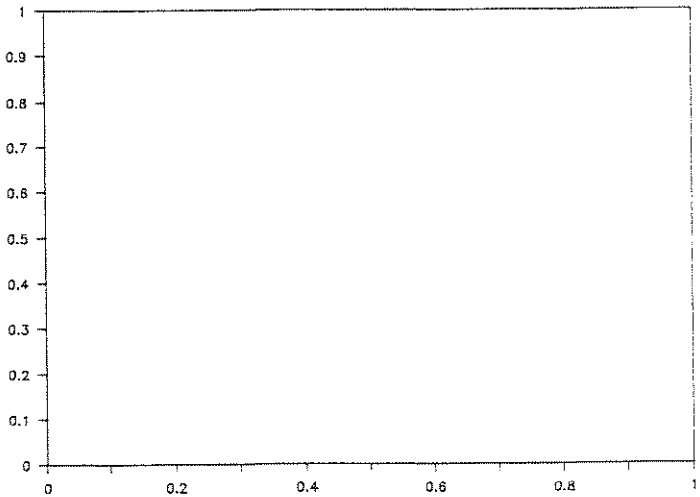

UNABLE TO RECOVER TEST DATA

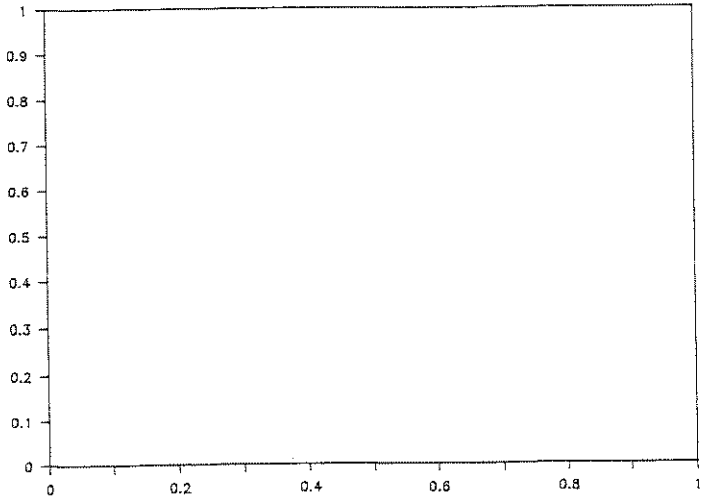

UNABLE TO RECOVER TEST DATA

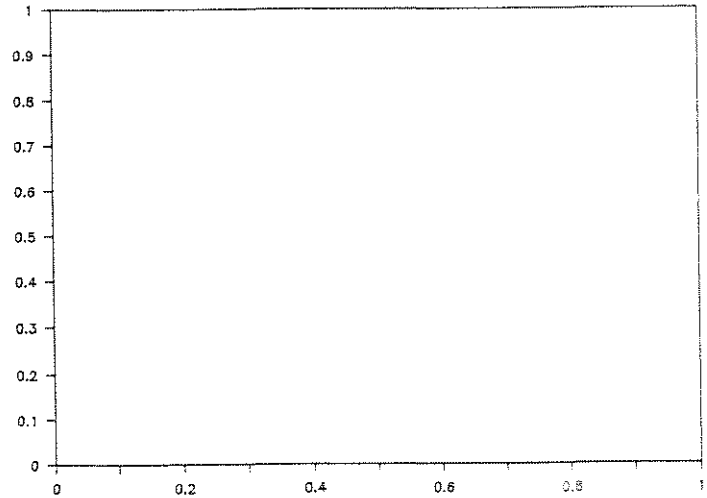

15GF103: 1000PSI: CV: 0.5HZ: 2": P

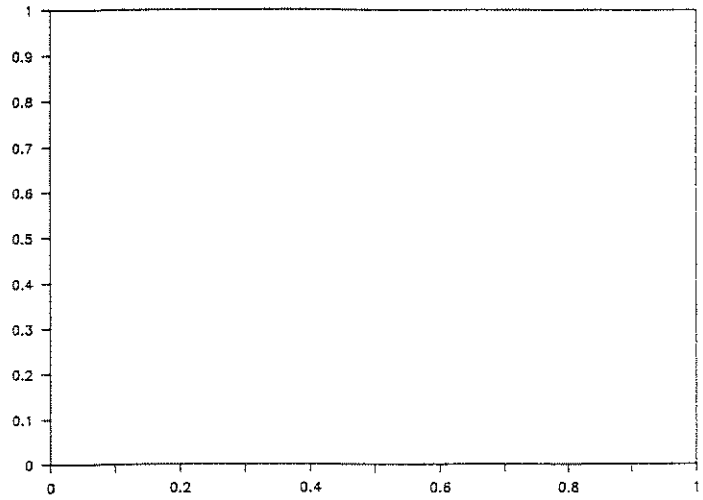

15GF104: 1000PSI: SIN: 0.5HZ: 2": P

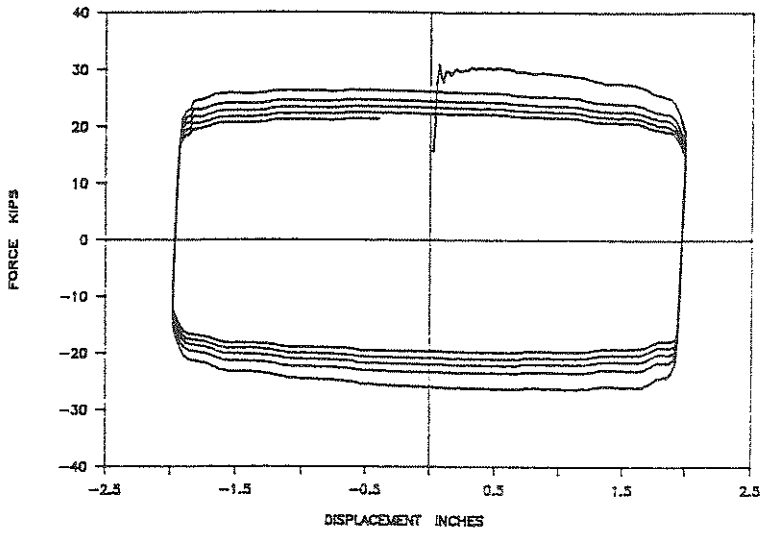

UNABLE TO RECOVER TEST DATA

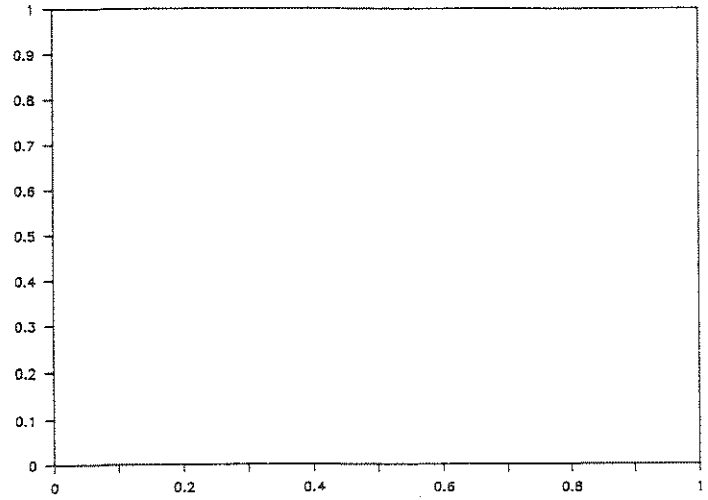

15GF104: 1000PSI: SIN: 0.5HZ: 2": P

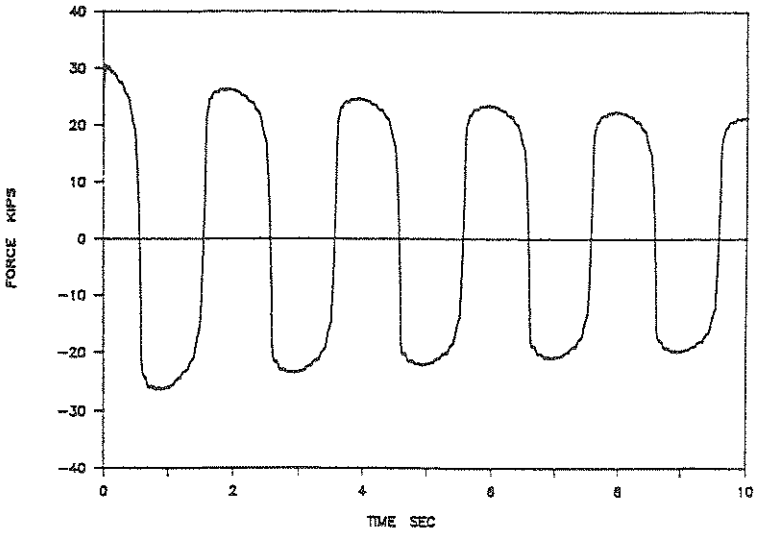

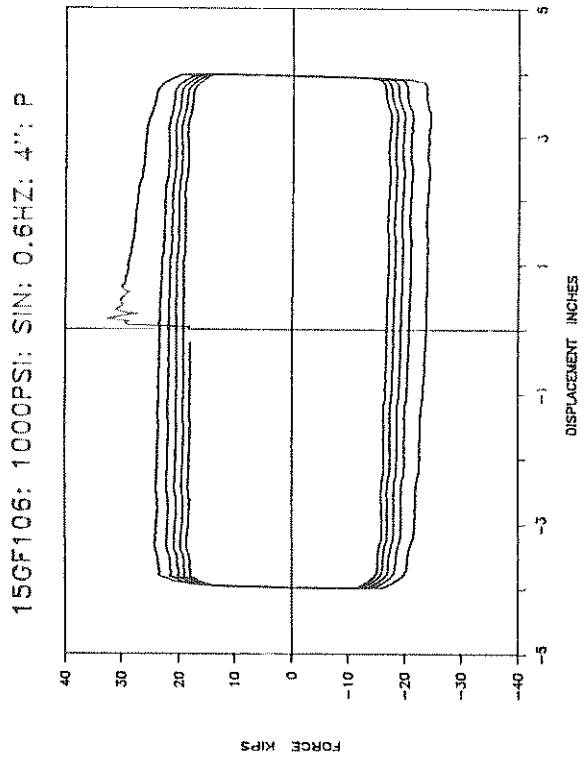
15GF106: 1000PSI: SIN: 0.6HZ: 4": P
FORCE KIPS
DISPLACEMENT INCHES

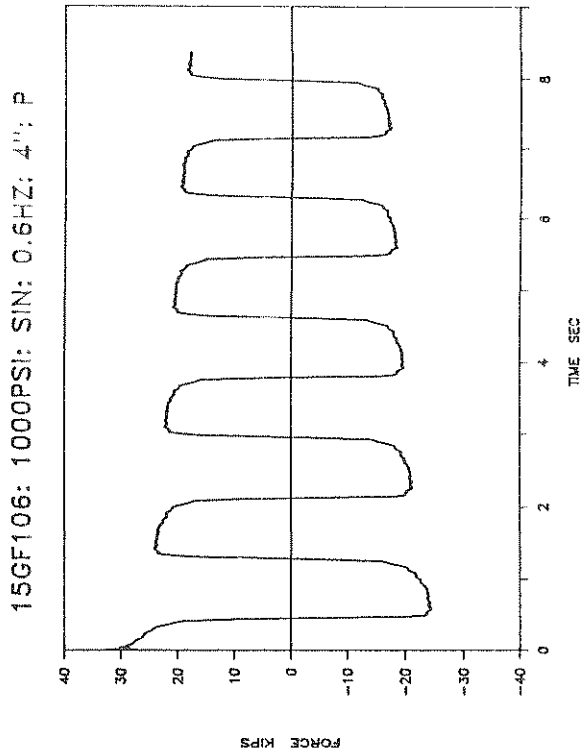
15GF106: 1000PSI: SIN: 0.6HZ: 4": P
FORCE KIPS
TIME SEC

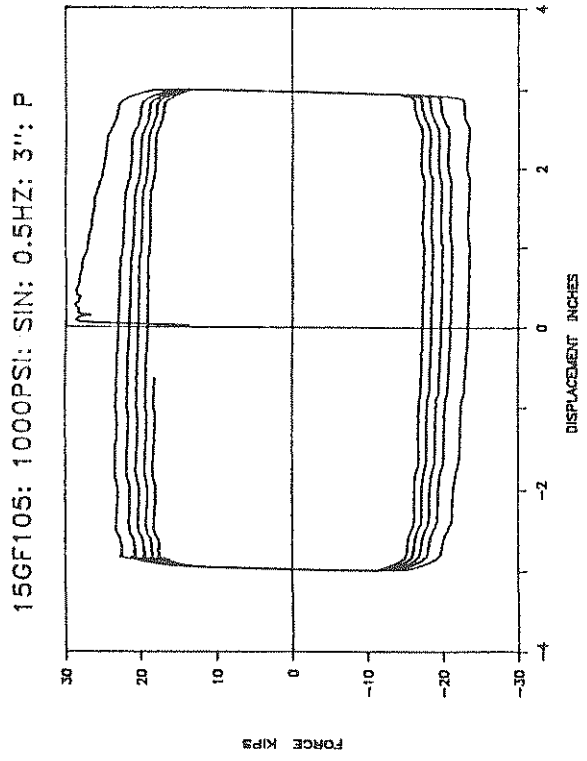
15GF105: 1000PSI: SIN: 0.5HZ: 3": P
FORCE KIPS
DISPLACEMENT INCHES

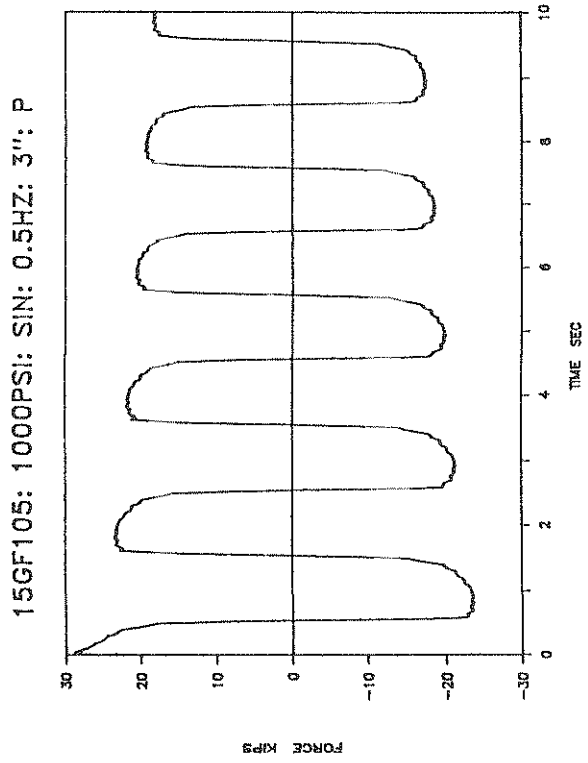
15GF105: 1000PSI: SIN: 0.5HZ: 3": P
FORCE KIPS
TIME SEC

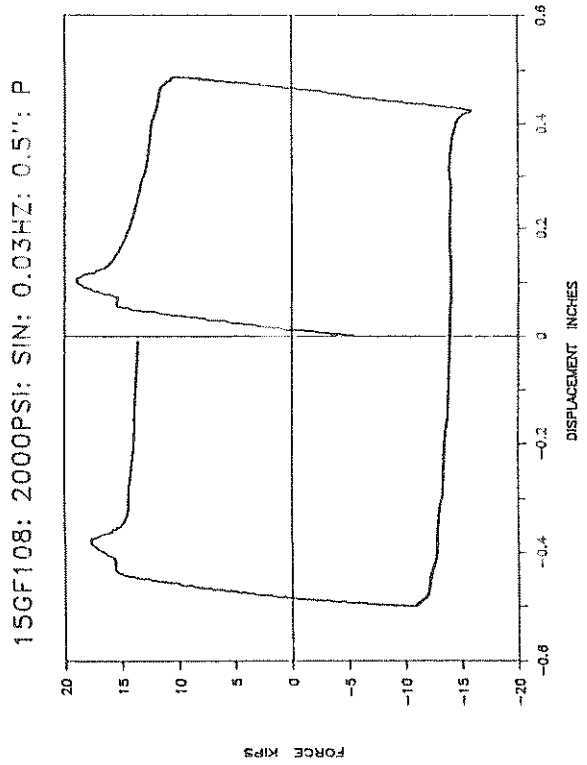
15GF108: 2000PSI: SIN: 0.03HZ: 0.5": P
FORCE KIPS
DISPLACEMENT INCHES

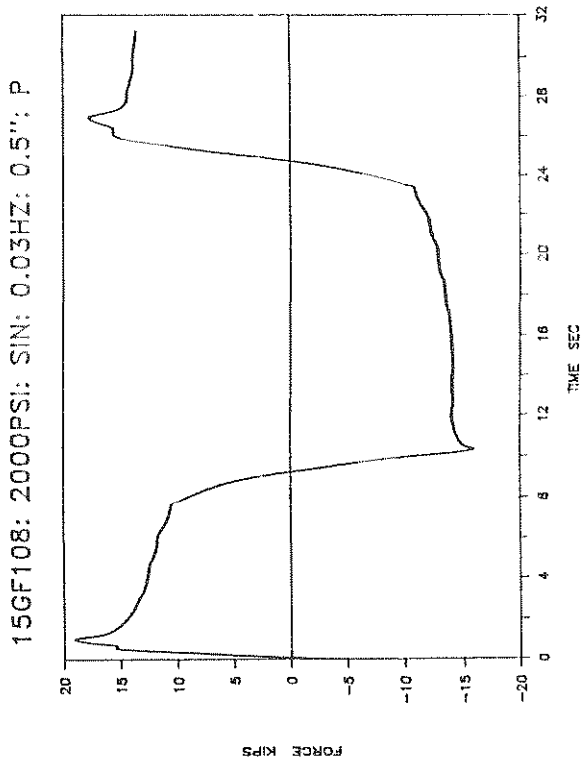
15GF108: 2000PSI: SIN: 0.03HZ: 0.5": P
FORCE KIPS
TIME SEC

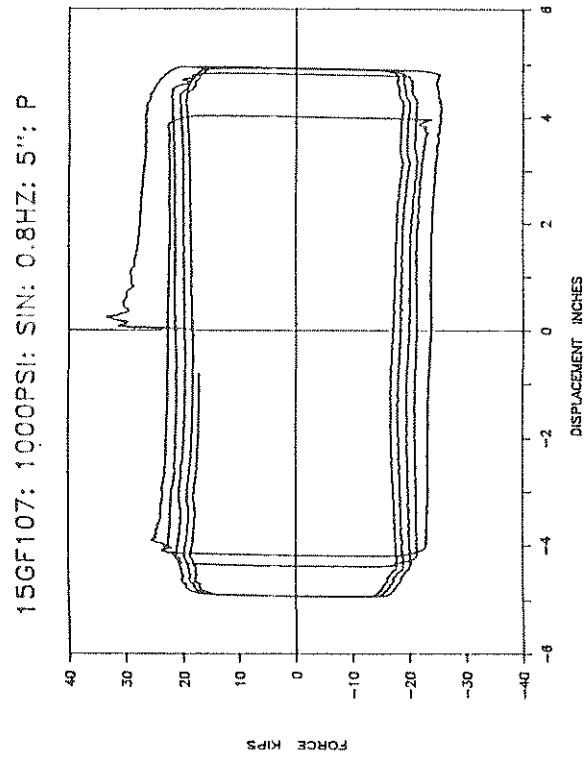
15GF107: 1000PSI: SIN: 0.8HZ: 5": P
FORCE KIPS
DISPLACEMENT INCHES

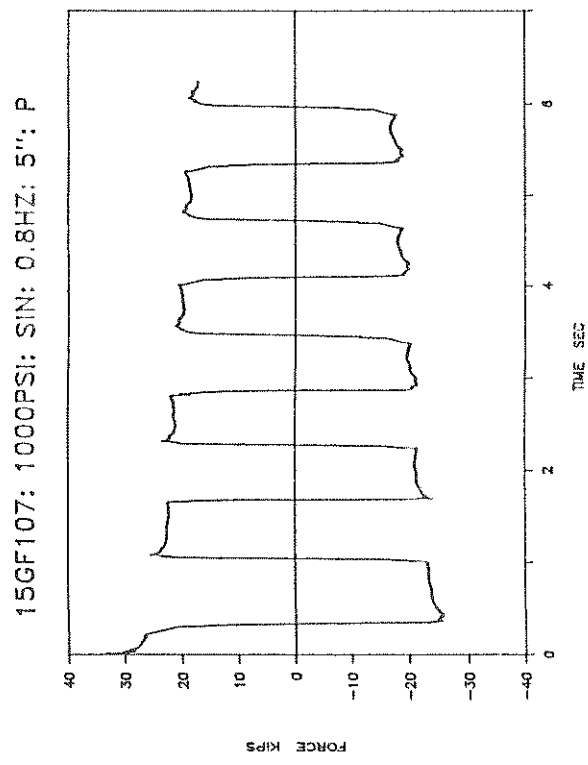
15GF107: 1000PSI: SIN: 0.8HZ: 5": P
FORCE KIPS
TIME SEC

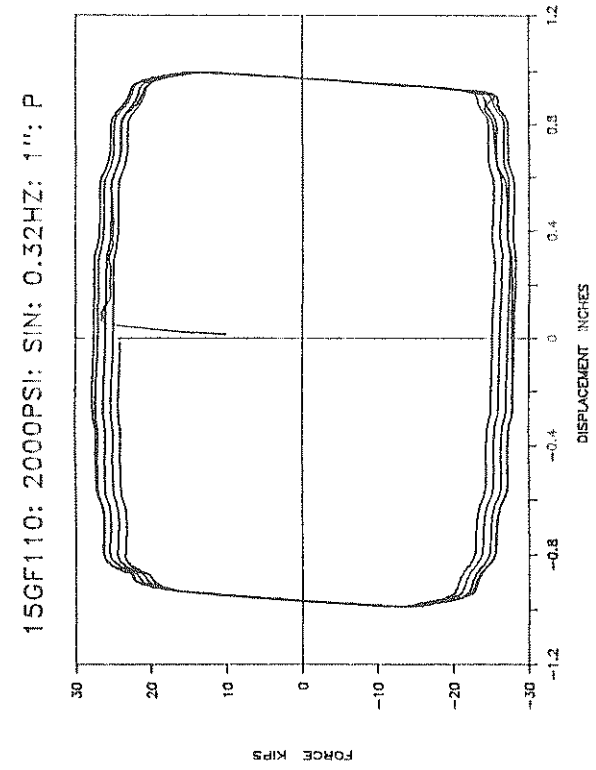
15GF110: 2000PSI: SIN: 0.32HZ: 1": P
FORCE KIPS
DISPLACEMENT INCHES

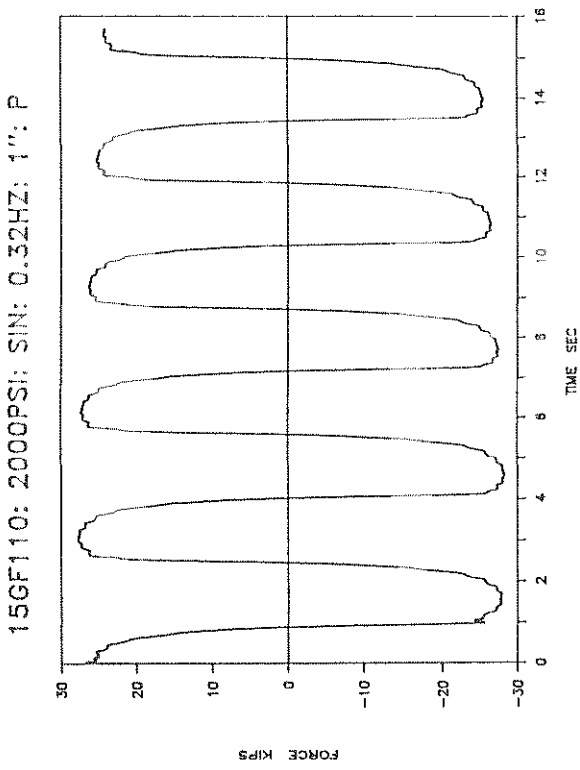
15GF110: 2000PSI: SIN: 0.32HZ: 1": P
FORCE KIPS
TIME SEC

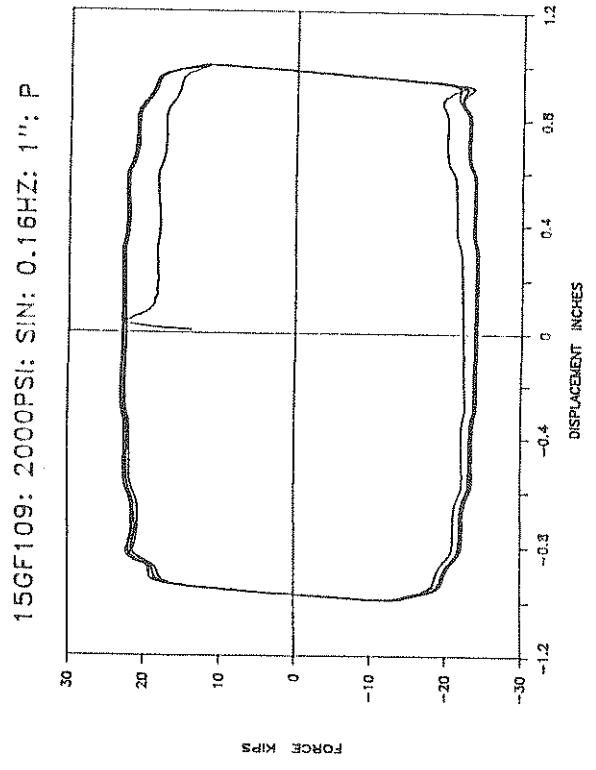
15GF109: 2000PSI: SIN: 0.16HZ: 1": P
FORCE KIPS
DISPLACEMENT INCHES

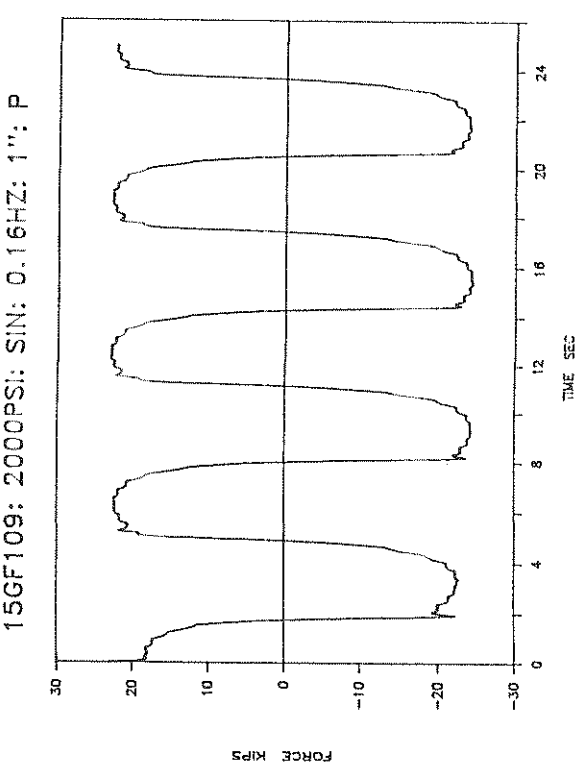
15GF109: 2000PSI: SIN: 0.16HZ: 1": P
FORCE KIPS
TIME SEC

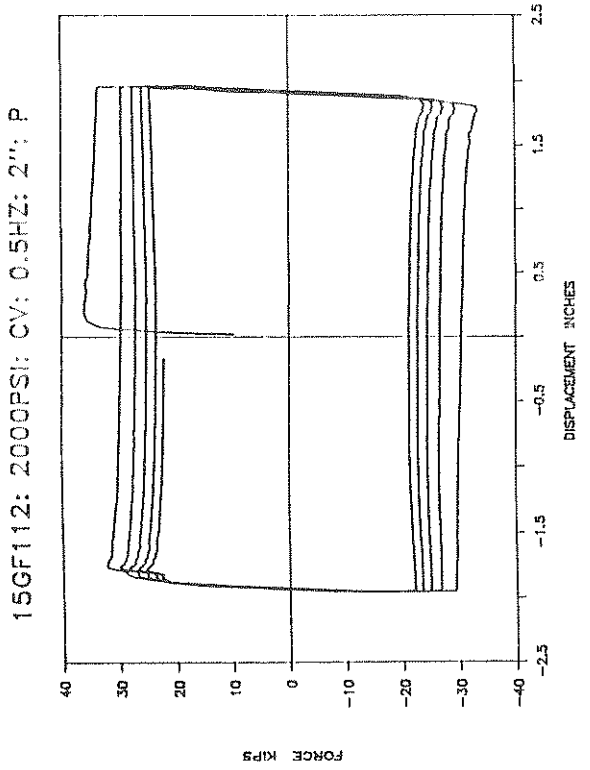
15GF112: 2000PSI: CV: 0.5HZ: 2": P
FORCE KIPS
DISPLACEMENT INCHES

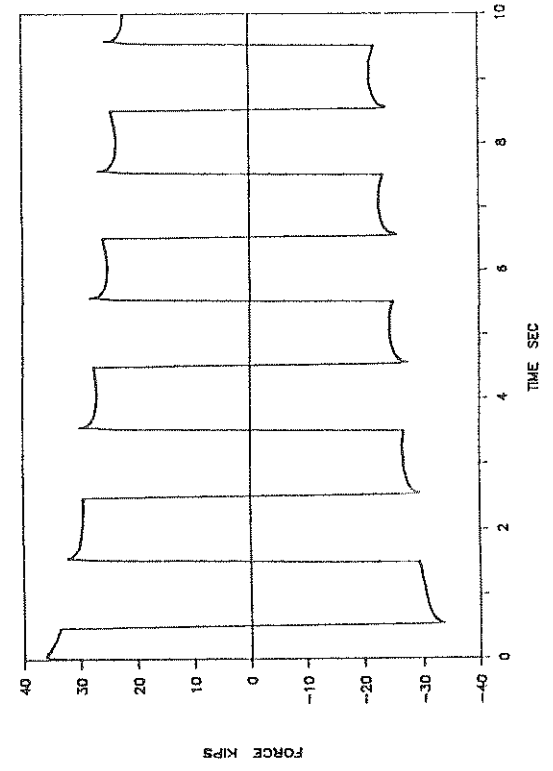
15GF112: 2000PSI: CV: 0.5HZ: 2": P
FORCE KIPS
TIME SEC

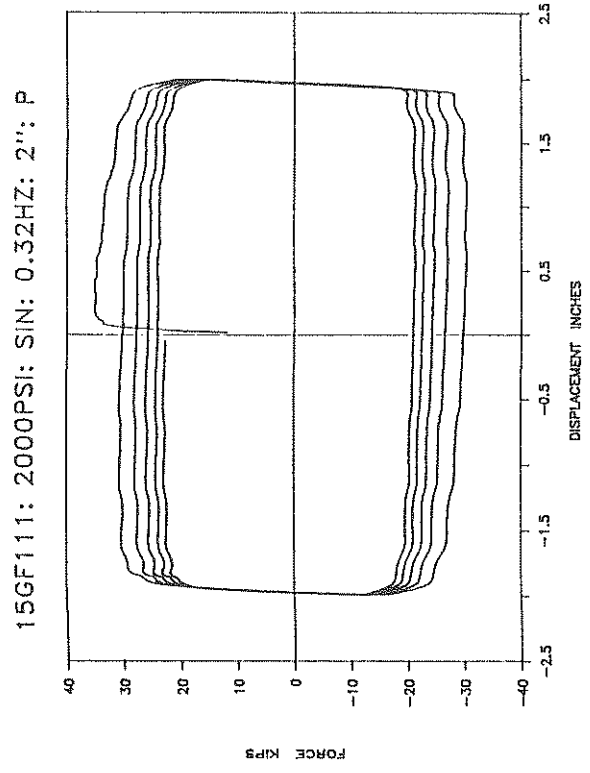
15GF111: 2000PSI: SIN: 0.32HZ: 2": P
FORCE KIPS
DISPLACEMENT INCHES

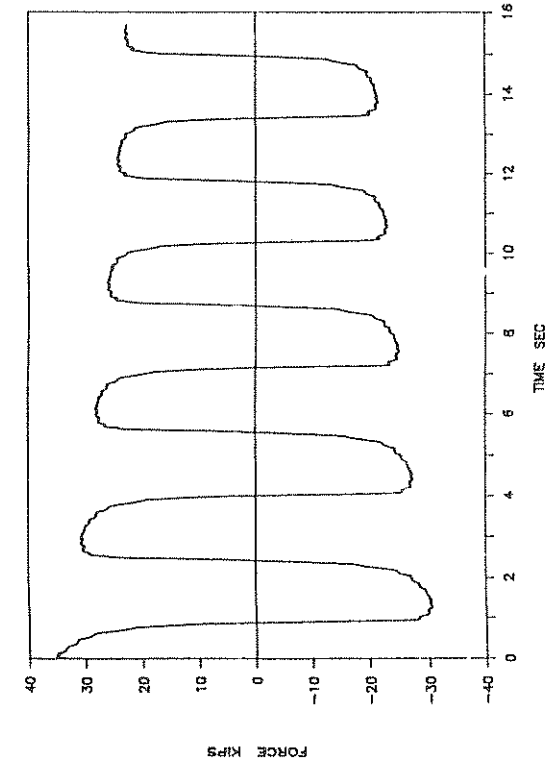
15GF111: 2000PSI: SIN: 0.32HZ: 2": P
FORCE KIPS
TIME SEC

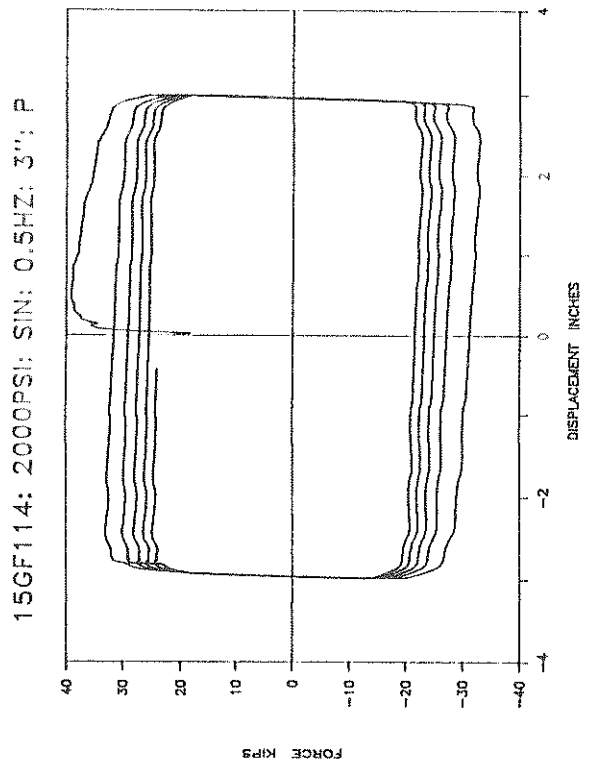
15GF114: 2000PSI: SIN: 0.5HZ: 3": P
FORCE KIPS
DISPLACEMENT INCHES

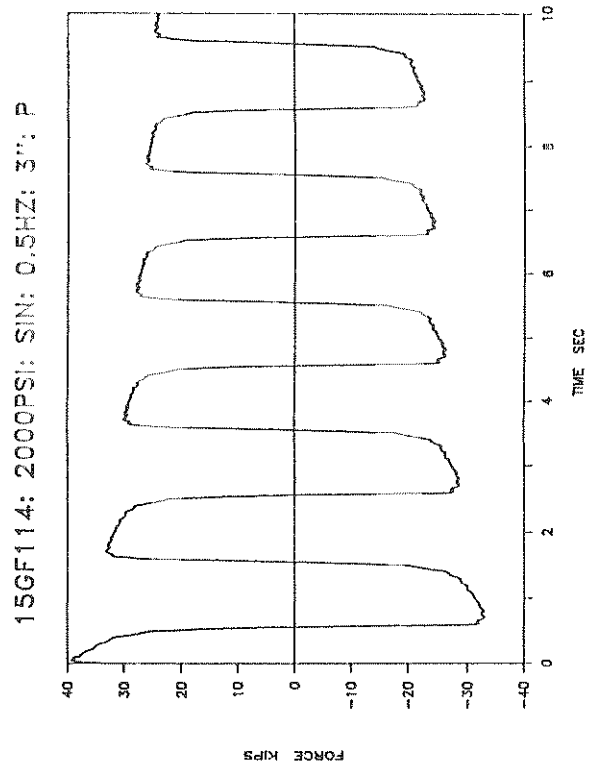
15GF114: 2000PSI: SIN: 0.5HZ: 3": P
FORCE KIPS
TIME SEC

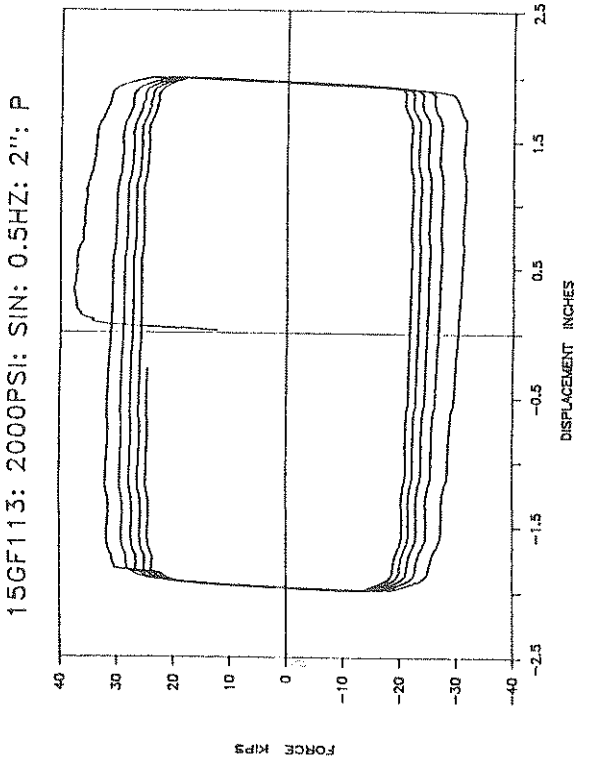
15GF113: 2000PSI: SIN: 0.5HZ: 2": P
FORCE KIPS
DISPLACEMENT INCHES

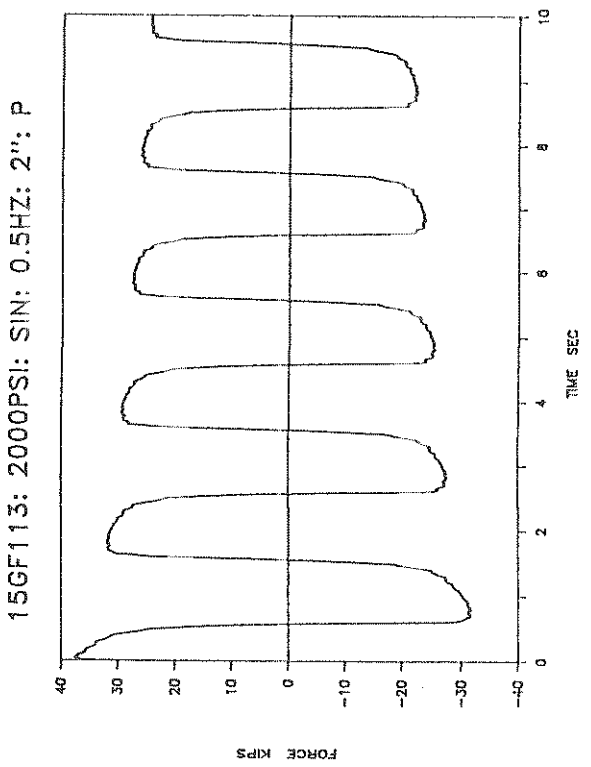
15GF113: 2000PSI: SIN: 0.5HZ: 2": P
FORCE KIPS
TIME SEC

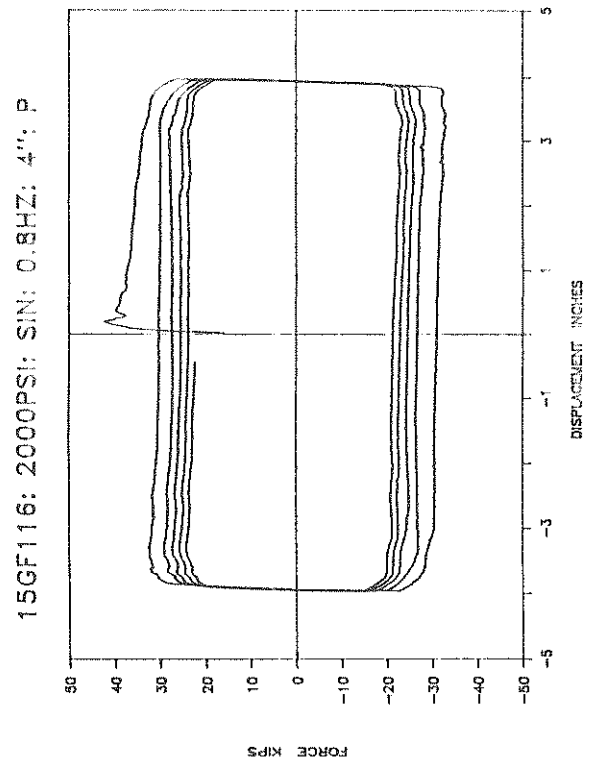
15GF116: 2000PSI: SIN: 0.8HZ: 4": P
FORCE KIPS
DISPLACEMENT INCHES

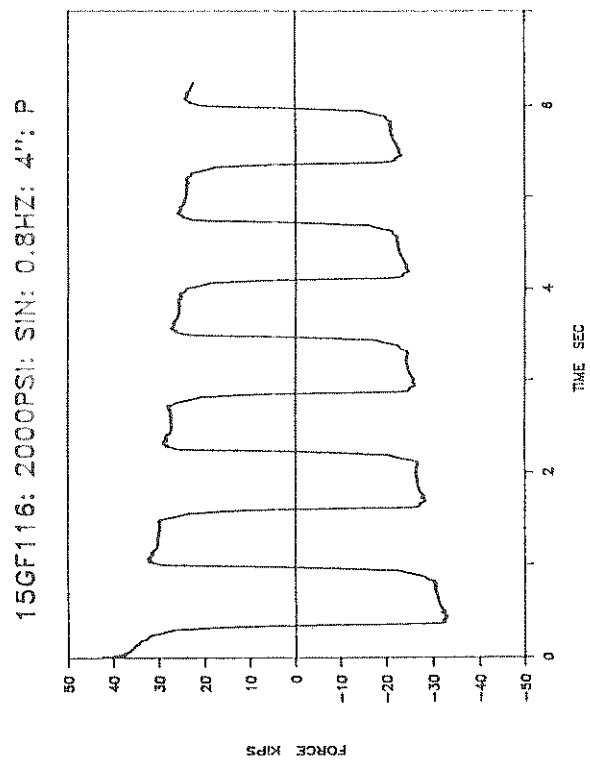
15GF116: 2000PSI: SIN: 0.8HZ: 4": P
FORCE KIPS
TIME SEC

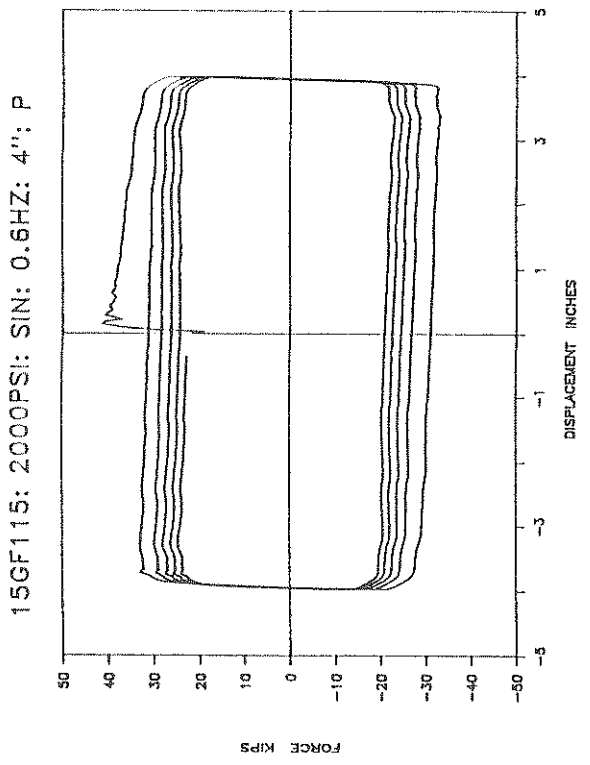
15GF115: 2000PSI: SIN: 0.6HZ: 4": P
FORCE KIPS
DISPLACEMENT INCHES

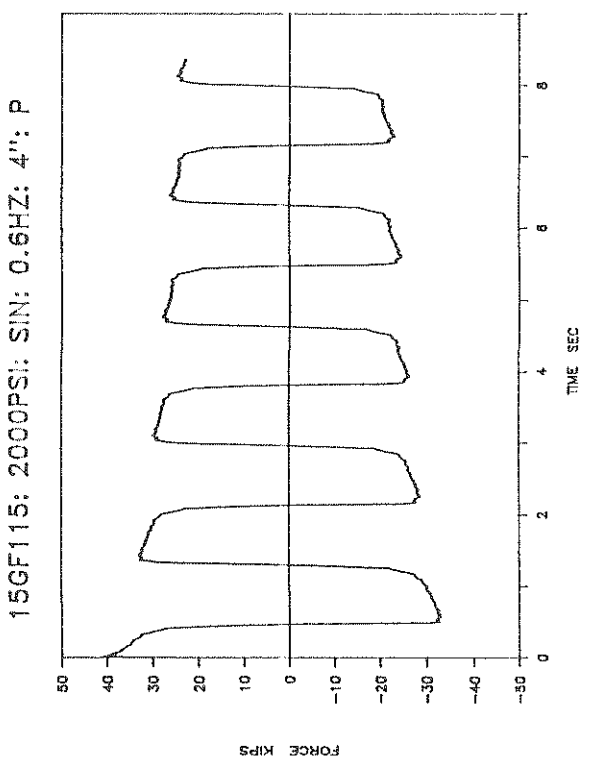
15GF115: 2000PSI: SIN: 0.6HZ: 4": P
FORCE KIPS
TIME SEC

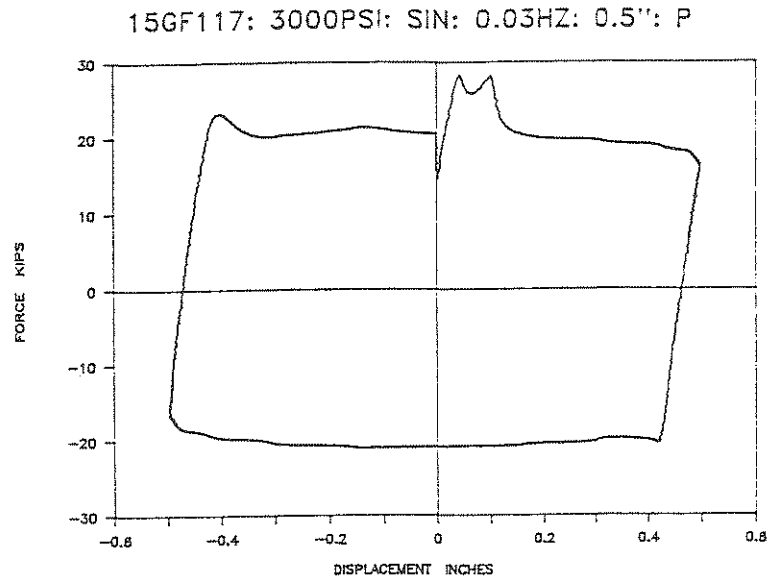
15GF117: 3000PSI: SIN: 0.03HZ: 0.5": P
FORCE KIPS
DISPLACEMENT INCHES

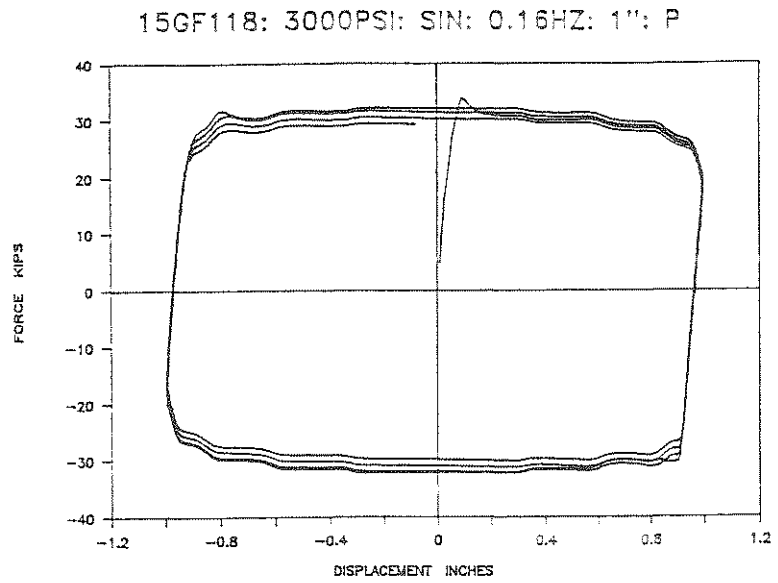
15GF118: 3000PSI: SIN: 0.16HZ: 1": P
FORCE KIPS
DISPLACEMENT INCHES

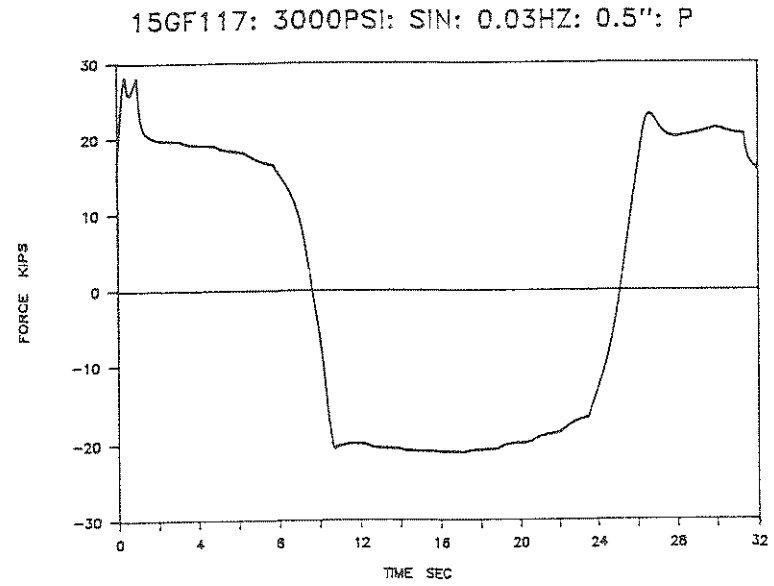
15GF117: 3000PSI: SIN: 0.03HZ: 0.5": P
FORCE KIPS
TIME SEC

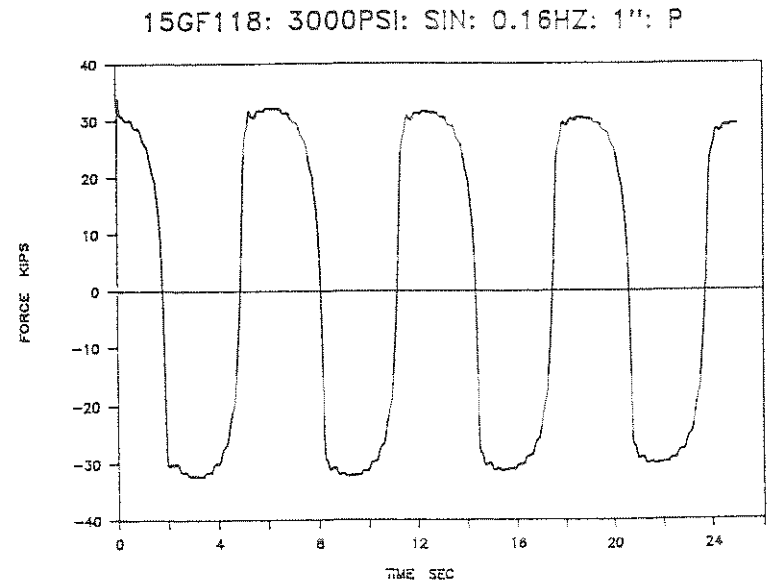
15GF118: 3000PSI: SIN: 0.16HZ: 1": P
FORCE KIPS
TIME SEC

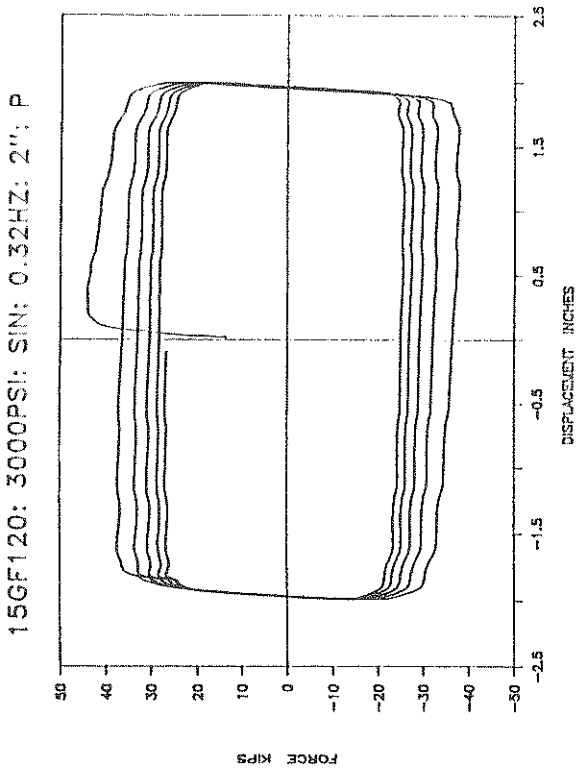
15GF120: 3000PSI: SIN: 0.32HZ: 2": P
FORCE KIPS
DISPLACEMENT INCHES

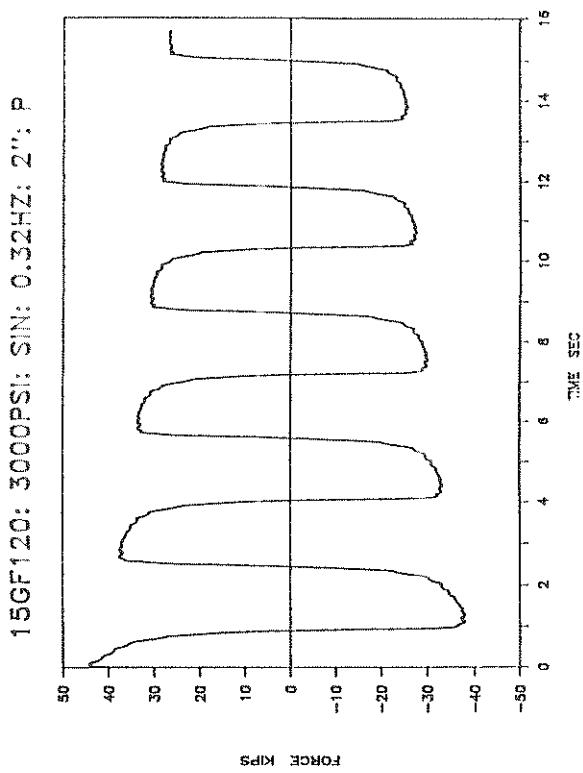
15GF120: 3000PSI: SIN: 0.32HZ: 2": P
FORCE KIPS
TIME SEC

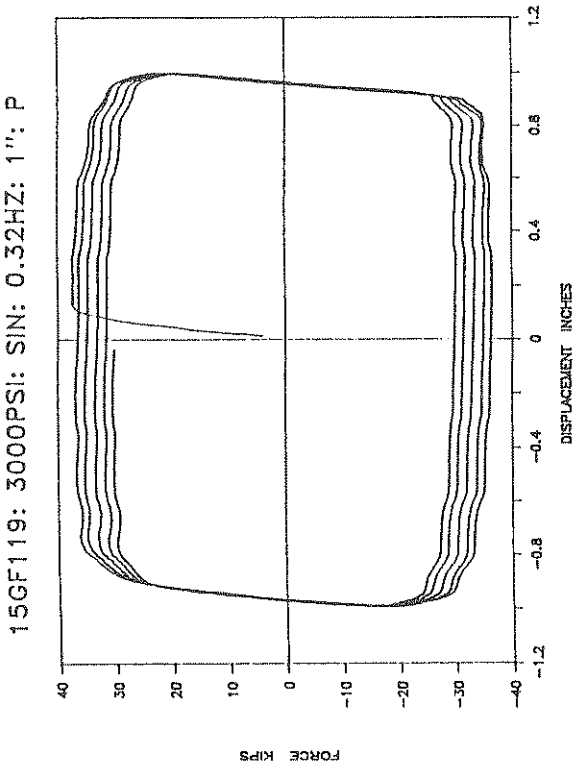
15GF119: 3000PSI: SIN: 0.32HZ: 1": P
FORCE KIPS
DISPLACEMENT INCHES

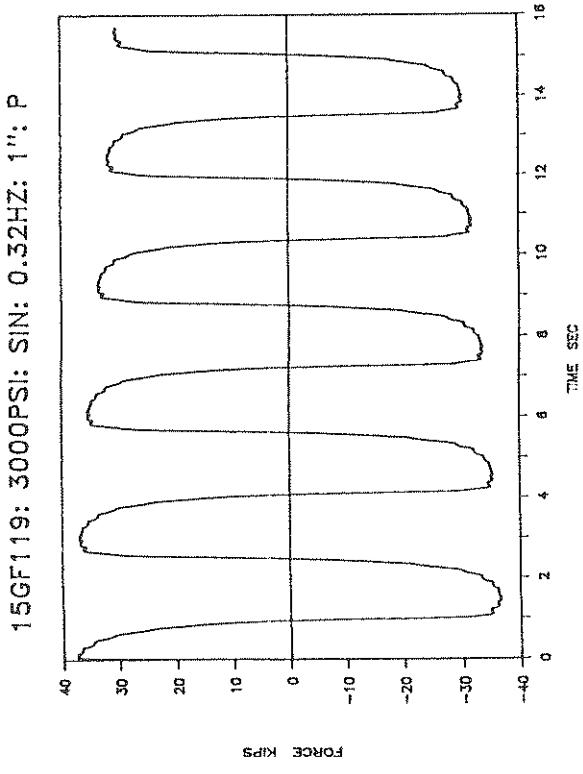
15GF119: 3000PSI: SIN: 0.32HZ: 1": P
FORCE KIPS
TIME SEC

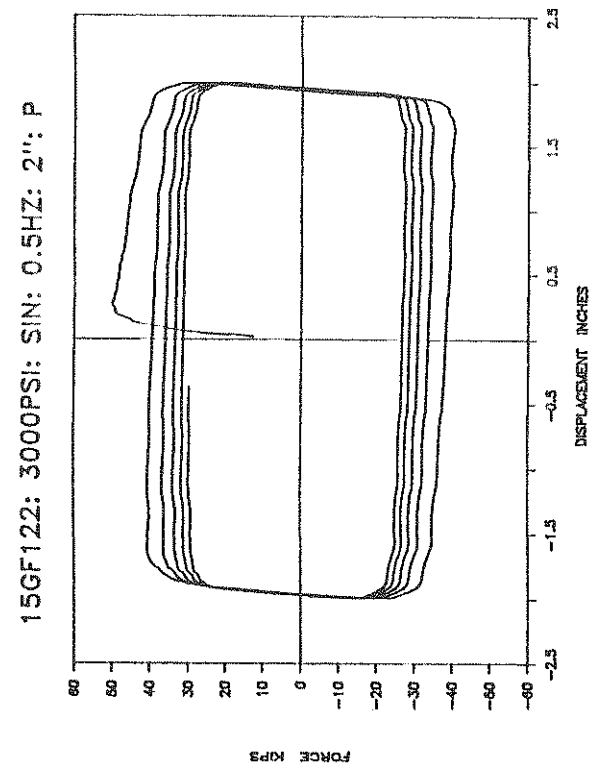
15GF122: 3000PSI: SIN: 0.5HZ: 2": P
FORCE KIPS
DISPLACEMENT INCHES

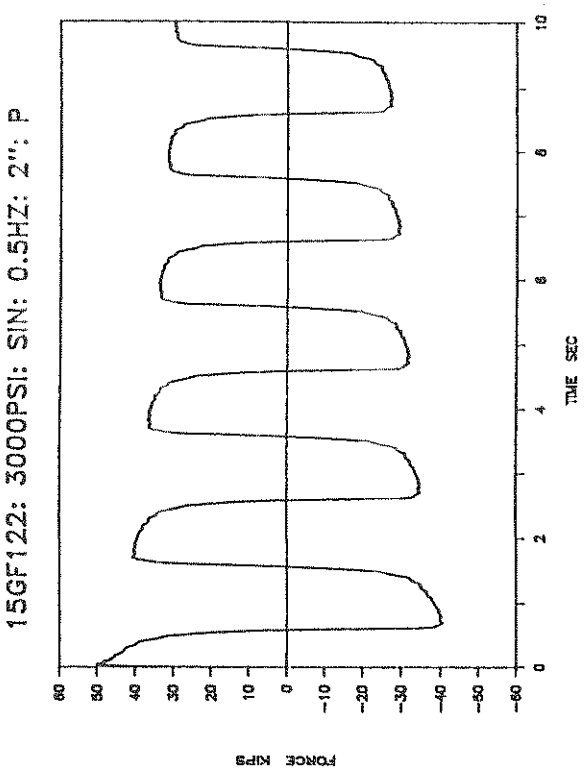
15GF122: 3000PSI: SIN: 0.5HZ: 2": P
FORCE KIPS
TIME SEC

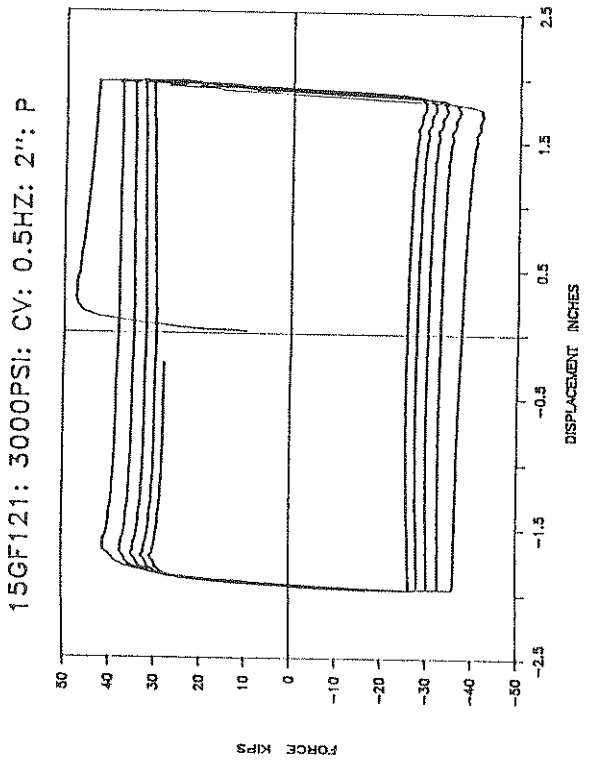
15GF121: 3000PSI: CV: 0.5HZ: 2": P
FORCE KIPS
DISPLACEMENT INCHES

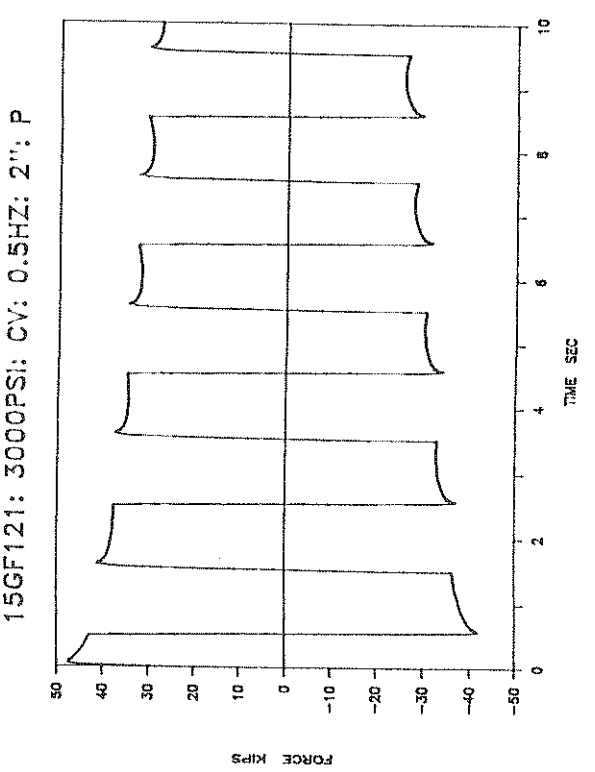
15GF121: 3000PSI: CV: 0.5HZ: 2": P
FORCE KIPS
TIME SEC

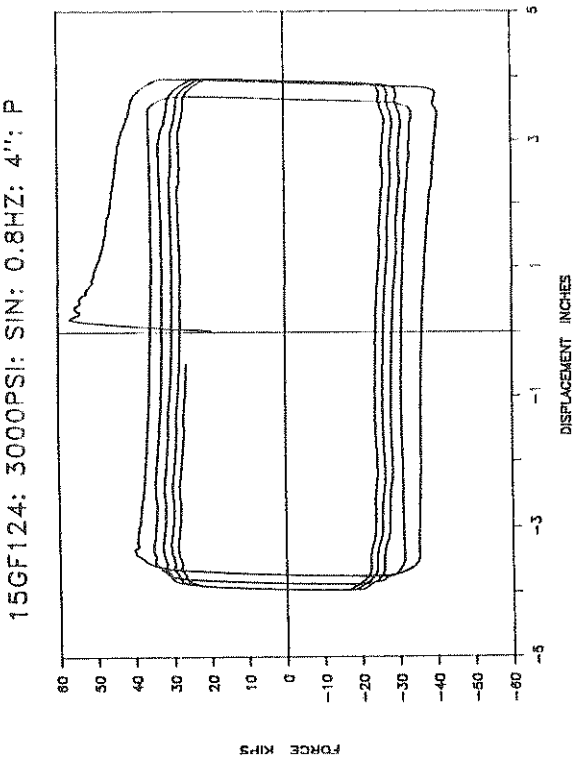
15GF124: 3000PSI: SIN: 0.8HZ: 4": P
FORCE KIPS
DISPLACEMENT INCHES

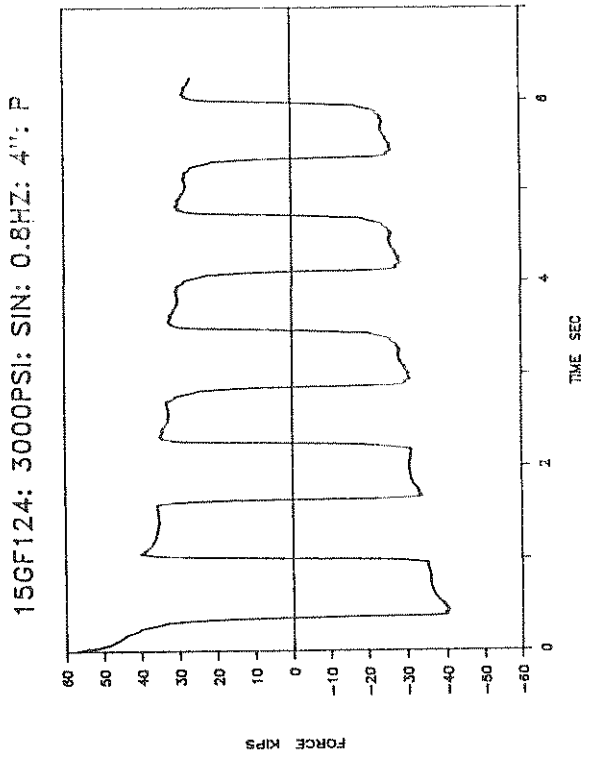
15GF124: 3000PSI: SIN: 0.8HZ: 4": P
FORCE KIPS
TIME SEC

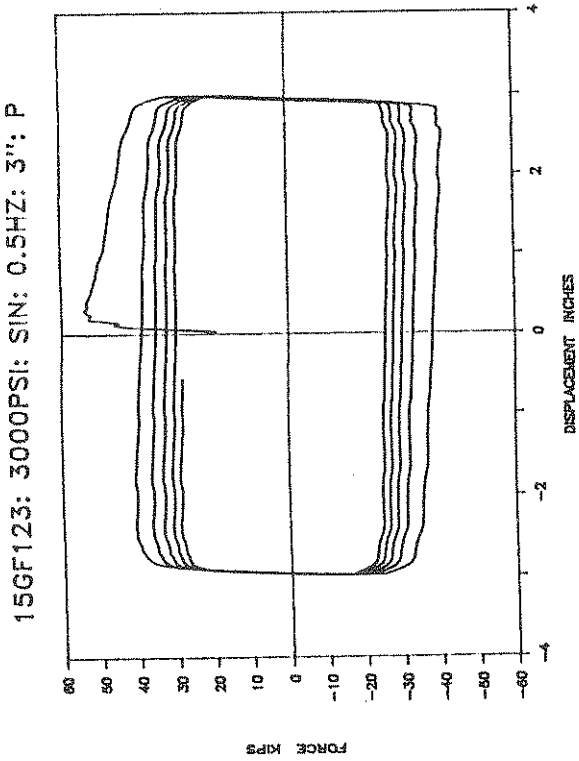
15GF123: 3000PSI: SIN: 0.5HZ: 3": P
FORCE KIPS
DISPLACEMENT INCHES

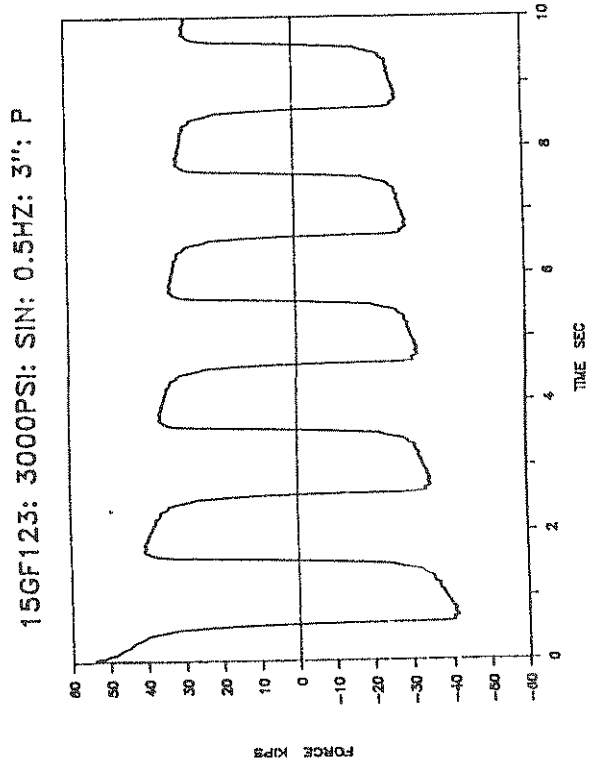
15GF123: 3000PSI: SIN: 0.5HZ: 3": P
FORCE KIPS
TIME SEC

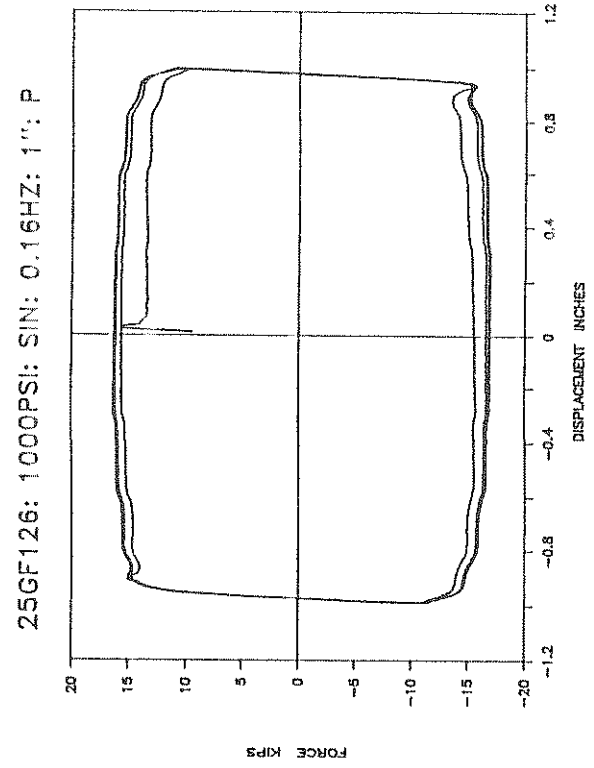
25GF126: 1000PSI: SIN: 0.16HZ: 1": P
FORCE KIPS
DISPLACEMENT INCHES

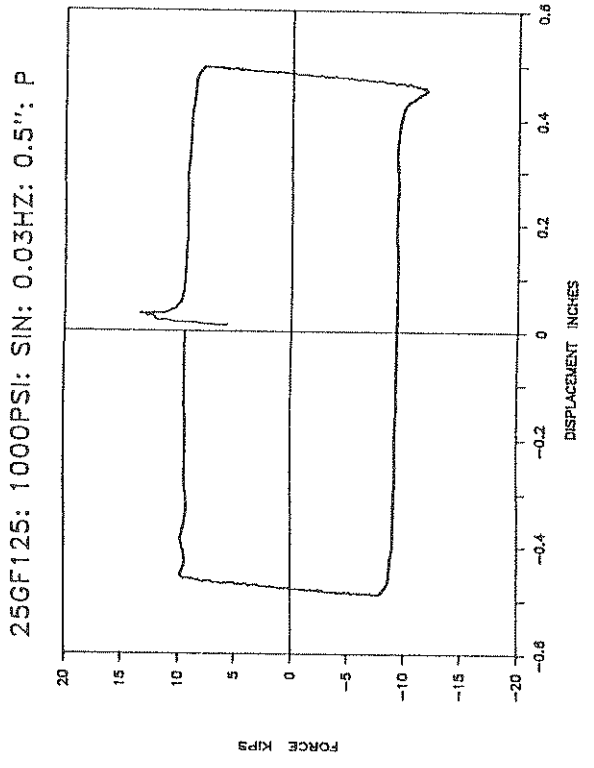
25GF125: 1000PSI: SIN: 0.03HZ: 0.5": P
FORCE KIPS
DISPLACEMENT INCHES

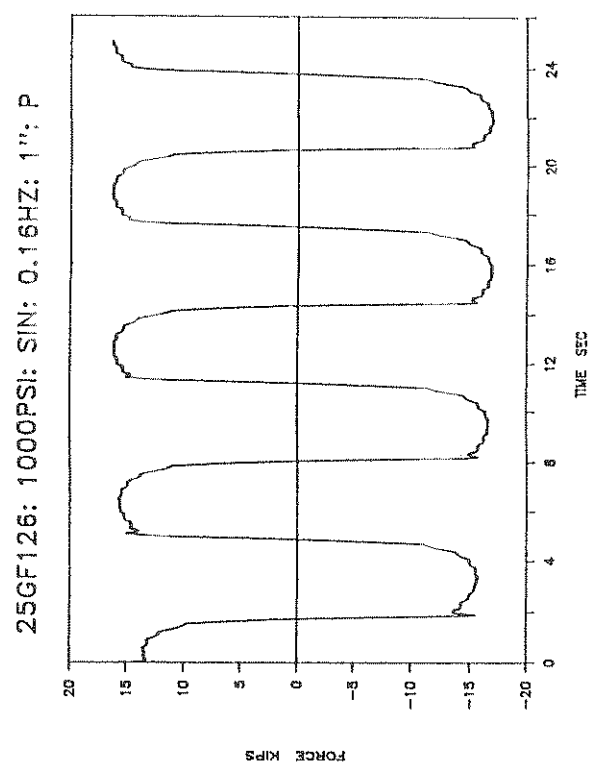
25GF126: 1000PSI: SIN: 0.16HZ: 1": P
FORCE KIPS
TIME SEC

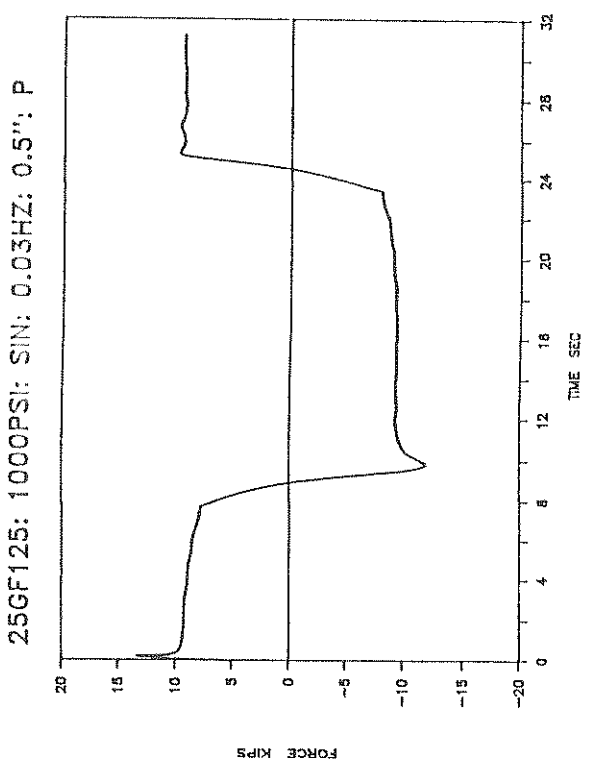
25GF125: 1000PSI: SIN: 0.03HZ: 0.5": P
FORCE KIPS
TIME SEC

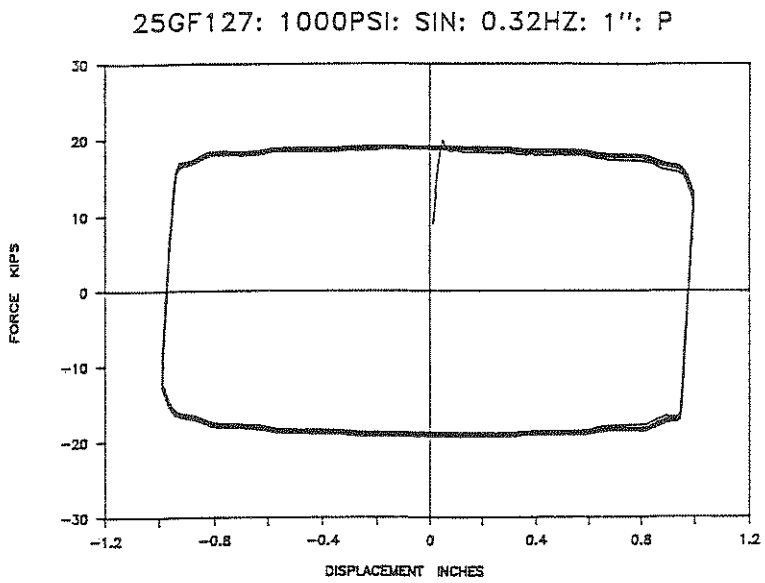
25GF127: 1000PSI: SIN: 0.32HZ: 1": P
FORCE KIPS
DISPLACEMENT INCHES
30
20
10
0
-10
-20
-30
-1.2
-0.8
-0.4
0
0.4
0.8
1.2

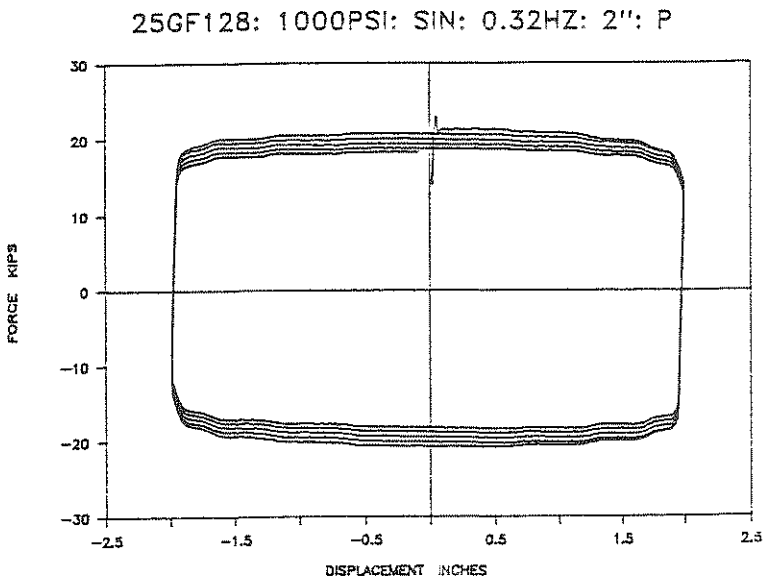
25GF128: 1000PSI: SIN: 0.32HZ: 2": P
FORCE KIPS
DISPLACEMENT INCHES
30
20
10
0
-10
-20
-30
-2.5
-1.5
-0.5
0.5
1.5
2.5

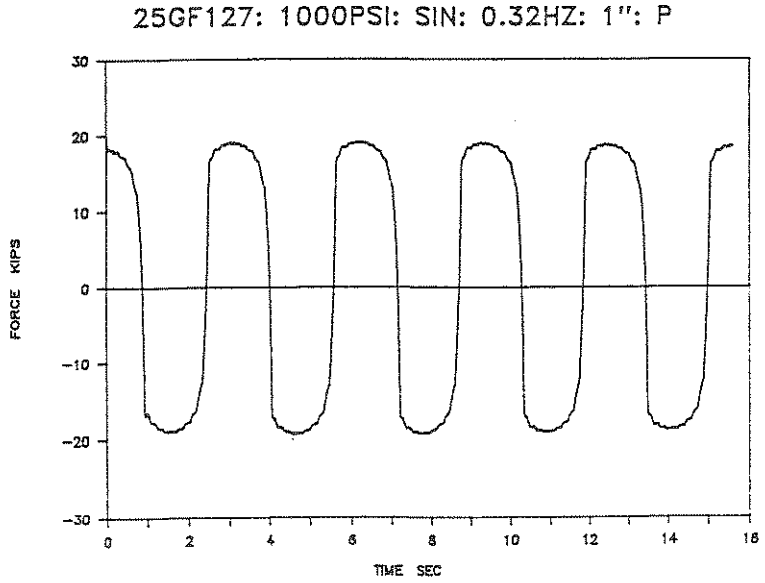
25GF127: 1000PSI: SIN: 0.32HZ: 1": P
FORCE KIPS
TIME SEC
30
20
10
0
-10
-20
-30
0
2
4
6
8
10
12
14
16

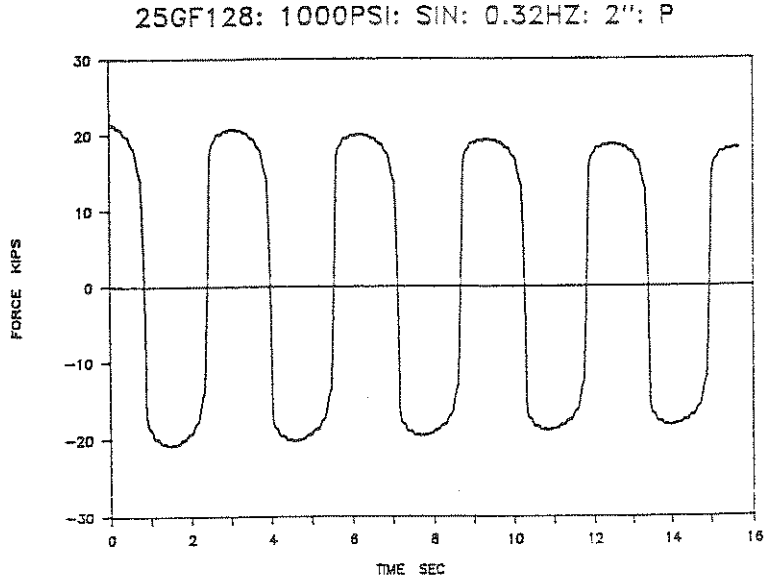
25GF128: 1000PSI: SIN: 0.32HZ: 2": P
FORCE KIPS
TIME SEC
30
20
10
0
-10
-20
-30
0
2
4
6
8
10
12
14
16

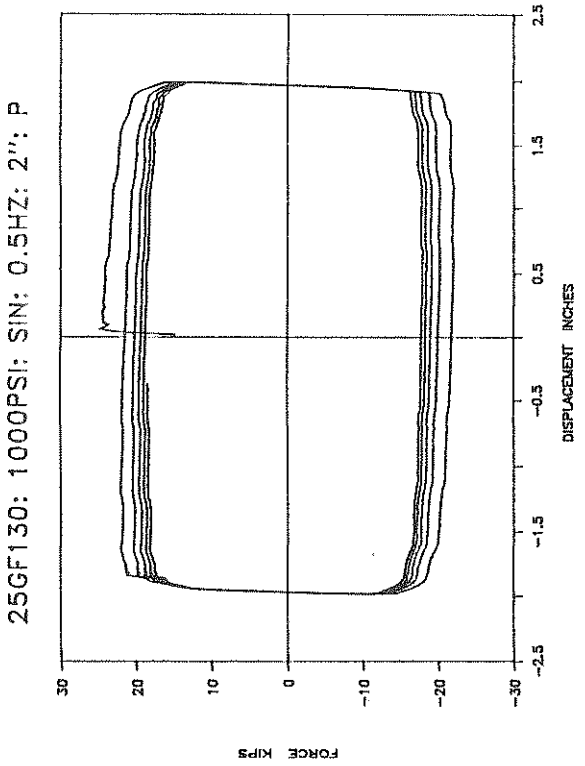
25GF130: 1000PSI: SIN: 0.5HZ: 2": P
FORCE KIPS
DISPLACEMENT INCHES

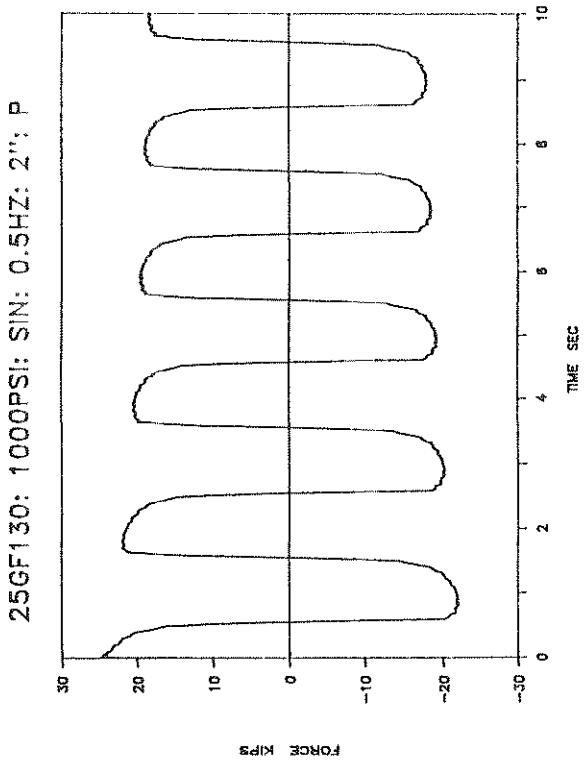
25GF130: 1000PSI: SIN: 0.5HZ: 2": P
FORCE KIPS
TIME SEC

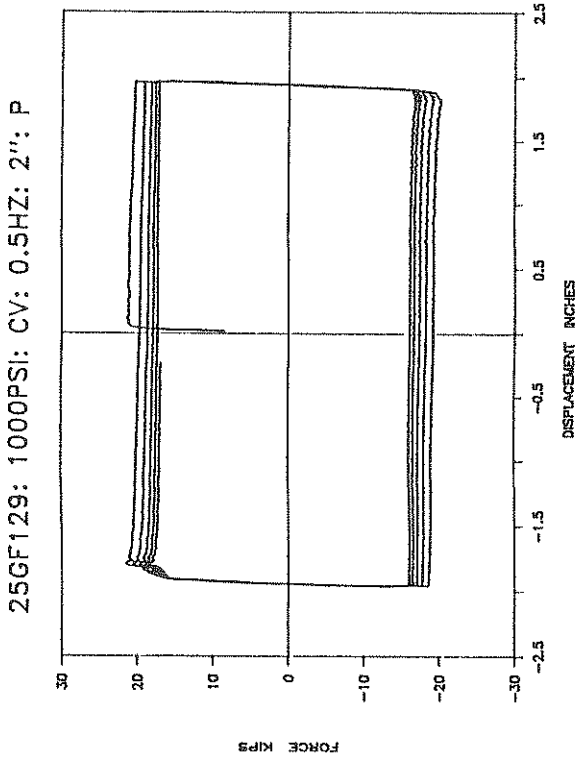
25GF129: 1000PSI: CV: 0.5HZ: 2": P
FORCE KIPS
DISPLACEMENT INCHES

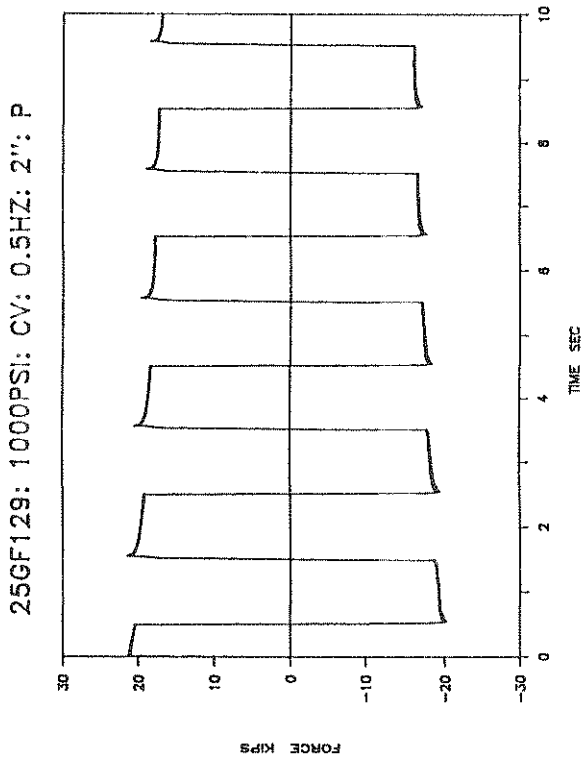
25GF129: 1000PSI: CV: 0.5HZ: 2": P
FORCE KIPS
TIME SEC

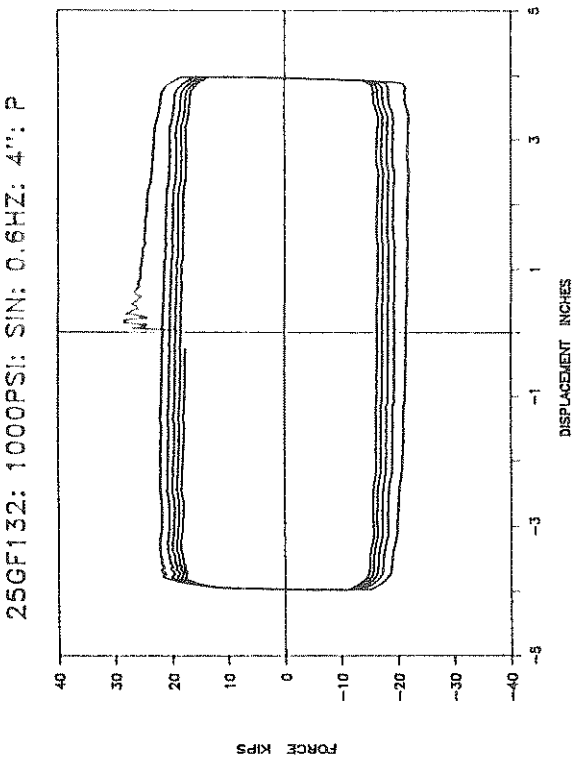
25GF132: 1000PSI: SIN: 0.6HZ: 4": P
FORCE KIPS
DISPLACEMENT INCHES

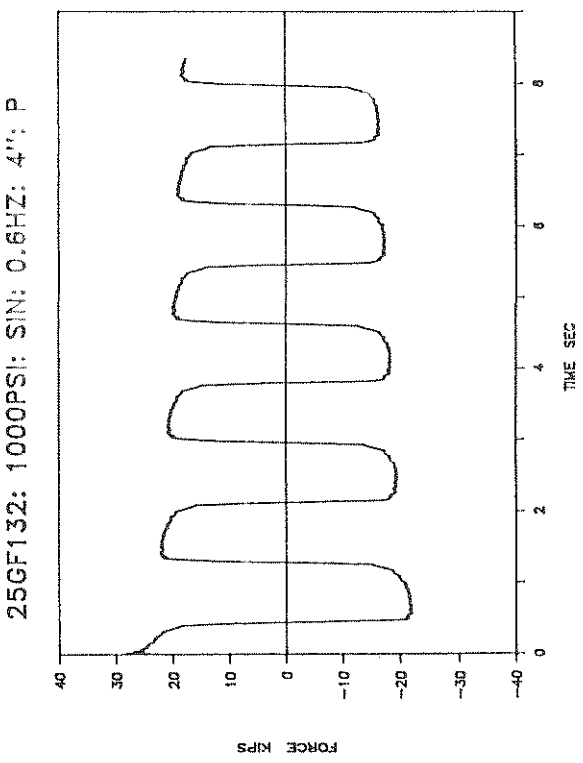
25GF132: 1000PSI: SIN: 0.6HZ: 4": P
FORCE KIPS
TIME SEC

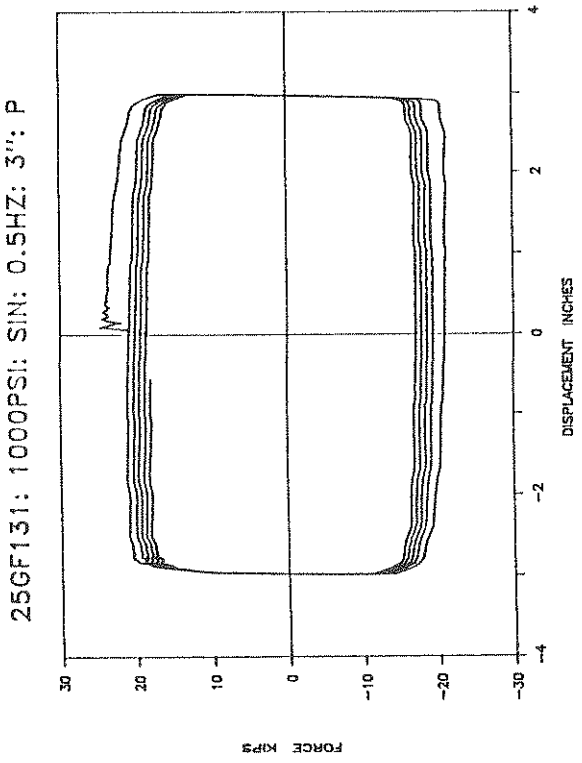
25GF131: 1000PSI: SIN: 0.5HZ: 3": P
FORCE KIPS
DISPLACEMENT INCHES

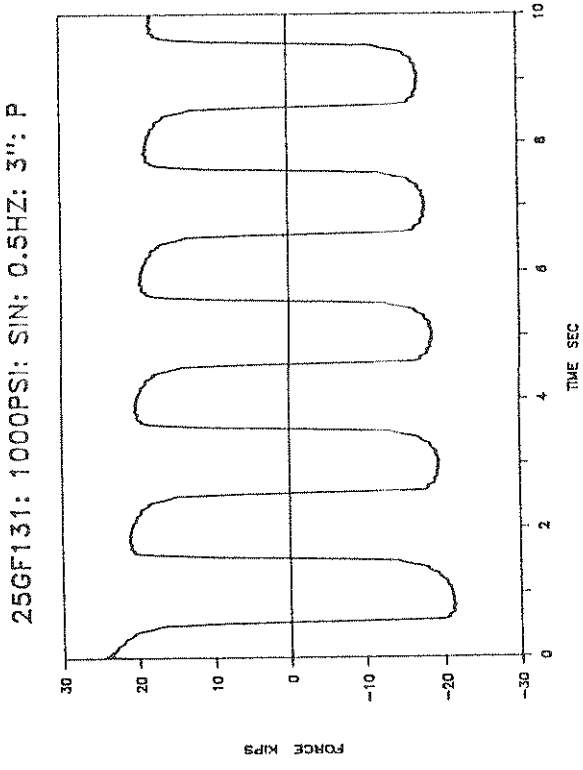
25GF131: 1000PSI: SIN: 0.5HZ: 3": P
FORCE KIPS
TIME SEC

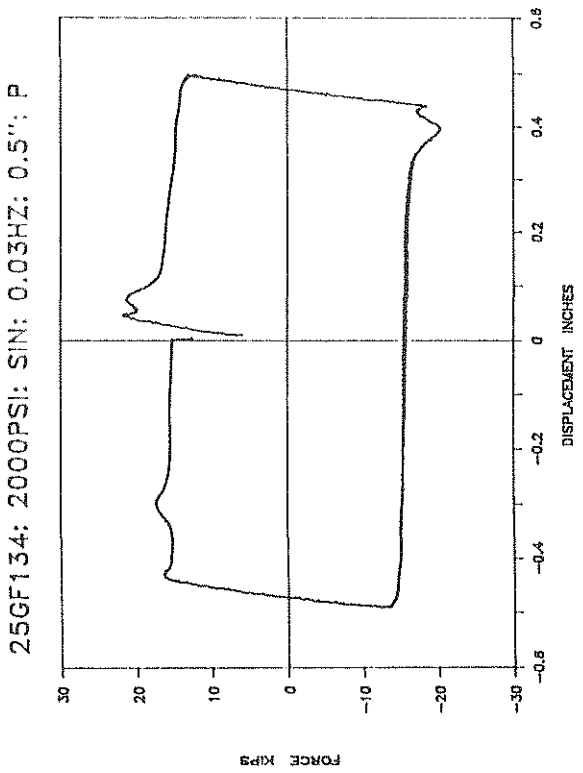
25GF134: 2000PSI: SIN: 0.03HZ: 0.5": P
FORCE KIPS
DISPLACEMENT INCHES

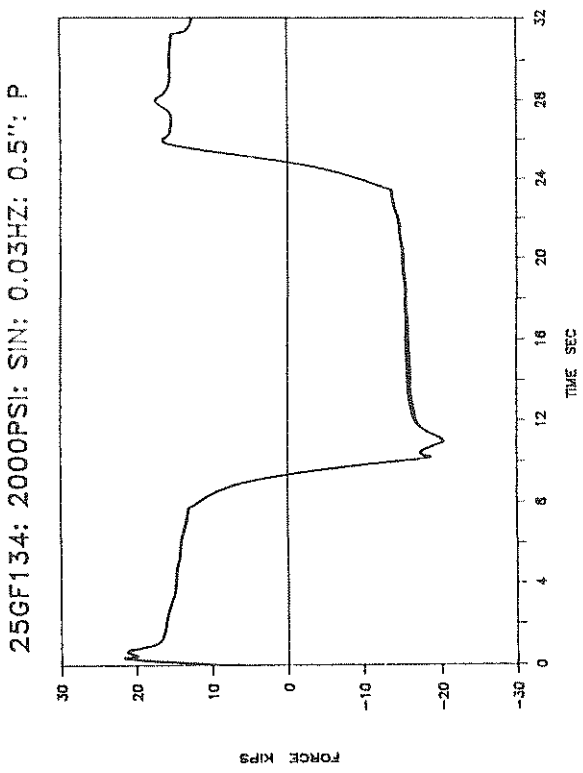
25GF134: 2000PSI: SIN: 0.03HZ: 0.5": P
FORCE KIPS
TIME SEC

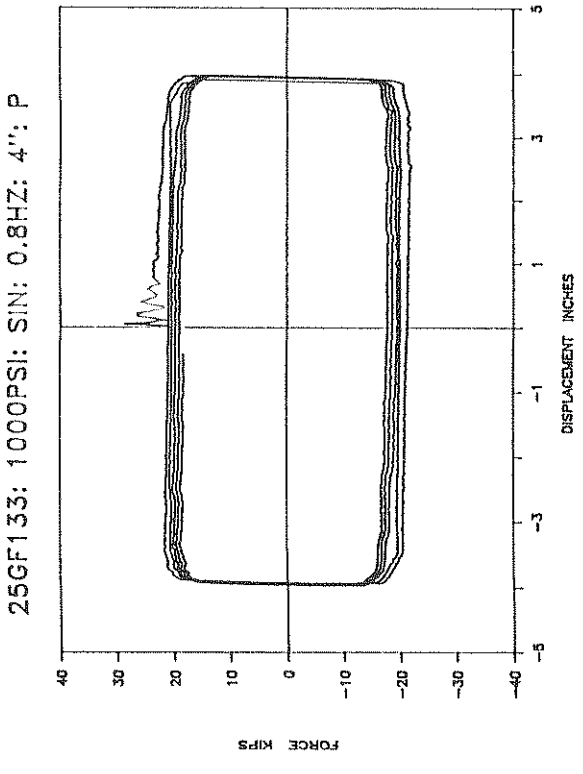
25GF133: 1000PSI: SIN: 0.8HZ: 4": P
FORCE KIPS
DISPLACEMENT INCHES

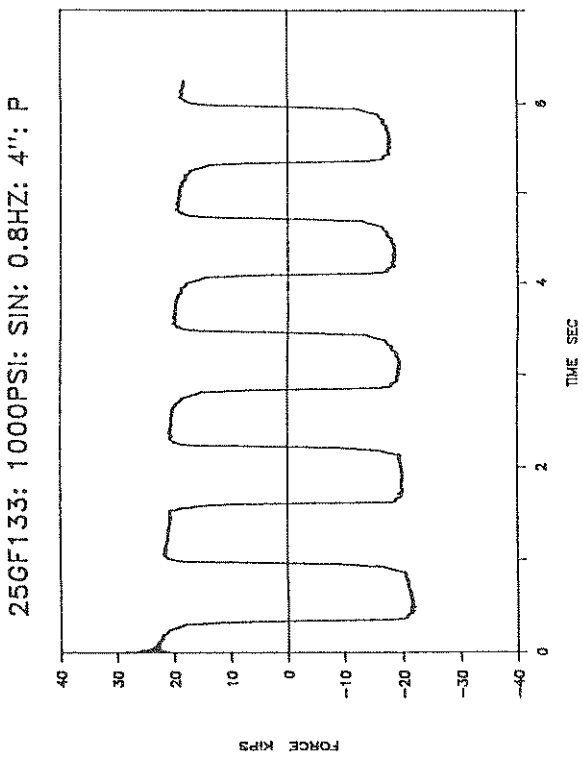
25GF133: 1000PSI: SIN: 0.8HZ: 4": P
FORCE KIPS
TIME SEC

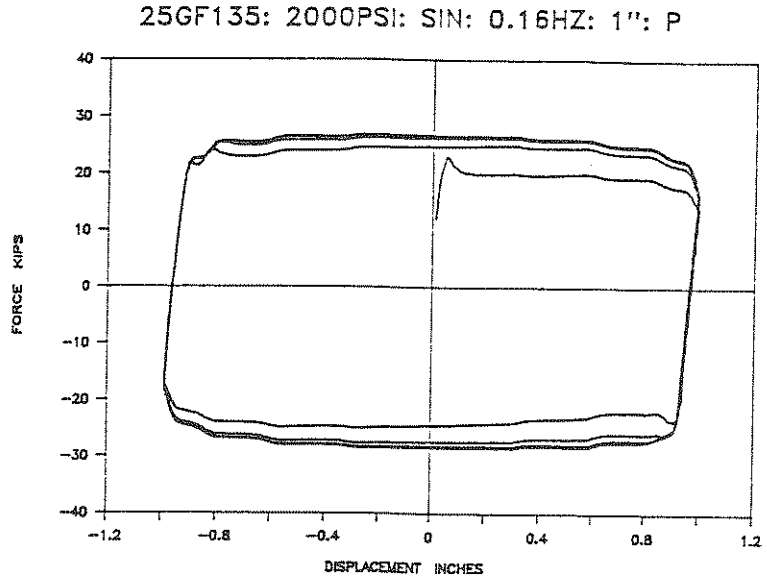
25GF135: 2000PSI: SIN: 0.16HZ: 1": P
FORCE KIPS
DISPLACEMENT INCHES
40
30
20
10
0
-10
-20
-30
-40
-1.2
-0.8
-0.4
0
0.4
0.8
1.2

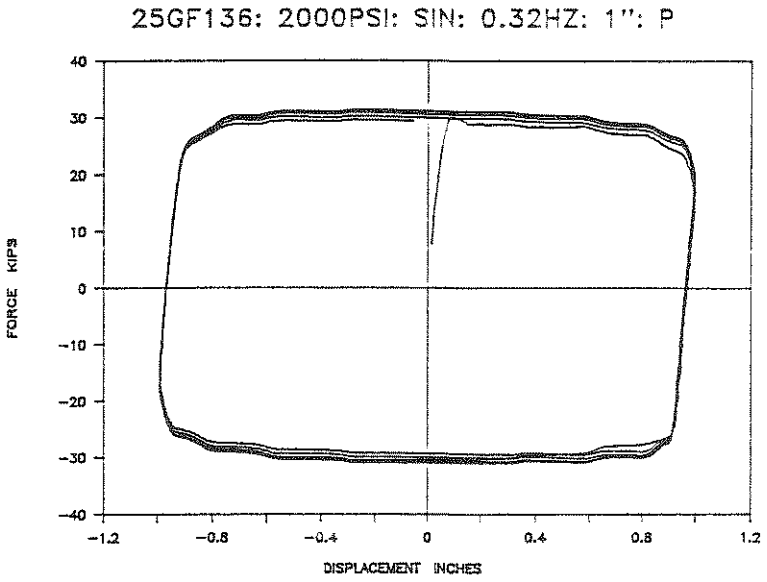
25GF136: 2000PSI: SIN: 0.32HZ: 1": P
FORCE KIPS
DISPLACEMENT INCHES
40
30
20
10
0
-10
-20
-30
-40
-1.2
-0.8
-0.4
0
0.4
0.8
1.2

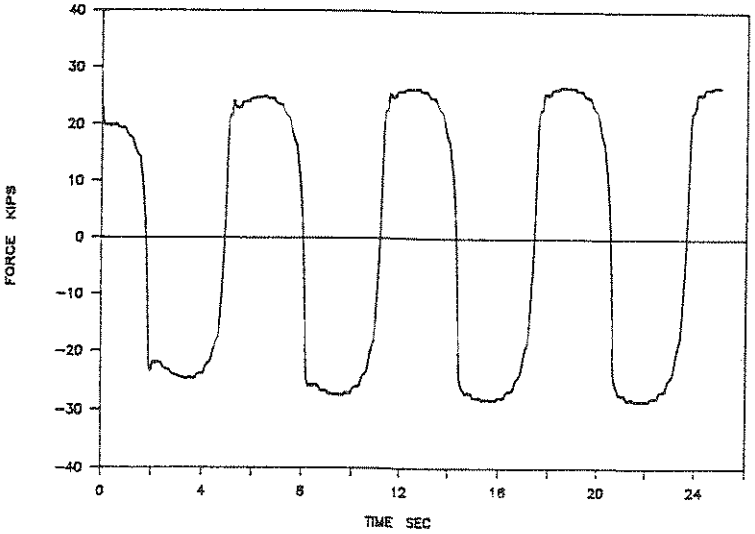
25GF135: 2000PSI: SIN: 0.16HZ: 1": P
FORCE KIPS
TIME SEC
40
30
20
10
0
-10
-20
-30
-40
0
4
8
12
16
20
24

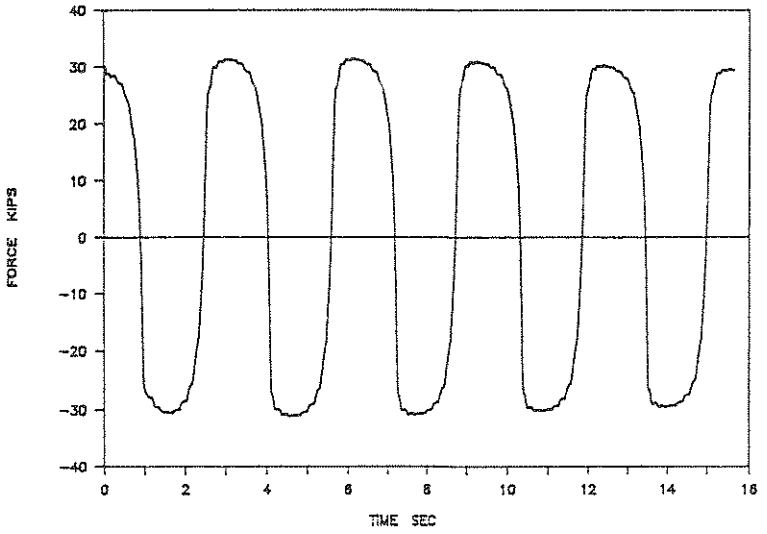
25GF136: 2000PSI: SIN: 0.32HZ: 1": P
FORCE KIPS
TIME SEC
40
30
20
10
0
-10
-20
-30
-40
0
2
4
6
8
10
12
14
16

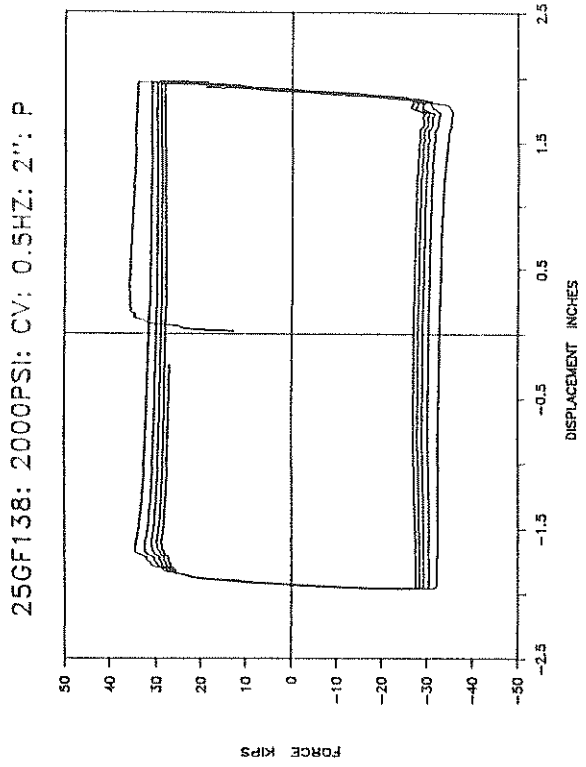
25GF138: 2000PSI: CV: 0.5HZ: 2": P
FORCE KIPS
DISPLACEMENT INCHES

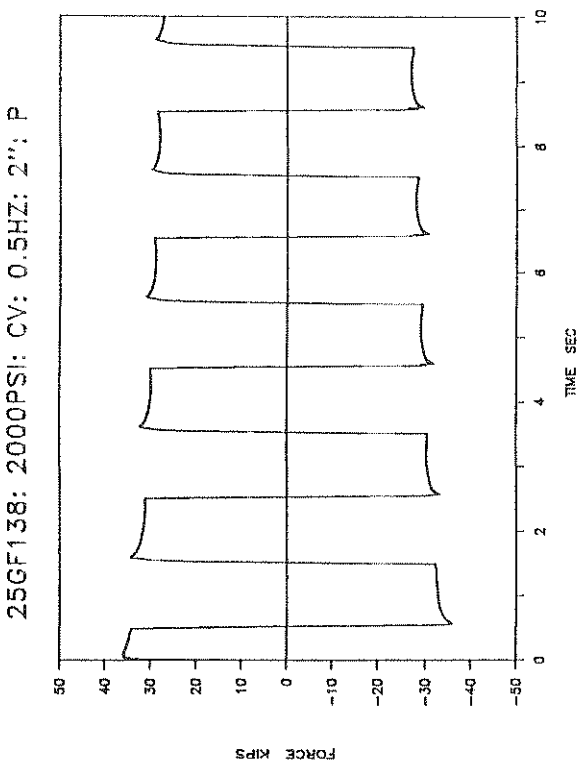
25GF138: 2000PSI: CV: 0.5HZ: 2": P
FORCE KIPS
TIME SEC

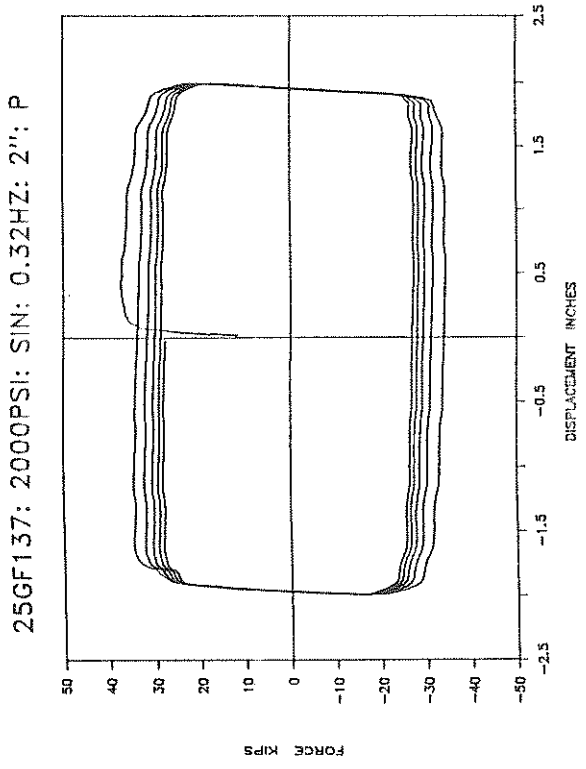
25GF137: 2000PSI: SIN: 0.32HZ: 2": P
FORCE KIPS
DISPLACEMENT INCHES

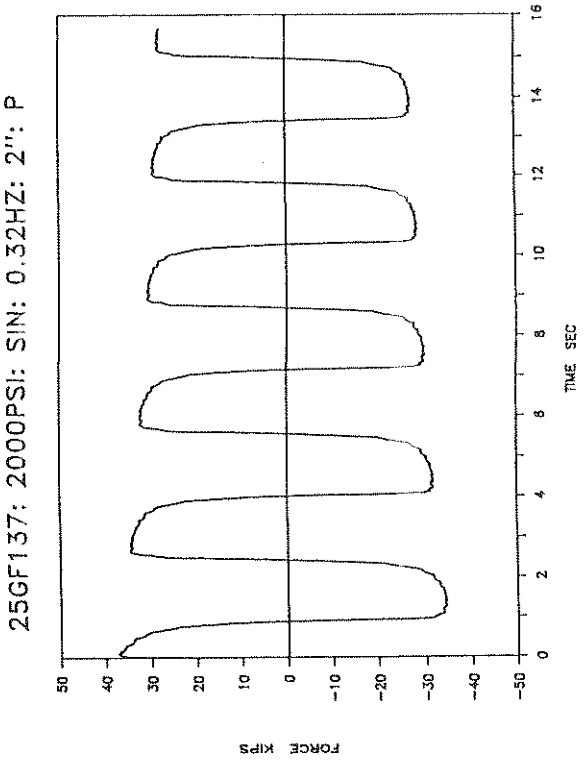
25GF137: 2000PSI: SIN: 0.32HZ: 2": P
FORCE KIPS
TIME SEC

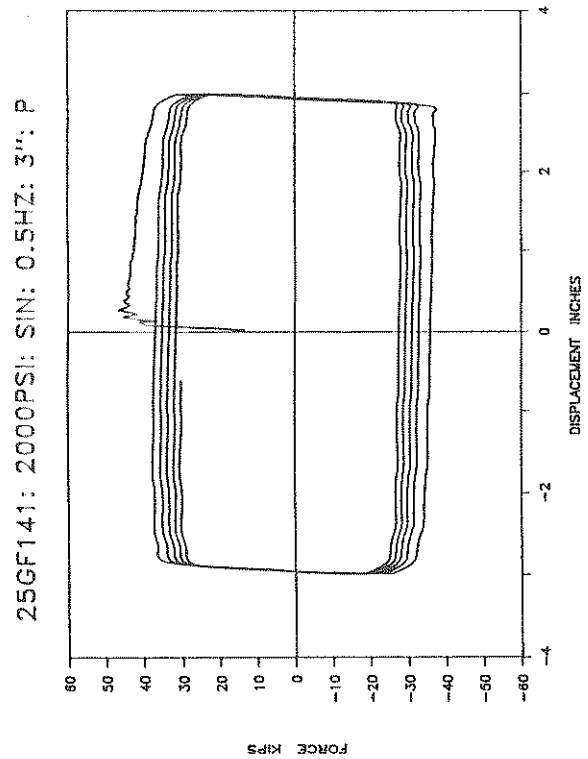
25GF141: 2000PSI: SIN: 0.5HZ: 3": P
FORCE KIPS
DISPLACEMENT INCHES

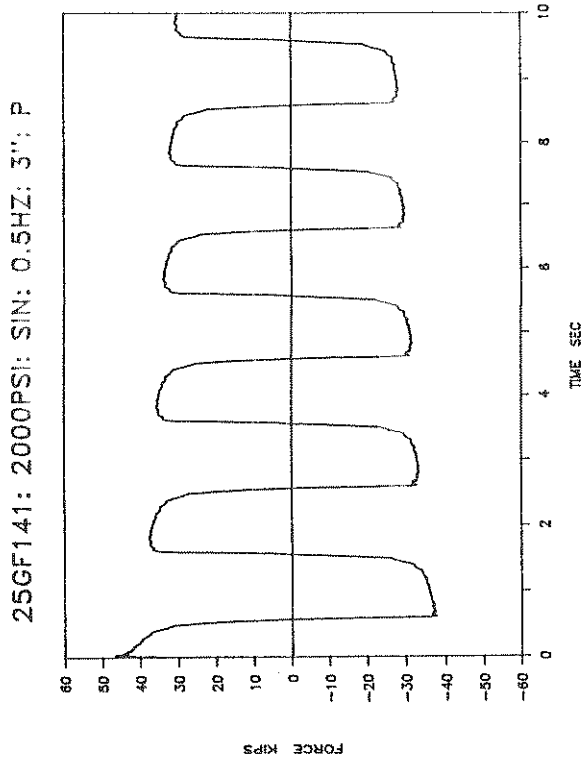
25GF141: 2000PSI: SIN: 0.5HZ: 3": P
FORCE KIPS
TIME SEC

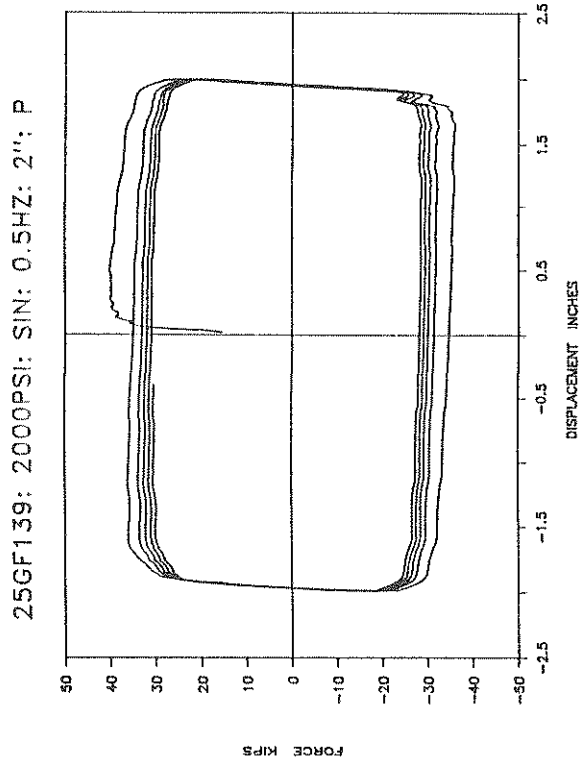
25GF139: 2000PSI: SIN: 0.5HZ: 2": P
FORCE KIPS
DISPLACEMENT INCHES

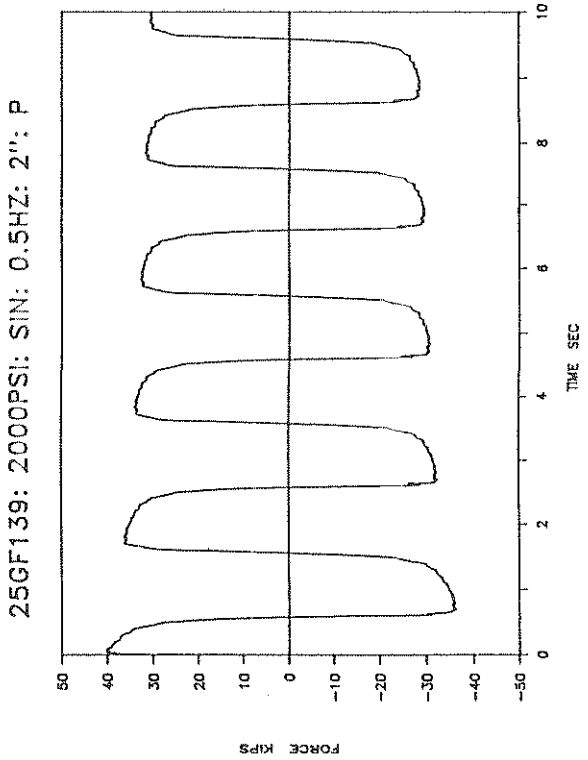
25GF139: 2000PSI: SIN: 0.5HZ: 2": P
FORCE KIPS
TIME SEC

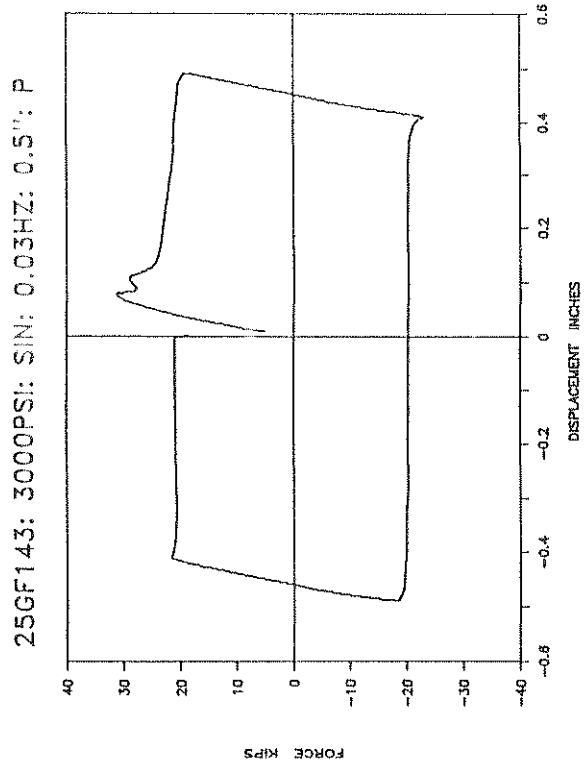
25GF143: 3000PSI: SIN: 0.03HZ: 0.5": P
FORCE KIPS
DISPLACEMENT INCHES

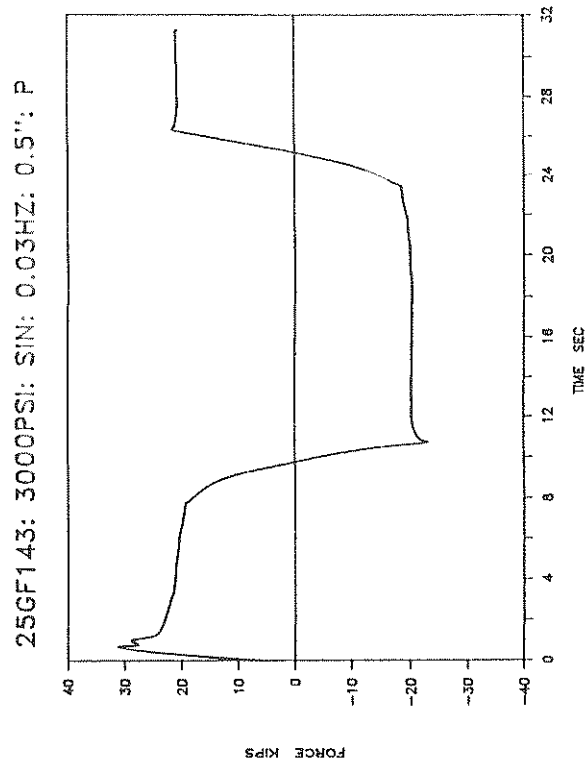
25GF143: 3000PSI: SIN: 0.03HZ: 0.5": P
FORCE KIPS
TIME SEC

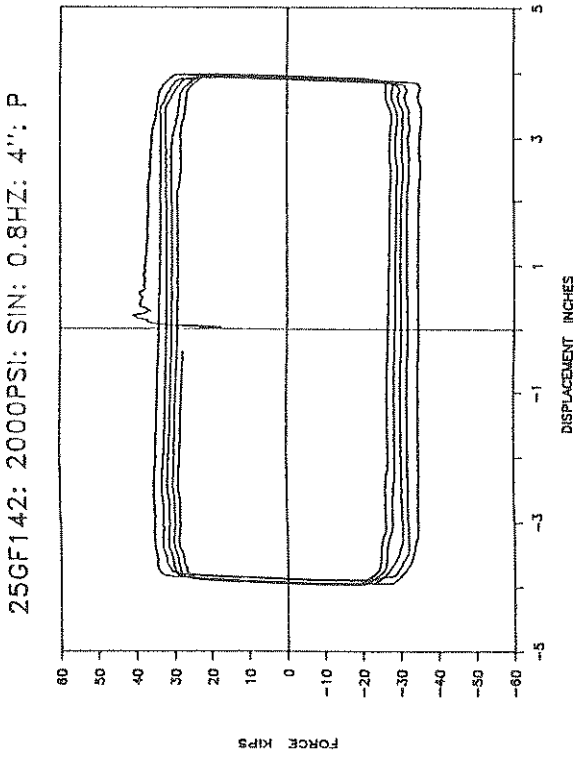
25GF142: 2000PSI: SIN: 0.8HZ: 4": P
FORCE KIPS
DISPLACEMENT INCHES

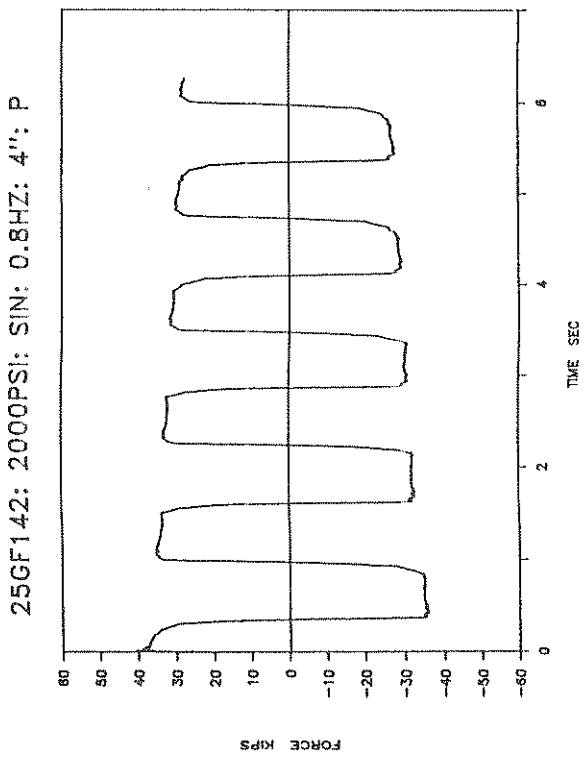
25GF142: 2000PSI: SIN: 0.8HZ: 4": P
FORCE KIPS
TIME SEC

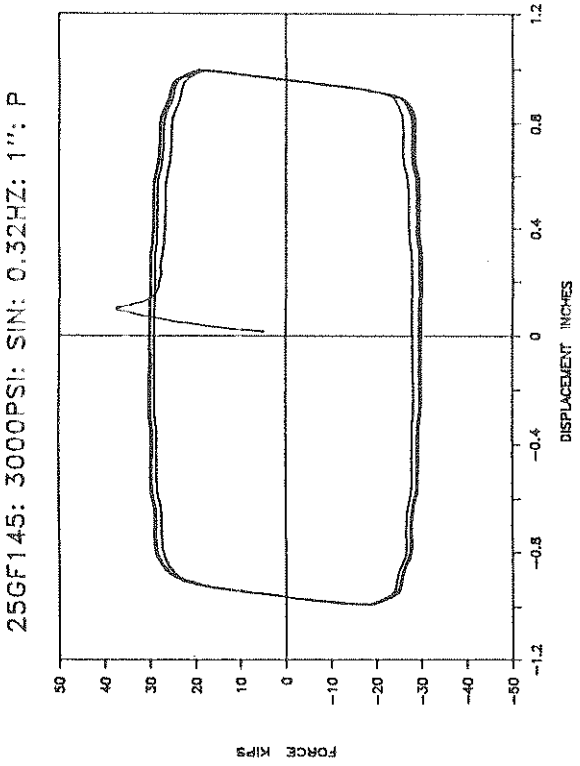
25GF145: 3000PSI: SIN: 0.32HZ: 1": P
FORCE KIPS
DISPLACEMENT INCHES

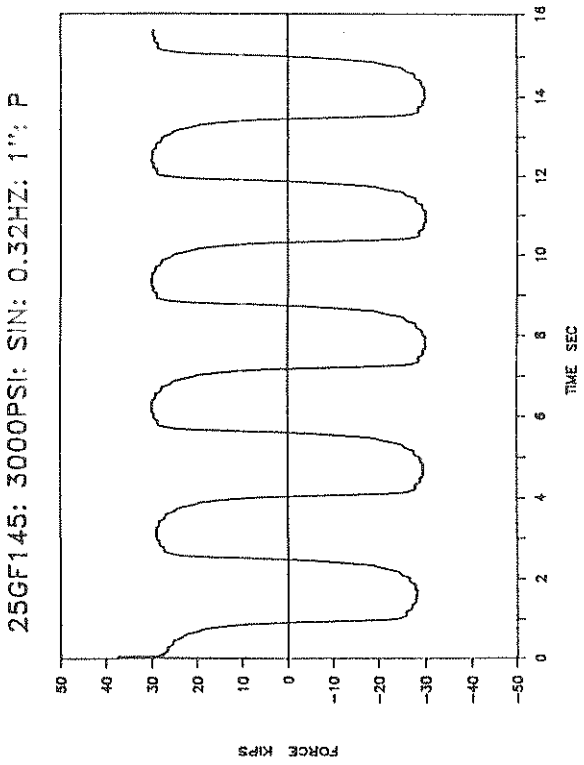
25GF145: 3000PSI: SIN: 0.32HZ: 1": P
FORCE KIPS
TIME SEC

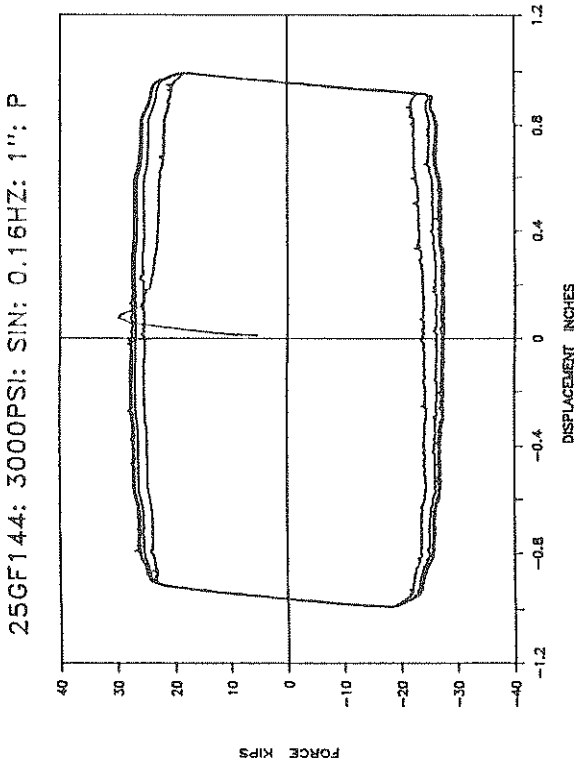
25GF144: 3000PSI: SIN: 0.16HZ: 1": P
FORCE KIPS
DISPLACEMENT INCHES

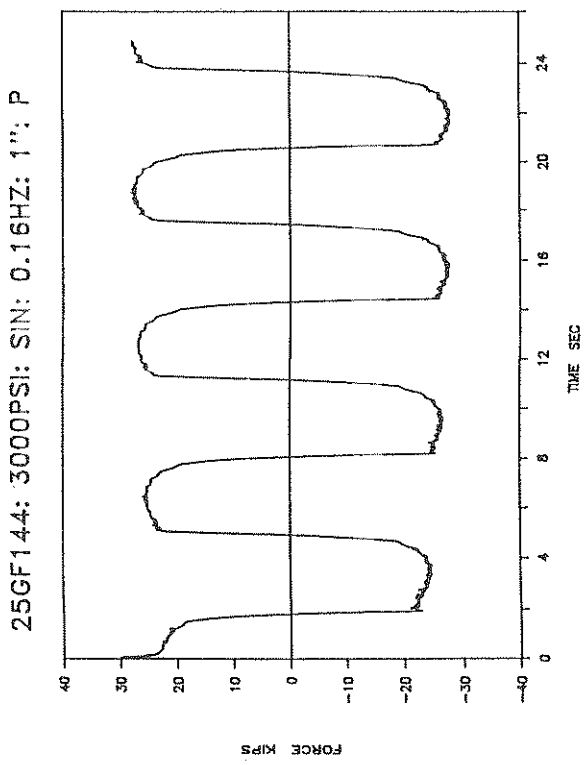
25GF144: 3000PSI: SIN: 0.16HZ: 1": P
FORCE KIPS
TIME SEC

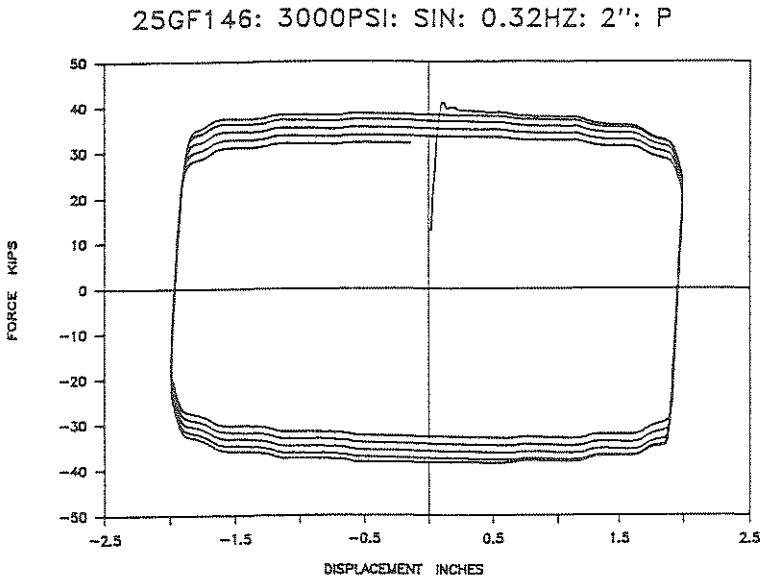
25GF146: 3000PSI: SIN: 0.32HZ: 2": P
FORCE KIPS
DISPLACEMENT INCHES

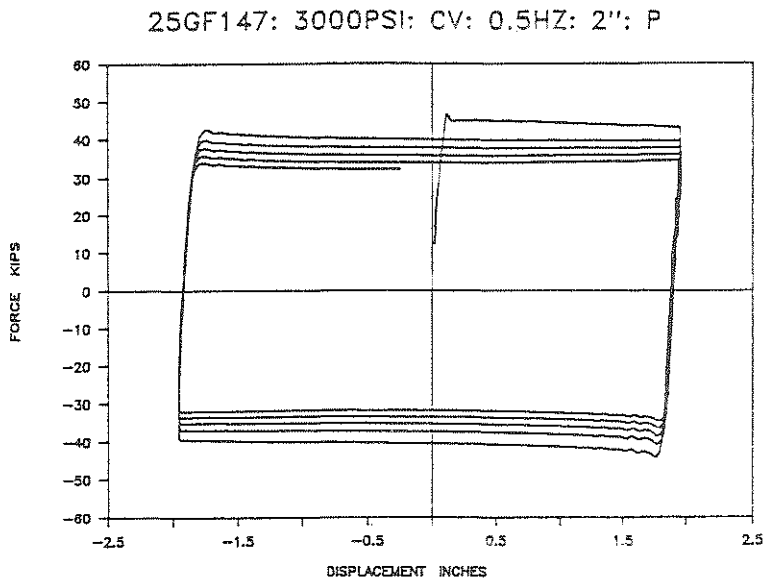
25GF147: 3000PSI: CV: 0.5HZ: 2": P
FORCE KIPS
DISPLACEMENT INCHES

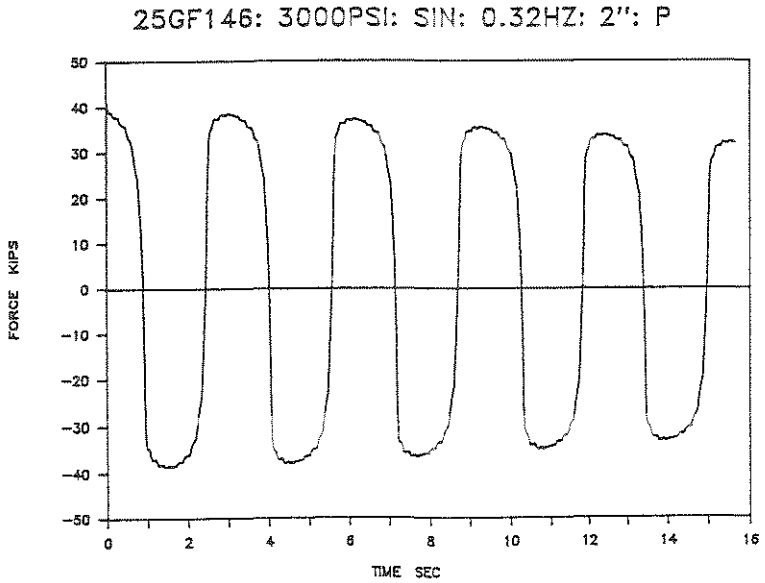
25GF146: 3000PSI: SIN: 0.32HZ: 2": P
FORCE KIPS
TIME SEC

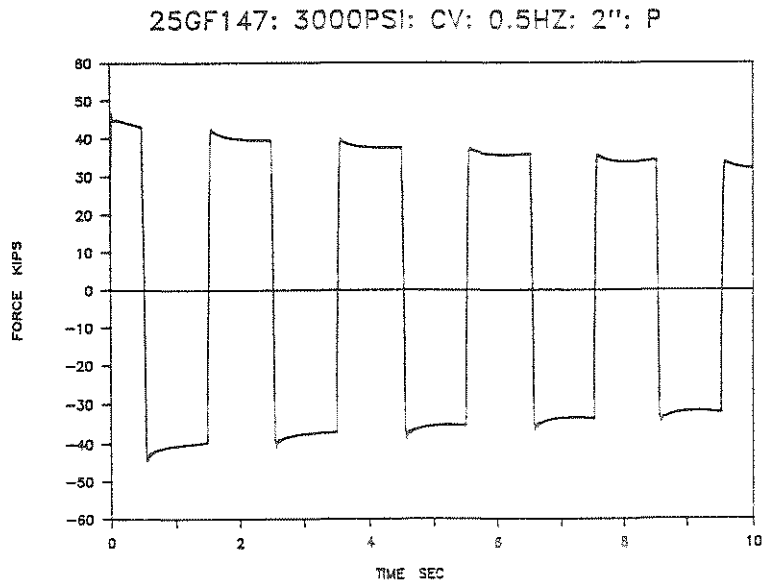
25GF147: 3000PSI: CV: 0.5HZ: 2": P
FORCE KIPS
TIME SEC

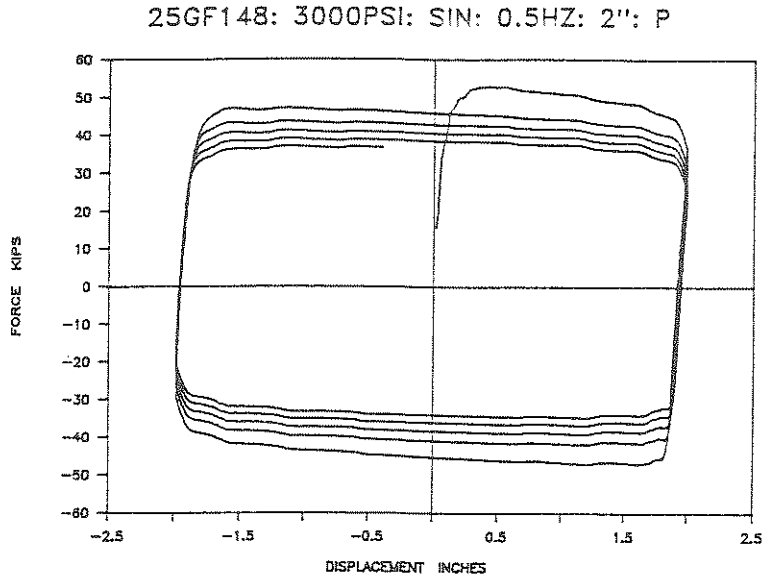
25GF148: 3000PSI: SIN: 0.5HZ: 2": P
FORCE KIPS
DISPLACEMENT INCHES

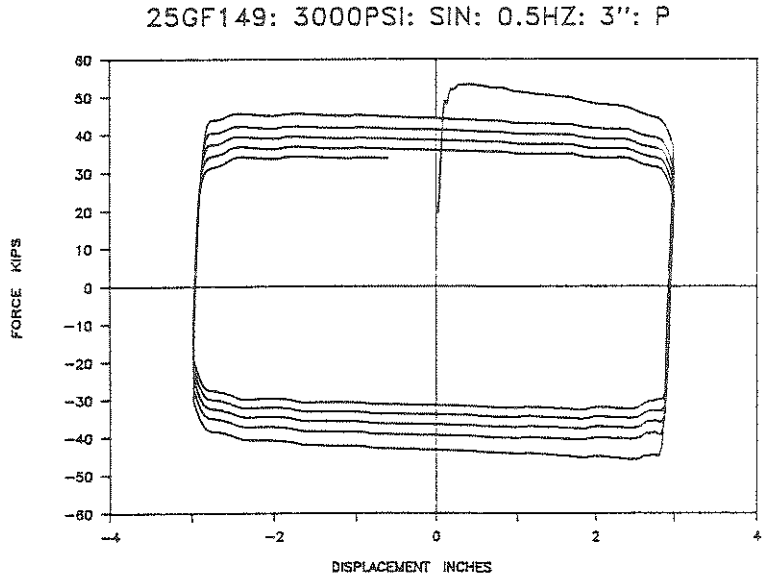
25GF149: 3000PSI: SIN: 0.5HZ: 3": P
FORCE KIPS
DISPLACEMENT INCHES

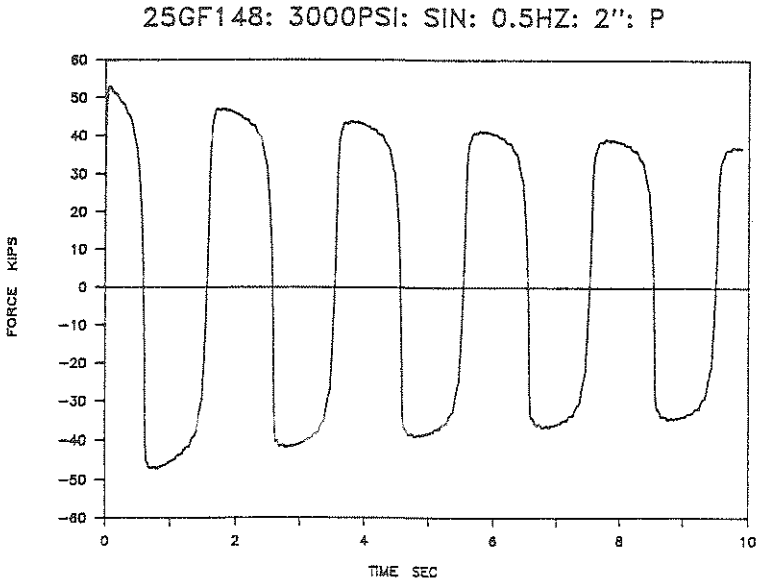
25GF148: 3000PSI: SIN: 0.5HZ: 2": P
FORCE KIPS
TIME SEC

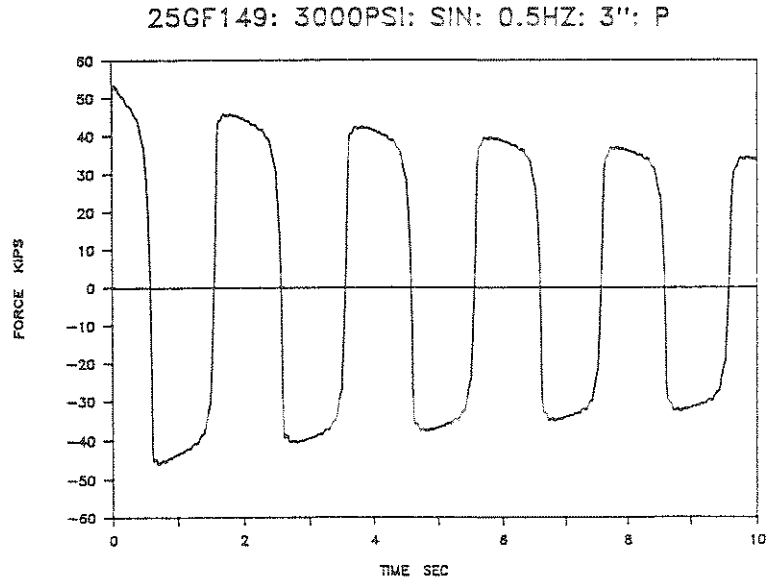
25GF149: 3000PSI: SIN: 0.5HZ: 3": P
FORCE KIPS
TIME SEC

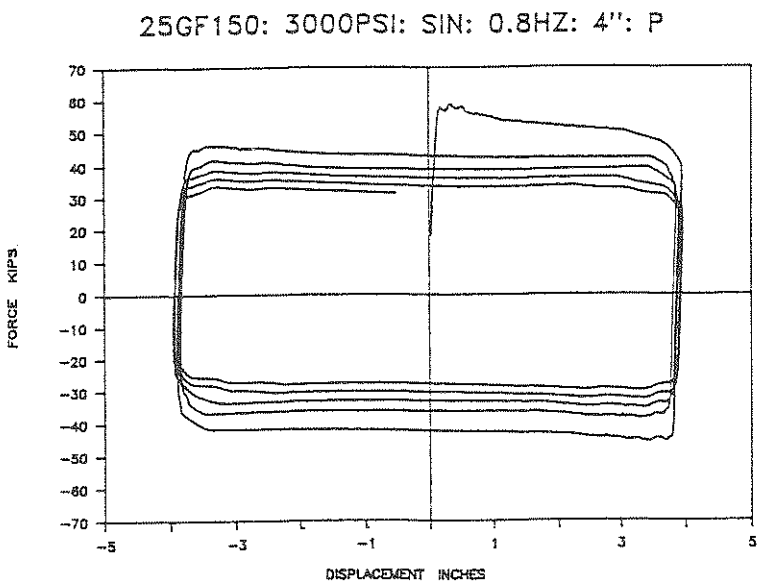
25GF150: 3000PSI: SIN: 0.8HZ: 4": P
FORCE KIPS
DISPLACEMENT INCHES

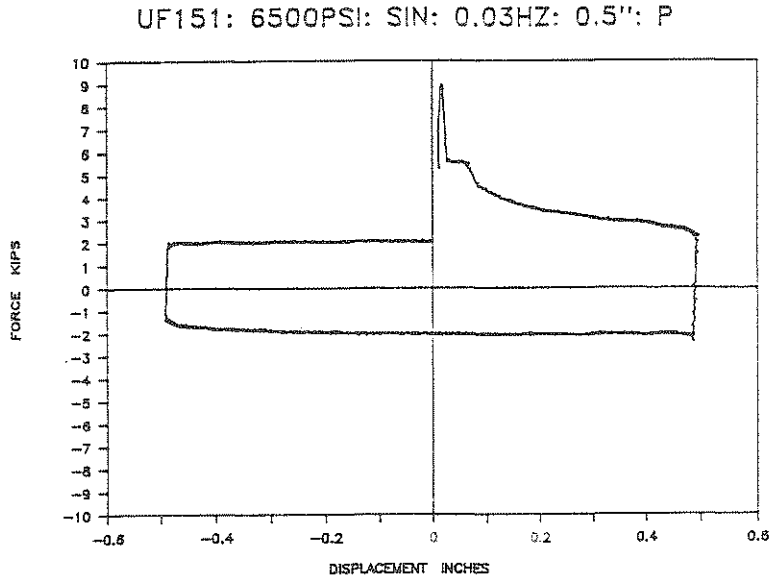
UF151: 6500PSI: SIN: 0.03HZ: 0.5": P
FORCE KIPS
DISPLACEMENT INCHES

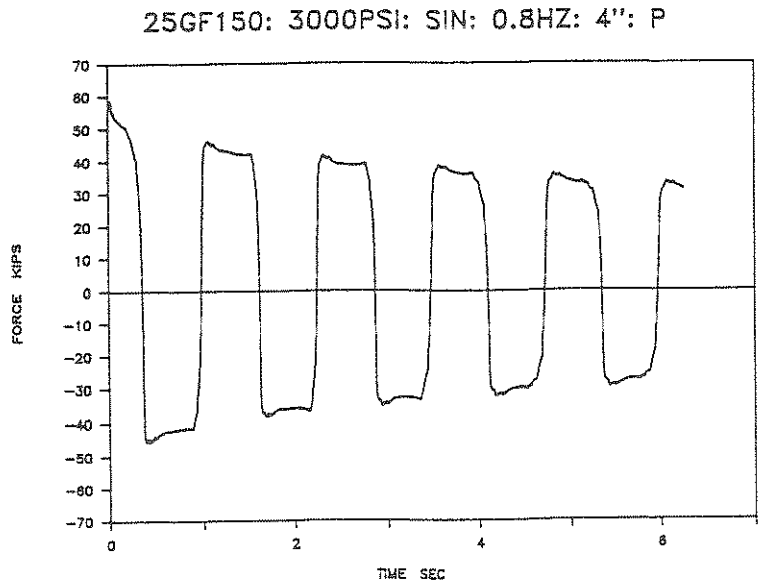
25GF150: 3000PSI: SIN: 0.8HZ: 4": P
FORCE KIPS
TIME SEC

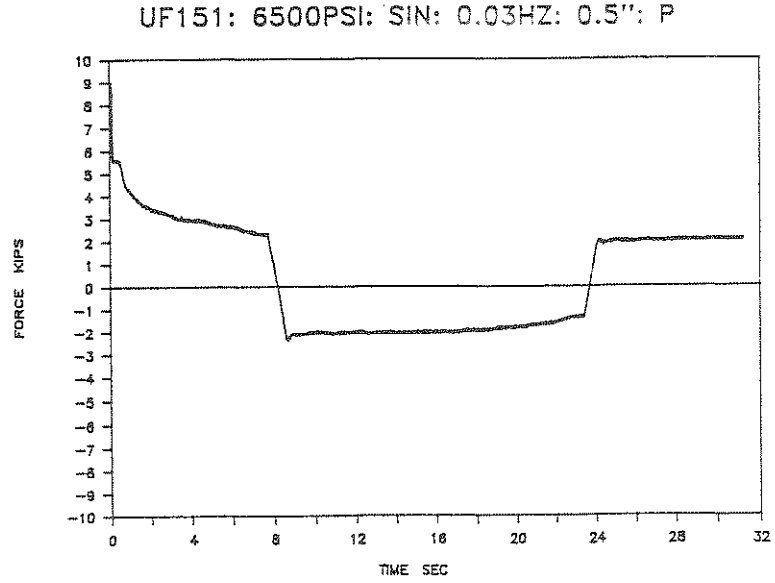
UF151: 6500PSI: SIN: 0.03HZ: 0.5": P
FORCE KIPS
TIME SEC

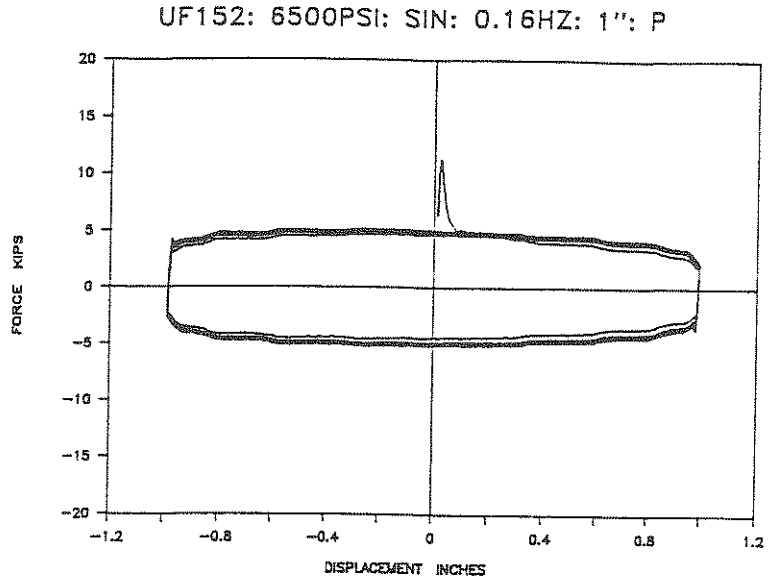
UF152: 6500PSI: SIN: 0.16HZ: 1": P
FORCE KIPS
DISPLACEMENT INCHES

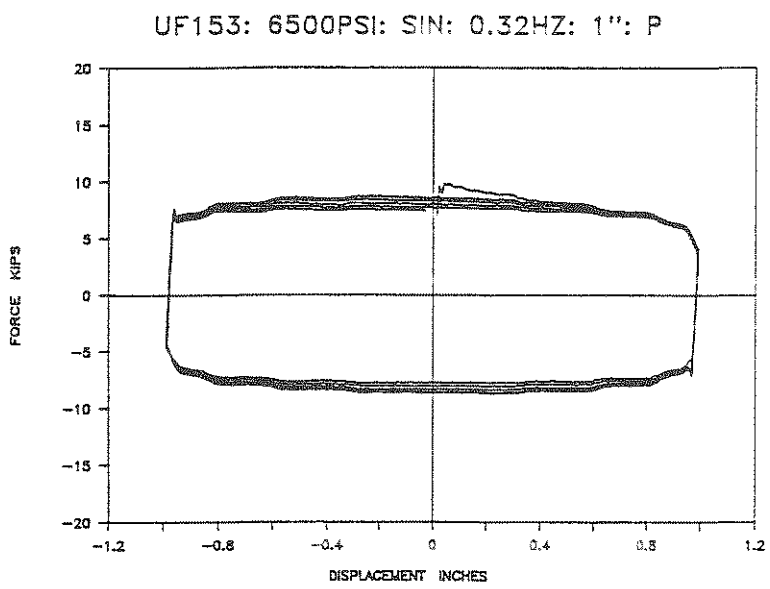
UF153: 6500PSI: SIN: 0.32HZ: 1": P
FORCE KIPS
DISPLACEMENT INCHES

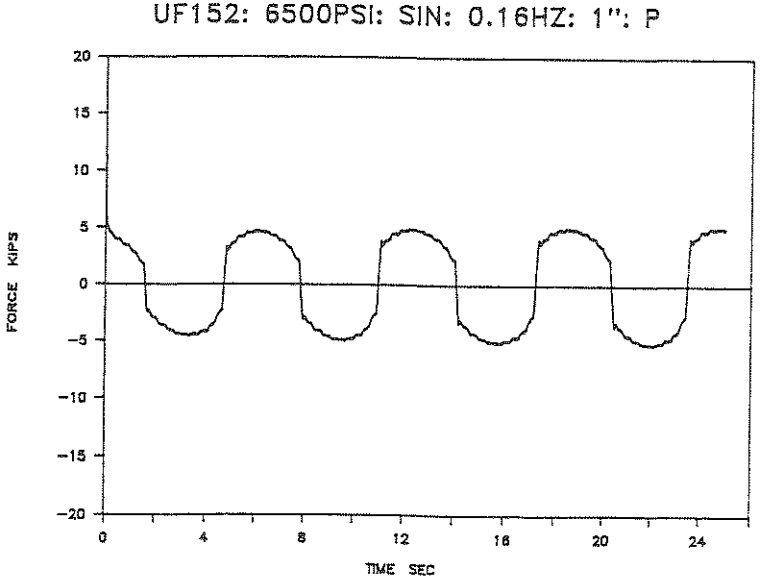
UF152: 6500PSI: SIN: 0.16HZ: 1": P
FORCE KIPS
TIME SEC

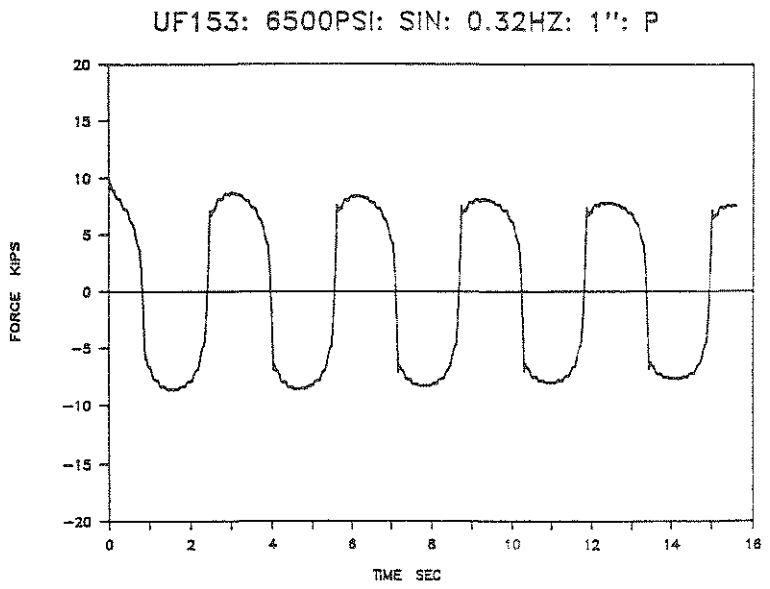
UF153: 6500PSI: SIN: 0.32HZ: 1": P
FORCE KIPS
TIME SEC

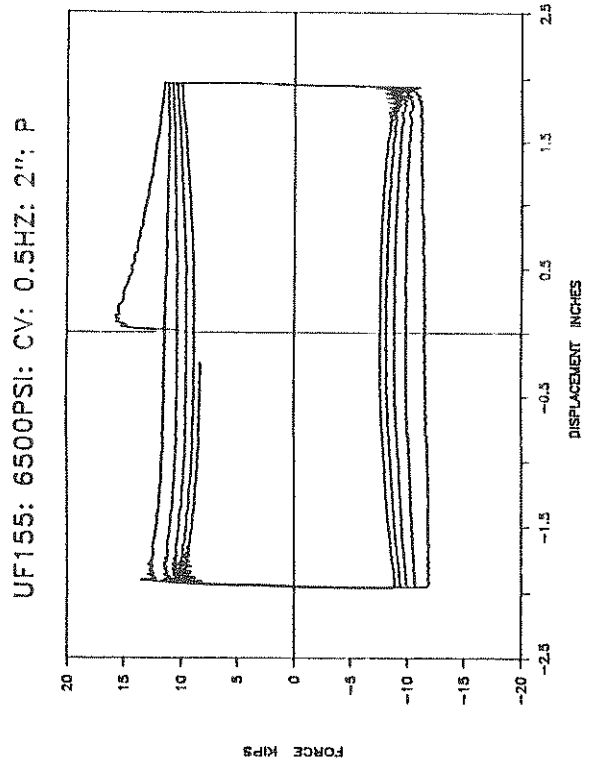
UF155: 6500PSI: CV: 0.5HZ: 2": P
FORCE KIPS
DISPLACEMENT INCHES

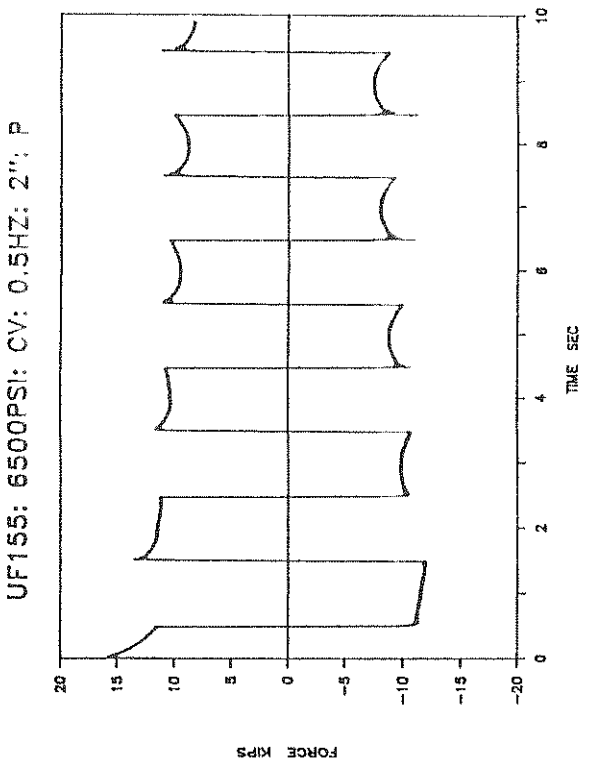
UF155: 6500PSI: CV: 0.5HZ: 2": P
FORCE KIPS
TIME SEC

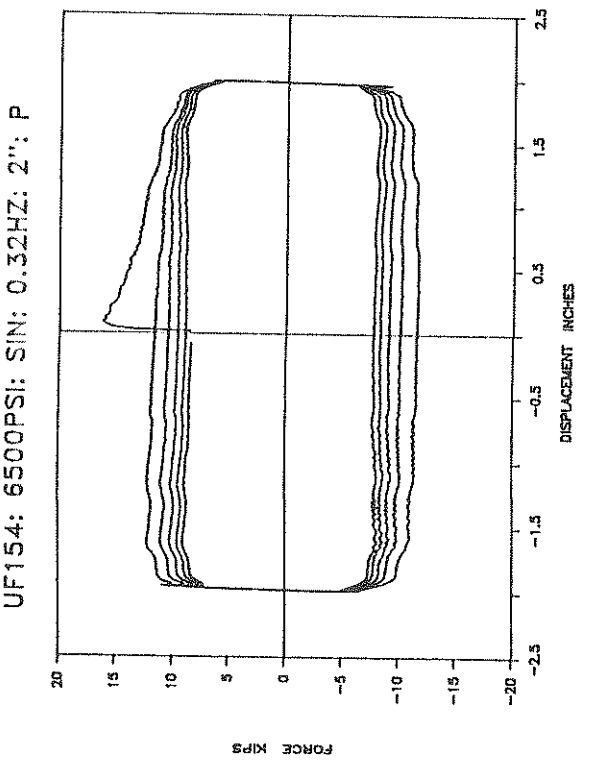
UF154: 6500PSI: SIN: 0.32HZ: 2": P
FORCE KIPS
DISPLACEMENT INCHES

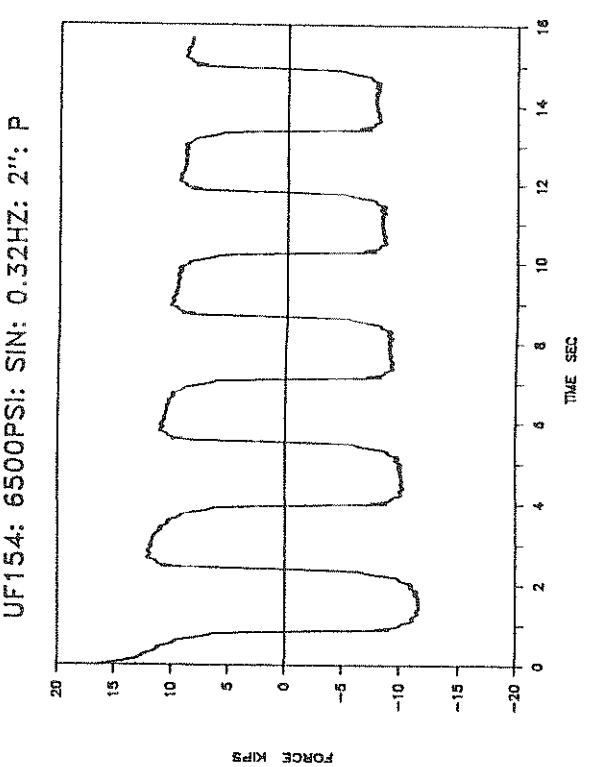
UF154: 6500PSI: SIN: 0.32HZ: 2": P
FORCE KIPS
TIME SEC

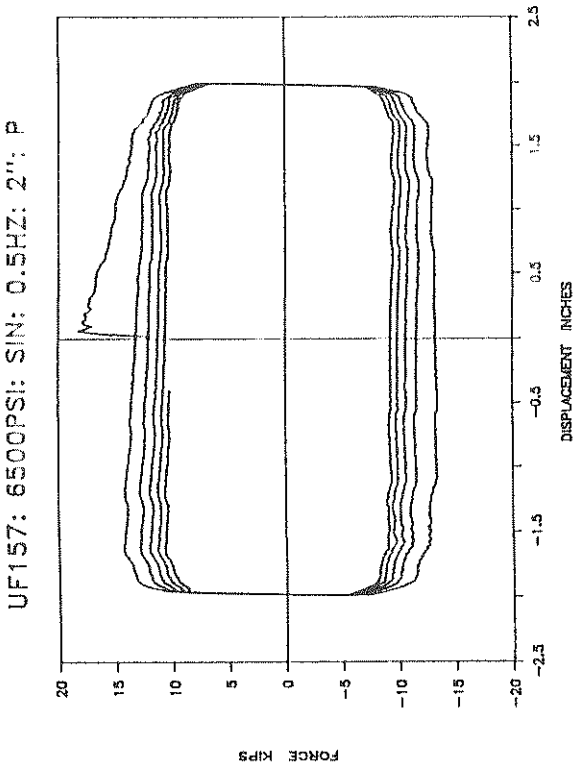
UF157: 6500PSI: SIN: 0.5HZ: 2": P
FORCE KIPS
DISPLACEMENT INCHES

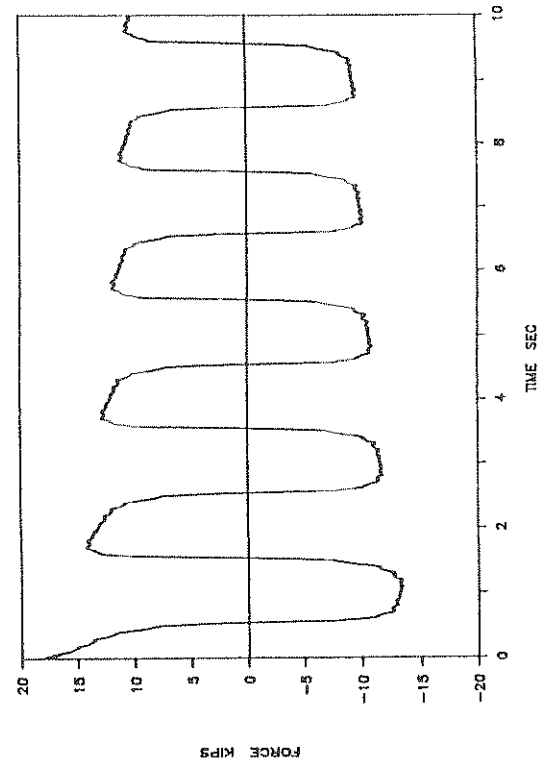
UF157: 6500PSI: SIN: 0.5HZ: 2": P
FORCE KIPS
TIME SEC

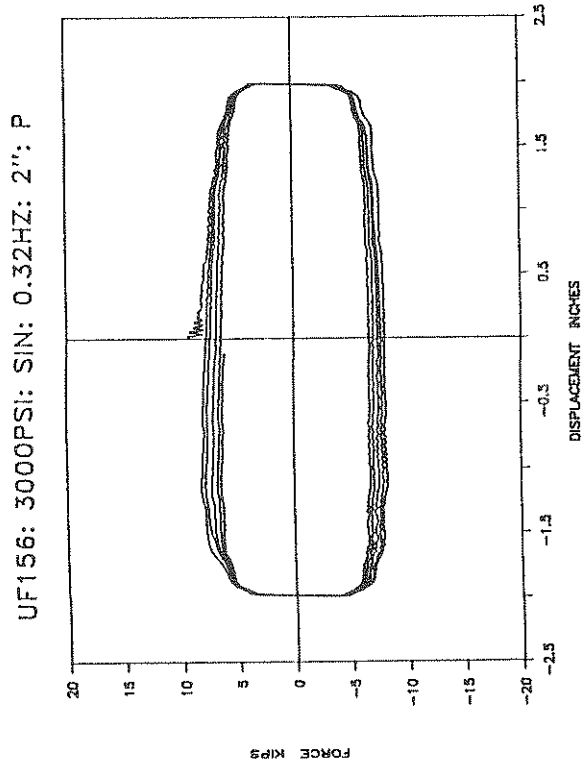
UF156: 3000PSI: SIN: 0.32HZ: 2": P
FORCE KIPS
DISPLACEMENT INCHES

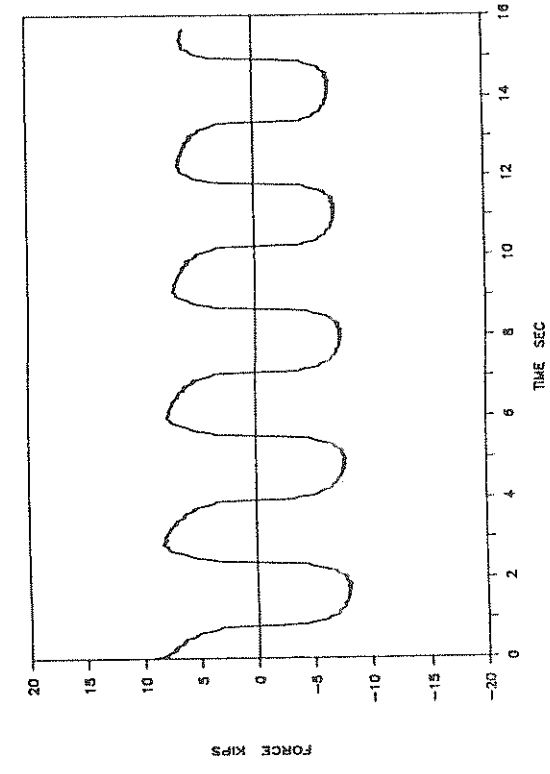
UF156: 3000PSI: SIN: 0.32HZ: 2": P
FORCE KIPS
TIME SEC

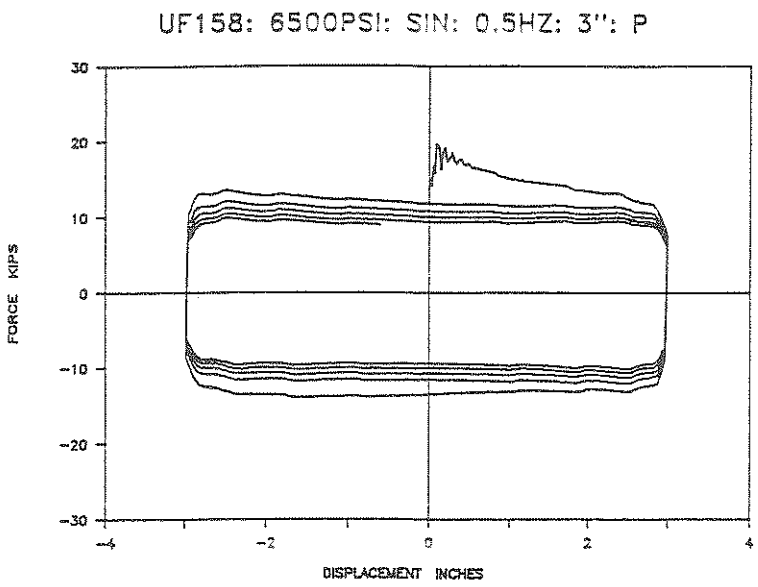
UF158: 6500PSI: SIN: 0.5HZ: 3": P
FORCE KIPS
DISPLACEMENT INCHES

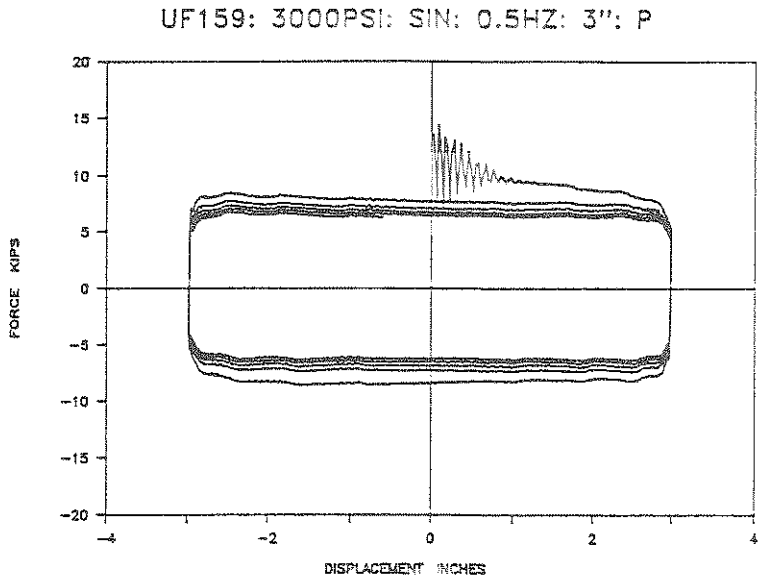
UF159: 3000PSI: SIN: 0.5HZ: 3": P
FORCE KIPS
DISPLACEMENT INCHES

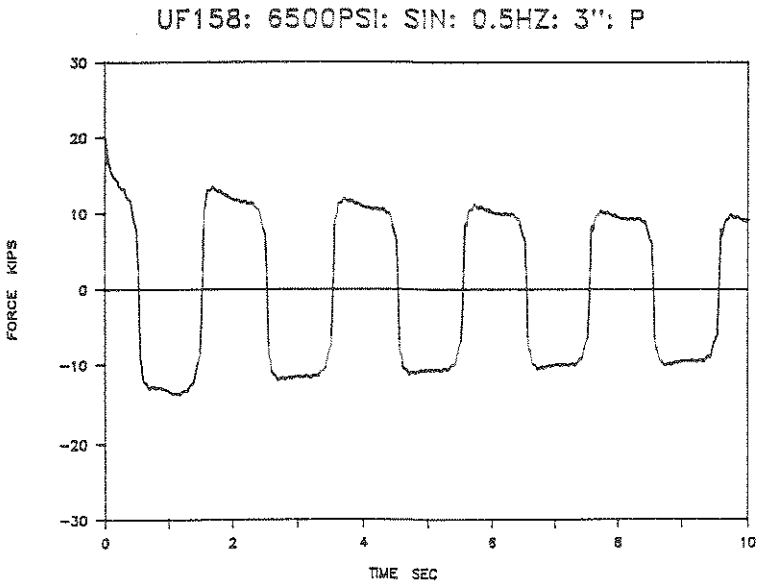
UF158: 6500PSI: SIN: 0.5HZ: 3": P
FORCE KIPS
TIME SEC

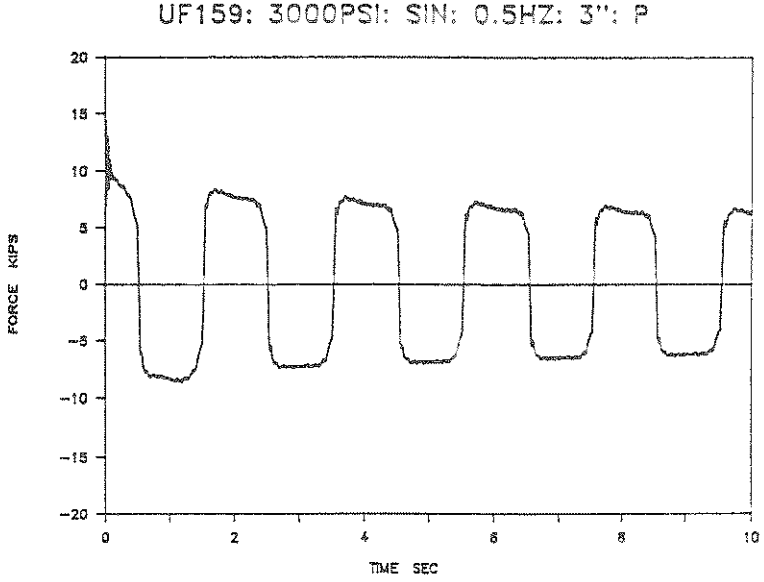
UF159: 3000PSI: SIN: 0.5HZ: 3": P
FORCE KIPS
TIME SEC

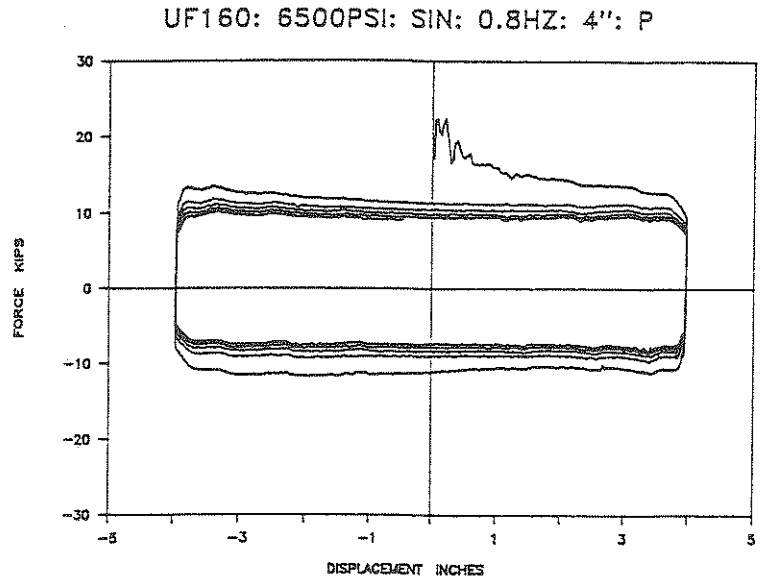
UF160: 6500PSI: SIN: 0.8HZ: 4": P
FORCE KIPS
DISPLACEMENT INCHES

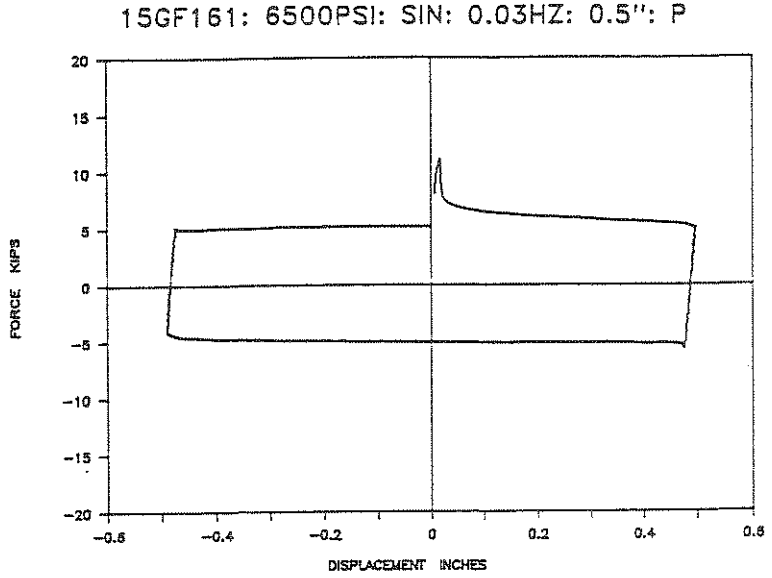
15GF161: 6500PSI: SIN: 0.03HZ: 0.5": P
FORCE KIPS
DISPLACEMENT INCHES

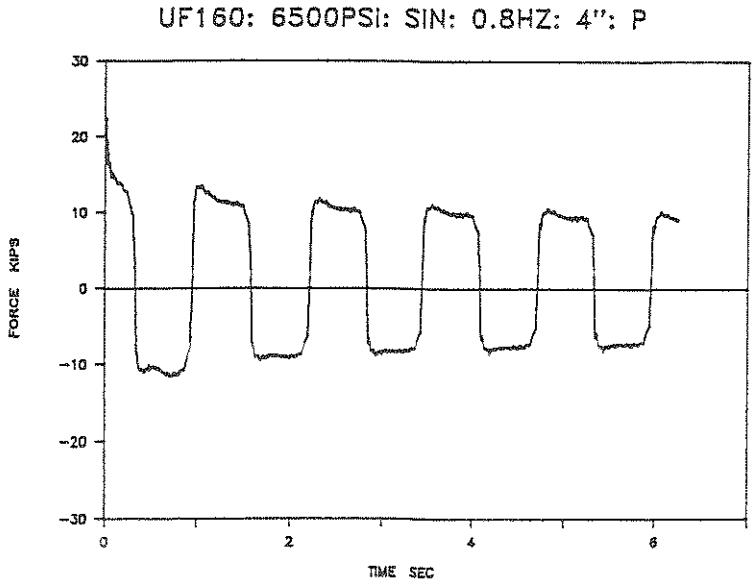
UF160: 6500PSI: SIN: 0.8HZ: 4": P
FORCE KIPS
TIME SEC

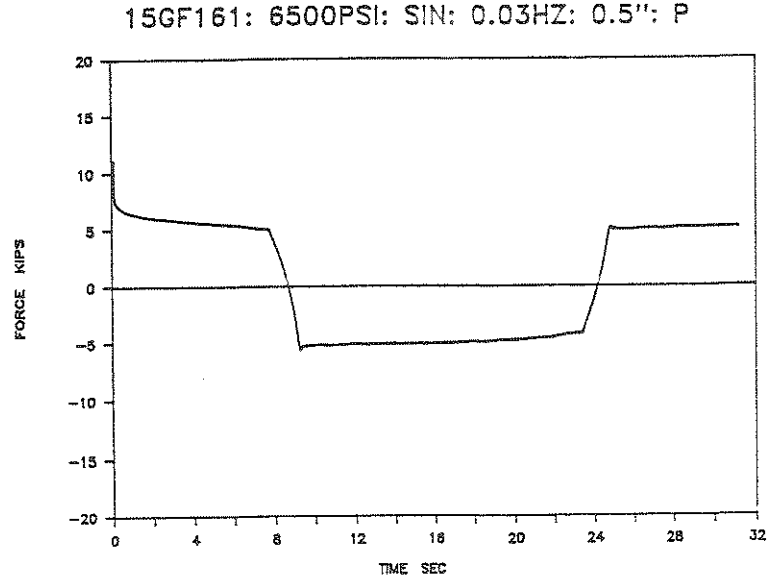
15GF161: 6500PSI: SIN: 0.03HZ: 0.5": P
FORCE KIPS
TIME SEC

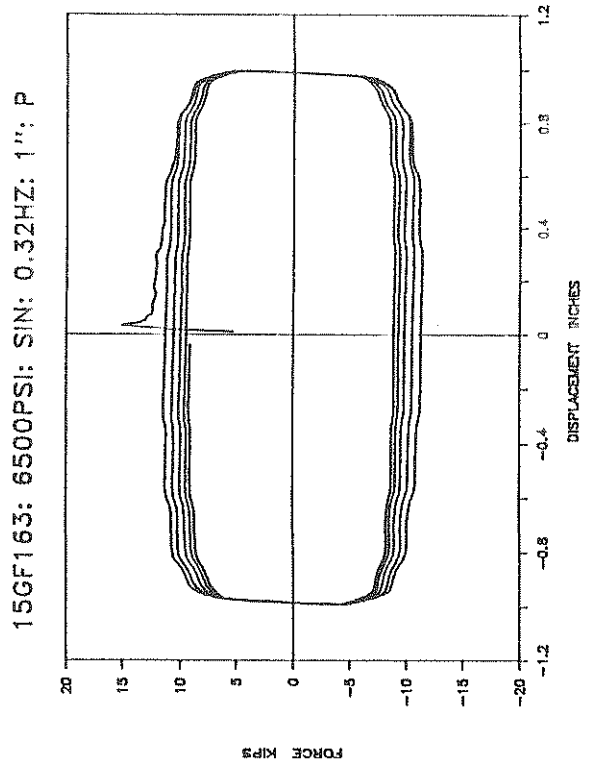
15GF163: 6500PSI: SIN: 0.32HZ: 1": P
FORCE KIPS
DISPLACEMENT INCHES

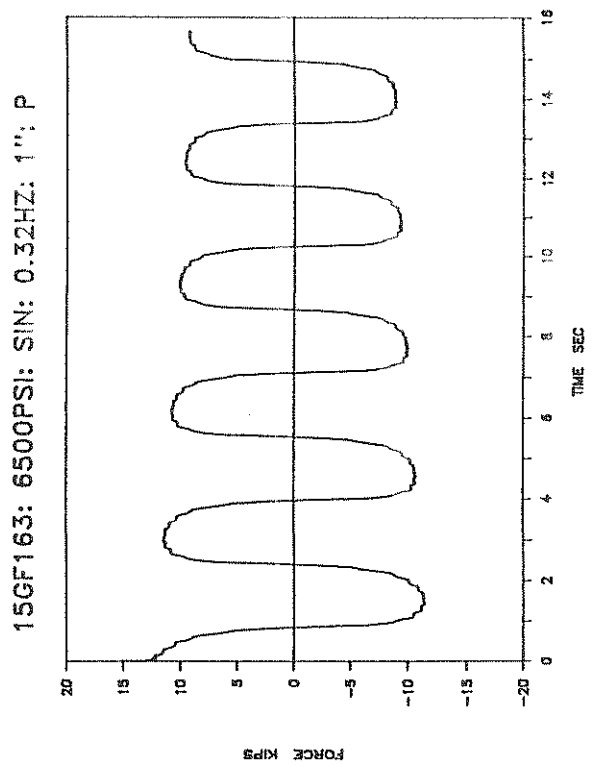
15GF163: 6500PSI: SIN: 0.32HZ: 1": P
FORCE KIPS
TIME SEC

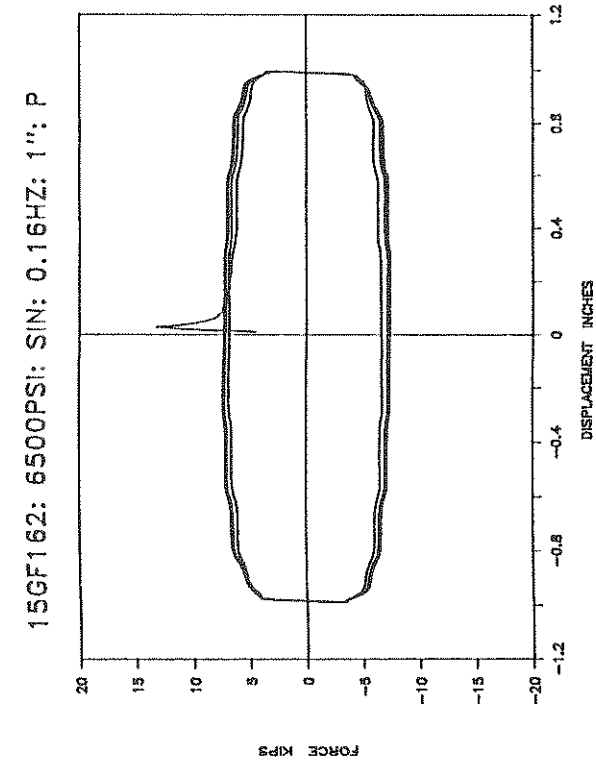
15GF162: 6500PSI: SIN: 0.16HZ: 1": P
FORCE KIPS
DISPLACEMENT INCHES

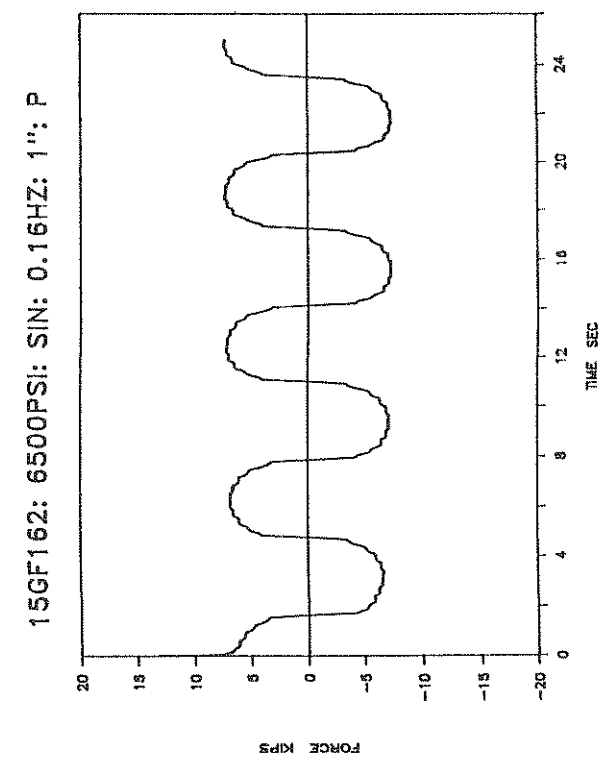
15GF162: 6500PSI: SIN: 0.16HZ: 1": P
FORCE KIPS
TIME SEC

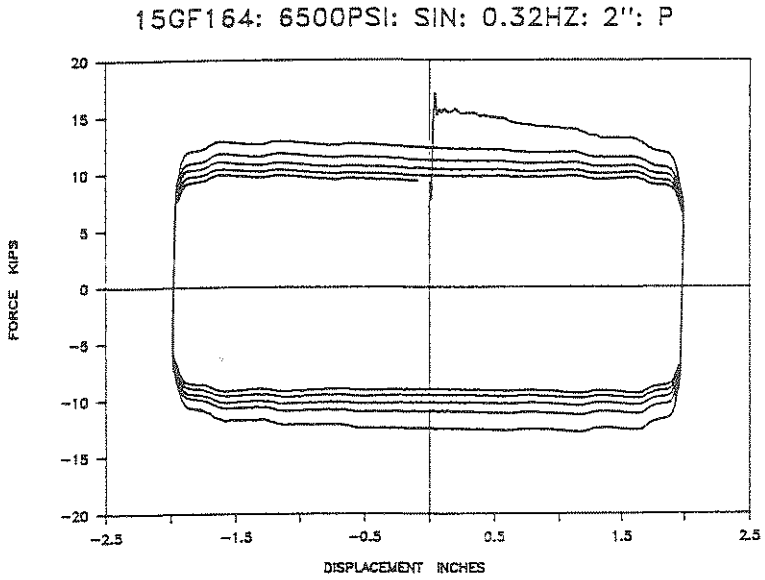
15GF164: 6500PSI: SIN: 0.32HZ: 2": P
FORCE KIPS
DISPLACEMENT INCHES

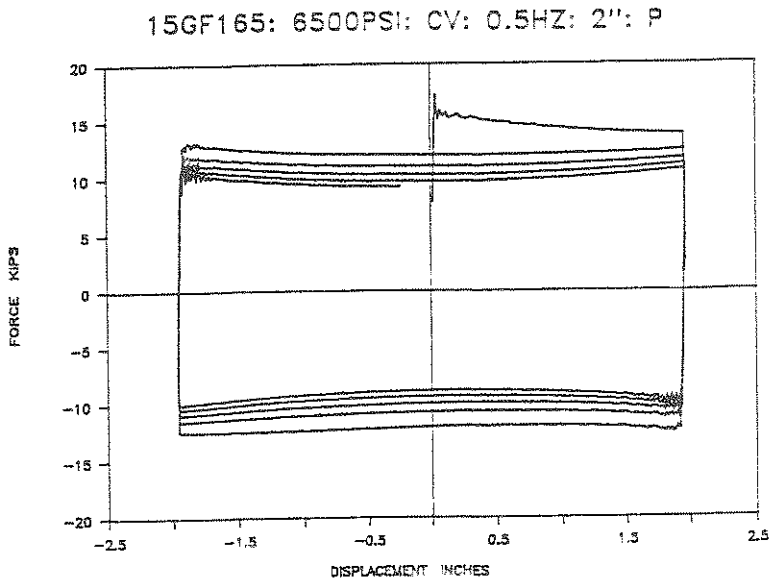
15GF165: 6500PSI: CV: 0.5HZ: 2": P
FORCE KIPS
DISPLACEMENT INCHES

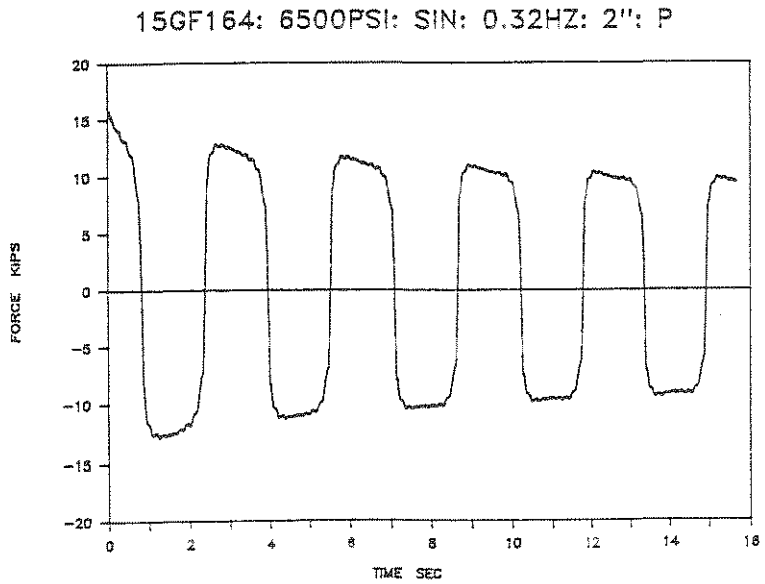
15GF164: 6500PSI: SIN: 0.32HZ: 2": P
FORCE KIPS
TIME SEC

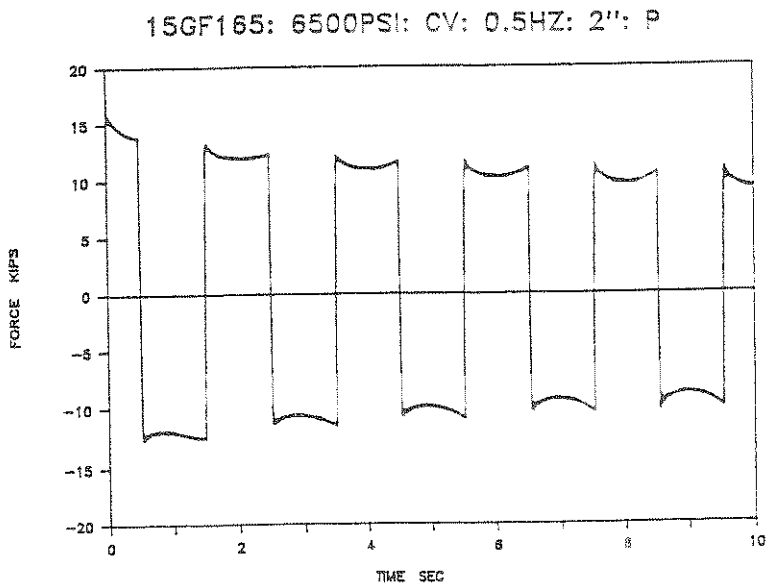
15GF165: 6500PSI: CV: 0.5HZ: 2": P
FORCE KIPS
TIME SEC

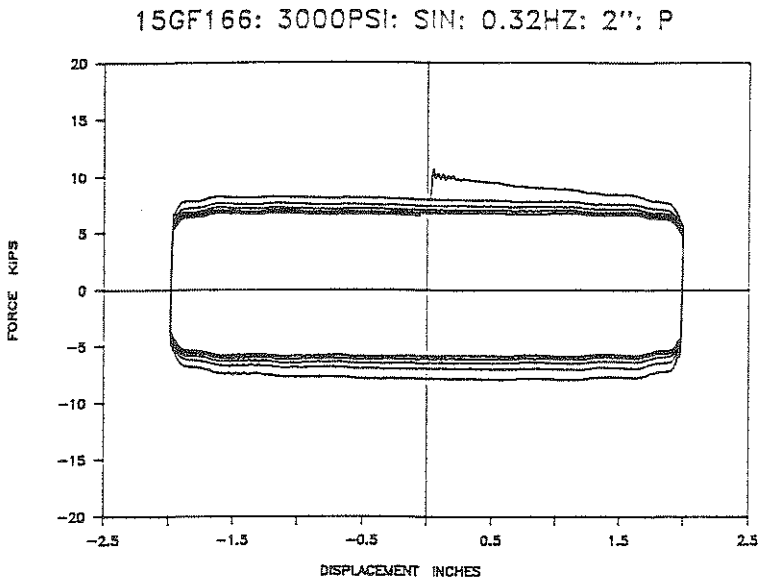
15GF166: 3000PSI: SIN: 0.32HZ: 2": P
FORCE KIPS
DISPLACEMENT INCHES

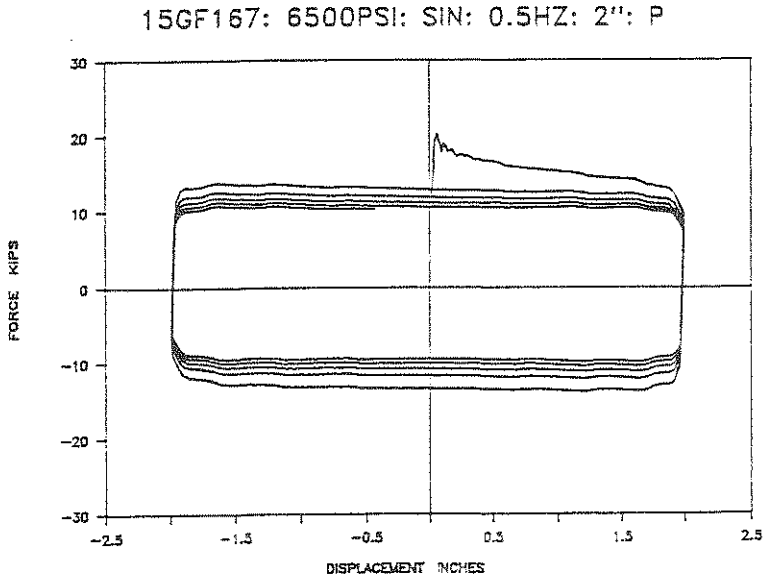
15GF167: 6500PSI: SIN: 0.5HZ: 2": P
FORCE KIPS
DISPLACEMENT INCHES

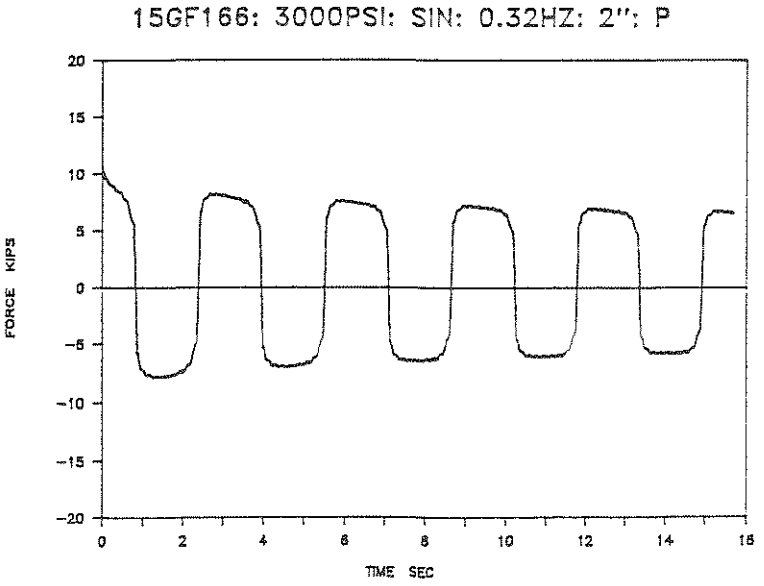
15GF166: 3000PSI: SIN: 0.32HZ: 2": P
FORCE KIPS
TIME SEC

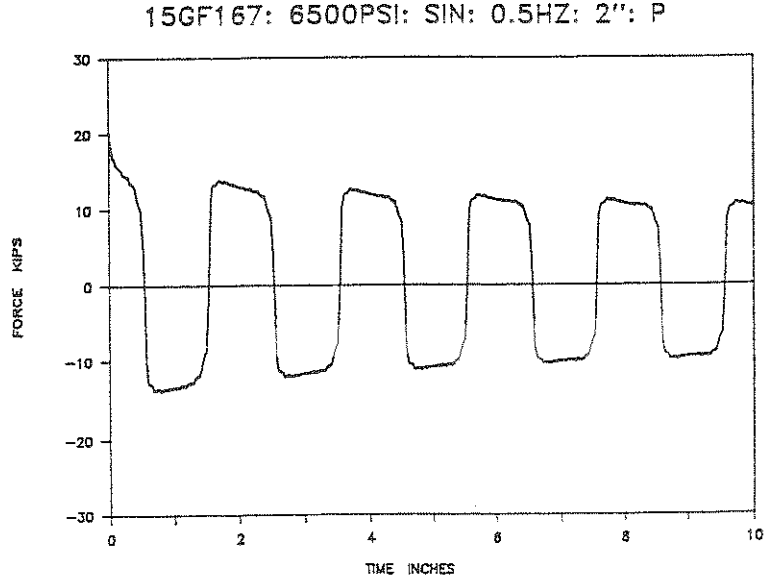
15GF167: 6500PSI: SIN: 0.5HZ: 2": P
FORCE KIPS
TIME INCHES

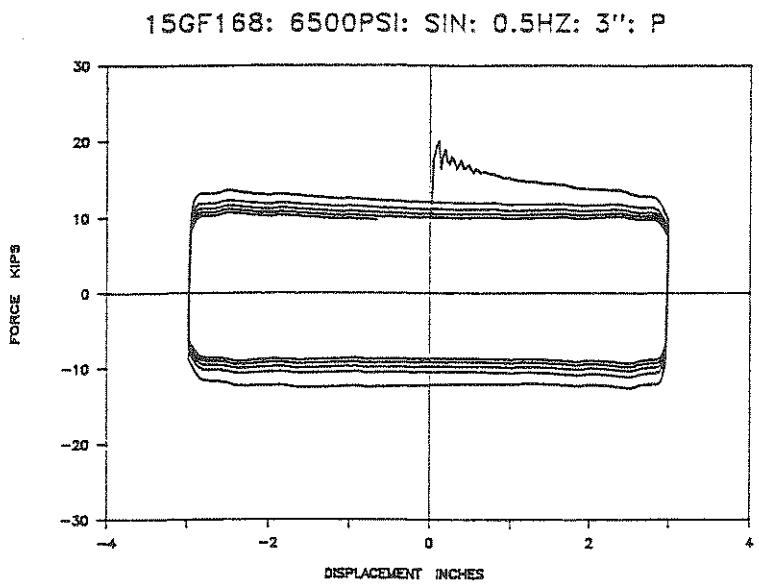
15GF168: 6500PSI: SIN: 0.5HZ: 3": P
FORCE KIPS
DISPLACEMENT INCHES

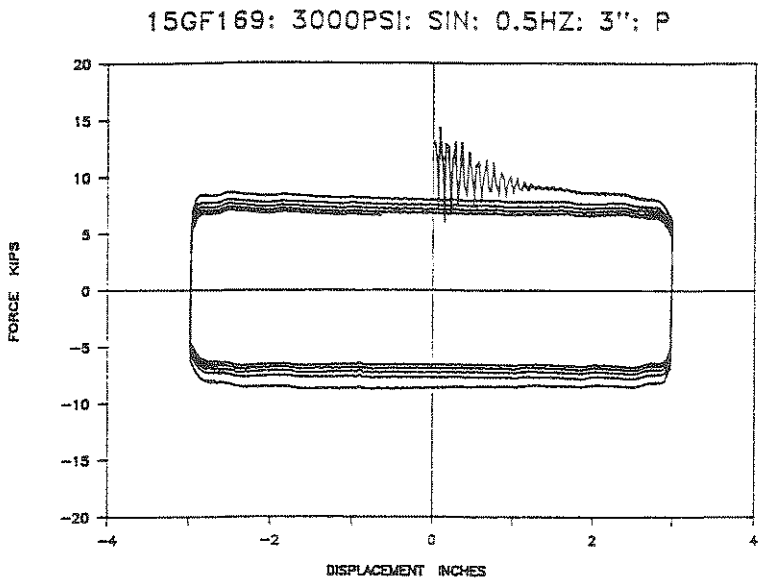
15GF169: 3000PSI: SIN: 0.5HZ: 3": P
FORCE KIPS
DISPLACEMENT INCHES

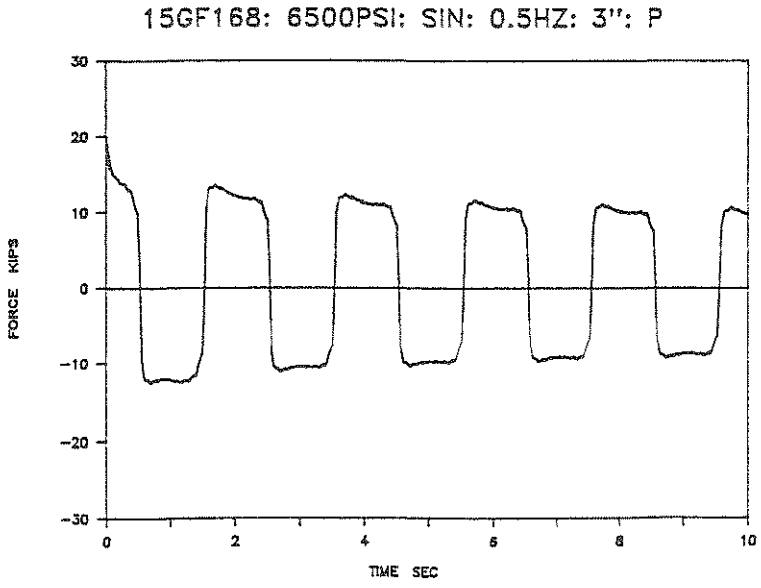
15GF168: 6500PSI: SIN: 0.5HZ: 3": P
FORCE KIPS
TIME SEC

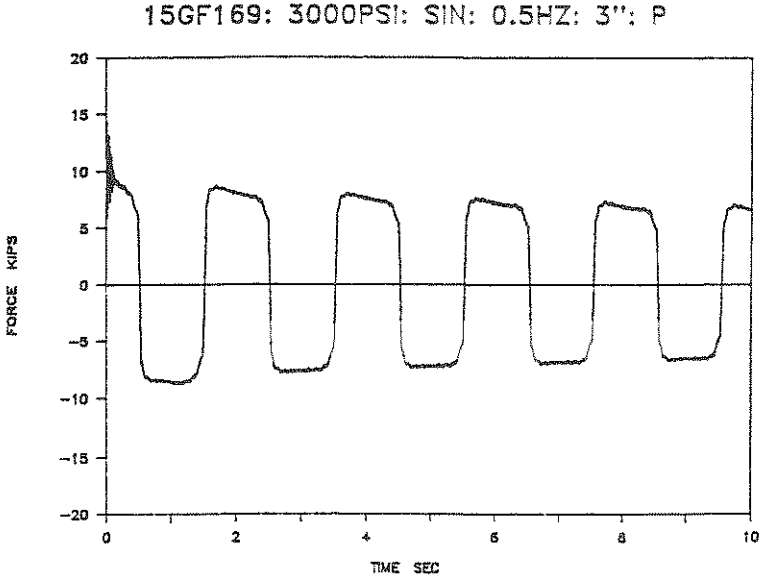
15GF169: 3000PSI: SIN: 0.5HZ: 3": P
FORCE KIPS
TIME SEC

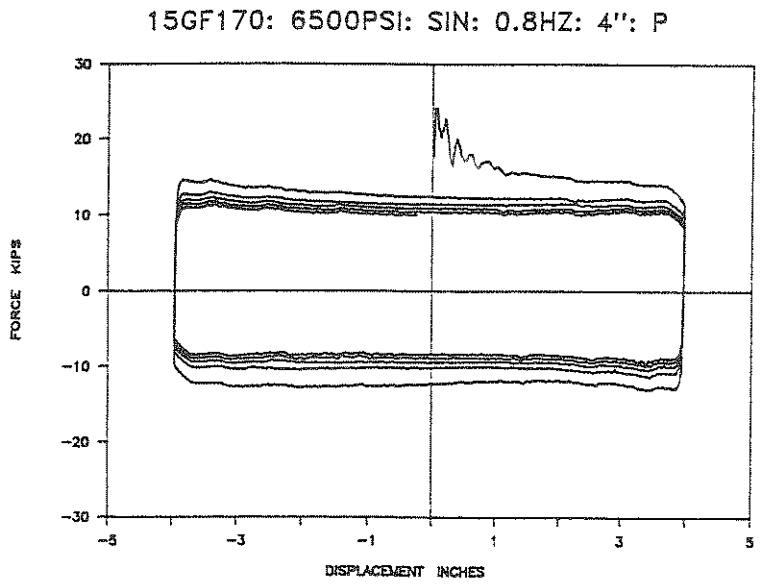
15GF170: 6500PSI: SIN: 0.8HZ: 4": P
FORCE KIPS
DISPLACEMENT INCHES

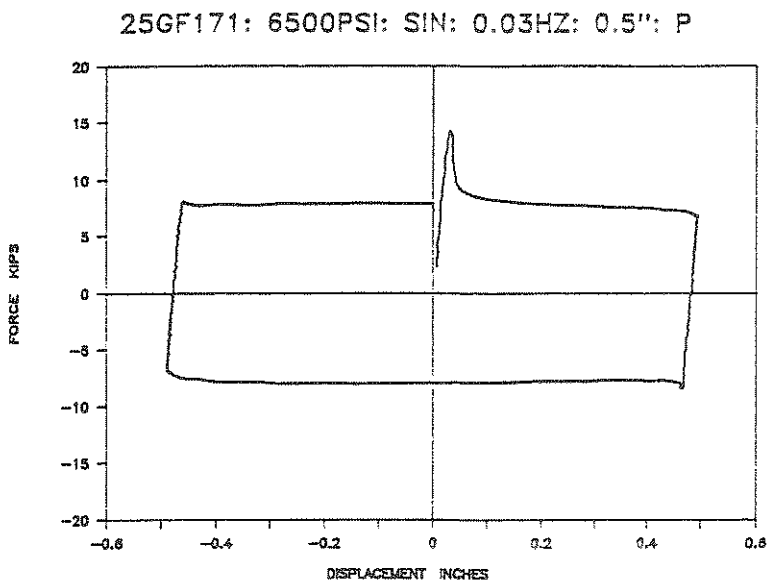
25GF171: 6500PSI: SIN: 0.03HZ: 0.5": P
FORCE KIPS
DISPLACEMENT INCHES

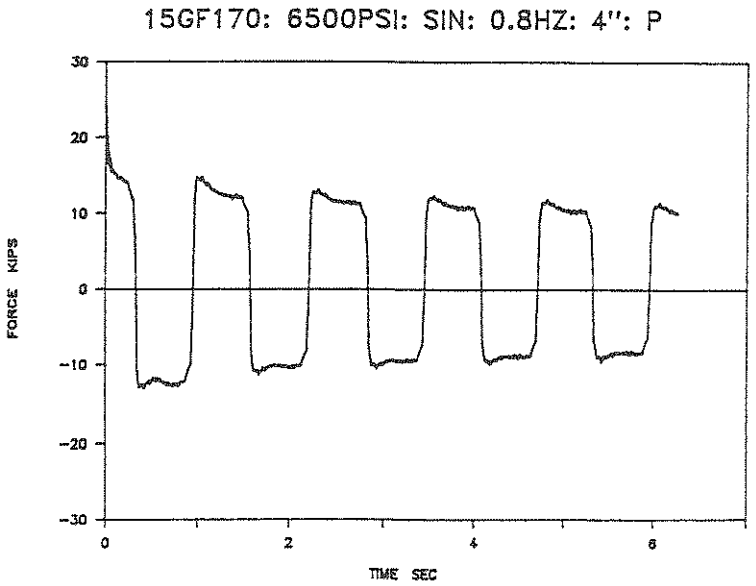
15GF170: 6500PSI: SIN: 0.8HZ: 4": P
FORCE KIPS
TIME SEC

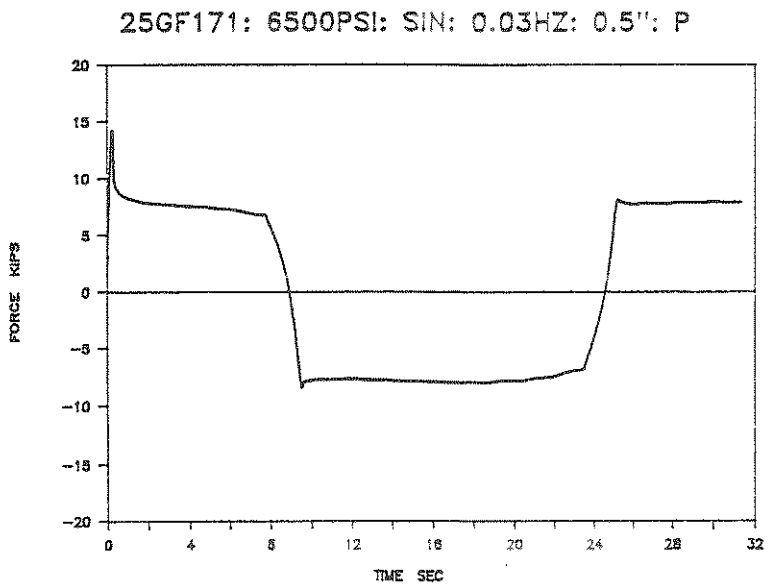
25GF171: 6500PSI: SIN: 0.03HZ: 0.5": P
FORCE KIPS
TIME SEC

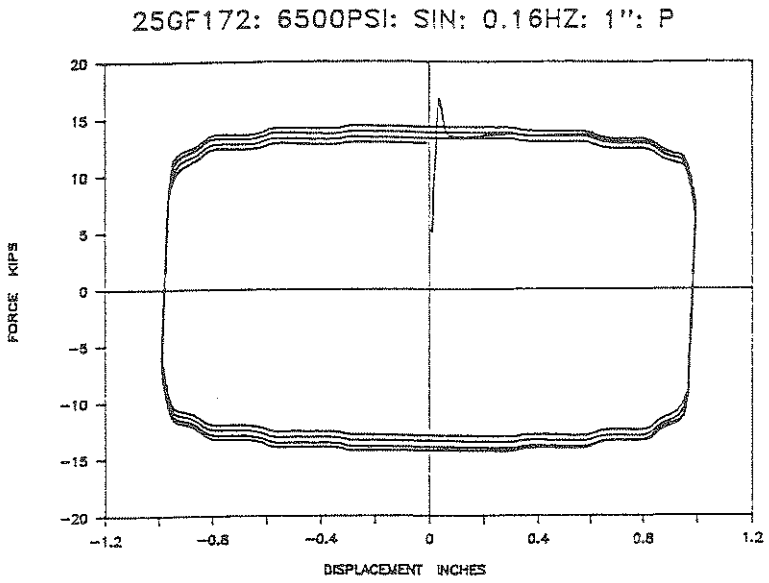
25GF172: 6500PSI: SIN: 0.16HZ: 1": P
FORCE KIPS
DISPLACEMENT INCHES

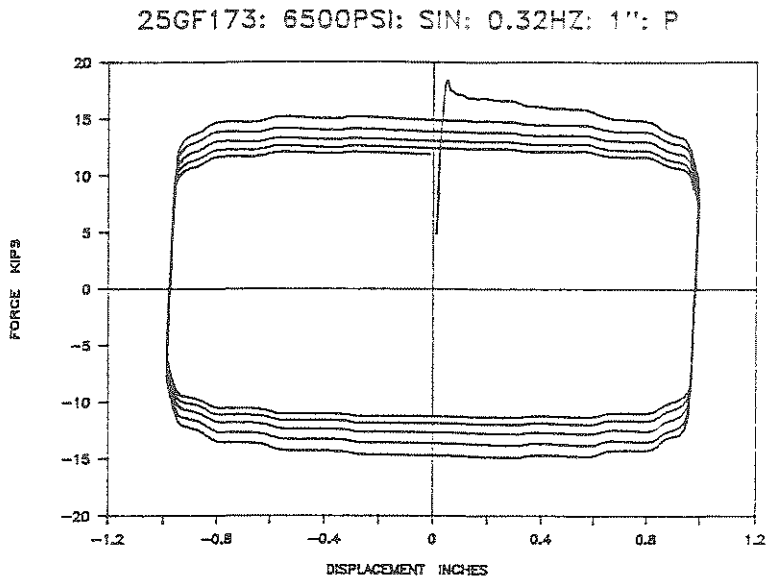
25GF173: 6500PSI: SIN: 0.32HZ: 1": P
FORCE KIPS
DISPLACEMENT INCHES

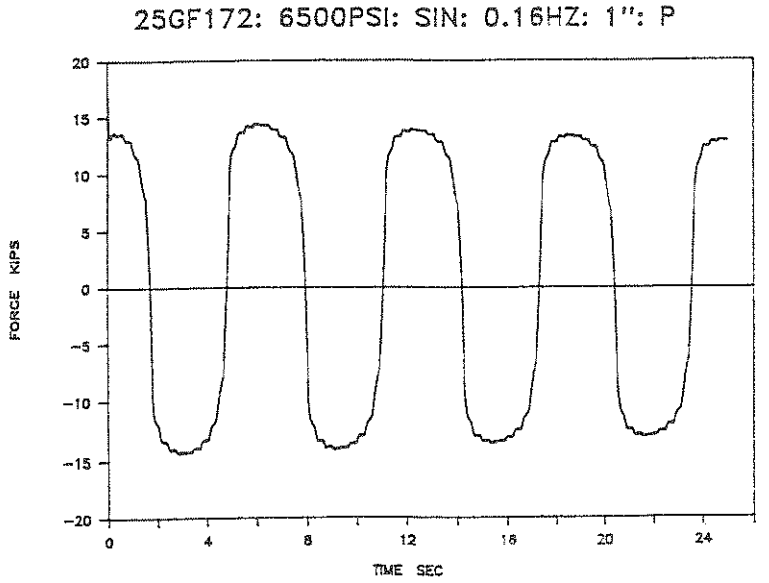
25GF172: 6500PSI: SIN: 0.16HZ: 1": P
FORCE KIPS
TIME SEC

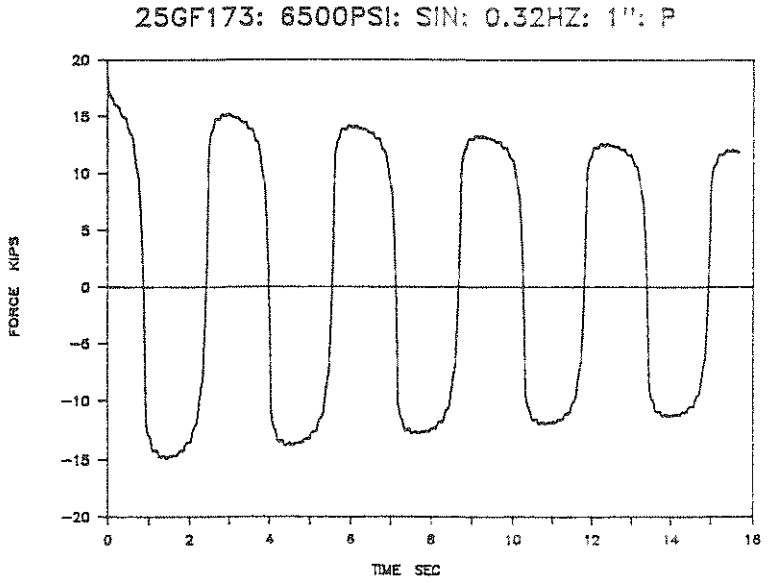
25GF173: 6500PSI: SIN: 0.32HZ: 1": P
FORCE KIPS
TIME SEC

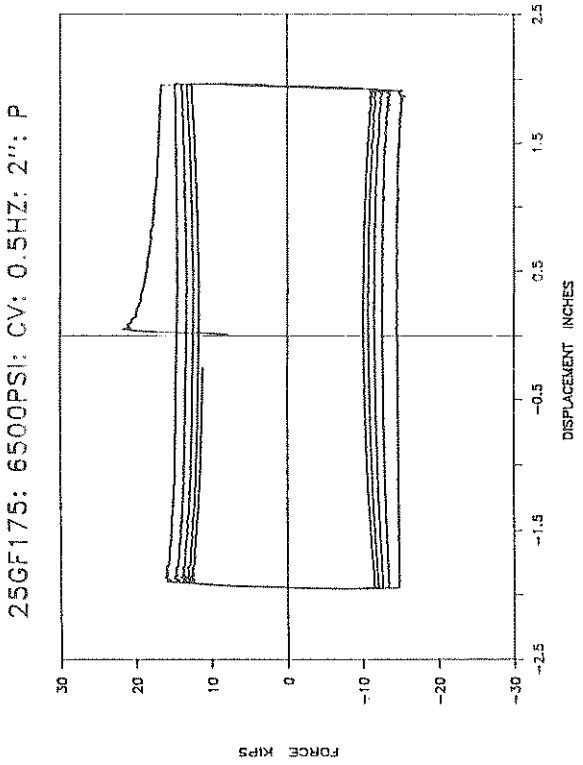
25GF175: 6500PSI: CV: 0.5HZ: 2": P
FORCE KIPS
DISPLACEMENT INCHES

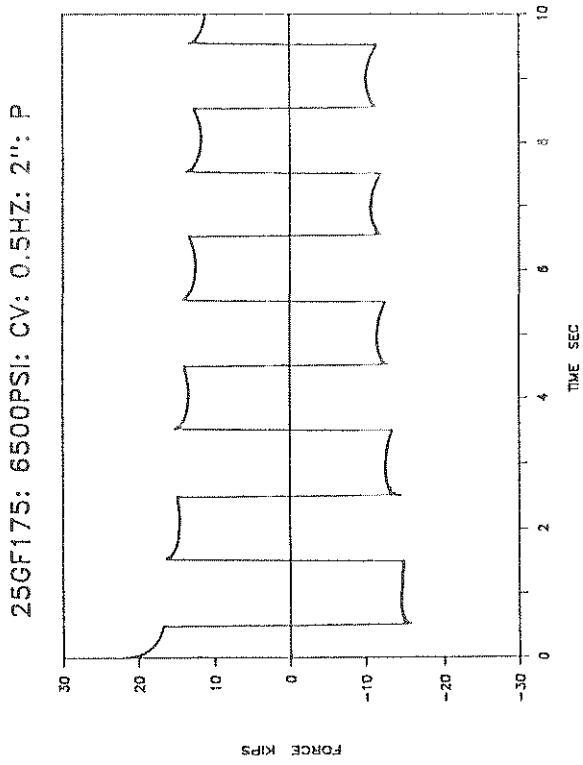
25GF175: 6500PSI: CV: 0.5HZ: 2": P
FORCE KIPS
TIME SEC

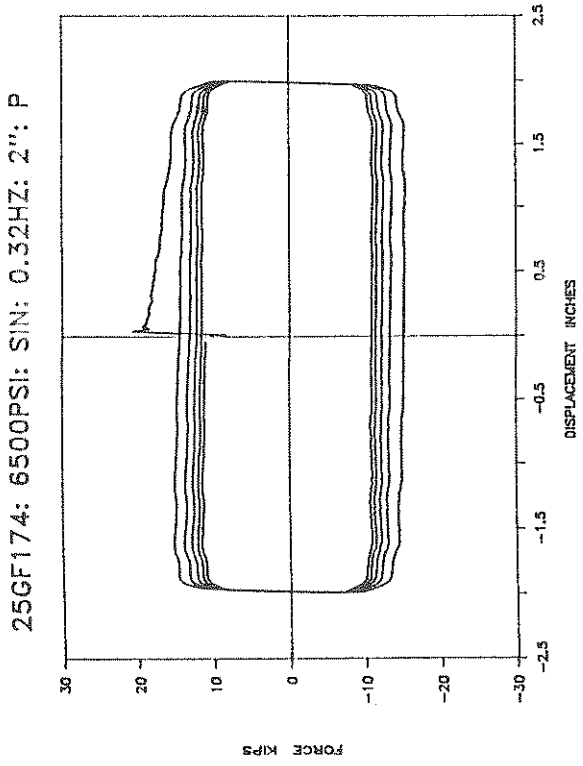
25GF174: 6500PSI: SIN: 0.32HZ: 2": P
FORCE KIPS
DISPLACEMENT INCHES

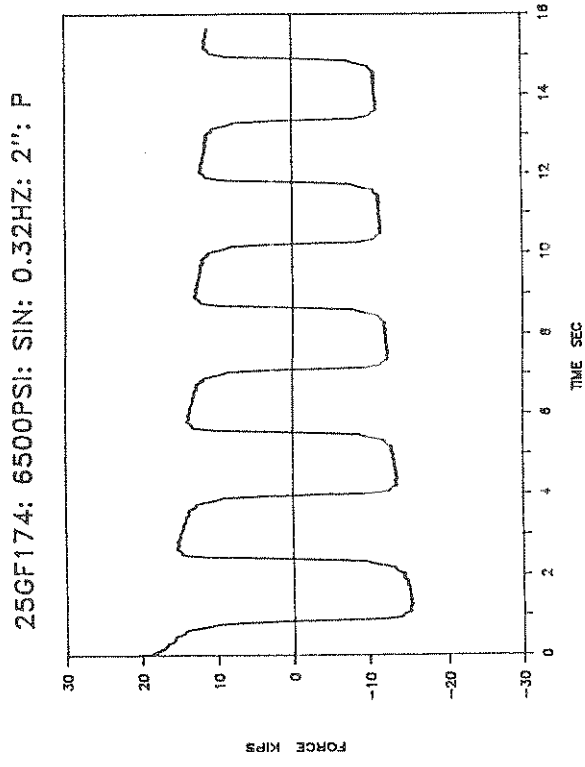
25GF174: 6500PSI: SIN: 0.32HZ: 2": P
FORCE KIPS
TIME SEC

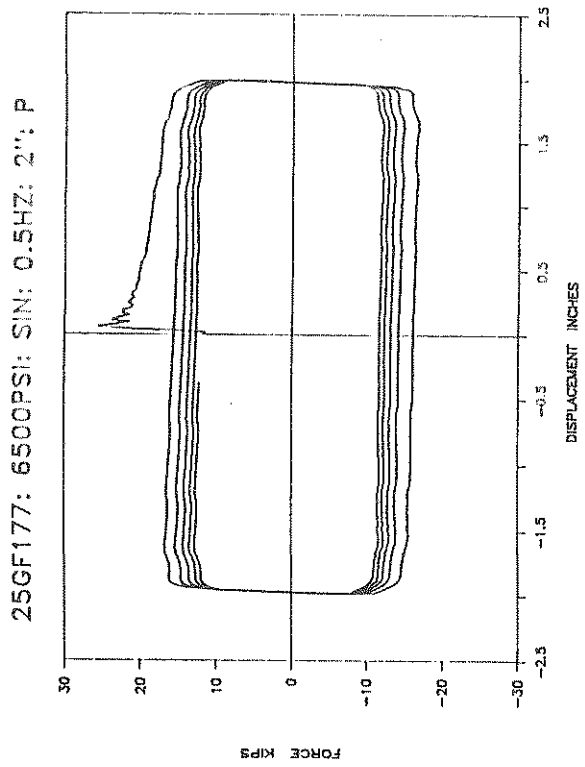
25GF177: 6500PSI: SIN: 0.5HZ: 2": P
FORCE KIPS
DISPLACEMENT INCHES

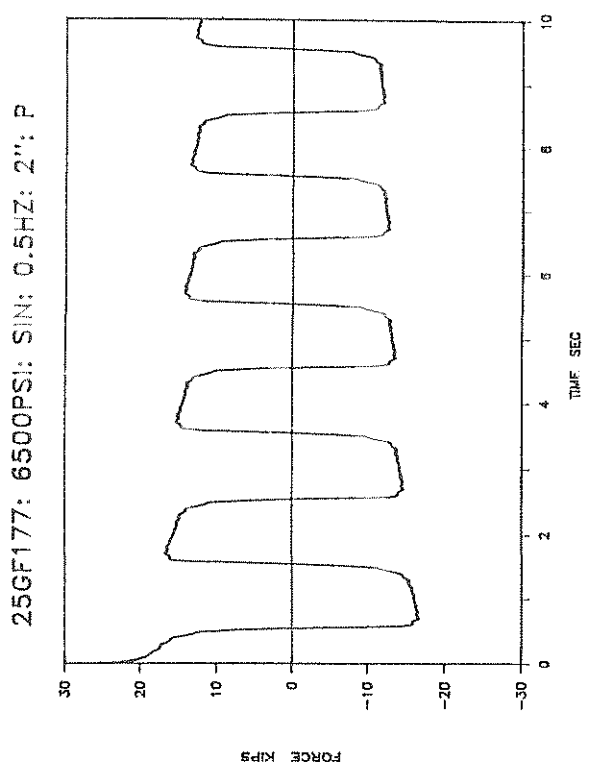
25GF177: 6500PSI: SIN: 0.5HZ: 2": P
FORCE KIPS
TIME SEC

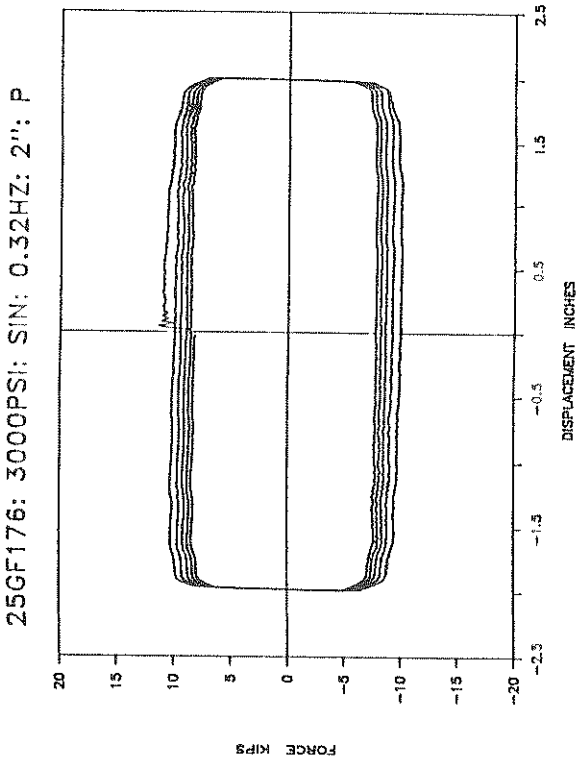
25GF176: 3000PSI: SIN: 0.32HZ: 2": P
FORCE KIPS
DISPLACEMENT INCHES

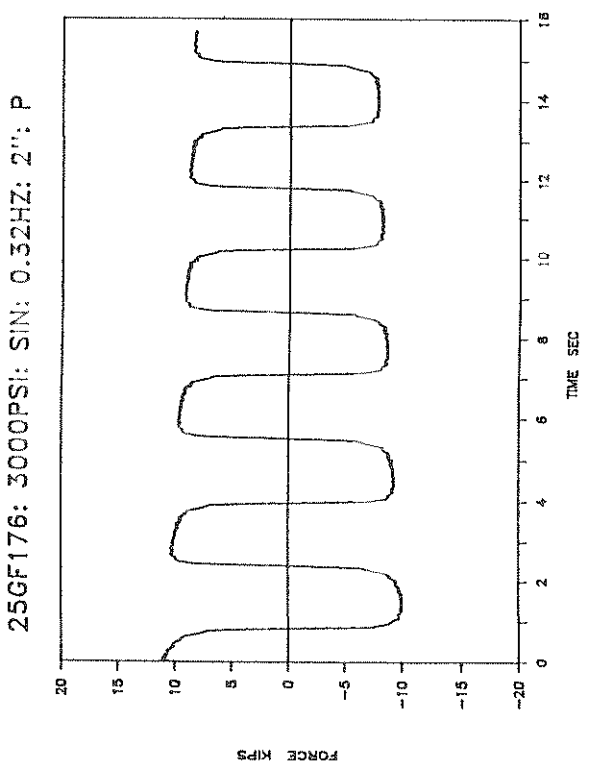
25GF176: 3000PSI: SIN: 0.32HZ: 2": P
FORCE KIPS
TIME SEC

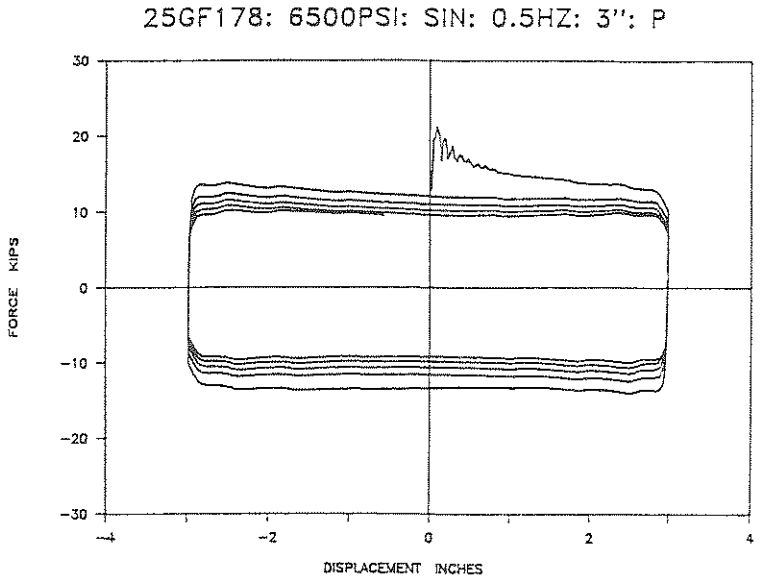
25GF178: 6500PSI: SIN: 0.5HZ: 3": P
FORCE KIPS
DISPLACEMENT INCHES

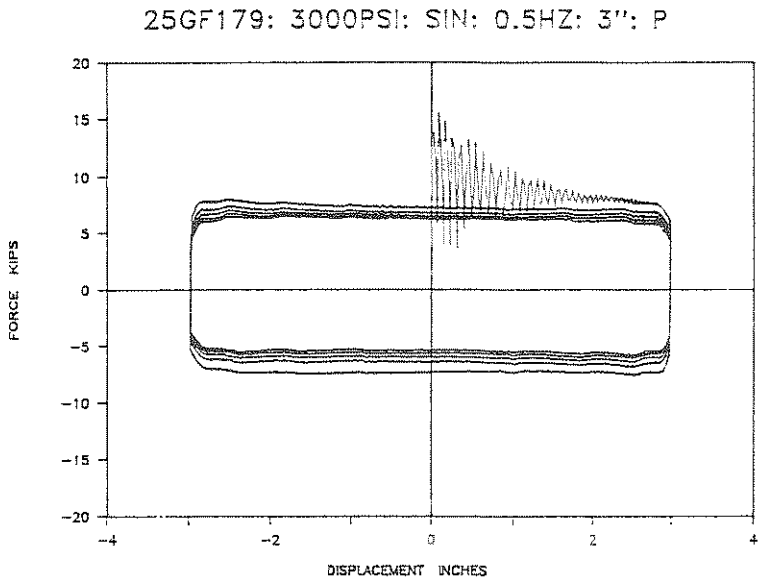
25GF179: 3000PSI: SIN: 0.5HZ: 3": P
FORCE KIPS
DISPLACEMENT INCHES

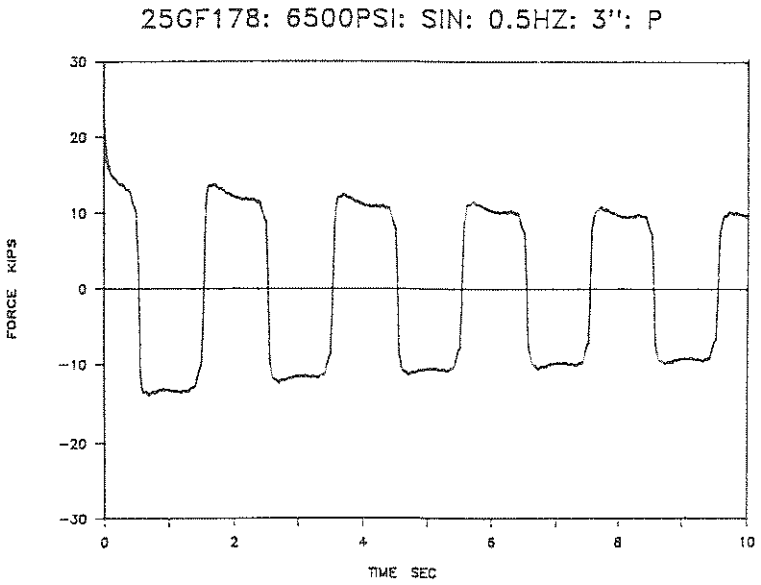
25GF178: 6500PSI: SIN: 0.5HZ: 3": P
FORCE KIPS
TIME SEC

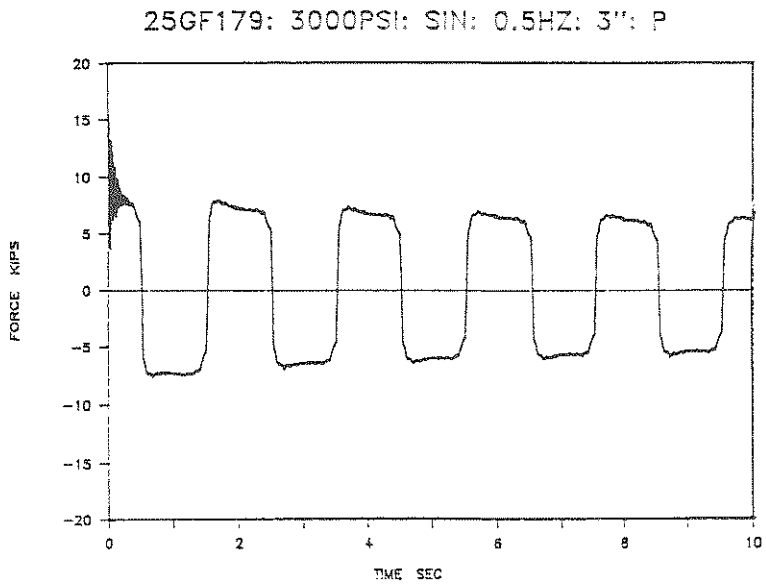
25GF179: 3000PSI: SIN: 0.5HZ: 3": P
FORCE KIPS
TIME SEC

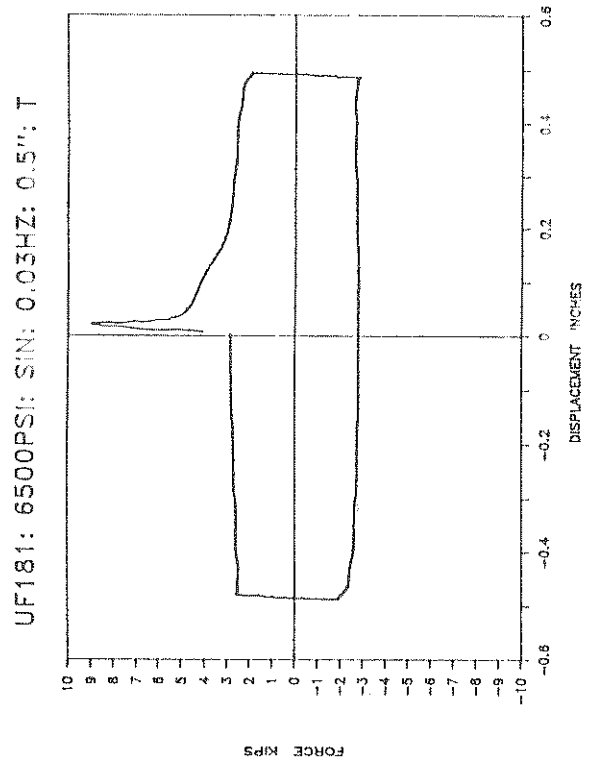
UF181: 6500PSI: SIN: 0.03HZ: 0.5": T
FORCE KIPS
DISPLACEMENT INCHES

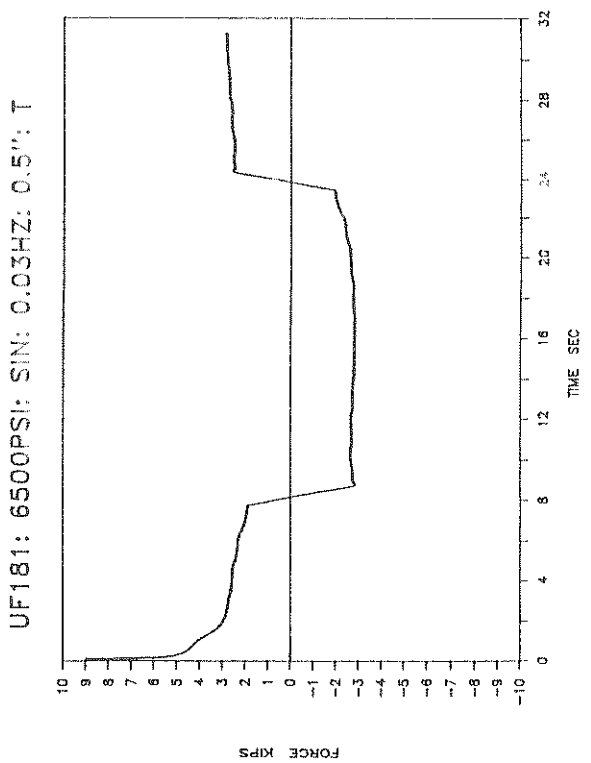
UF181: 6500PSI: SIN: 0.03HZ: 0.5": T
FORCE KIPS
TIME SEC

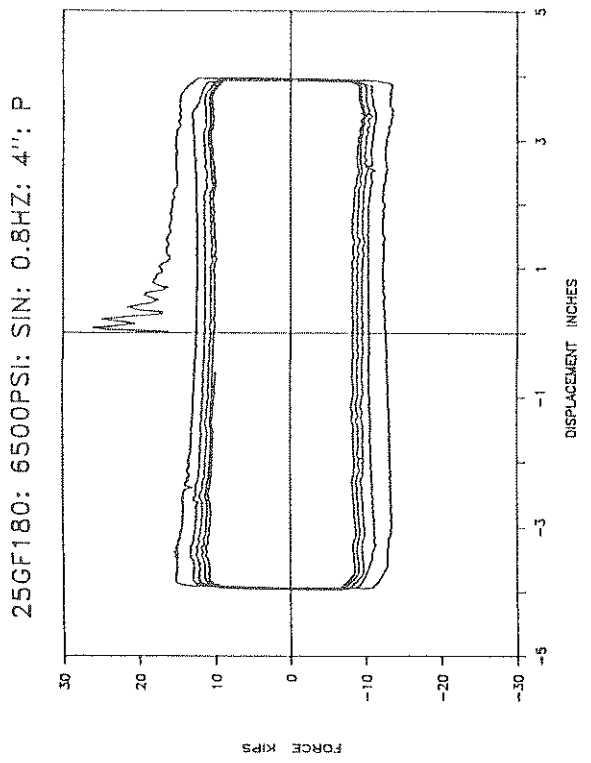
25GF180: 6500PSI: SIN: 0.8HZ: 4": P
FORCE KIPS
DISPLACEMENT INCHES

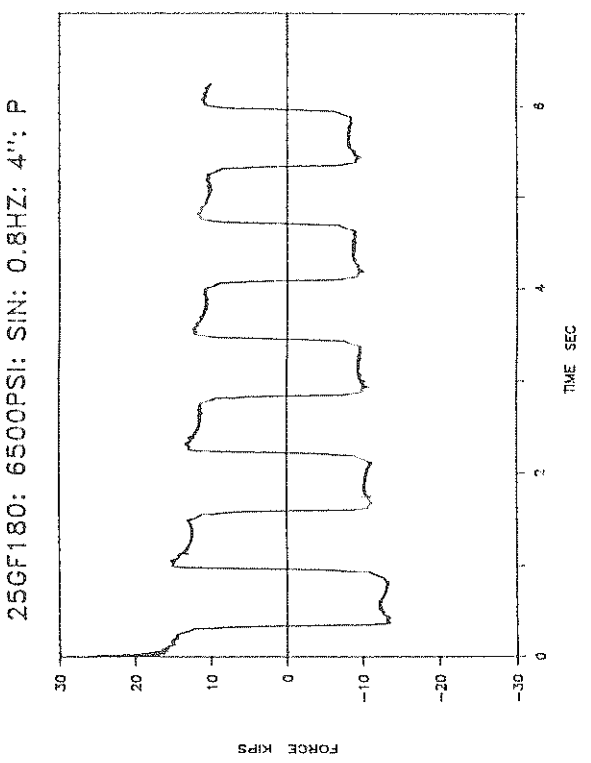
25GF180: 6500PSI: SIN: 0.8HZ: 4": P
FORCE KIPS
TIME SEC

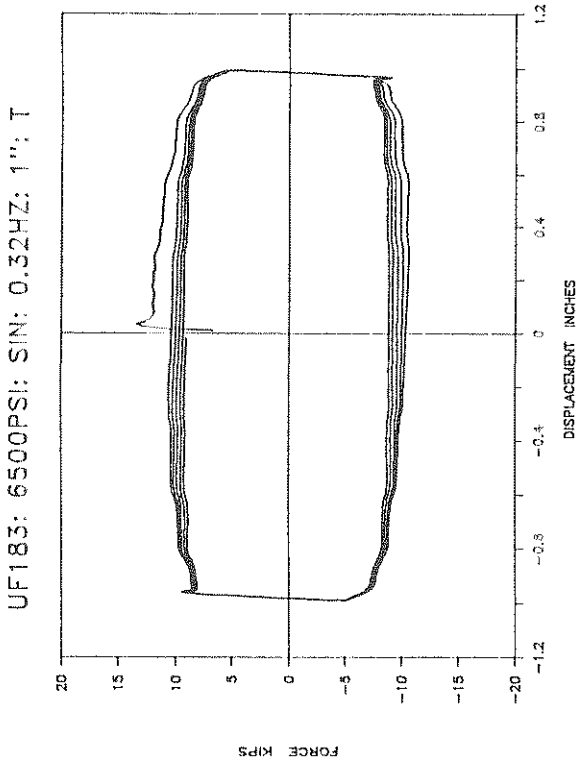
UF183: 6500PSI: SIN: 0.32HZ: 1": T
FORCE KIPS
DISPLACEMENT INCHES

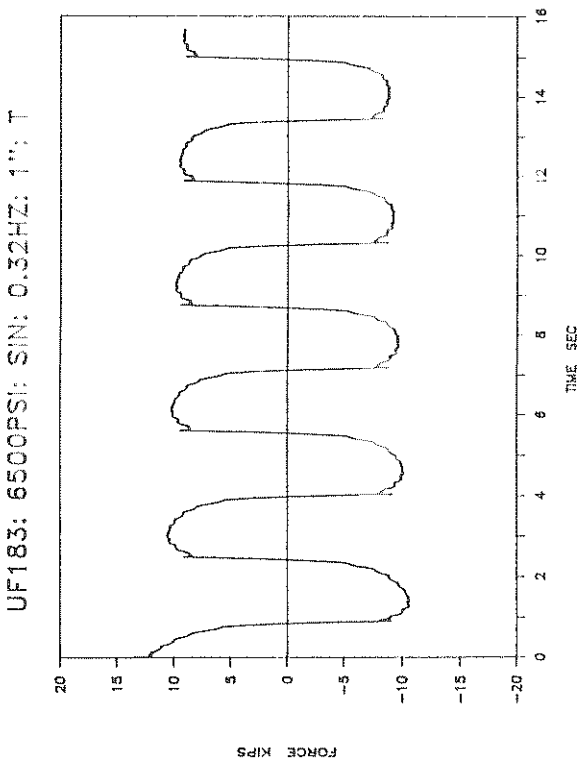
UF183: 6500PSI: SIN: 0.32HZ: 1": T
FORCE KIPS
TIME SEC

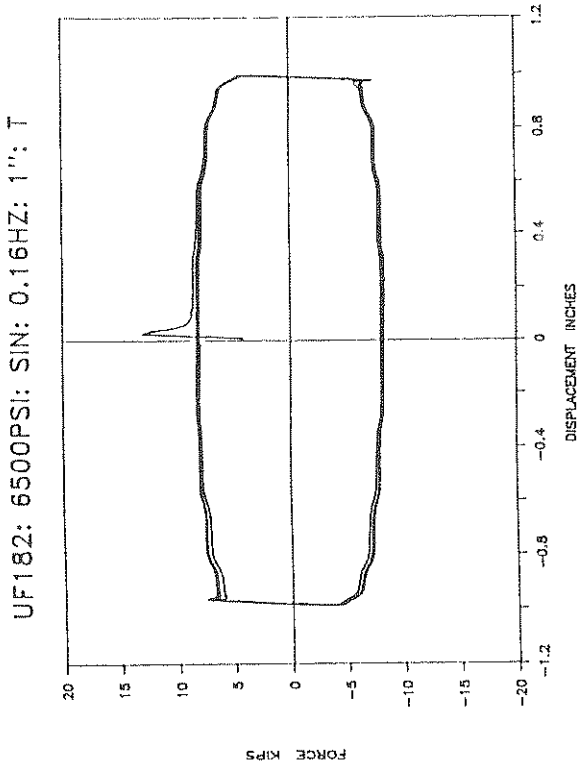
UF182: 6500PSI: SIN: 0.16HZ: 1": T
FORCE KIPS
DISPLACEMENT INCHES

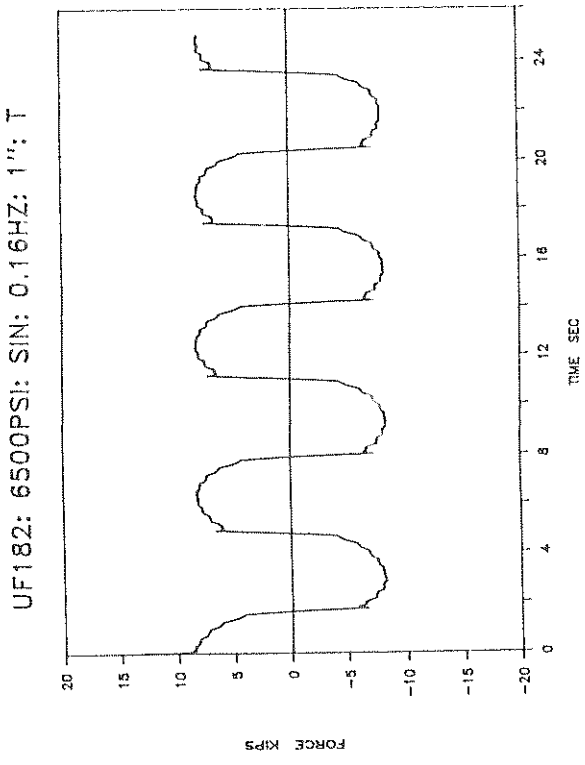
UF182: 6500PSI: SIN: 0.16HZ: 1": T
FORCE KIPS
TIME SEC

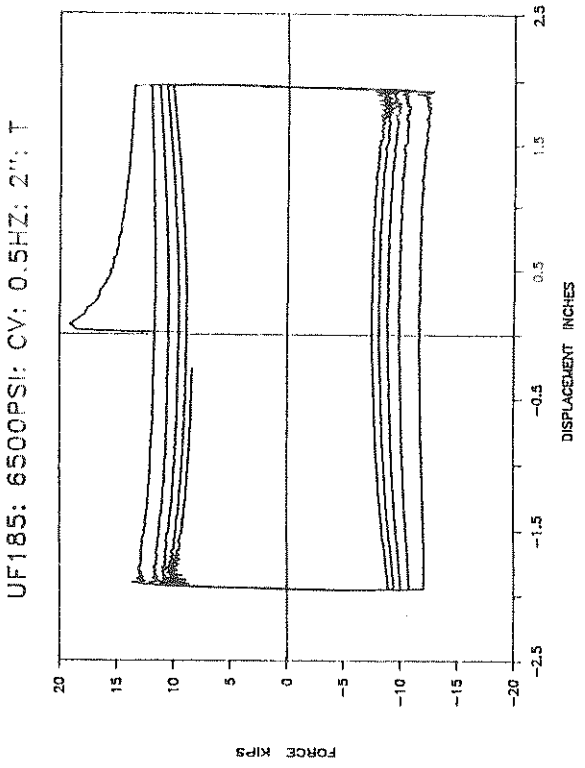
UF185: 6500PSI: CV: 0.5HZ: 2": T
FORCE KIPS
DISPLACEMENT INCHES

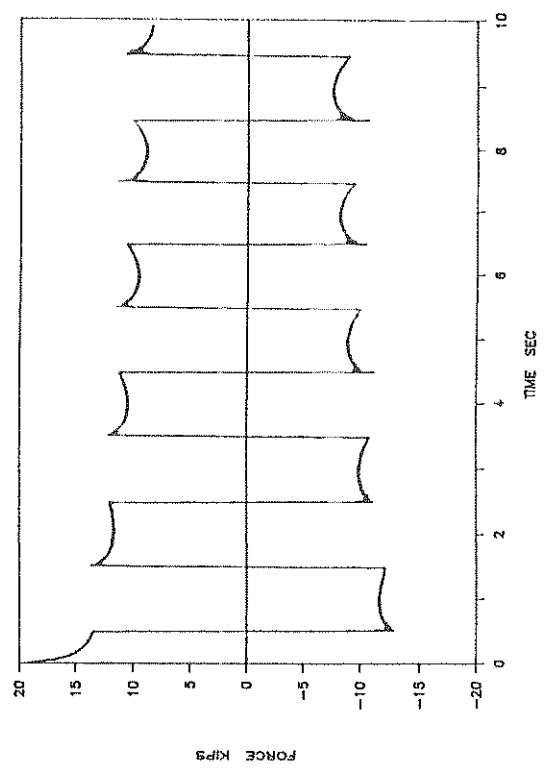
UF185: 6500PSI: CV: 0.5HZ: 2": T
FORCE KIPS
TIME SEC

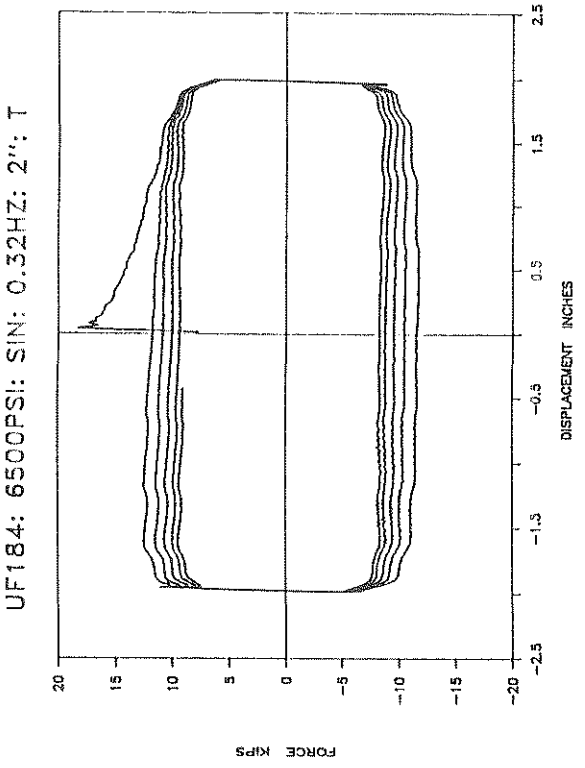
UF184: 6500PSI: SIN: 0.32HZ: 2": T
FORCE KIPS
DISPLACEMENT INCHES

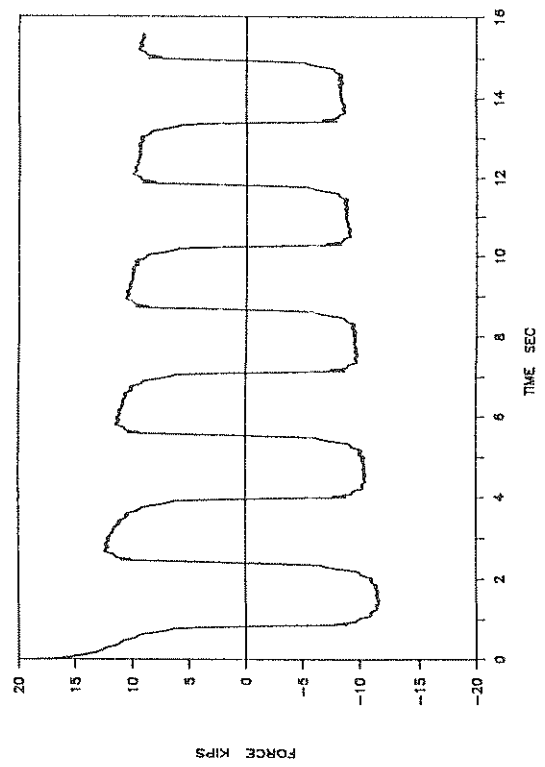
UF184: 6500PSI: SIN: 0.32HZ: 2": T
FORCE KIPS
TIME SEC

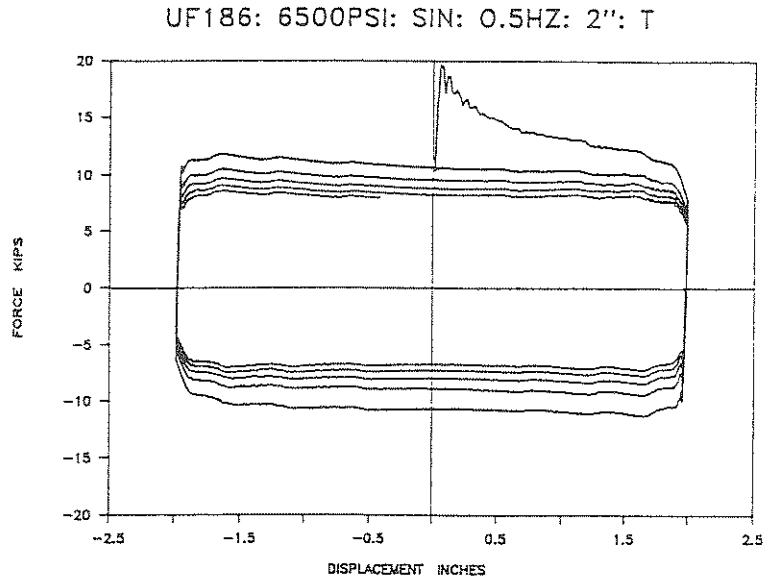
UF186: 6500PSI: SIN: 0.5HZ: 2": T
FORCE KIPS
DISPLACEMENT INCHES

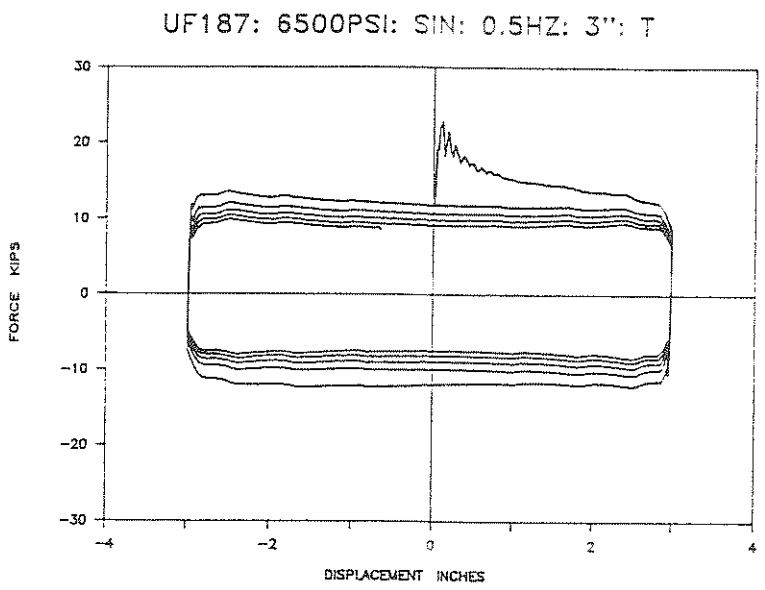
UF187: 6500PSI: SIN: 0.5HZ: 3": T
FORCE KIPS
DISPLACEMENT INCHES

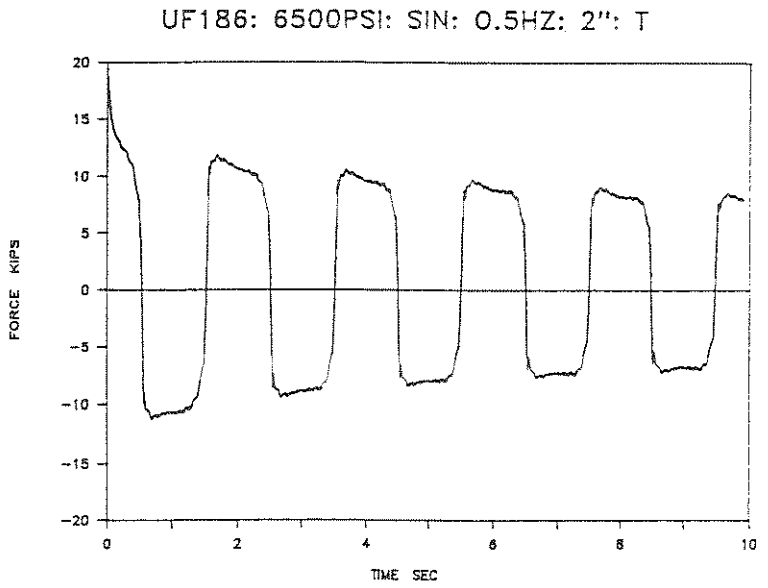
UF186: 6500PSI: SIN: 0.5HZ: 2": T
FORCE KIPS
TIME SEC

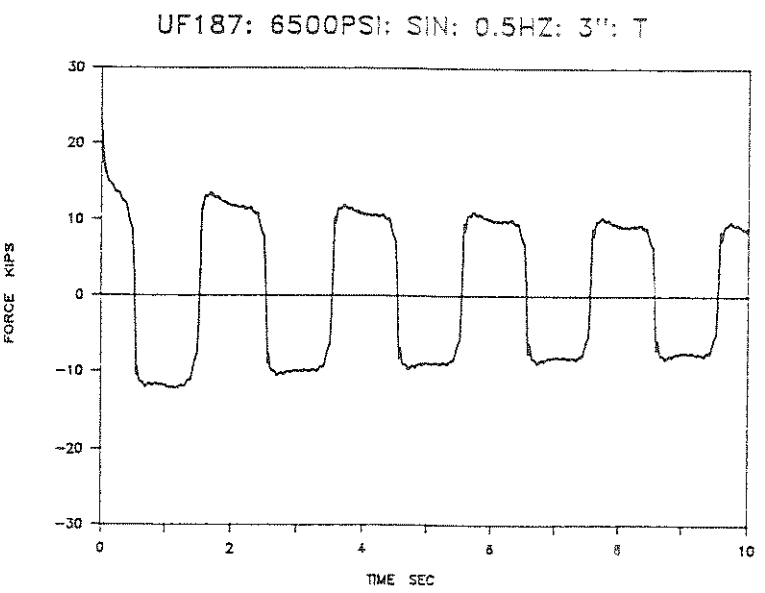
UF187: 6500PSI: SIN: 0.5HZ: 3": T
FORCE KIPS
TIME SEC

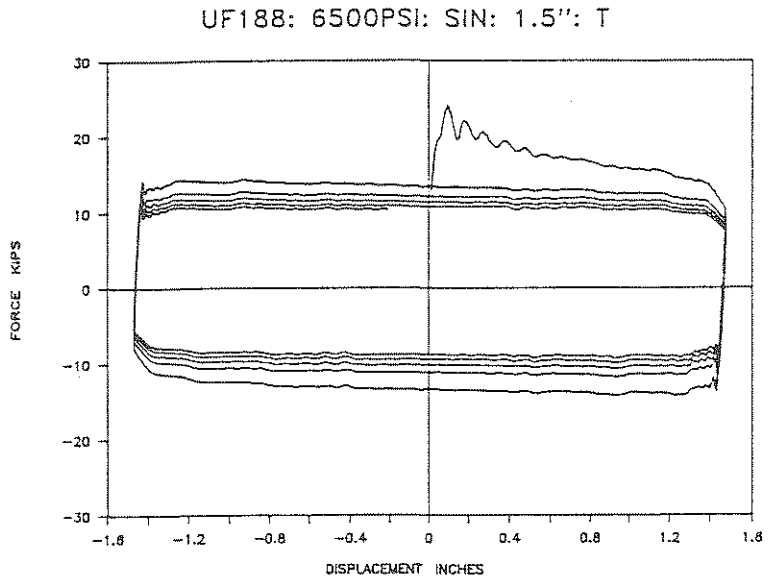
UF188: 6500PSI: SIN: 1.5": T
FORCE KIPS
DISPLACEMENT INCHES

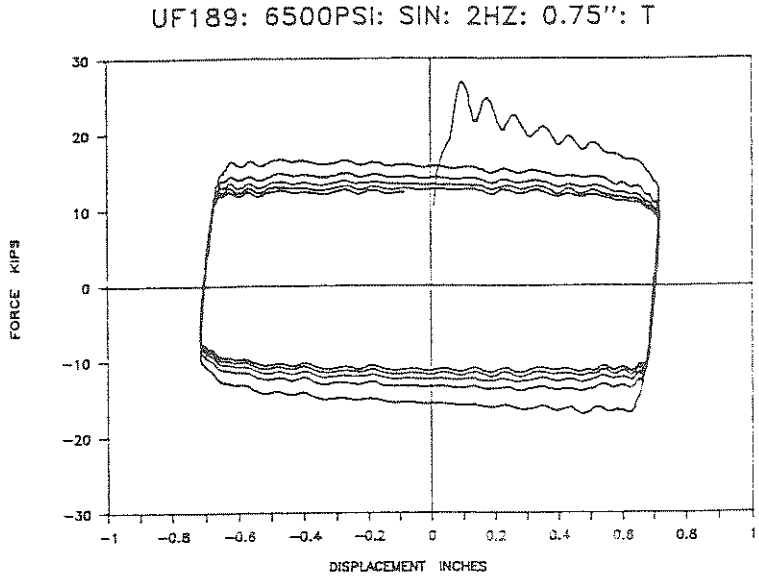
UF189: 6500PSI: SIN: 2HZ: 0.75": T
FORCE KIPS
DISPLACEMENT INCHES

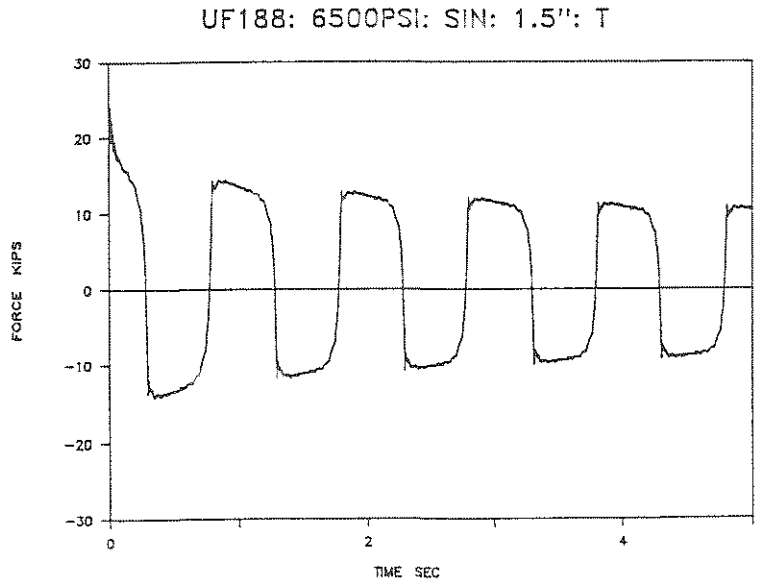
UF188: 6500PSI: SIN: 1.5": T
FORCE KIPS
TIME SEC

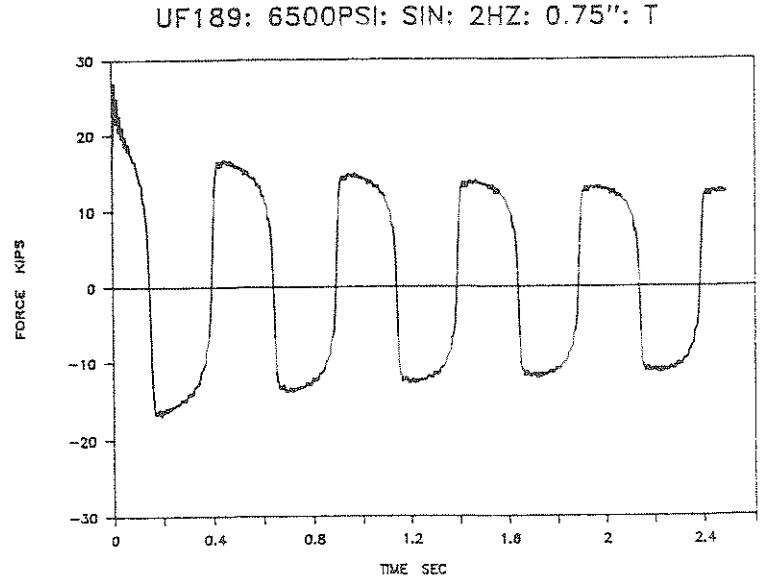
UF189: 6500PSI: SIN: 2HZ: 0.75": T
FORCE KIPS
TIME SEC

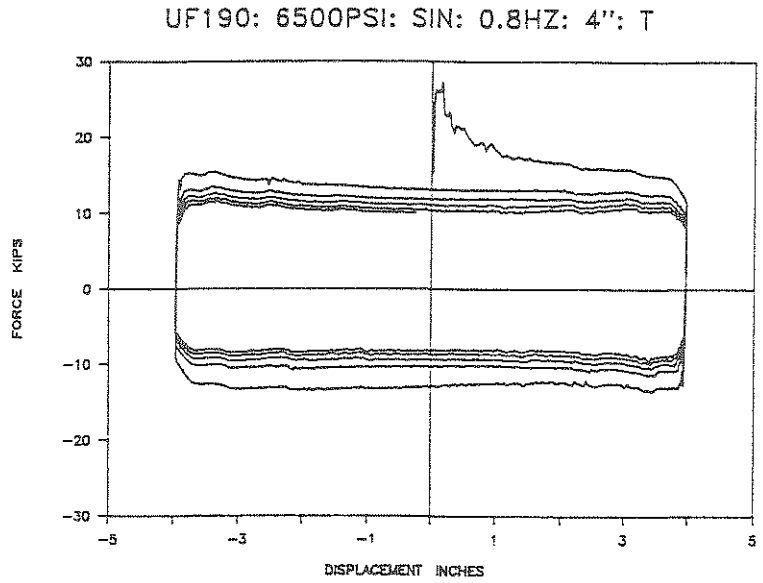
UF190: 6500PSI: SIN: 0.8HZ: 4": T
FORCE KIPS
DISPLACEMENT INCHES

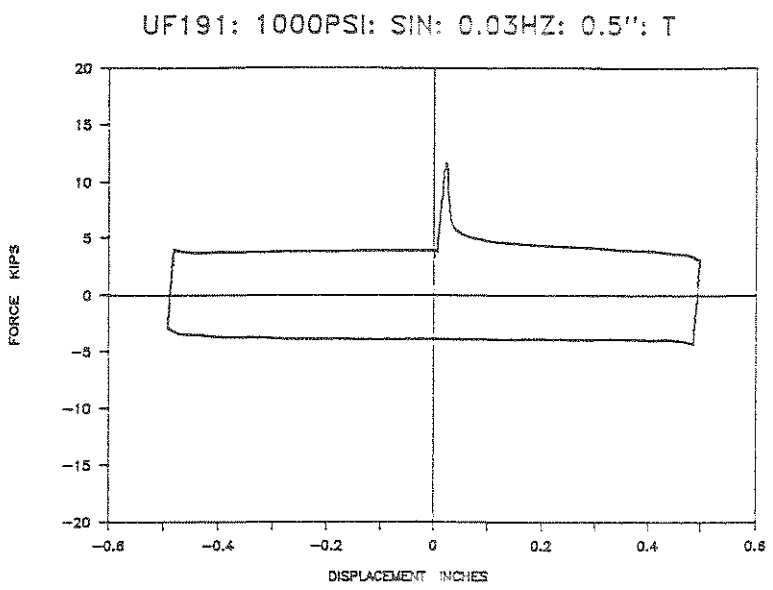
UF191: 1000PSI: SIN: 0.03HZ: 0.5": T
FORCE KIPS
DISPLACEMENT INCHES

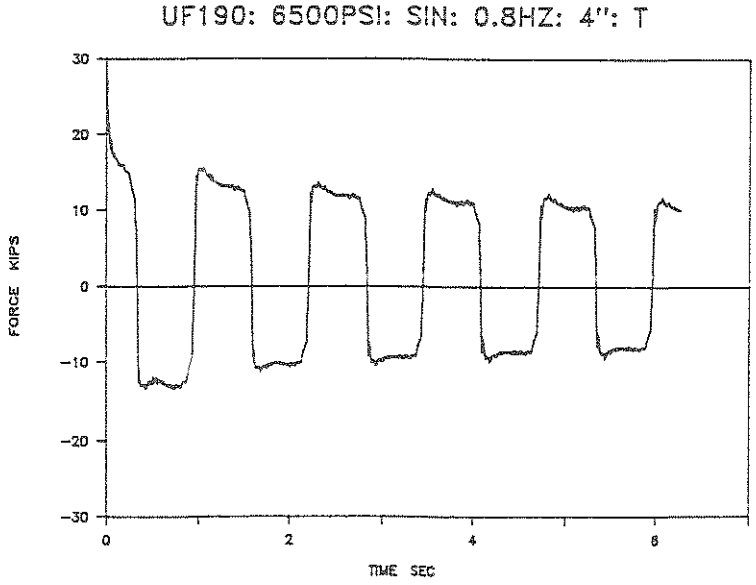
UF190: 6500PSI: SIN: 0.8HZ: 4": T
FORCE KIPS
TIME SEC

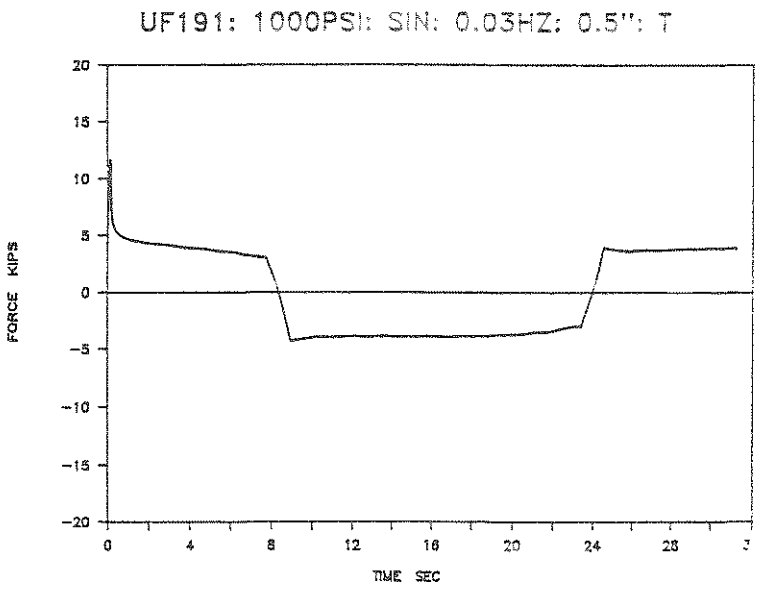
UF191: 1000PSI: SIN: 0.03HZ: 0.5": T
FORCE KIPS
TIME SEC

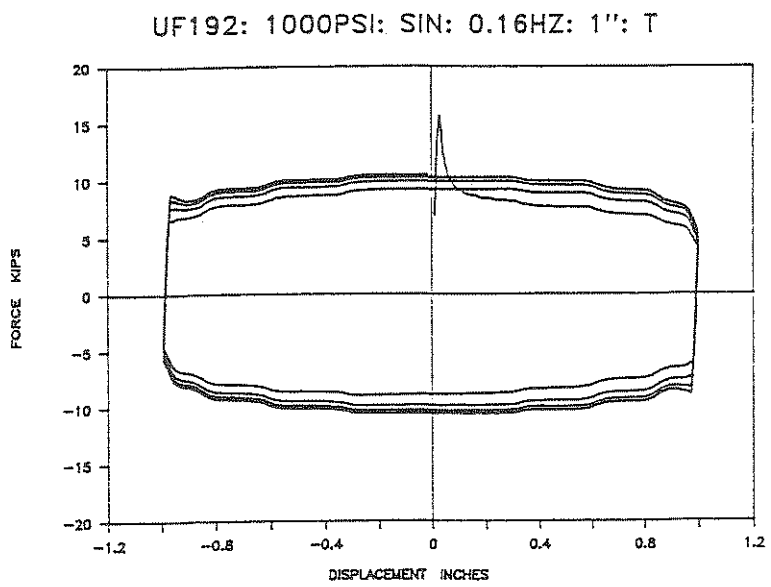
UF192: 1000PSI: SIN: 0.16HZ: 1": T
FORCE KIPS
DISPLACEMENT INCHES

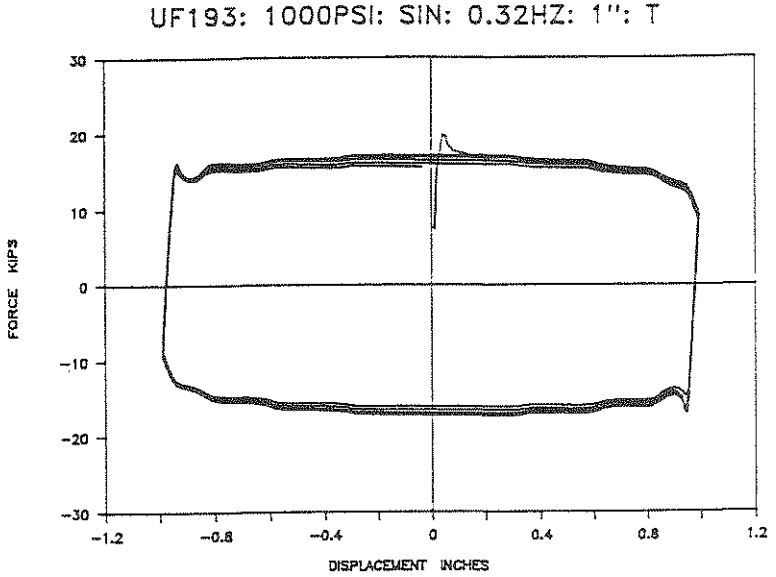
UF193: 1000PSI: SIN: 0.32HZ: 1": T
FORCE KIPS
DISPLACEMENT INCHES

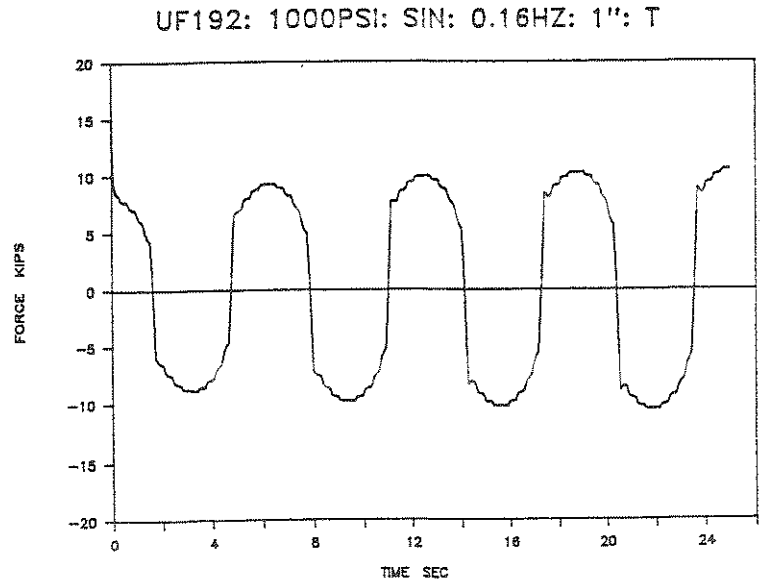
UF192: 1000PSI: SIN: 0.16HZ: 1": T
FORCE KIPS
TIME SEC

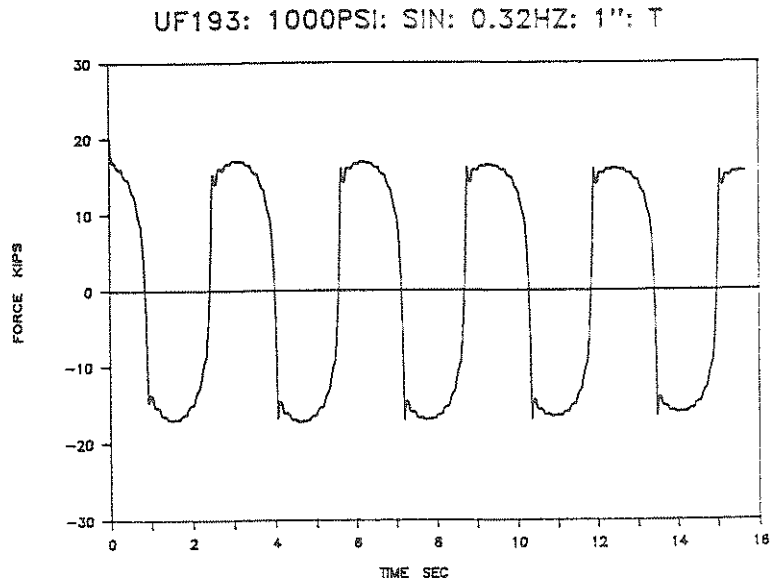
UF193: 1000PSI: SIN: 0.32HZ: 1": T
FORCE KIPS
TIME SEC

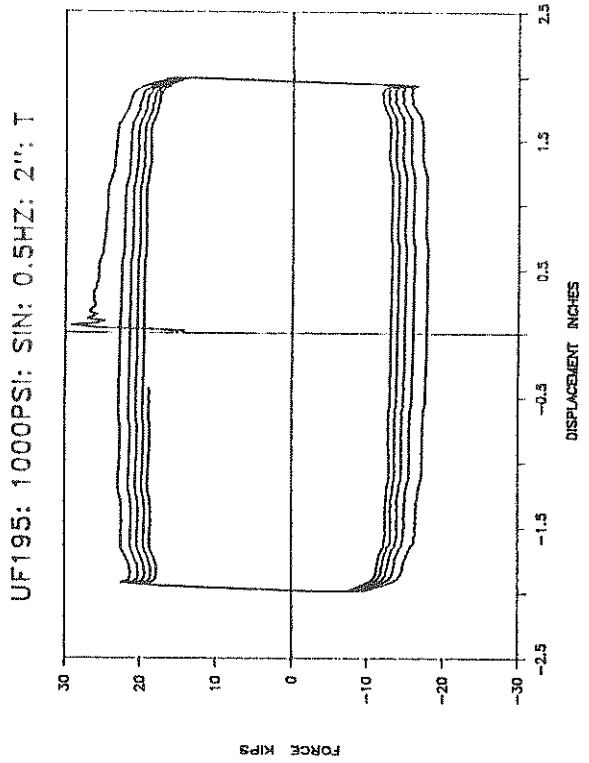
UF195: 1000PSI: SIN: 0.5HZ: 2": T
FORCE KIPS
DISPLACEMENT INCHES

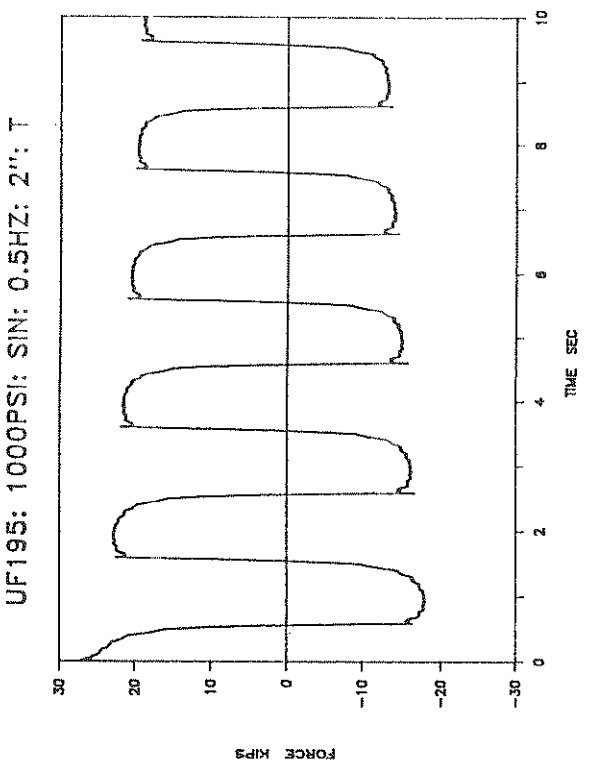
UF195: 1000PSI: SIN: 0.5HZ: 2": T
FORCE KIPS
TIME SEC

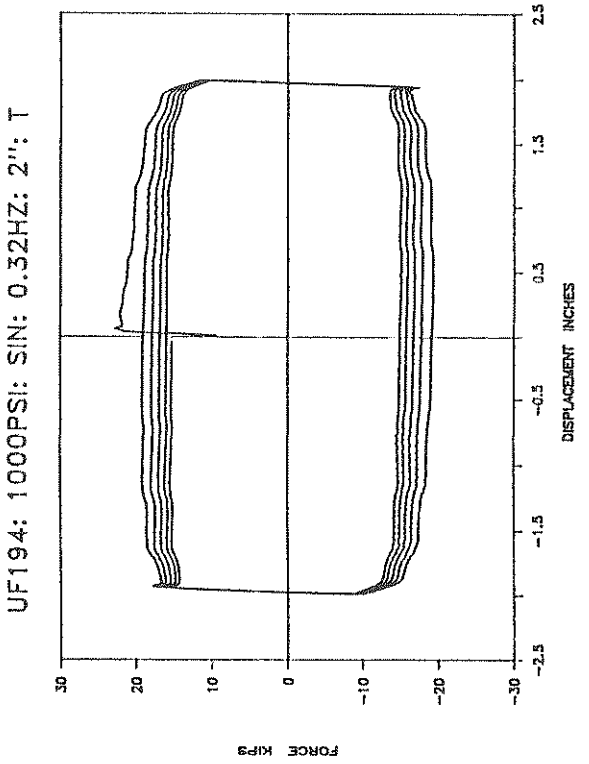
UF194: 1000PSI: SIN: 0.32HZ: 2": T
FORCE KIPS
DISPLACEMENT INCHES

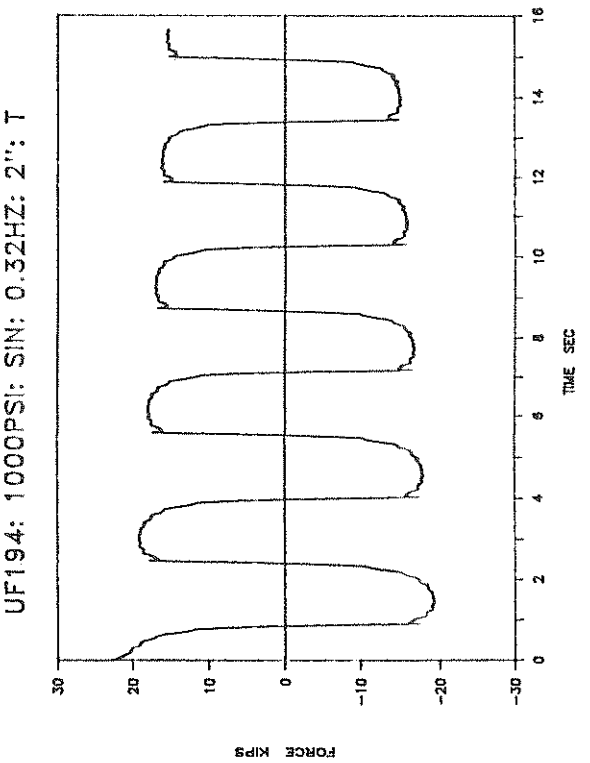
UF194: 1000PSI: SIN: 0.32HZ: 2": T
FORCE KIPS
TIME SEC

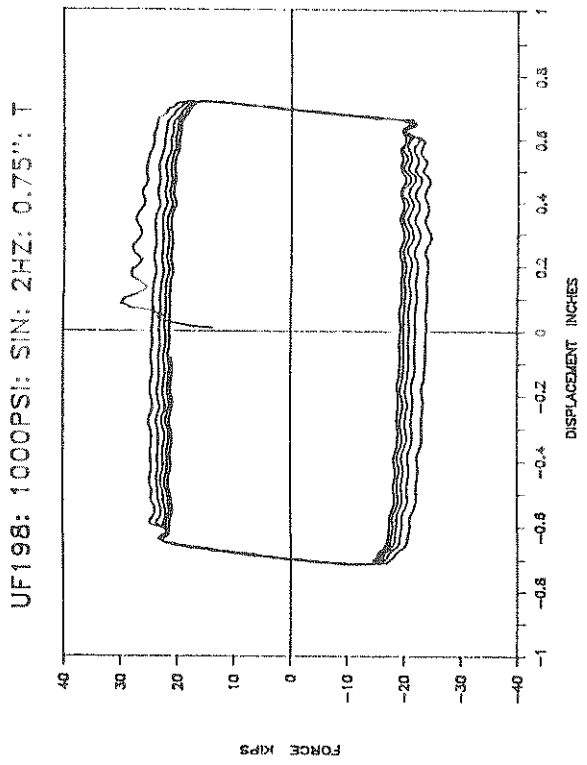
UF198: 1000PSI: SIN: 2HZ: 0.75": T
FORCE KIPS
DISPLACEMENT INCHES

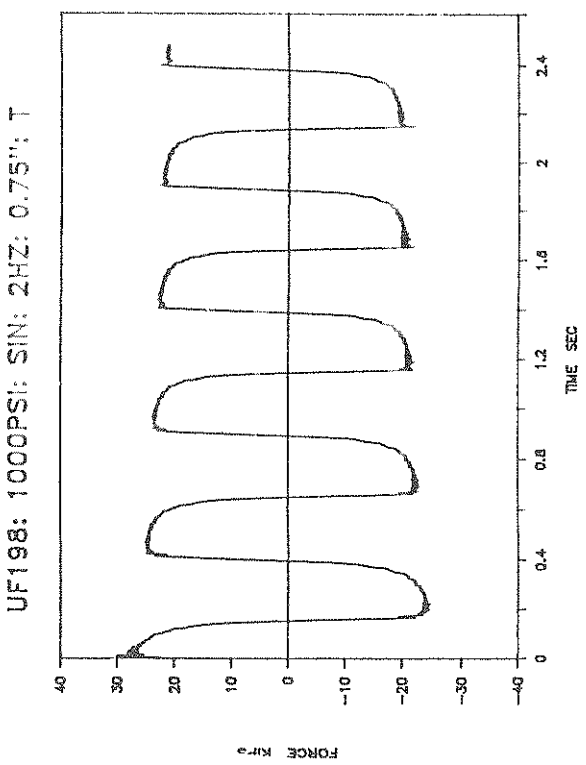
UF198: 1000PSI: SIN: 2HZ: 0.75": T
FORCE KIPS
TIME SEC

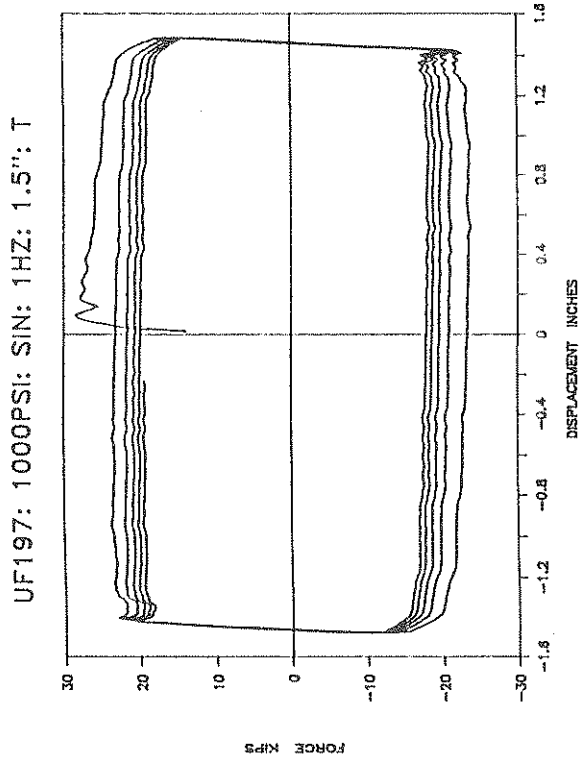
UF197: 1000PSI: SIN: 1HZ: 1.5": T
FORCE KIPS
DISPLACEMENT INCHES

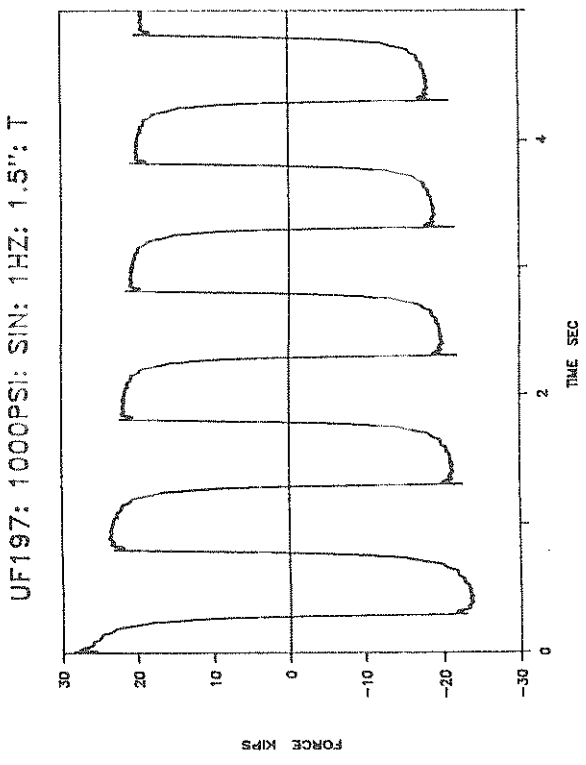
UF197: 1000PSI: SIN: 1HZ: 1.5": T
FORCE KIPS
TIME SEC

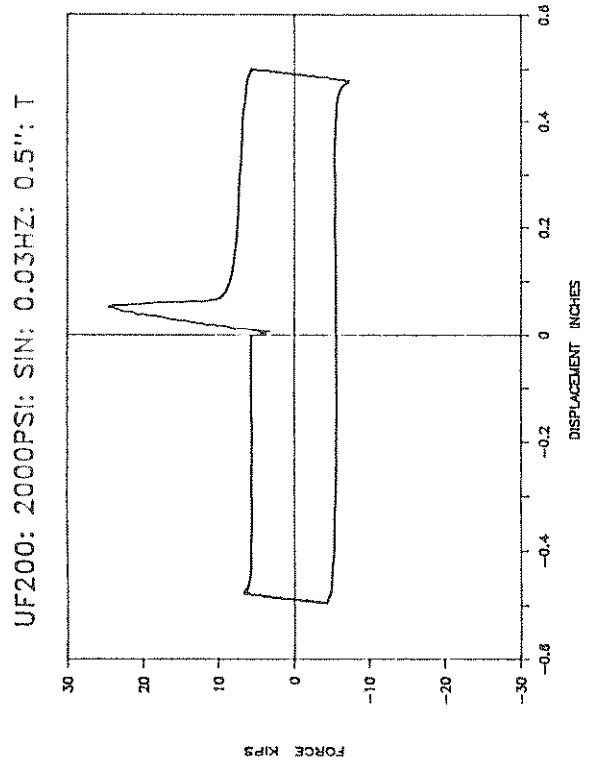
UF200: 2000PSI: SIN: 0.03HZ: 0.5": T
FORCE KIPS
DISPLACEMENT INCHES

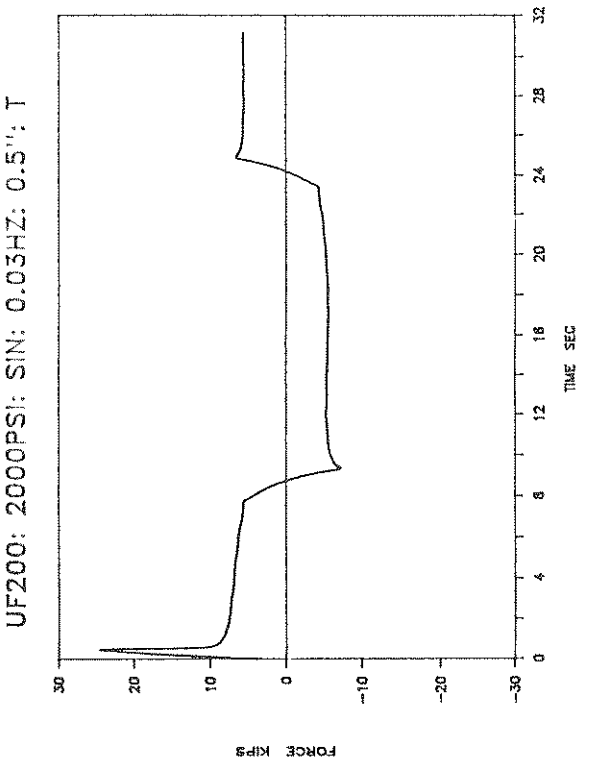
UF200: 2000PSI: SIN: 0.03HZ: 0.5": T
FORCE KIPS
TIME SEC

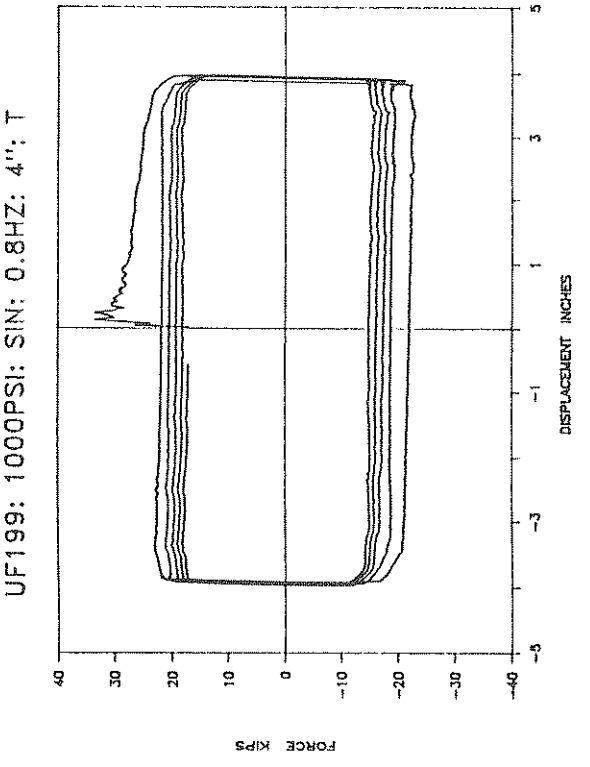
UF199: 1000PSI: SIN: 0.8HZ: 4": T
FORCE KIPS
DISPLACEMENT INCHES

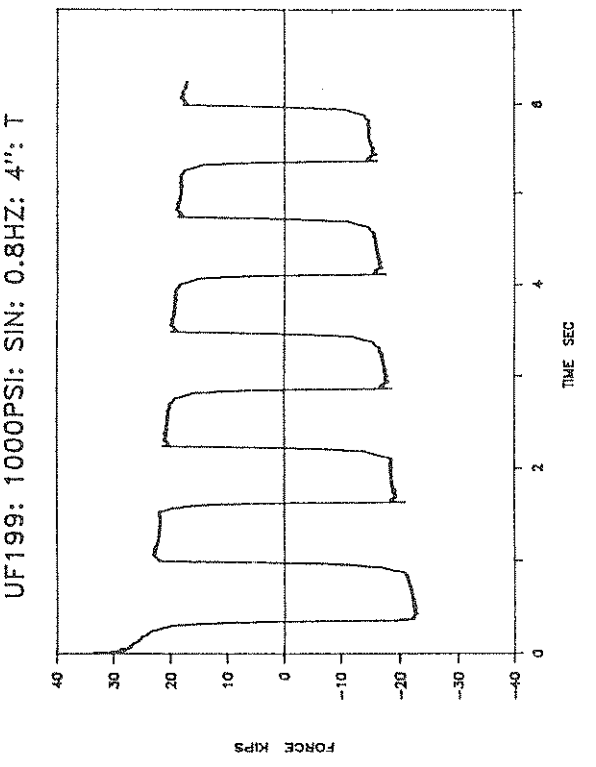
UF199: 1000PSI: SIN: 0.8HZ: 4": T
FORCE KIPS
TIME SEC

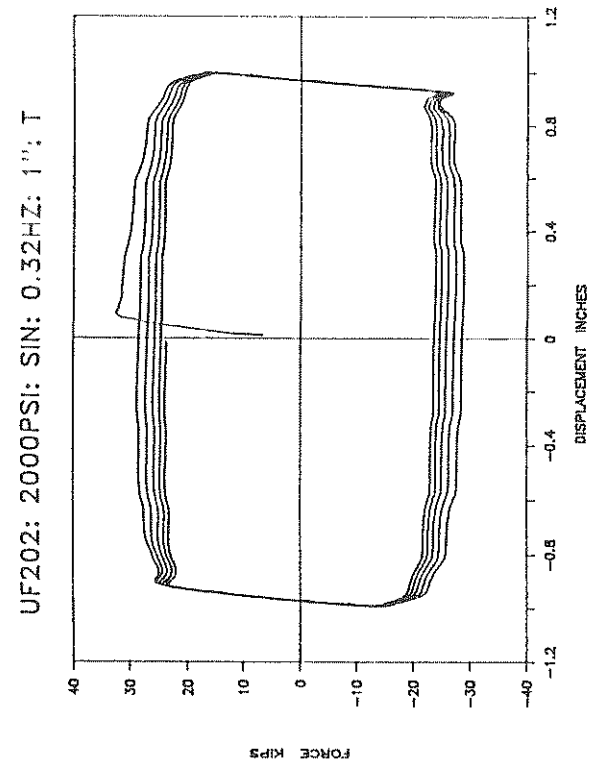
UF202: 2000PSI: SIN: 0.32HZ: 1": T
FORCE KIPS
DISPLACEMENT INCHES

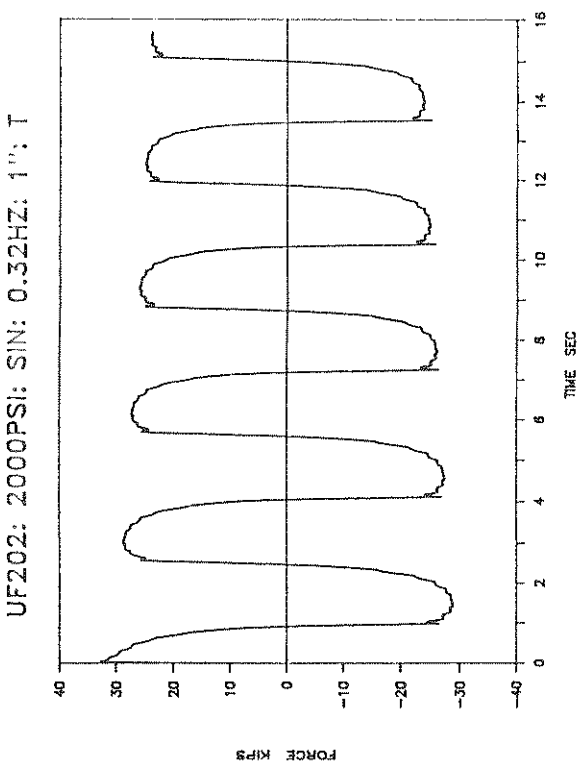
UF202: 2000PSI: SIN: 0.32HZ: 1": T
FORCE KIPS
TIME SEC

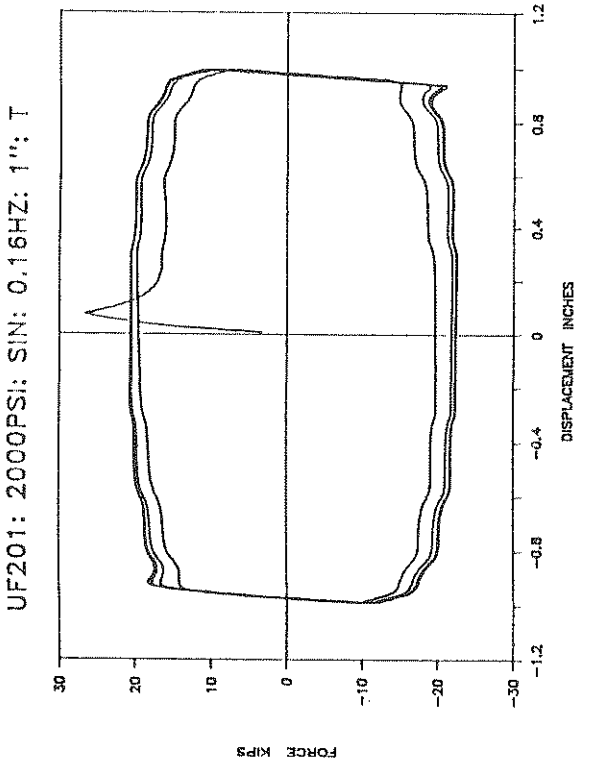
UF201: 2000PSI: SIN: 0.16HZ: 1": T
FORCE KIPS
DISPLACEMENT INCHES

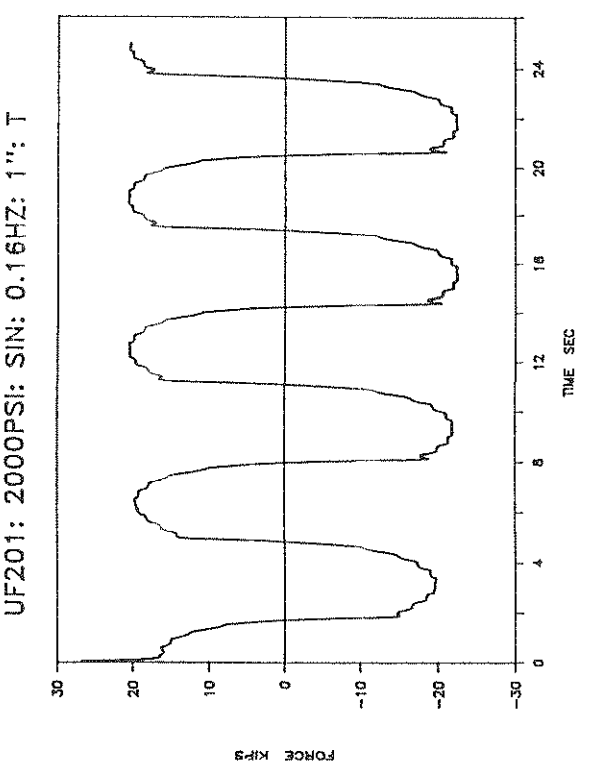
UF201: 2000PSI: SIN: 0.16HZ: 1": T
FORCE KIPS
TIME SEC

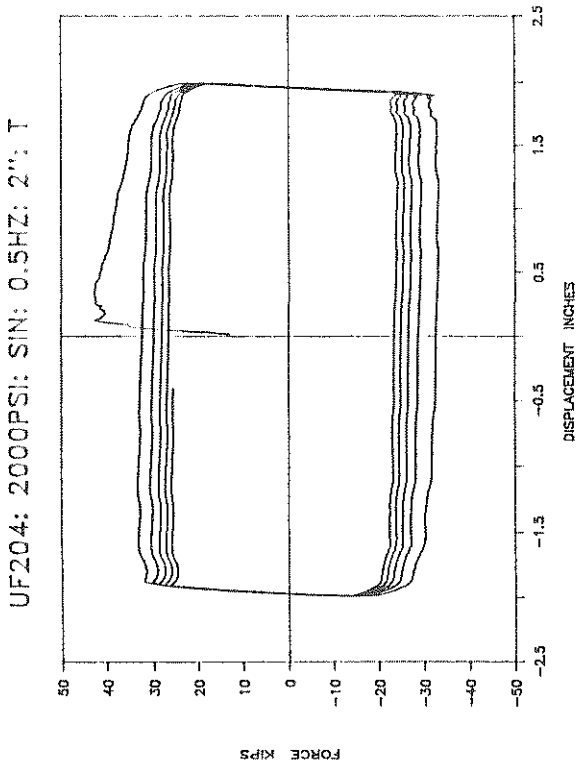
UF204: 2000PSI: SIN: 0.5HZ: 2": T
FORCE KIPS
DISPLACEMENT INCHES

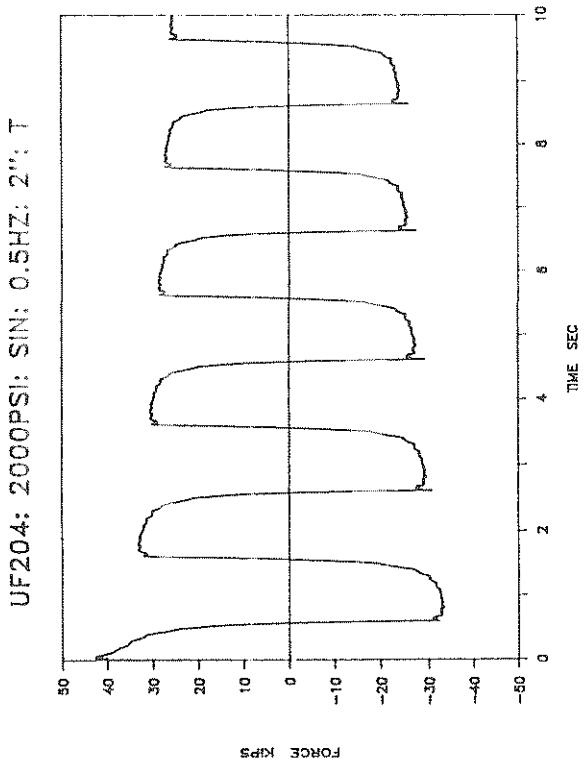
UF204: 2000PSI: SIN: 0.5HZ: 2": T
FORCE KIPS
TIME SEC

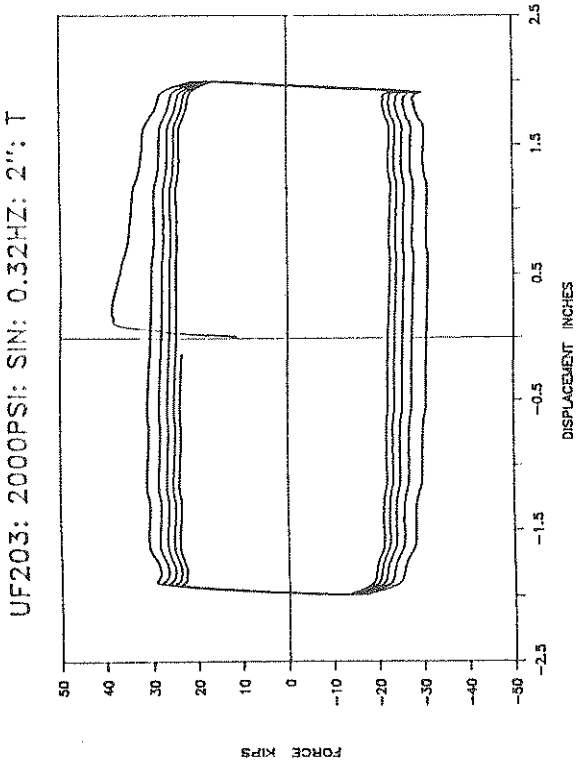
UF203: 2000PSI: SIN: 0.32HZ: 2": T
FORCE KIPS
DISPLACEMENT INCHES

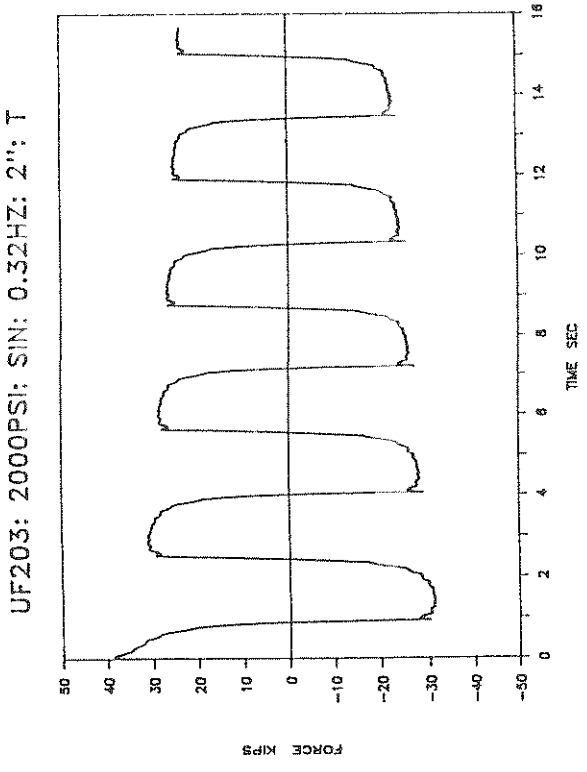
UF203: 2000PSI: SIN: 0.32HZ: 2": T
FORCE KIPS
TIME SEC

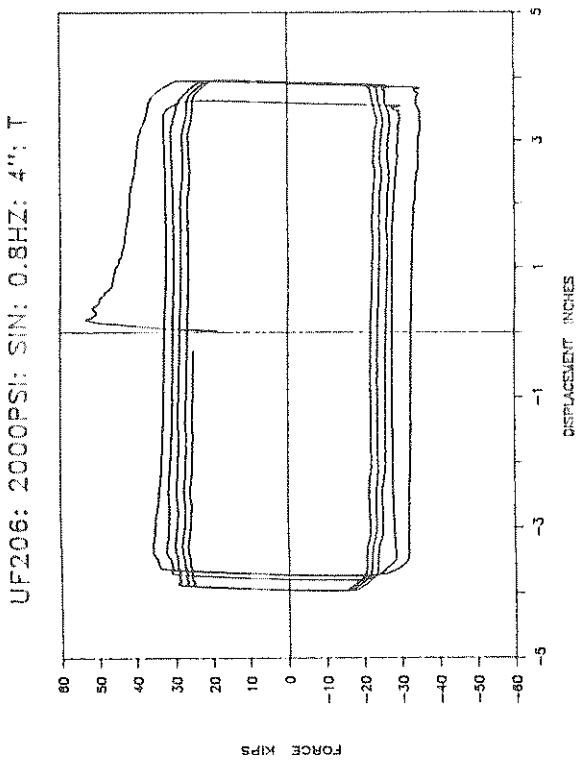
UF206: 2000PSI: SIN: 0.8HZ: 4": T
FORCE KIPS
DISPLACEMENT INCHES

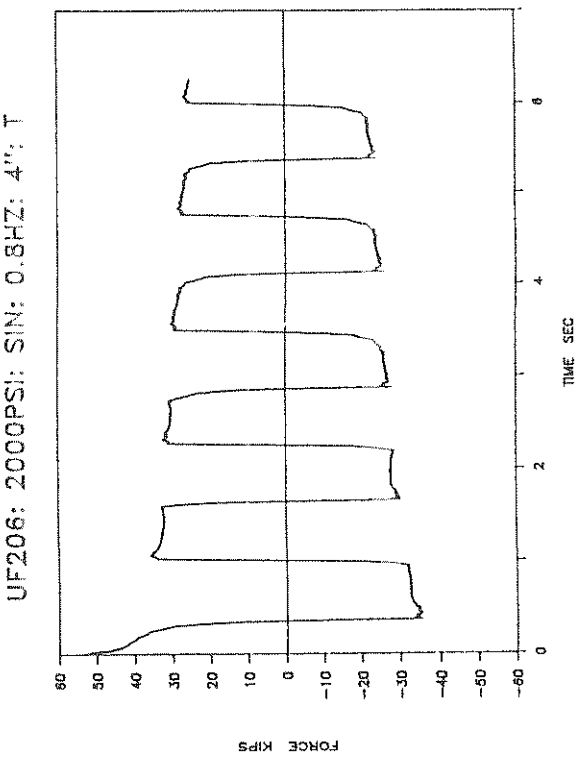
UF206: 2000PSI: SIN: 0.8HZ: 4": T
FORCE KIPS
TIME SEC

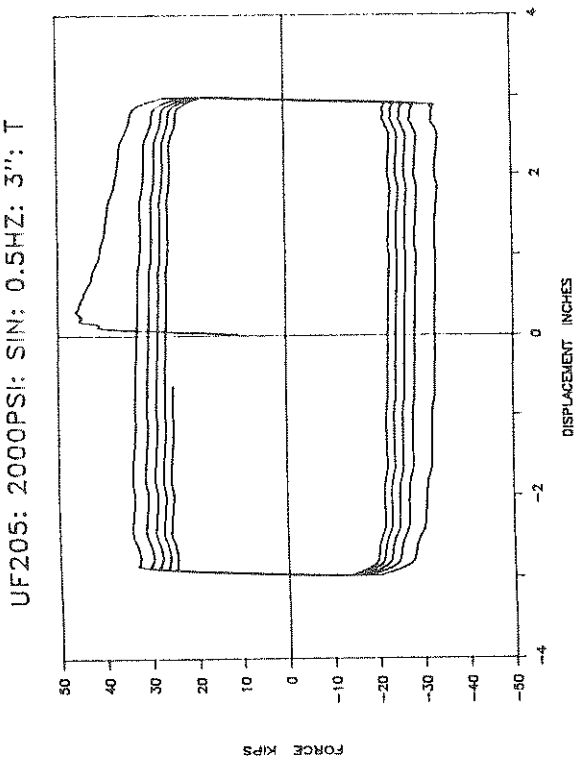
UF205: 2000PSI: SIN: 0.5HZ: 3": T
FORCE KIPS
DISPLACEMENT INCHES

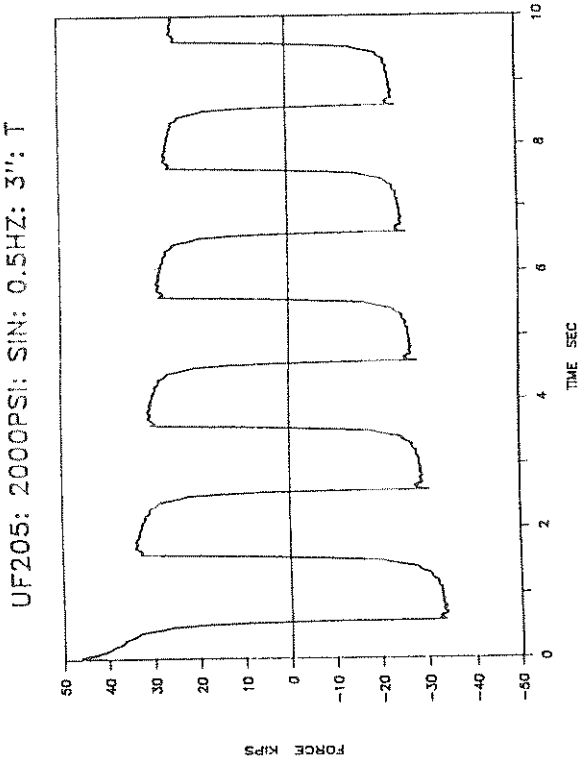
UF205: 2000PSI: SIN: 0.5HZ: 3": T
FORCE KIPS
TIME SEC

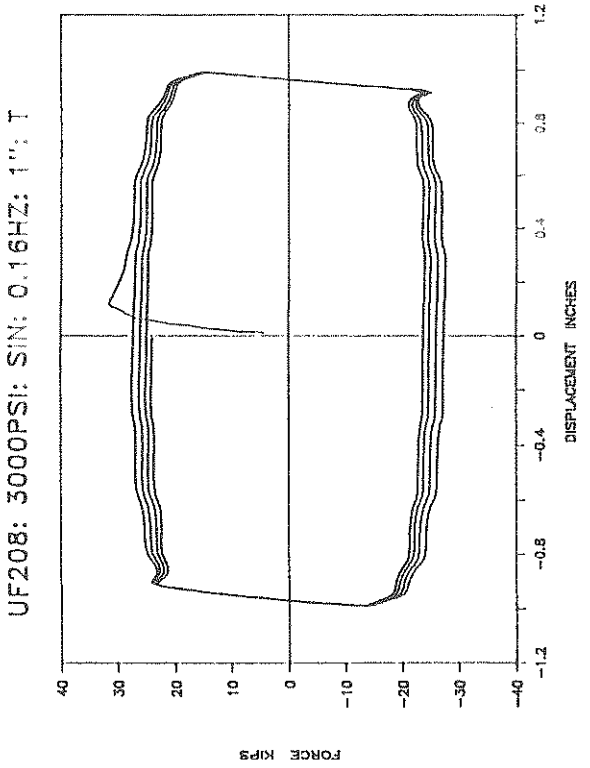
UF208: 3000PSI: SIN: 0.16HZ: 1": T
FORCE KIPS
DISPLACEMENT INCHES

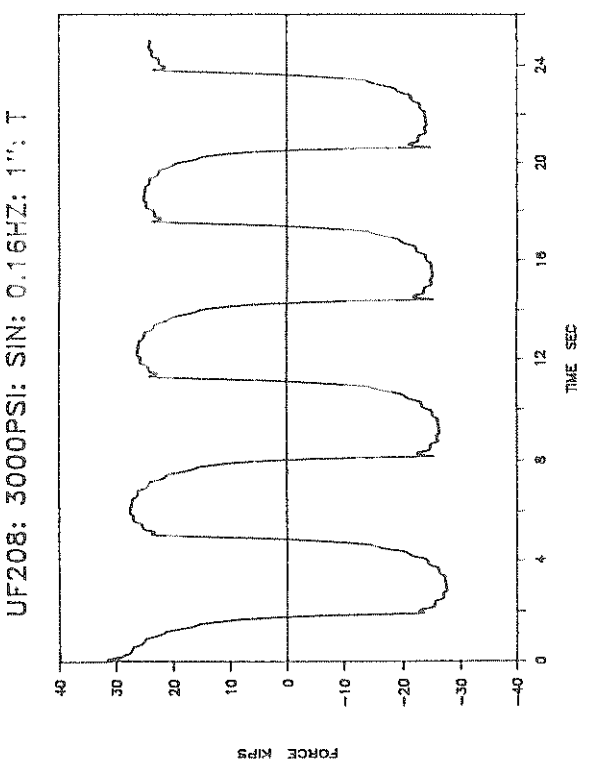
UF208: 3000PSI: SIN: 0.16HZ: 1": T
FORCE KIPS
TIME SEC

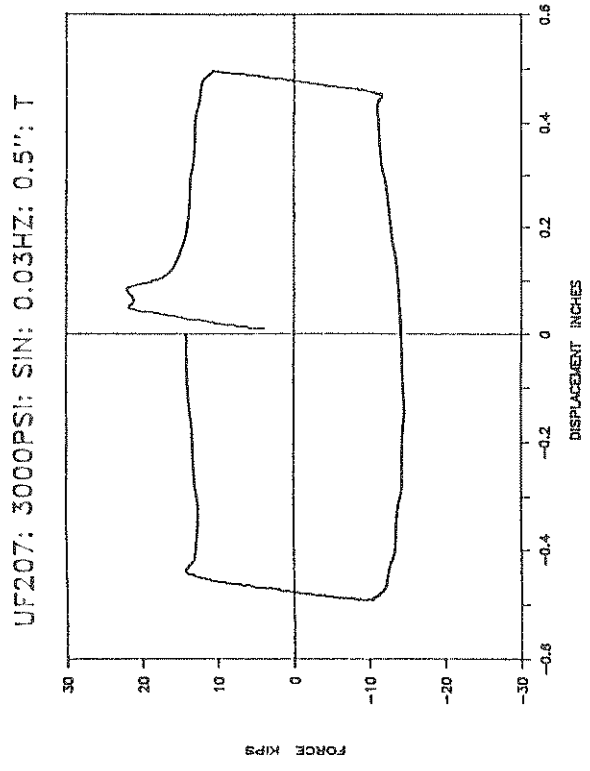
UF207: 3000PSI: SIN: 0.03HZ: 0.5": T
FORCE KIPS
DISPLACEMENT INCHES

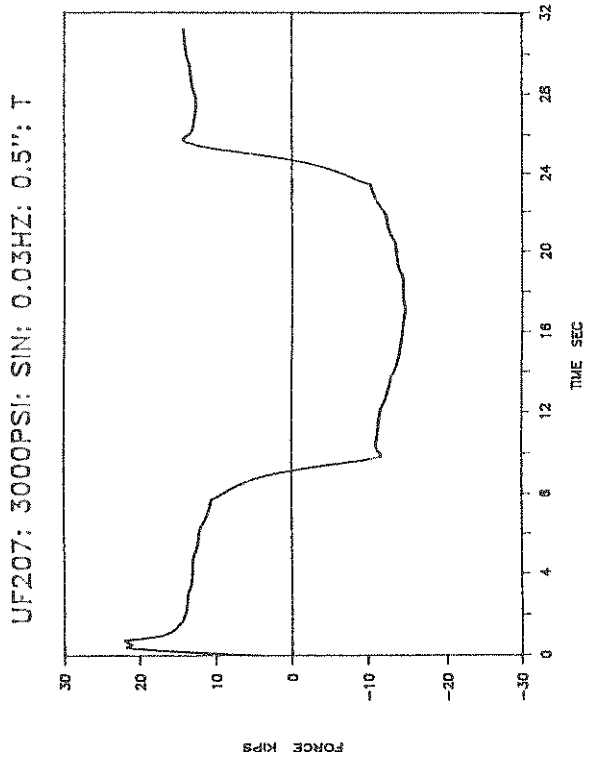
UF207: 3000PSI: SIN: 0.03HZ: 0.5": T
FORCE KIPS
TIME SEC

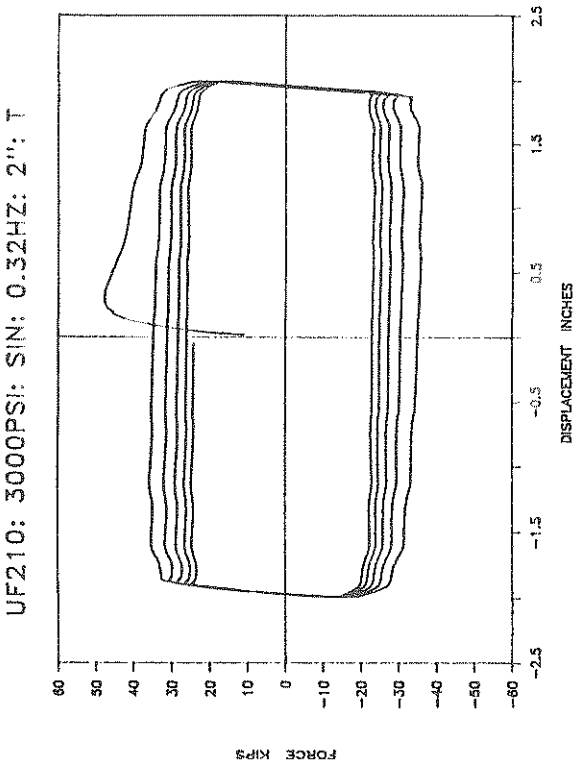
UF210: 3000PSI: SIN: 0.32HZ: 2": T
FORCE KIPS
DISPLACEMENT INCHES

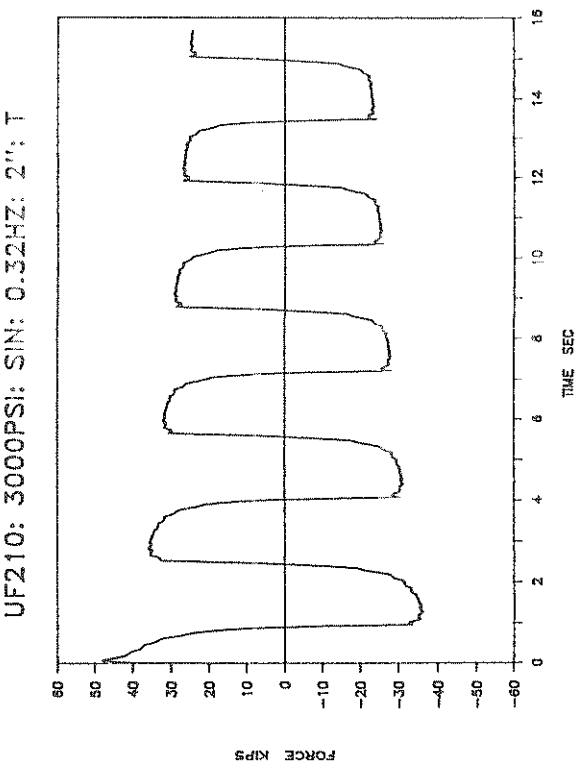
UF210: 3000PSI: SIN: 0.32HZ: 2": T
FORCE KIPS
TIME SEC

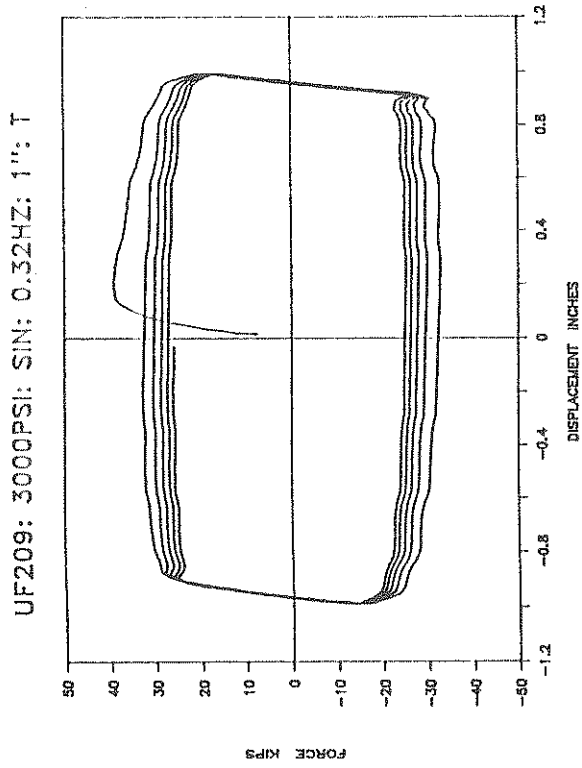
UF209: 3000PSI: SIN: 0.32HZ: 1": T
FORCE KIPS
DISPLACEMENT INCHES

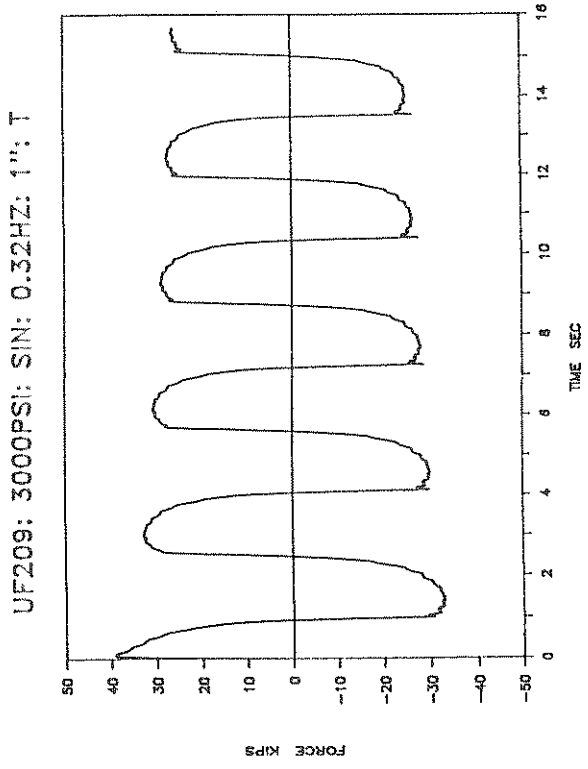
UF209: 3000PSI: SIN: 0.32HZ: 1": T
FORCE KIPS
TIME SEC

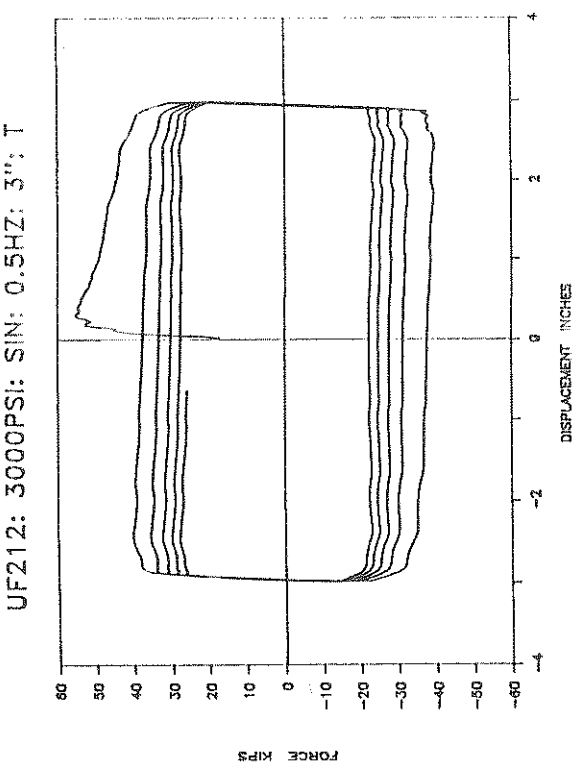
UF212: 3000PSI: SIN: 0.5HZ: 3": T
FORCE KIPS
DISPLACEMENT INCHES

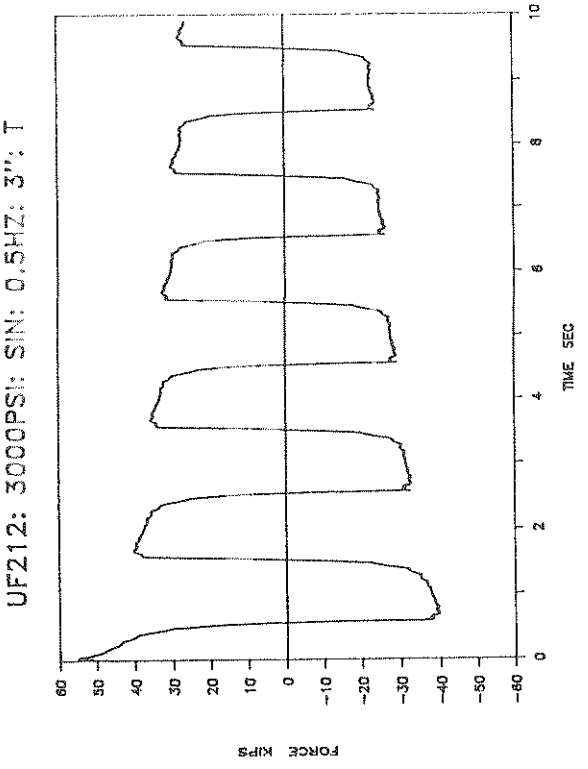
UF212: 3000PSI: SIN: 0.5HZ: 3": T
FORCE KIPS
TIME SEC

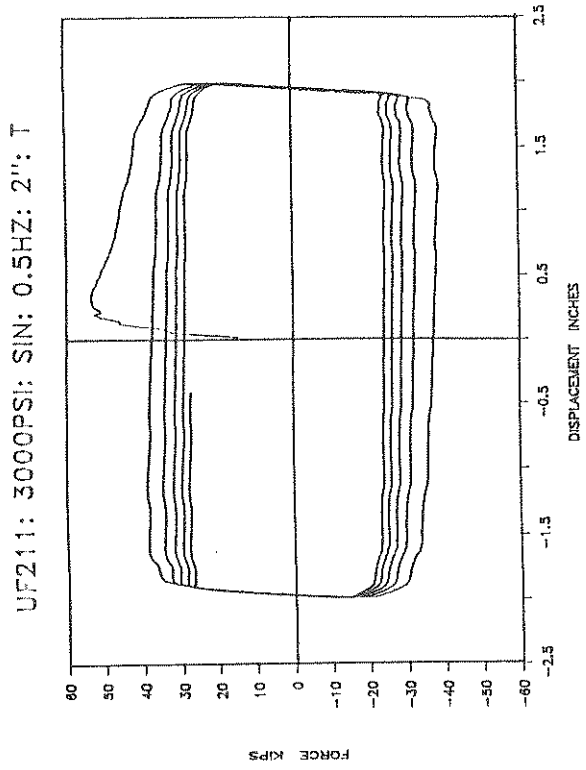
UF211: 3000PSI: SIN: 0.5HZ: 2": T
FORCE KIPS
DISPLACEMENT INCHES

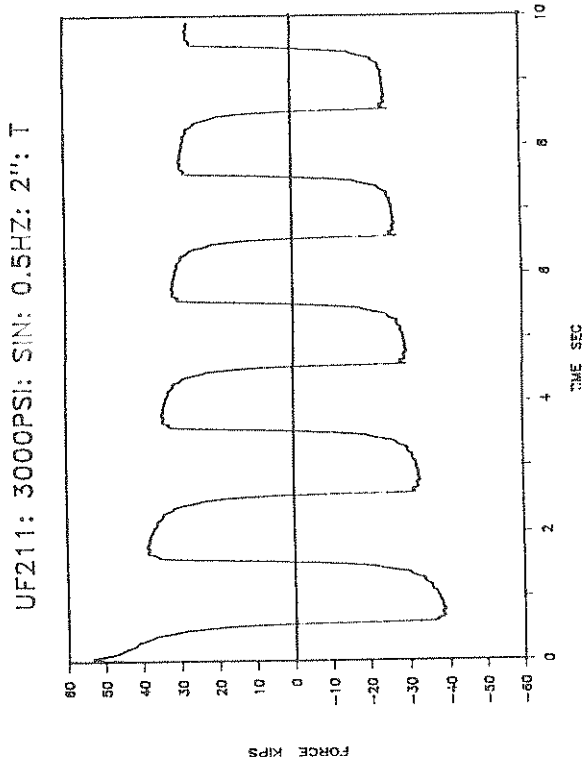
UF211: 3000PSI: SIN: 0.5HZ: 2": T
FORCE KIPS
TIME SEC

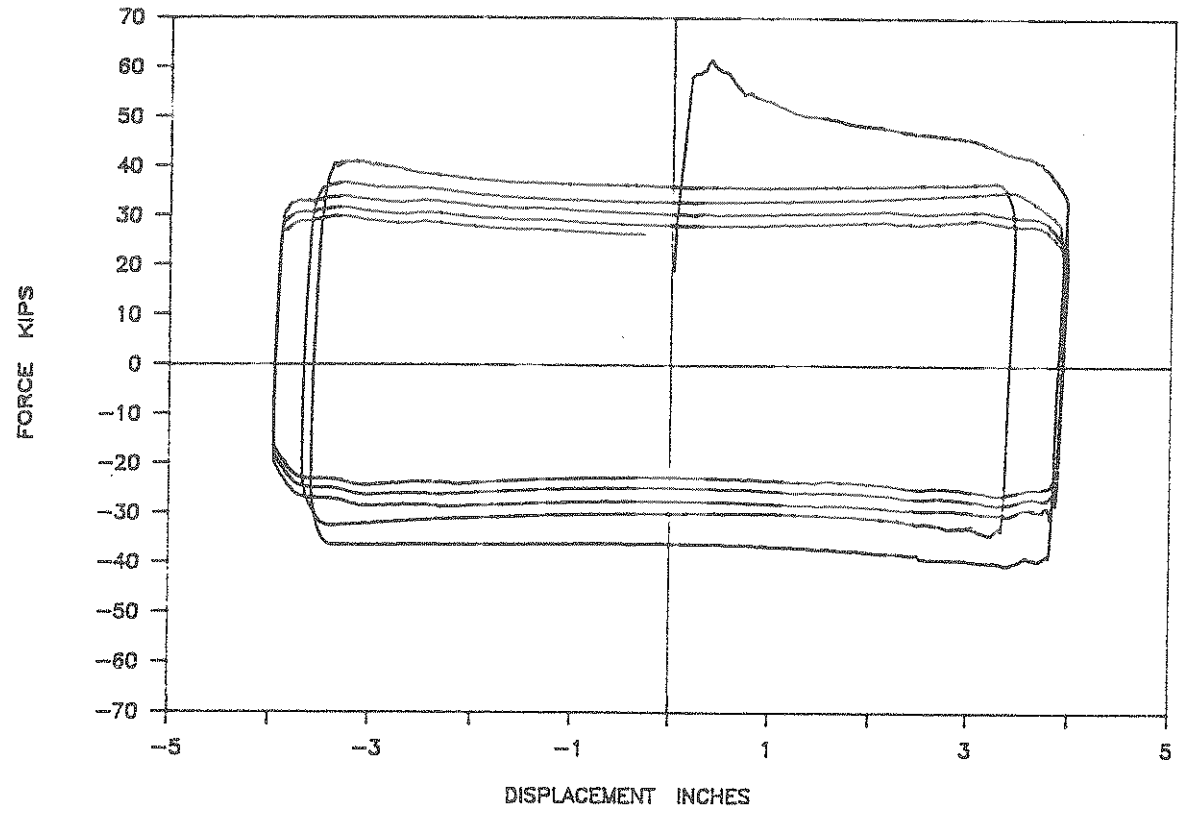
UF213: 3000PSI: SIN: 0.8HZ: 4": T
FORCE KIPS
70
60
50
40
30
20
10
0
-10
-20
-30
-40
-50
-60
-70
-5
-3
-1
1
3
5
DISPLACEMENT INCHES

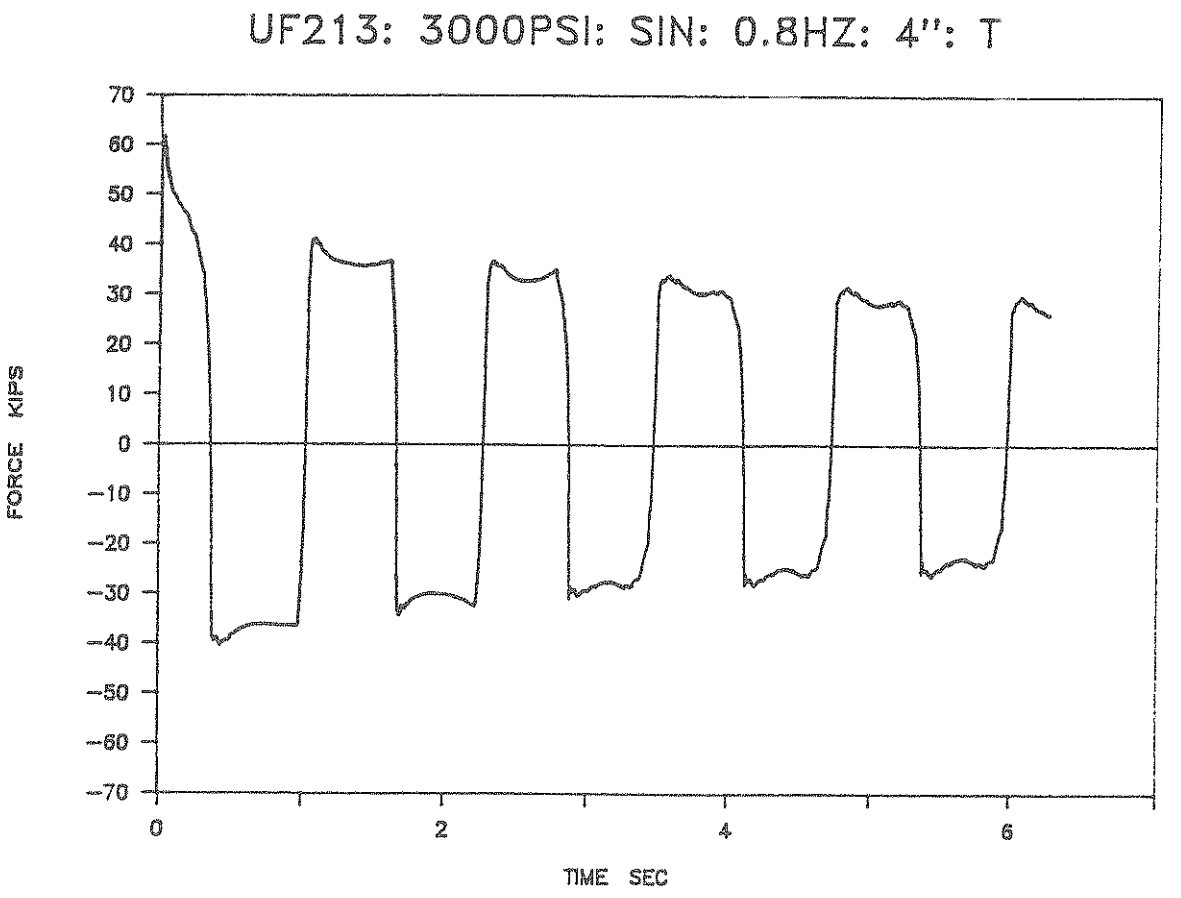
UF213: 3000PSI: SIN: 0.8HZ: 4": T
FORCE KIPS
70
60
50
40
30
20
10
0
-10
-20
-30
-40
-50
-60
-70
0
2
4
6
TIME SEC

NATIONAL CENTER FOR EARTHQUAKE ENGINEERING RESEARCH
LIST OF PUBLISHED TECHNICAL REPORTS

The National Center for Earthquake Engineering Research (NCEER) publishes technical reports on a variety of subjects related to earthquake engineering written by authors funded through NCEER. These reports are available from both NCEER's Publications Department and the National Technical Information Service (NTIS). Requests for reports should be directed to the Publications Department, National Center for Earthquake Engineering Research, State University of New York at Buffalo, Red Jacket Quadrangle, Buffalo, New York 14261. Reports can also be requested through NTIS, 5285 Port Royal Road, Springfield, Virginia 22161. NTIS accession numbers are shown in parenthesis, if available.

NCEER-87-0001 "First-Year Program in Research, Education and Technology Transfer," 3/5/87, (PB88-134275/AS).

NCEER-87-0002 "Experimental Evaluation of Instantaneous Optimal Algorithms for Structural Control," by R.C. Lin, T.T. Soong and A.M. Reinhorn, 4/20/87, (PB88-134341/AS).

NCEER-87-0003 "Experimentation Using the Earthquake Simulation Facilities at University at Buffalo," by A.M. Reinhorn and R.L. Ketter, to be published.

NCEER-87-0004 "The System Characteristics and Performance of a Shaking Table," by J.S. Hwang, K.C. Chang and G.C. Lee, 6/1/87, (PB88-134259/AS).

NCEER-87-0005 "A Finite Element Formulation for Nonlinear Viscoplastic Material Using a Q Model," by O. Gyebi and G. Dasgupta, 11/2/87, (PB88-213764/AS).

NCEER-87-0006 "Symbolic Manipulation Program (SMP) - Algebraic Codes for Two and Three Dimensional Finite Element Formulations," by X. Lee and G. Dasgupta, 11/9/87, (PB88-219522/AS).

NCEER-87-0007 "Instantaneous Optimal Control Laws for Tall Buildings Under Seismic Excitations," by J.N. Yang, A. Akbarpour and P. Ghaemmaghami, 6/10/87, (PB88-134333/AS).

NCEER-87-0008 "IDARC: Inelastic Damage Analysis of Reinforced Concrete Frame - Shear-Wall Structures," by Y.J. Park, A.M. Reinhorn and S.K. Kunnath, 7/20/87, (PB88-134325/AS).

NCEER-87-0009 "Liquefaction Potential for New York State: A Preliminary Report on Sites in Manhattan and Buffalo," by M. Budhu, V. Vijayakumar, R.F. Giese and L. Baumgras, 8/31/87, (PB88-163704/AS). This report is available only through NTIS (see address given above).

NCEER-87-0010 "Vertical and Torsional Vibration of Foundations in Inhomogeneous Media," by A.S. Veletsos and K.W. Dotson, 6/1/87, (PB88-134291/AS).

NCEER-87-0011 "Seismic Probabilistic Risk Assessment and Seismic Margins Studies for Nuclear Power Plants," by Howard H.M. Hwang, 6/15/87, (PB88-134267/AS). This report is available only through NTIS (see address given above).

NCEER-87-0012 "Parametric Studies of Frequency Response of Secondary Systems Under Ground-Acceleration Excitations," by Y. Yong and Y.K. Lin, 6/10/87, (PB88-134309/AS).

NCEER-87-0013 "Frequency Response of Secondary Systems Under Seismic Excitation," by J.A. HoLung, J. Cai and Y.K. Lin, 7/31/87, (PB88-134317/AS).

NCEER-87-0014 "Modelling Earthquake Ground Motions in Seismically Active Regions Using Parametric Time Series Methods," by G.W. Ellis and A.S. Cakmak, 8/25/87, (PB88-134283/AS).

NCEER-87-0015 "Detection and Assessment of Seismic Structural Damage," by E. DiPasquale and A.S. Cakmak, 8/25/87, (PB88-163712/AS).

NCEER-87-0016 "Pipeline Experiment at Parkfield, California," by J. Isenberg and E. Richardson, 9/15/87, (PB88-163720/AS).

NCEER-87-0017 "Digital Simulation of Seismic Ground Motion," by M. Shinozuka, G. Deodatis and T. Harada, 8/31/87, (PB88-155197/AS). This report is available only through NTIS (see address given above).

NCEER-87-0018 "Practical Considerations for Structural Control: System Uncertainty, System Time Delay and Truncation of Small Control Forces," J.N. Yang and A. Akbarpour, 8/10/87, (PB88-163738/AS).

NCEER-87-0019 "Modal Analysis of Nonclassically Damped Structural Systems Using Canonical Transformation," by J.N. Yang, S. Sarkani and F.X. Long, 9/27/87, (PB88-187851/AS).

NCEER-87-0020 "A Nonstationary Solution in Random Vibration Theory," by J.R. Red-Horse and P.D. Spanos, 11/3/87, (PB88-163746/AS).

NCEER-87-0021 "Horizontal Impedances for Radially Inhomogeneous Viscoelastic Soil Layers," by A.S. Veletsos and K.W. Dotson, 10/15/87, (PB88-150859/AS).

NCEER-87-0022 "Seismic Damage Assessment of Reinforced Concrete Members," by Y.S. Chung, C. Meyer and M. Shinozuka, 10/9/87, (PB88-150867/AS). This report is available only through NTIS (see address given above).

NCEER-87-0023 "Active Structural Control in Civil Engineering," by T.T. Soong, 11/11/87, (PB88-187778/AS).

NCEER-87-0024 Vertical and Torsional Impedances for Radially Inhomogeneous Viscoelastic Soil Layers," by K.W. Dotson and A.S. Veletsos, 12/87, (PB88-187786/AS).

NCEER-87-0025 "Proceedings from the Symposium on Seismic Hazards, Ground Motions, Soil-Liquefaction and Engineering Practice in Eastern North America," October 20-22, 1987, edited by K.H. Jacob, 12/87, (PB88-188115/AS).

NCEER-87-0026 "Report on the Whittier-Narrows, California, Earthquake of October 1, 1987," by J. Pantelic and A. Reinhorn, 11/87, (PB88-187752/AS). This report is available only through NTIS (see address given above).

NCEER-87-0027 "Design of a Modular Program for Transient Nonlinear Analysis of Large 3-D Building Structures," by S. Srivastav and J.F. Abel, 12/30/87, (PB88-187950/AS).

NCEER-87-0028 "Second-Year Program in Research, Education and Technology Transfer," 3/8/88, (PB88-219480/AS).

NCEER-88-0001 "Workshop on Seismic Computer Analysis and Design of Buildings With Interactive Graphics," by W. McGuire, J.F. Abel and C.H. Conley, 1/18/88, (PB88-187760/AS).

NCEER-88-0002 "Optimal Control of Nonlinear Flexible Structures," by J.N. Yang, F.X. Long and D. Wong, 1/22/88, (PB88-213772/AS).

NCEER-88-0003 "Substructuring Techniques in the Time Domain for Primary-Secondary Structural Systems," by G.D. Manolis and G. Juhn, 2/10/88, (PB88-213780/AS).

NCEER-88-0004 "Iterative Seismic Analysis of Primary-Secondary Systems," by A. Singhal, L.D. Lutes and P.D. Spanos, 2/23/88, (PB88-213798/AS).

NCEER-88-0005 "Stochastic Finite Element Expansion for Random Media," by P.D. Spanos and R. Ghanem, 3/14/88, (PB88-213806/AS).

NCEER-88-0006 "Combining Structural Optimization and Structural Control," by F.Y. Cheng and C.P. Pantelides, 1/10/88, (PB88-213814/AS).

NCEER-88-0007 "Seismic Performance Assessment of Code-Designed Structures," by H.H-M. Hwang, J-W. Jaw and H-J. Shau, 3/20/88, (PB88-219423/AS).

NCEER-88-0008 "Reliability Analysis of Code-Designed Structures Under Natural Hazards," by H.H-M. Hwang, H. Ushiba and M. Shinozuka, 2/29/88, (PB88-229471/AS).

NCEER-88-0009 "Seismic Fragility Analysis of Shear Wall Structures," by J-W Jaw and H.H-M. Hwang, 4/30/88.

NCEER-88-0010 "Base Isolation of a Multi-Story Building Under a Harmonic Ground Motion - A Comparison of Performances of Various Systems," by F-G Fan, G. Ahmadi and I.G. Tadjbakhsh, 5/18/88.

NCEER-88-0011 "Seismic Floor Response Spectra for a Combined System by Green's Functions," by F.M. Lavelle, L.A. Bergman and P.D. Spanos, 5/1/88.

NCEER-88-0012 "A New Solution Technique for Randomly Excited Hysteretic Structures," by G.Q. Cai and Y.K. Lin, 5/16/88.

NCEER-88-0013 "A Study of Radiation Damping and Soil-Structure Interaction Effects in the Centrifuge," by K. Weissman, supervised by J.H. Prevost, 5/24/88.

NCEER-88-0014 "Parameter Identification and Implementation of a Kinematic Plasticity Model for Frictional Soils," by J.H. Prevost and D.V. Griffiths, to be published.

NCEER-88-0015 "Two- and Three- Dimensional Dynamic Finite Element Analyses of the Long Valley Dam," by D.V. Griffiths and J.H. Prevost, 6/17/88.

NCEER-88-0016 "Damage Assessment of Reinforced Concrete Structures in Eastern United States," by A.M. Reinhorn, M.J. Seidel, S.K. Kunnath and Y.J. Park, 6/15/88.

NCEER-88-0017 "Dynamic Compliance of Vertically Loaded Strip Foundations in Multilayered Viscoelastic Soils," by S. Ahmad and A.S.M. Israil, 6/17/88.

NCEER-88-0018 "An Experimental Study of Seismic Structural Response With Added Viscoelastic Dampers," by R.C. Lin, Z. Liang, T.T. Soong and R.H. Zhang, 6/30/88.

NCEER-88-0019 "Experimental Investigation of Primary - Secondary System Interaction," by G.D. Manolis, G. Juhn and A.M. Reinhorn, 5/27/88.

NCEER-88-0020 "A Response Spectrum Approach For Analysis of Nonclassically Damped Structures," by J.N. Yang, S. Sarkani and F.X. Long, 4/22/88.

NCEER-88-0021 "Seismic Interaction of Structures and Soils: Stochastic Approach," by A.S. Veletsos and A.M. Prasad, 7/21/88.

NCEER-88-0022 "Identification of the Serviceability Limit State and Detection of Seismic Structural Damage," by E. DiPasquale and A.S. Cakmak, 6/15/88.

NCEER-88-0023 "Multi-Hazard Risk Analysis: Case of a Simple Offshore Structure," by B.K. Bhartia and E.H. Vanmarcke, 7/21/88.

NCEER-88-0024 "Automated Seismic Design of Reinforced Concrete Buildings," by Y.S. Chung, C. Meyer and M. Shinozuka, 7/5/88.

NCEER-88-0025 "Experimental Study of Active Control of MDOF Structures Under Seismic Excitations," by L.L. Chung, R.C. Lin, T.T. Soong and A.M. Reinhorn, 7/10/88, (PB89-122600/AS).

NCEER-88-0026 "Earthquake Simulation Tests of a Low-Rise Metal Structure," by J.S. Hwang, K.C. Chang, G.C. Lee and R.L. Ketter, 8/1/88.

NCEER-88-0027 "Systems Study of Urban Response and Reconstruction Due to Catastrophic Earthquakes," by F. Kozin and H.K. Zhou, 9/22/88, to be published.

NCEER-88-0028 "Seismic Fragility Analysis of Plane Frame Structures," by H.H-M. Hwang and Y.K. Low, 7/31/88.

NCEER-88-0029 "Response Analysis of Stochastic Structures," by A. Kardara, C. Bucher and M. Shinozuka, 9/22/88, to be published.

NCEER-88-0030 "Nonnormal Accelerations Due to Yielding in a Primary Structure," by D.C.K. Chen and L.D. Lutes, 9/19/88.

NCEER-88-0031 "Design Approaches for Soil-Structure Interaction," by A.S. Veletsos, A.M. Prasad and Y. Tang, to be published.

NCEER-88-0032 "A Re-evaluation of Design Spectra for Seismic Damage Control," by C.J. Turkstra and A.G. Tallin, 11/7/88.

NCEER-88-0033 "The Behavior and Design of Noncontact Lap Splices Subjected to Repeated Inelastic Tensile Loading," by V.E. Sagan, P. Gergely and R.N. White, to be published.

NCEER-88-0034 "Seismic Response of Pile Foundations," by S.M. Mamoon, P.K. Banerjee and S. Ahmad, 11/1/88.

NCEER-88-0035 "Modeling of R/C Building Structures With Flexible Floor Diaphragms (IDARC2)," by A.M. Reinhorn, S.K. Kunnath and N. Panahshahi, 9/7/88, to be published.

NCEER-88-0036 "Solution of the Dam-Reservoir Interaction Problem Using a Combination of FEM, BEM with Particular Integrals, Modal Analysis, and Substructuring," by C-S. Tsai, G.C. Lee and R.L. Ketter, 12/88, to be published.

NCEER-88-0037 "Optimal Placement of Actuators for Structural Control," by F.Y. Cheng and C.P. Pantelides, 8/15/88.

NCEER-88-0038 "Teflon Bearings in Aseismic Base Isolation: Experimental Studies and Mathematical Modeling," by A. Mokha, M.C. Constantinou and A.M. Reinhorn, 12/5/88.

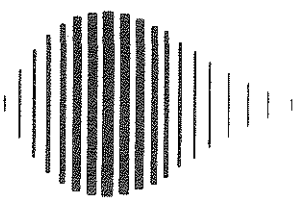

National Center for Earthquake Engineering Research
State University of New York at Buffalo